Dual Photo- and Thermo-Responsive Copolymers Based on Spiropyrans:

Synthesis and Self-Assembly into Nanostructured Materials

Dissertation

Zur Erlangung des akademischen Grades doctor rerum naturalium

(Dr. rer. Nat.)

Vorgelegt dem Rat der Chemisch-Geowissenschaftlichen Fakultät der Friedrich-Schiller-Universität Jena

Von M.Sc. Oliver Grimm

Geboren am 30. August 1987 in Seligenstadt

Gutachter:

1. Felix H. Schacher

2. Benjamin Dietzek

Tag der Verteidigung: 05.02.2020

"A straight line may be the shortest distance between two points, but it is by no means the most interesting."

-Robert Holmes

Table of Contents

1 Acknowledgements / Danksagung

Ich möchte diese Arbeit, mit dem in meinen Augen wichtigsten Teil beginnen, denn diese Arbeit wäre nicht möglich gewesen ohne die umfangreiche Hilfe aller beteiligten Personen. Mir ist im Laufe meiner Promotion von so einigen Leuten geholfen worden und die wichtigsten sind im Folgenden genannt.

Allen voran möchte ich Prof. Dr. Felix H. Schacher danken für die Möglichkeit in seiner Arbeitsgruppe diese Arbeit anzufertigen. Er sorgte für ein überragendes Arbeitsklima und stand mir immer mit Rat und Tat zur Seite. Besonders zu erwähnen ist an dieser Stelle der Lötkolben, der für den Bau der Beleuchtungsutensilien benötigt wurde.

Als nächstes danke ich Prof. Dr. Benjamin Dietzek für die Übernahme des Zweitgutachten. Sowie einigen sehr interessanten Diskussionen in Master-Verteidigungen, die mich in meiner Arbeit sehr vorangebracht haben.

Ich möchte allen Kooperationspartnern danken Daniel Zalami, Dr. Uwe Gerken und Prof. Dr. Jürgen Köhler aus Bayreuth.

Des Weiteren möchte ich allen Master-, Bachelor- und Forschungspraktikanten die einen großen Teil der Arbeit übernommen haben. Sarina C. Maßmann deren Arbeit mir sehr bei einer Publikation geholfen hat. Jonas Eichhorn der mir sehr bei der Arbeit mit den Mizellen, Lisa Volkmann inzwischen Wiedenhöft, die mir bei einem Großteil der Membranmessungen durchgeführt hat. Thomas Choisnet für die wiederkehrende Motivation mit guter Laune ins Labor zu kommen. Albert Altenburg, Cesar Marzola und Prof. Dr. Hisham Essawy für die vielen Synthesen und Membranen. Ich danke außerdem meinem HiWi Jacob Künne, der mich mit immer ausreichend Monomer versorgt hat. Abschließend sei noch Hanna Träger gedankt, für ihre Bachelor-Arbeit bei mir, den wunderbaren Vortrag über energetisiertes Wasser und ihre (leider) Abschiedsfeier.

Jenseits meiner Promotion möchte ich Malek Seibh erwähnen, den ich auf seinem Weg zum Bundessieger Jugend Forscht begleiten durfte.

Ich danke allen die im Rahmen meiner Promotion für mich Messungen übernommen haben. Dazu zählen Dr. Grit Festag und Katja König für die Wartung und Messung der SEC, Dr. Peter Bellsted und Friederike Pielenz, sowie der gesamten NMR-Abteilung, Felix und Iuliia für die SEM-Messungen, Philip und Moritz für die TEM und cryo-TEM Messungen, den Werkstätten und Glasbläserei für den Bau von verschiedenen, speziellen Geräten und Johanna für die Hilfe mit den Blender Abbildungen.

Ich danke der gesamten Arbeitsgruppe für die freundliche Aufnahmen Mark Billing, Anne Böhm, Felix Wendler, Dr. Christian Pietsch, Oliver Eckardt, Robert Deubler, Christoph Hörenz, Ulrike Günther, Tobias Rudolph und Moritz von der Lühe.

Ich möchte außerdem allen Arbeitsgruppenmitgliedern danke die im Laufe der Zeit dazugekommen sind. Felix Wendler, Philip Biehl, Carsten Rössel, Dr. Iuliia Romanenko, Johanna Elter, Lisa Volkmann, Johannes Max, Dr. Jessica Tom, Moritz Köhler, Jan-Hendrik Kruse, Yves Carstensen, Katja König, Peter Mons und Katrin Kuwalcuk. Ihr habe das Arbeitsumfeld geschaffen, in dem sich mit viel Spaß und ausgesprochen Produktiv arbeiten lässt. Ich erinnere mich sehr gerne an große Rollen Luftpolster-Folie, Arbeitsgruppenkalender, Spieleabende, „Streichelzoos“, Wandertage und endlos lange Vorträge mit lustigen Männchen auf Klassenfahrten

Ich danke meinem Büro, Wendy, Bob, Christoph und Johanna mit denen ich viel Spaß hatte angefangen bei Wackelaugen über Nerf-Gun Kämpfe bis hin zu einer ganzen Menge Luftballons.

Ebenso zu erwähnen sind alle Menschen, mit denen ich Sport gemacht habe, was zugegebenen Maßen eine ganze Menge waren. Hier sei meine Freeletics-Gruppe in Jena Ost sowie den Jugger und Lacrosse Teams im USV. Ebenso sei meiner Boulder-Gruppe aus Moritz, Johanna und Björn gedankt. In der Heimat ist noch die DLRG Hainburg zu nennen, die mir unzählige Stunden am Telefon abgerungen haben. Aber auch für einen gelungen Ausgleich gesorgt haben.

Des Weiteren sei an dieser Stelle noch die Doppelkopf-Runde bestehend aus, Johannes, Johanna, Carsten, Jonas und Daniel Costabel gedankt.

Ich danke Jessica für die unsagbare Hilfe die sie mir bei erstellen dieser Arbeit war. Sie hat die Arbeit nicht nur Korrektur gelesen, sondern mich auch bei allen was es so jenseits des Arbeitens gibt unterstützt hat. Angefangen bei Kuchen backen über Whiskey-Abende bis zur Organisation von Pool-Partys. Du hast mir viel Arbeit abgenommen, und diese Arbeit würde ohne dich sicherlich anders aussehen. Danke dafür.

Ich danke außerdem meinen Geschwistern, Simone und Tobias, sowie meinen Eltern Ursula und Roland samt Partner die mich während meiner gesamten Zeit in Jena nach besten Kräften unterstütz haben. Die Zeit mit euch war ein guter Ausgleich und ihr habt mich sehr motiviert nicht aufzugeben.

Ich hoffe ich habe niemanden vergessen, fall doch fühle er/sie/es sich an dieser Stelle erwähnt.

2 Abbreviations

$<R_H>_{n,app}$	Number-weighted hydrodynamic radius
^1A	Molecule A in the singlet ground state
$^1A^*$	Molecule A in the singlet exited state
^3A	Molecule A in the triplet state
AIBN	Azobis(isobutyronitrile)
ANOVA	Analysis of variances
ATRP	Atom transfer radical polymerisation
AzoMA	Methacrylate-based azobenzenes
BlocBuilder-MA	(2-[*N*-tert-butyl-N-(1-diethoxyphosphoryl-2,2-di-methylpropyl)aminoxy]-2-methyl propionic acid
BSP	2-((3´,3´-dimethylspiro[chromene-2,2´-indolin]-6-yl)oxy) acrylate
BSPA	2-((3´,3´-dimethylspiro[chromene-2,2´-indolin]-6-yl)oxy) ethylacrylate
CRP	Controlled radical polymerisation
d	Pathlength of a cuvette
Đ	Dispersity
DC	Decomposition
DCM	Dichloromethane
DLS	Dynamic light scattering
DMAc	Dimethylacetamide
DMF	Dimethylformamide
DMSO	Dimethyl sulfoxide
dn/dc	Refractive index increment
DoE	Design of experiment
DOSY	Diffusion ordered spectroscopy
DP	Degree of polymerisation
Δp	Transmembrane pressure
ε	Molar extinction coefficient at specific wavelength
eSEM	Environmental SEM
FRP	Free radical polymerisation
Hg(Xe)	Xenon doped mercury lamp
I_0	Intensity without sample
insol	Insoluble
IR	Infra-red
k	Reaction speed
λ	Wavelength
LCST	Lower Critical solution temperature
LED	Light emitting diode
M/I	Monomer to initiator
MALLS	Multi-angle light scattering
MC	Merocyanine-form
MCH^+	Protonated merocyanine
MMA	Methyl methacrylate
M_n	Number-weighted molecular weight
MSD	Mean square displacement
NEt_3	Triethylamine
NIPAAm	*N*-isopropylacrylamide
NMP	Nitroxide-mediated polymerisation
NMR	Nuclear magnetic resonance
p	Packing parameter
PEG	Polyethylene glycol

PEO	Poly(ethylene oxide)
PI	Polyisoprene
PMDETA	*N,N,N',N'',N''*-pentamethyldiethylenetriamine
PMMA	Poly(methyl methacrylate)
PNIPAAm	Poly(*N*-isopropylacrylamide)
POEGMA	Poly(oligoethyleneglycole) methacrylate
PS	Polystyrene
PU	Polyurethane
RAFT	Reversible addition–fragmentation chain-transfer
RI	Refractive index
SEC	Size exclusion chromatography
SEM	Scanning electron microscopy
SG-1	Diethyl (1-(tert-butyl(hydroxy)amino)-2,2-dimethylpropyl)phosphonate radical
SLS	Static light scattering
SNIPS	Self-assembly non-solvent induced phase separation
sol	Soluble
SP	Spiropyran-form
SPA	2-(3´,3´-dimethyl-6-nitrospiro[chromene-2,2´-indolin]-1´-yl)ethyl acrylate
SPH^+	Protonated spiropyran
$SP\text{-}NO_2$	2-(3´,3´-Dimethyl-6-nitro-3´H-spiro[chromene-2,2´-indol]-1´-yl)-ethanol
SP-OH	Trimethyl-6-hydroxyspiro-(2H-1-benzopyran-2,2'indoline)
SPOT	Single particle orbit tracking
TDE	Thiodiethanol
TEGA	2-(2-(2-methoxyethoxy) ethoxy) ethyl acrylate
TEM	Transmission electron microscopy
TEMPO	2,2,6,6-tetramethylpiperidinyloxy
THF	Tetrahydrofuran
TRIS	Tris(hydroxymethyl)aminomethane
UCST	Upper critical solution temperature
UV	Ultraviolet
Vis	Visible light

3 Introduction to Thermo- and Photo-Responsive Materials

Parts of this chapter have been published in Grimm, O.; Wendler, F.; Schacher, F., Micellization of Photo-Responsive Block Copolymers. *Polymers* **2017,** *9* (9), 396.[1]

The field of responsive or "smart" materials has expanded over the last decades owing to their unique functional applications, and their ability to respond to numerous triggers (Figure 1). Common stimuli that are applied to alter the properties of responsive materials include temperature, mechanical force, electromagnetic fields, pH, and solvent.

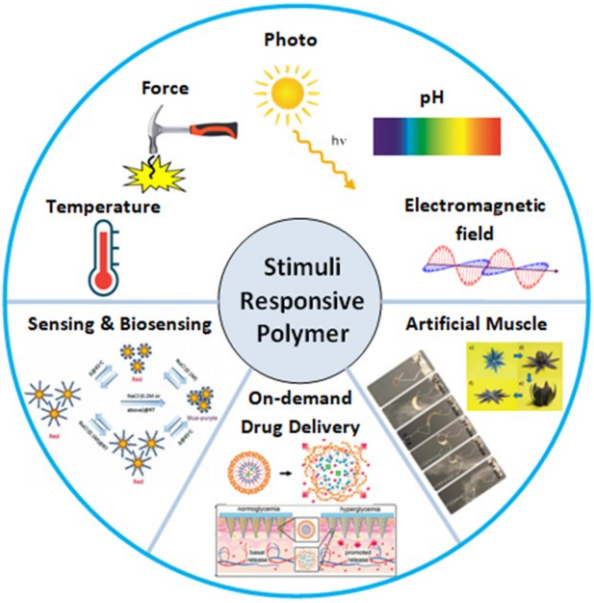

Figure 1: Summary of common stimuli and the potential applications of stimuli-responsive polymeric materials.[2] Published by The Royal Society of Chemistry.

The response of materials towards a stimulus is as diverse as their fields of application.[3] In everyday life, thermo-responsive materials are omnipresent. Many thermo-responsive materials are applied as sensors to detect the stimulus directly, *e.g.*, the different thermal expansion of two metals in a bimetal thermometer. A further and more complex response to temperature is seen in shape memory materials, which are able to recover their original shape in the presence of a specific stimulus.[4] Certain alloys such as Nitinol, an alloy of nickel and tin, can return to their original shape formed at an elevated temperature upon heating to this temperature once again. This enables such materials to be used in guided wires or stents in medical applications. Utilising polymers as responsive materials instead of metal alloys those materials are cheaper to produce or process and the tailoring of the materials is more variable.[5]

In addition to a straightforward or direct material response towards a specific stimulus, the response can also be used indirectly, *e.g.*, in thermal paper used to print receipts with heating rather than ink. This type of paper is coated with a mixture of crystal violet lactone, a pH-responsive dye, and a weak acid such as Bisphenol A. When this mixture is melted, the dye is protonated and becomes coloured.[6] Besides the organic-based system just discussed, this strategy also works using inorganic crystals, which also change colour upon melting.[7] The temperature-induced colour change of these materials can be tuned precisely, such that it is possible to apply them as thermometers. The liquid crystal thermometer appears black, and, depending on the temperature the coloured background is revealed. This type of thermometer is cheaper than conventional thermometers and easy to use.

The thermochromic behaviour, which generally manifests from a change in conformation, can also be triggered by irradiation rather than temperature. Such materials are omnipresent in modern society, with a very well-known example being transition lenses in prescription glasses as an alternative to sunglasses. Here, a glass containing silver halides dissociate upon UV irradiation darkening the material, and this is then reversed by thermal bleaching.[8] More recent research attempts to replace the glass matrix with a polymeric one, which enables various organic molecules (*e.g.*, spiropyran and diarylethene) for a more rapid response to UV light.[9]

Photochromic materials can also be used for optical data storage. This application of photochromic materials was suggested by Hirshberg in 1956,[10] and is still a hot topic that continues to be researched.[11-12] However, the photo-responsive materials are in most cases small molecules, whilst polymeric materials are more commonly used as bicontinuous matrix materials in organic solar cells.[13]

As shown above, there are a vast number of strategies that can be used to form stimuli-responsive materials. However, the combination of two stimuli in one material, and the tailoring of the properties of the newly formed material, is currently only conceivable using polymeric materials. The most straight forward and commonly applied method to access such materials is chain-growth polymerisation, and in most cases controlled radical polymerisation is chosen due to its chemical robustness and broad variety of amenable monomers. This method enables us to form polymeric materials that can respond to multiple stimuli relatively simply by combining different monomers into one material. When both stimuli can be addressed independently from each other, they are said to be orthogonal. This orthogonality is necessary so that both input stimuli can be applied independently from each other to obtain a measurable response for each stimulus separately. This is necessary to be able to decouple cause and effect on the polymeric material.

In this dissertation, a combination of multiple stimuli (light and temperature) is investigated since both stimuli can be applied independently from each other in aqueous media. First, the various photo-responsive moieties that have been incorporated within polymers is reviewed (chapter 3.2). Amongst which, spiropyran (SP) is well-known and transforms from a non-polar form to a zwitterionic merocyanine (MC) form. We then focus on thermo-responsive polymers, specifically poly(*N*-isopropylacrylamide) (PNIPAAm) as the most famous and representative thermo-responsive polymer, as well as oligoethylenoxide derivatives, which are gaining more popularity in research (chapter 3.3).

The expected behaviour of such orthogonally responsive materials is investigated, highlighting the difficulties associated with measuring both responses simultaneously (chapter 4). It is rather difficult and complex to measure the response of a material subjected to two stimuli simultaneously. This is because the response of the polymer to one stimulus is suppressed in many cases, or the investigation requires very complex and expensive equipment. The use of absorption spectrophotometry is a relatively simple and highly accessible tool for characterisation; however, the experimental setup to probe the responsive behaviour requires substantial optimisation.

The formation of a dual stimuli-responsive material using chain-growth polymerisation also enables block extension to form block copolymers (chapter 3.4). The combination of a hydrophilic and hydrophobic segment can lead to a broad variety of assembled structures. These structures, predominately micelles or asymmetric membranes, are investigated at the end of this chapter.

3.1 Copolymerisation of Various Functional Monomers

Polymers can be synthesised *via* two mechanisms: chain-growth or step-growth.[14] In step-growth, two repeating units react with each other to form a dimer. This process is repeated such that a polymer is formed in a stepwise manner. This approach is mostly used in polyaddition or polycondensation reactions. For step-growth polymerisations, a functional group A reacts with a functional group B. Both functional groups can be located in the same molecule (AB-type monomer), or one monomer has the same functionality multiple times and reacts with a second monomer bearing the opposite functionality at least twice (AABB-type). Compared with chain-growth polymerisation, step-growth polymerisation is limited to a smaller variety of polymerisable monomers, and high chain length polymers are only achievable at high conversions.

Conversely, in chain-growth polymerisation, an initiator decomposes and reacts with a monomer to form an active end. This active chain then continues to react further with other monomers. The chain then continues to grow until it terminates irreversibly by radical recombination or disproportionation (Figure 2).

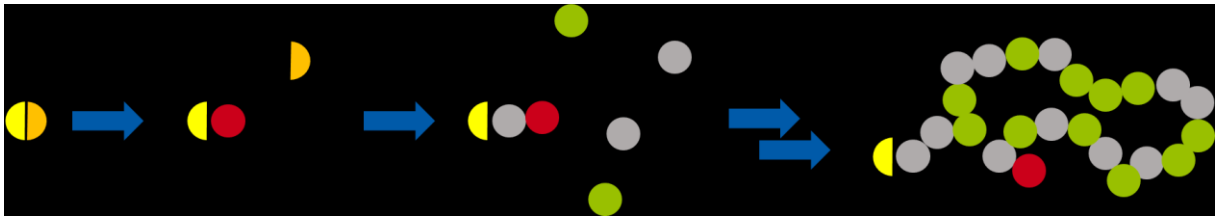

Figure 2: Schematic of a copolymerisation of two different monomers polymerising via chain-growth polymerisation: (i) initiator decomposition, (ii) initiation, and (iii) chain-growth.

In chain-growth polymerisation, the monomer must bear a polymerisable moiety; this is typically a double bond, but can also include epoxides, which can be modified to tune the reactivity of the monomer. Certain modifications also permit the copolymerisation of two or more monomers to form well-defined copolymers with relative ease.

In a copolymerisation, the active end group exhibits varying reactivity towards each monomer in the reaction mixture.[15] In the example depicted in Figure 2, the active end group has no preference for either monomer, and this results in the formation of a random copolymer. However, when the end group of one monomer has a higher reactivity towards the same monomer, a gradient copolymer is formed. In an extreme case, this can even result in the formation of block-like copolymers called tapered copolymers. In very rare cases, the reactive end group reacts preferentially with the other monomer present leading to the formation of alternating copolymers.

The particular built-in ratio exhibited in a copolymerisation is independent of the polymerisable group utilised in chain-growth polymerisation. The reactive group can react with an anion, a cation or a radical depending on the initiator used and its decomposition product (anion, cation or radical). Ionic polymerisation,[16] whilst particularly vulnerable to impurities such as polar protic solvents or oxygen, it is highly advantageous over radical polymerisation due to the repulsion between the charged end groups. This repulsion prevents interchain coupling, making ionic polymerisation a truly “living” system. Provided no termination agent is added, the chain end continues to grow until all monomer is consumed. A second monomer can then be added to access block copolymers since the end group can

stay alive for weeks. However, this method is not very robust towards impurities and can only be performed in polar aprotic or unipolar solvents.

Radical-based systems are much more robust than ionic systems, tolerating the presence of impurities and protic solvents.[17] However, the end groups can react with each other, leading to premature termination of the polymerisation and broader molecular weight distributions. Termination occurs *via* two main pathways: recombination of two reactive end groups, as well as disproportionation. Transfer reactions can also occur, *e.g.*, the abstraction of a secondary proton from a neighbouring polymer chain, or through backbiting whereby a hydrogen atom is abstracted from a tertiary carbon along the polymer backbone by the active chain end in a single polymer chain. In the latter case, radicals are formed along the polymer backbone leading to polymer branching. In general, the high reactivity of radicals leads to poorer control and higher dispersity materials when compared to ionic polymerisations. Furthermore, the presence of termination and transfer reactions in radical polymerisations prevents the formation of truly "living" polymers.

Nevertheless, the synthetic ease and large variety of monomers amenable with radical polymerisation makes it highly attractive to achieve a controlled radical polymerisation. Since 1956, where Szwarc[18] reported one of the first single-electron transfer polymerisations, significant progress has been made to improve the control over radical polymerisations with the arrival of so-called quasi-living systems where the end group is capped reversibly.[19-22] Controlled radical polymerisation can be classified into three main techniques (see Figure 3): transition metal-mediated radical polymerisation,[23] reversible addition-fragmentation chain-transfer (RAFT) polymerisation,[24] and nitroxide-mediated polymerisation (NMP).[25] In transition metal-mediated polymerisation, which in most cases refers to atom transfer radical polymerisation (ATRP), a transition metal catalyst (typically copper) cleaves and recombines the end group from the growing polymer chains (typically a halogen such as bromine). Whilst in RAFT polymerisation, a thiocarbonyl thio compound transfers radicals between chains. Similarly to ATRP, NMP exploits a stable or persistent nitroxide radical that reversibly caps the active radicals due to temperature. As the nitroxide radical is highly stable or persistent, it is not reactive enough to initiate a polymerisation itself, while the active polymer chain end is highly reactive and further propagates by the addition of monomer, or irreversibly terminates.

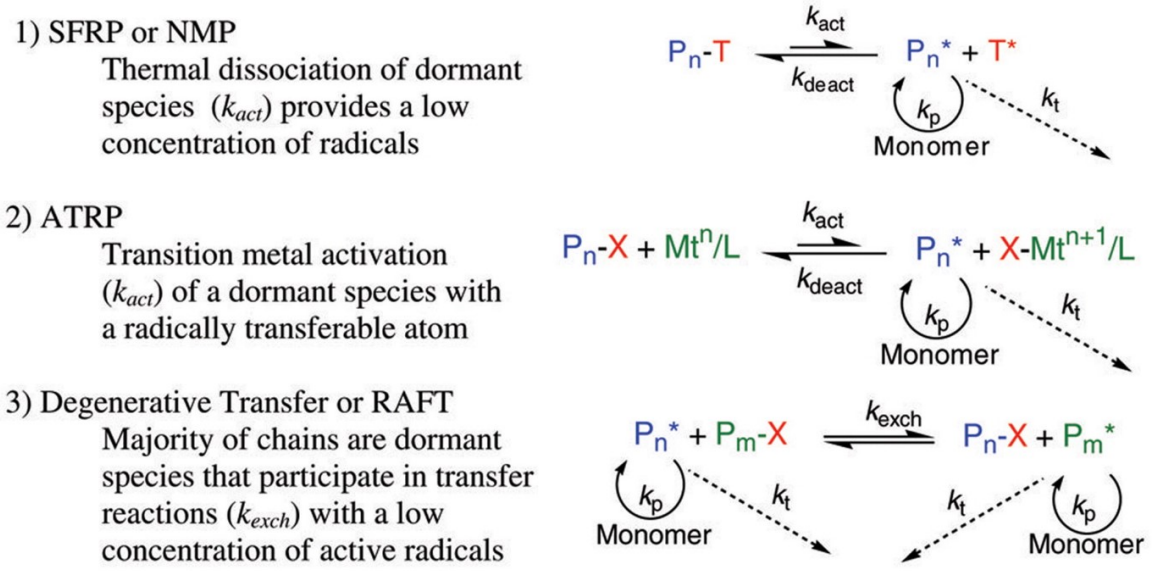

Figure 3: Summary of the three key controlled radical polymerisation techniques available and their accepted mechanisms. Reprinted from [21] with permission from Elsevier.

In all cases, the active chain end can be in a dormant inactive state or in a growing active state. In the dormant state, the polymer chain is protected, and neither termination nor growth occurs. In the active state, additional monomer is added to the radical end group, and the polymer chain continues to grow. The equilibrium between the dormant and active state favours the dormant species in well-controlled systems to reduce the number of active radicals present at any given time and prevent unwanted termination processes. In this way, more well-defined polymers are achieved. While it is possible to suppress unwanted side reactions of termination and transfer, they can never be completely eliminated in radical processes. This is why controlled radical polymerisation processes are never described as truly living systems. Despite this downfall, controlled radical polymerisation techniques are favoured over ionic systems because they are synthetically simple, incredibly robust to the presence of impurities, are amenable to a large variety of monomer classes from ethene to vinyl-containing molecules, and can be performed in a variety of solvents including beer,[17] and even blood.[26] With the advent of controlled radical polymerisation, well-defined polymer architectures can now be easily accessed with high chain-end fidelity, such that the formation of block copolymers is feasible.

In this thesis, we will concentrate on nitroxide-mediated polymerisation because of its synthetic simplicity and broad variety of possible monomers. The persistent nitroxide radical can be modified into a unimolecular NMP initiator with synthetic ease. Therefore, an initiating group such as styrene or MMA is linked to the nitroxide compound, which fixes the ratio of the initiating radical and end-capping nitroxide. This reduces the synthetic effort of a nitroxide-mediated polymerisation. The first NMP reported used an alkoxy amine, prepared by combining 2,2,6,6-tetramethyl piperidinyl oxy (TEMPO) with α-bromo styrene, to initiate and control the polymerisation of styrene (Scheme 1).[27]

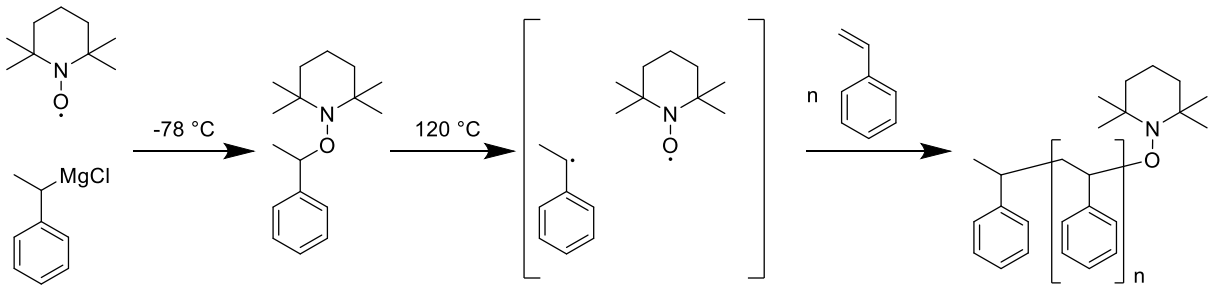

Scheme 1: Nitroxide-mediated polymerisation of styrene initiated with a unimolecular NMP initiator based on TEMPO as a persistent radical or capping agent.

Heating above a certain threshold temperature breaks the C-O covalent bond homolytically in the unimolecular initiator to form a stable nitroxide radical and a reactive styrene radical. The stable radical can then react reversibly with the reactive end group to reform a dormant species. However, the high temperature required of 120 °C for TEMPO-mediated NMP is a major drawback, which has led to the synthesis of a broad variety of nitroxides with improved reactivity. The most significant change for the increase in reactivity of TEMPO derivatives was obtained by the formation of an intermolecular hydrogen bond in close proximity to the nitroxide radical.[20] The addition of hydrogen at the α-carbon proved to significantly increase the initiator reactivity.[28-29] These developments made NMP compatible with other controlled radical polymerisation methods, as well as a very versatile and easy method for the successful polymerisation of numerous monomers; predominantly acrylates, acrylamides, 1,3-dienes, and acrylonitrile-based monomers.[30] In some cases, the addition of additional nitroxide radical to the reaction mixture improves the polymerisation control as the added persistent radical prevents uncontrolled transfer of the reactive chain end.

The ability to reactivate the chain end upon heating also simplifies the formation of block copolymers. In general, a macroinitiator is first required; for this, the unimolecular initiator is mixed with a monomer, the mixture is heated, and a polymer is formed. The mixture is cooled down and the polymer isolated and characterised before being applied as a macroinitiator. The macroinitiator is then mixed with a second monomer and heated again to thermally break the C-O bond to reactivate the chain end for continued polymer growth. In this way, it is possible to form the hydrophilic and hydrophobic segments of amphiphilic block copolymers, which are known to self-assemble in the solid-state, as well as in solution.

The monomers typically used in NMP (styrene- and acrylate-based) are not stimuli-responsive. In order to form such stimuli-responsive materials through NMP, one or more monomers must be combined that react to a specific stimulus. A stimuli-responsive polymer can be achieved in two ways: (i) a responsive molecule is covalently linked to a polymerisable unit before or after polymerisation; or (ii) the responsive behaviour only manifests in the polymer itself, not the monomeric unit. Photo-responsive materials are typically accessed through the first route, where a photo-sensitive moiety is chemically anchored onto the polymer pendant group; thermo-sensitive materials, however, are typically realised through the second pathway.

3.2 Photo-Responsive Monomers

Photo-responsive polymeric materials are obtained by linking a photo-responsive molecule covalently to the polymer chain, which then interacts with light of a specific wavelength. In most cases, this simply involves the absorption of light energy, which promotes the molecule into its excited electronic state (Figure 4).[31] In most cases, molecules simply relax from this excited state back to their ground state by emitting light of a lower energy due to non-radiative decay. From this excited state, photo-responsive molecules overcome a specific energy barrier to alter their conformation, or to break and/or form a specific chemical bond. Light as a stimulus is easily applied locally and does not interfere with other stimuli when applied at low doses.

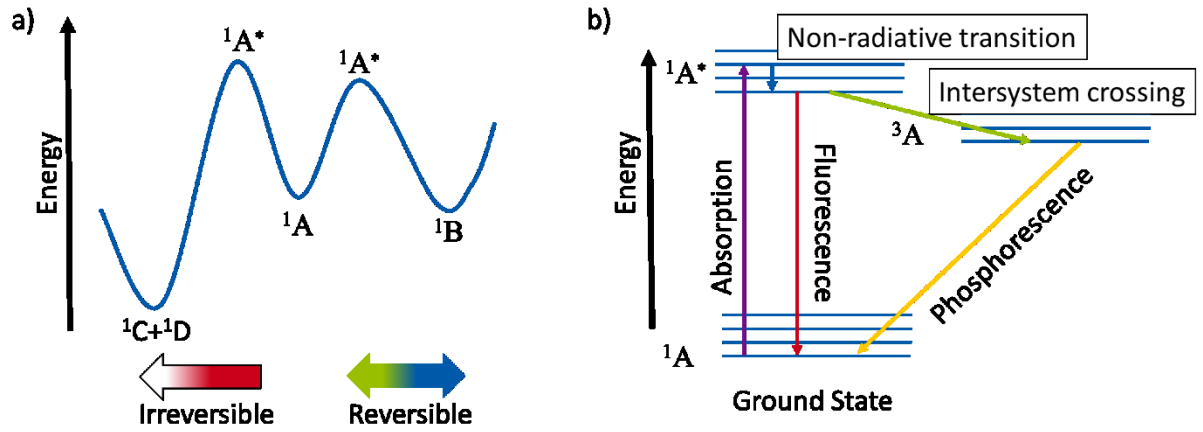

Figure 4: a) Simplified reaction coordinate diagram of molecule A (i) that is transformed reversibly to B and (ii) irreversibly to C + D. b) Simplified Jablonski diagram showing the energy pathways possible for an excited molecule upon irradiation.

Furthermore, the interaction of light with a photo-responsive molecule can either be of a reversible (^{1}A to ^{1}B) or irreversible (^{1}A to ^{1}C + ^{1}D) nature. A large variety of photo-responsive molecules have been synthesised over the last several decades. Many of these molecules possessed a polymerisable functional group for the synthesis of photo-responsive polymers. Focusing on reversible systems, the behaviour of spiropyran-based polymers remains of high interest; spiropyrans switch reversibly between a non-polar spiropyran (SP)-form to a zwitterionic merocyanine (MC)-form.[32] We will now briefly outline common irreversible and reversible photo-responsive moieties that have been incorporated within polymers and block copolymers.

3.2.1 Irreversibly Photo-Responsive Monomers

Most irreversible photoreactions that have been reported exhibit a response in the far UV region, and result in photo-cleavage of side groups as well as the introduction of irreversible crosslinks *via* photocycloadditions or photo-rearrangement reactions (Figure 5). The former approach was inspired by photo-labile protecting groups; *e.g.*, pyrenylmethyl esters,[33] *o*-nitrobenzyl esters,[34] coumarinyl esters,[35] and *p*-methoxy-phenacyl esters;[36] all of which have been investigated during the second half of the last century.[37] In this regard, the group of Zhao introduced two fundamental examples both presenting a block copolymer consisting of a hydrophilic PEO block and a hydrophobic and photo-responsive polymethacrylate-based segment.[38-39] The respective cleavage of either the pyrenylmethyl or *o*-nitrobenzyl groups upon UV irradiation (365 nm) shifted the hydrophilic/hydrophobic balance of the amphiphilic block copolymer through the generation of hydrophilic poly(methacrylic acid). This led to swelling or even dissociation of the micellar aggregates in aqueous media and a release of the

encapsulated Nile Red, which was used as a model drug. In particular, *o*-nitrobenzyl chromophores have been discussed as promising candidates for biological applications since stimulation with NIR light is possible. Consequently, several block copolymers bearing *o*-nitrobenzyl ester groups in the side chain in combination with blocks of PEO/PEG or POEGMA,[40-48] polystyrene,[49-51] poly(methyl acrylate),[52] poly(2-ethyl-2-oxazoline),[53] or polydimethylacrylamide[54] have been synthesised and investigated in terms of their response upon irradiation with far UV light. Another example was reported by Liu and Dong, where the photo-controlled release of the anticancer drug doxorubicin was demonstrated using a biodegradable polypeptide-based poly(*S*-(*o*-nitrobenzyl)-L-cysteine)-*block*-poly(ethylene oxide) block copolymer. The materials formed spherical micelles in aqueous media and exhibited a significant reduction in size after irradiation.[55] The combination of any photo-response with other stimuli, *e.g.*, temperature, is favourable because the release mechanism could be initiated more effectively and thus more controlled. In order to modify the responsive behaviour of copolymers, dual,[56-69] triple,[70-71] and even quadruple responsive systems have been realised.[72-73] Furthermore, the incorporation of *o*-nitrobenzyl esters in the main chain[74-75] or at the block junction can be realised *via* divergent polymerisation,[76-80] convergent coupling,[80-87] or even using a combination of both strategies[88-90] to prepare photolytically cleavable amphiphilic block copolymers.

3.2.2 Reversible Photo-Responsive Monomers

In general, UV light within the range of 200–400 nm provides enough energy to break bonds, induce cis-trans isomerisation, and enable cycloaddition reactions. The most important chromophores we will discuss in this section are azobenzenes,[91-92] spiropyrans,[93] cinnamoyl esters,[94] and diarylethenes.[95] These common photo-responsive molecules are shown in Figure 5.

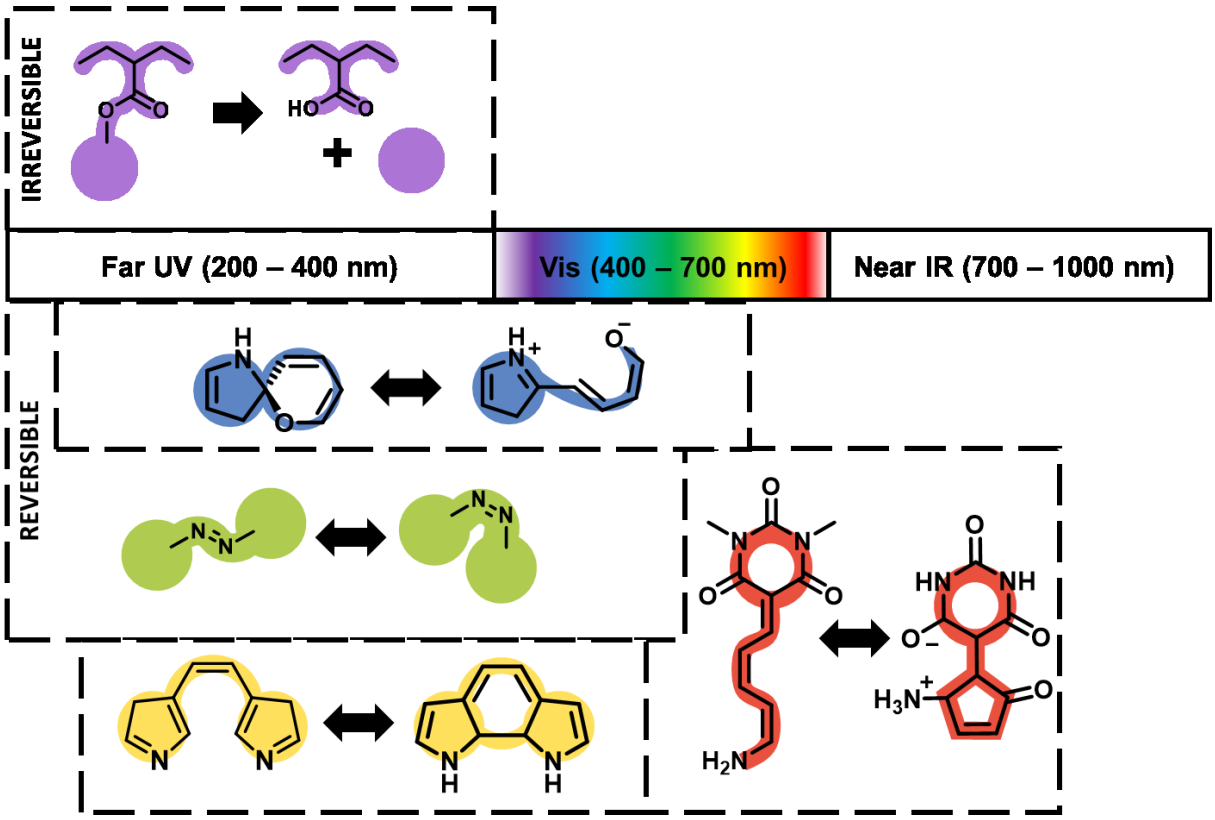

Figure 5: Overview of the typical photo-responsive moieties incorporated within polymers according to their typical excitation wavelength.[1]

The photochromism of heterocyclic 1,2-diarylethenes, a subclass of fulgides, has been known since 1905.[96] In 1988, the substitution pattern of these photochromic systems was extended considerably by Irie and Mohri.[97] The ring closure of single-molecule diarylethenes is typically triggered at 325 nm (the back reaction to the cis-form often occurs upon irradiation at 488 nm).[98] However, depending on the substitution pattern, this wavelength can vary from 313 to 405 nm (the corresponding back reaction is then triggered from 405 to 546 nm).[97, 99] These photo-responsive diarylethenes can be incorporated into polymers either within the main chain or in the side chain. Stellacci et al.[100] also reported the synthesis and successful polymerisation of diarylethene-based monomers. The modification of a suitable diarylethene with a polymerisable styrene group enabled Nishi et al.[101] to synthesise poly(diarylethene)-*block*-polystyrene *via* reversible addition–fragmentation chain-transfer polymerisation (RAFT). The RAFT end group was cleaved, and the resulting thiol adsorbed onto gold nanoparticles to form photochromic hybrid nanoparticles in toluene. The same photo-responsive monomer was used by Kobatake[102] to prepare poly(diarylethene)-*block*-PNIPAAm using surface-initiated polymerisation from silica nanoparticles. These nanoparticles were investigated both in water and THF.

The first azo dye was synthesised by Martius in 1863. In the following year, Griess reported the coupling reaction of related diazonium compounds.[103] However, it was not until 1937 that the reversible cis-trans isomerisation of azobenzene was proven by Hartley.[104] After irradiation of a sample in benzene with blue light, they observed different dipole moments compared to a non-irradiated sample. Previously, the light-responsive behaviour of azobenzene was ascribed to some sort of oxidation process; following this experiment, a new rationale for this behaviour was adopted.[105] A great variety of azobenzenes with varying substituents have been prepared that exhibit excitation wavelengths in the far UV[91-92] to 410 nm[106] range, with the corresponding back isomerisation process, generally mediated by thermal relaxation or irradiation at 500 nm, respectively. The first polymer containing an azobenzene photo-responsive group was synthesised by Ringsdorf et al. in 1984.[107] They first prepared the monomer 6-[4-(4-cyano-phenylazo)phenoxyhexyl acrylate before performing a free radical copolymerisation with the corresponding benzoate, which resulted in a liquid crystalline copolymer. Then in 1989, Angeloni et al. compared the spectroscopic properties of main-chain and side-chain azobenzene-functionalised polymers with the corresponding monomers, and found that the substitution pattern has the largest effect on the resulting absorbance maximum.[108] This effect is also exhibited by block copolymers consisting of a polystyrene (PS), poly(methyl methacrylate) (PMMA), poly(β-acetyl galactose ethyl methacrylate) or poly(ethylene glycol) (PEG) block in combination with various polymeric azobenzenes.[109-113] In that regard, the first block copolymer containing a photo-responsive azobenzene segment was synthesised by Se et al. in 1997 through side-chain modification of a poly(styrene-*block*-*N,N*-dimethyl-4-vinylphenethylamine) block copolymer prepared by sequential anionic polymerisation with *p,p'*-bis(chloromethyl)azobenzene.[114] In another example, the copolymerisation of methacrylate-based azobenzenes (AzoMA) with *N*-isopropyl acrylamide (NIPAAm) with varying amounts of NIPAAm was shown by Ueki et al., and this significantly affected the thermo-response characteristics of the resulting copolymers upon irradiation.[115] The change in dipole moment of the azobenzene was used by Concellón et al. to reversibly load aqueous block copolymer micelles.[116] They prepared poly(ethylene glycol)-*block*-poly(2,6-diacylaminopyridine) (PEG-*b*-PDAP) *via* RAFT polymerisation, and loaded these micellar assemblies with *N*(1)-[12-(4-(4'-isobutyloxyphenyldiazo)phenoxy)dodecyloxy)] thymine ($tAZO_i$). Afterwards, the load could be reversibly released upon irradiation with UV light.[117]

Many of the photo-responsive molecules are known for their thermo-chromatic behaviour. The thermally induced colour change of spiropyran-based compounds in solution has been known since the 1920s.[118-119] The origin of this colour change is the light- or temperature-induced cleavage of a bond between a tertiary carbon and a cyclic heteroatom, thereby switching between a bicyclic spiropyran-form and a zwitterionic merocyanine-form. The first detailed report on the photo-response of this class of molecules was published by Fischer et al. in 1954.[120] Since then, a multitude of spiropyrans with differing substitution patterns have been synthesised.[121-122] Benzospiropyran molecules exist predominantly in the open form upon irradiation at 365 nm, switching to the closed ring upon irradiation at 560 nm typically (Figure 6).[123-125] Copolymers containing spiropyran moieties were intensively studied by Smets in 1972, including a copolymer with MMA synthesised *via* free radical polymerisation.[126] The first copolymer containing spiropyran was synthesised by Krongauz et al. in 1981 by modifying benzospiropyran with an acrylate group followed by free radical polymerisation.[127] The first reported block copolymer was an ABA-type and was prepared by De Los Santos et al. in 1999.[128] They modified the B segment of PMMA-*b*-PU-*b*-PMMA with different spiropyran molecules. Since then, various examples of spiropyran-containing amphiphilic diblock terpolymers have been reported,[129-130] generally consisting of a PEG block, and various poly(benzospiropyran) segments with different comonomers. Comparing the absorption maxima of the spiropyran compounds used in polymers or copolymers, they do not differ significantly from the reported monomeric spiropyran compounds.[131] Nevertheless, the synthesis of amphiphilic block copolymers leads to many potential and varied applications from polymeric liquid crystals to photo-responsive block copolymer micelles.[132-136]

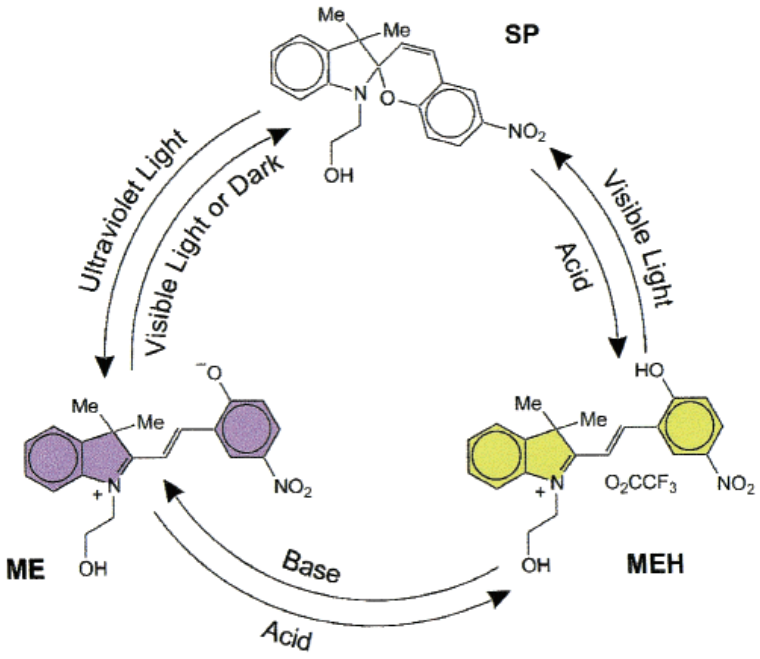

Figure 6: The switching cycle of nitro-spiropyran separated into three states by Raymo and Giordani. The colours indicate the observed colour in acetonitrile. Reprinted with permission from Ref. [123]. Copyright 2001 American Chemical Society.

It is possible to trigger micelle formation by addressing the spiropyran as shown by Guragain et al.,[135] as well as to control the release rate of encapsulated cargo in the case of core-crosslinked micelles as shown by Wang et al.[133] Menon et al.[136] synthesised an amphiphilic block copolymer consisting of poly(spiropyran methacrylate)-*block*-poly(3-*O*-4-vinylbenzoyl-D-glucopyranose), which forms 200 nm micelles in aqueous solution that can be loaded in the dark with coumarin, and which release their load upon irradiation at 360 nm UV light. They further demonstrated that the micelles can be reformed

upon irradiation with green light (560 nm). In that respect, coupling a thermo-responsive block to the spiropyran-containing segment further enables the formation of micelles by temperature changes.[137] Very recently, Zhang and coworkers used RAFT polymerisation to prepare P(NIPAAm)-*b*-poly(*N*-acryloyl glycine) diblock copolymers, which they subsequently functionalised with benzospiropyran ($PNIPAAm_{94}$-*b*-$P(NAG_{19}$-*co*-$NAGSP_{30})$). These multiple stimuli-responsive block copolymers formed spherical or worm-like micelles in water, depending on the temperature (above or below the LCST of PNIPAAm) or by irradiation with light (switching between the merocyanine and spiropyran form).[132]

All photo-responsive molecules are switchable from one well-defined state to another well-defined state. During a single-molecule experiment, this leads to binary, discontinuous behaviour. However, for a larger number of molecules (*e.g.*, 1 mol), not all molecules switch simultaneously during irradiation. This leads to a continuous change from one state to another, which also makes it challenging to specify the exact number of molecules in a particular state at any given time. For this reason, it is necessary to irradiate photo-responsive polymeric materials until no further change is observed and a threshold is reached. In contrast, thermo-responsive polymeric materials react simultaneously to a certain temperature.

3.3 Temperature-Responsive Polymers

The first reported stimuli-responsive polymers were temperature-responsive.[138] These materials are simple to investigate, and their water solubility permits their application in biological systems. Thermo-responsive polymers can exhibit an upper critical solution temperature (UCST) and/or a lower critical solution temperature (LCST). Polymers that show LCST behaviour are water-soluble at lower temperatures due to extensive hydrogen bonding. Upon heating above a certain temperature, the kinetic energy of the water molecules exceeds the binding energy of the hydrogen bonds, resulting in the coiled polymer chains to collapse simultaneously to form a globule (Figure 7).[139]

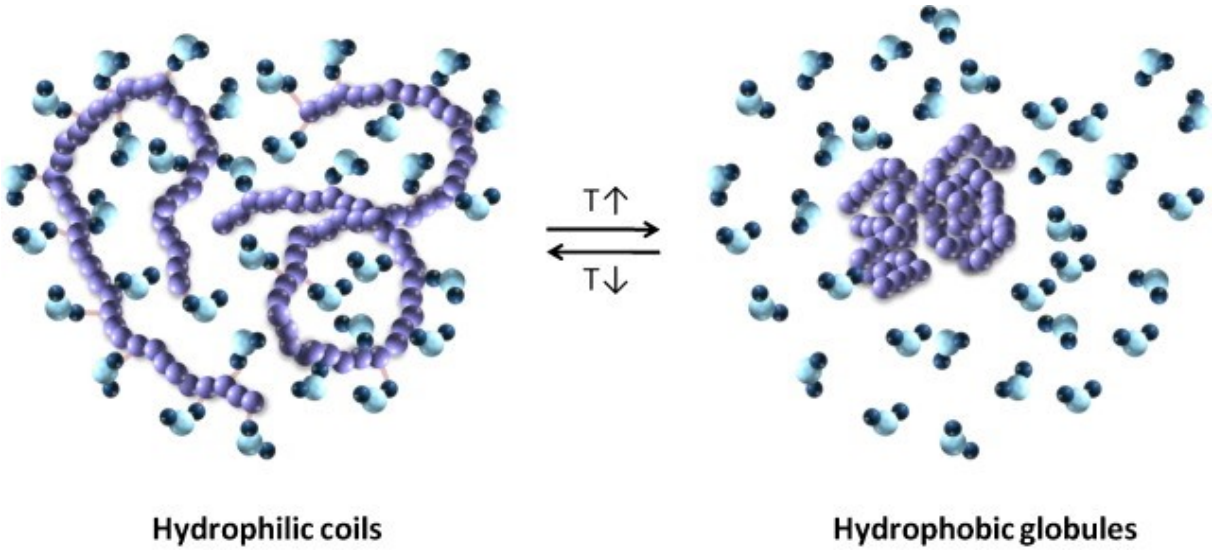

Figure 7: Schematic depicting the behaviour of a thermo-responsive polymer undergoing a coil-to-globule transition. Reprinted from Ref. [140], with permission from Elsevier.

In general, water molecules are attached to the polymer chain *via* hydrogen bonding forming a solvent hull around the polymer, and which further acts to stabilise it. Upon heating, the kinetic energy reaches a certain threshold where bonds break, and the solvent hull vanishes. The polymer coil collapses to a globule, and the polymer becomes insoluble. This transition temperature is not only temperature-

dependent, but also depends on complex interactions affecting the solvent hull such as the concentration of the polymer in solution, and in some cases also on the chain length of the polymer. The LCST is the lowest temperature observed for all possible polymer-solvent mixtures. Further effects on the LCST of thermo-responsive polymers can originate from cosolvents[141-142] and cosolutes.[143] In this dissertation, the polymer concentration was in most cases not varied. This means that a transition temperature or cloud point was determined and not the LCST.

The first synthesised and most investigated representative thermo-responsive polymer is poly(*N*-isopropylacrylamide) (PNIPAAm). The LCST behaviour was first investigated in 1968 by Heskins,[144] before being intensively investigated by Schild and Tirrell.[145-146] However, the phase transition hysteresis is still highly discussed,[147] and the thermo-response of the homopolymer exhibits complex behaviour depending on the chain length and end group, as well as on the presence of additives,[148] cosolvents,[149-150] or salt. Nevertheless, the convenient phase transition temperature of the homopolymer between room temperature and body temperature can be tuned by the incorporation of hydrophilic comonomers.

Various reports acknowledge a good polymerisability of acrylamides by controlled radical polymerisation techniques. A potential drawback is that the incorporation of a hydrophobic comonomer, as it applies for almost all photo-responsive molecules, leads to lower transition temperatures that trigger the response.[151-152] Consequently, the chosen thermo-responsive unit must also have a high transition temperature since it will be lowered by the incorporation of a hydrophobic copolymer. A monomer that is polymerisable using NMP and exhibits a higher transition temperature could provide an alternative. Poly(triethylenglycol monomethyl methacrylate) (PTEGA) meets all of these requirements.[153-155] Oligo ethylene glycol (meth-)acrylates are non-linear polyethylene glycol (PEG) analogues that exhibit a lower LCST compared to their linear analogues.[156] In order to create new polymer architectures, Rempp et al.[157] initiated the synthesis of 'macromers', 2 to 10 repetition units of oligo ethylene glycol in the side chain, and the number of which has increased over recent years.[152, 158] The incorporation of a comonomer with this class of thermo-responsive monomer does not broaden the transition temperature.[159]

3.4 Amphiphilic Block Copolymer Assemblies

In all cases discussed so far, both stimuli-responsive monomers were combined in a dual stimuli-responsive hydrophilic copolymer. Controlled radical polymerisation offers the possibility to form block copolymers. Therefore, first one segment is polymerised and separated from residual monomer. In the second step, the chain end is reinitiated and a second block using a different monomer is added. Polymers consisting of two different blocks self-assemble into defined structures depending on the packing parameter in the solid-state[160] and in solution[161] (Figure 8).

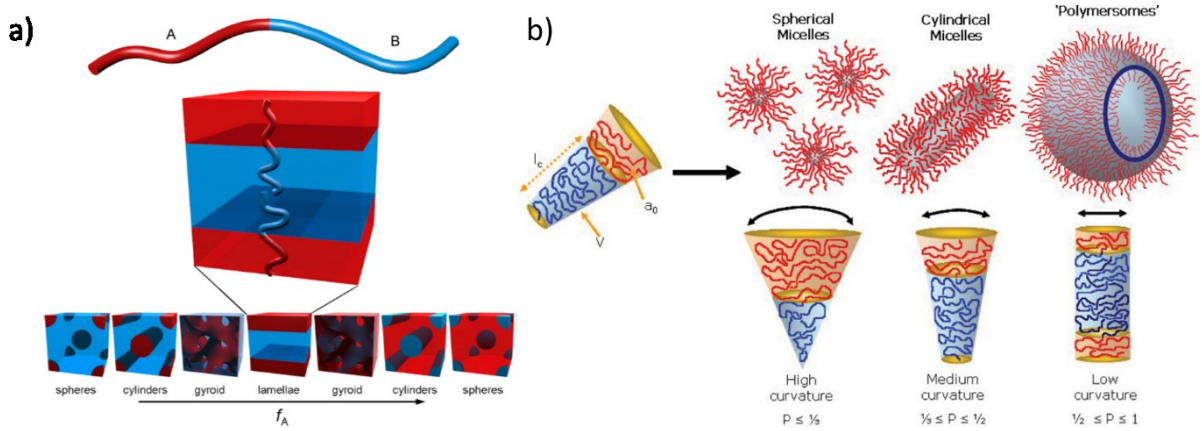

Figure 8: Structures formed by block copolymers with varying A/B ratios a) in the solid-state, Reprinted from Ref. [160], with permission from Elsevier, and b) in solution. Reprinted with permission from Ref. [162]

The self-assembled structure formed from block copolymers depends mainly on the volume-ratio of both blocks. Each block has a certain space requirement that favours certain structures in the solid-state and in solution. If the ratio is very high, spherical structures are more likely to form. As the ratio further increases, the structure goes from cylindrical, gyroid, and then to lamellar in the solid-state. Block copolymers consisting of a hydrophilic and a hydrophobic segment form interesting structures in aqueous solution. In solution, increasing volume ratios leads from spherical micelles over cylindrical micelles to vesicles.[163] The dual stimuli-responsive copolymer discussed so far is designed to be water-soluble, and the addition of a water-insoluble segment is relatively straight forward. Depending on the ratio of both blocks, stabilised micelles can be prepared in water (see chapter 6) or solid membranes (see chapter 7) can be formed. The response of these macro structures can then be compared to the dual-responsive behaviour observed for the dissolved copolymers.

3.5 Self-Assembly of Block Terpolymers into Micelles

The dual stimuli-responsive copolymers can coil freely in aqueous solution. If these copolymer chains are now brought in close proximity within a micellar assembly, they may affect each other and behave differently. Micellar systems are stabilised compartments in solution, and in our case consist of self-assembled block copolymers.[164] These block copolymers consist of a hydrophilic and a hydrophobic segment, which spontaneously self-assemble in a selective solvent such as water.[165] The morphology the block copolymer aggregate adopts in solution depends on the packing parameter, *i.e.*, the volume ratio between both segments in the selective solvent.[15] The possible morphologies range from spherical micelles to vesicles as shown in Figure 9.[166] The adopted morphology is also typically independent of the polymer architecture. The most simple architecture possible is a linear block copolymer, but micellisation has also been reported for more complex structures such as brush-like or ring copolymers.[161] The only real prerequisite for micelle formation being that the copolymer consists of two distinct functional segments.

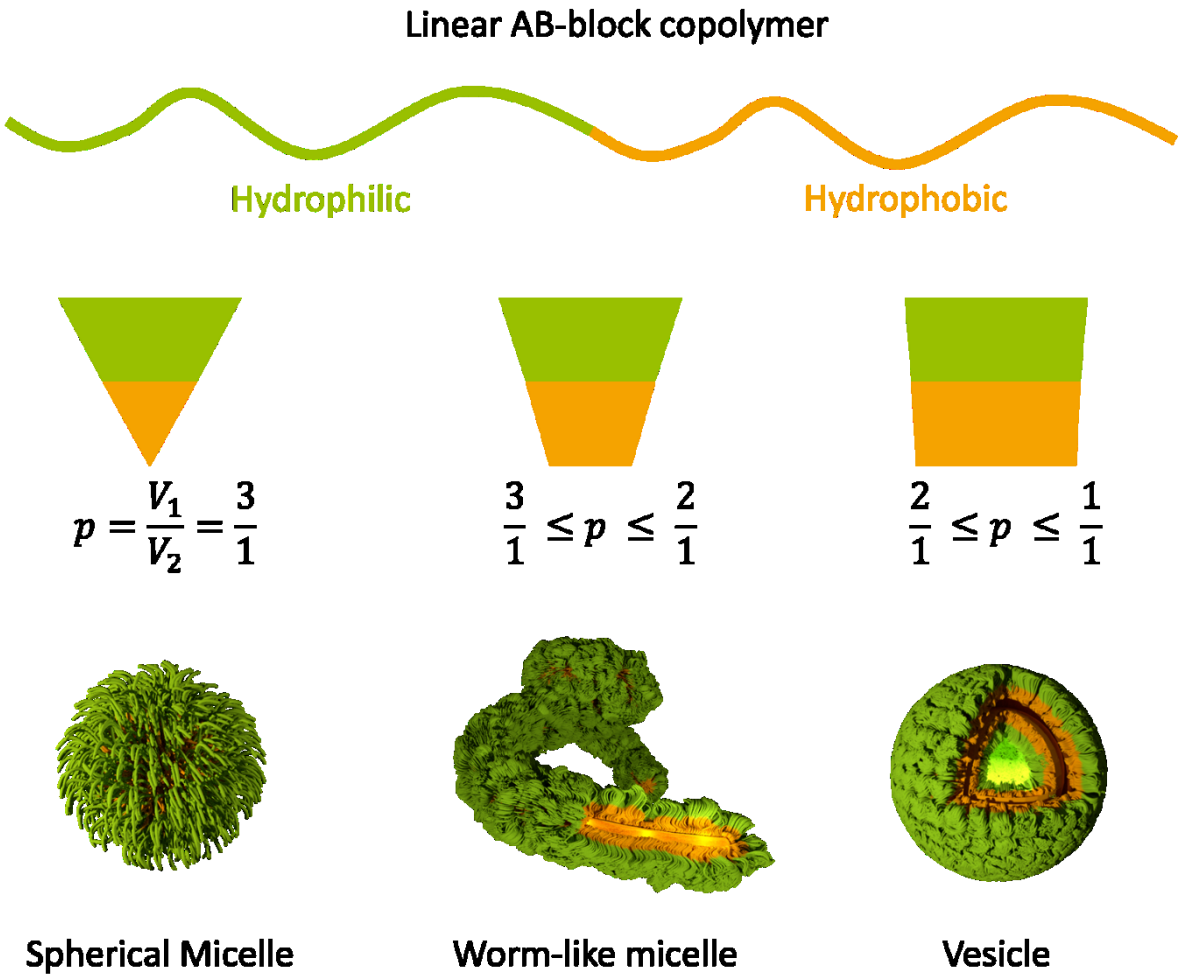

Figure 9: Impact of the packing parameter, p, on the resulting micellar morphology obtained.

If the core radius is significantly smaller than the total radius of the micelle, a hairy micelle is formed. If the hydrophobic segment is particularly insoluble in the selective solvent, the core will further collapse, reducing the volume percentage further in the final micelle. In this case, the hydrophilic chain ends can coil relatively freely. We can, therefore, expect that the behaviour of this responsive segment will not vary greatly from the responsive copolymers investigated previously. If a linear amphiphilic

block copolymer is used, the composition of the two segments predominantly controls the shape of the aggregate in solution. However, due to the collapse of the hydrophobic segment, even a block copolymer consisting of 50 % hydrophobic repetition units can still form spherical micelles.

3.5.1 Requirements for Micelle Formation

The formation of stable compartments in solution, *i.e.*, micelles or vesicles, is a delicate process that highly depends on the amphiphilic block copolymer used. Amphiphilic block copolymers consist of two distinct segments – one that is hydrophilic, and one that is hydrophobic. This difference in miscibility between blocks leads to their spontaneous self-assembly in the solid-state, as well as in solution. Micelles are generally formed under aqueous conditions, consistent with the present work, which results in the formation of a hydrophobic core and hydrophilic corona. While many techniques have been developed to prepare micellar structures,[167] in most cases the copolymer is first dissolved in a non-selective solvent that is capable of dissolving both blocks before the solvent is exchanged to a selective solvent. This selective solvent, typically water, only dissolves one specific block, which results in the formation of stable compartments in solution as depicted in Figure 10.

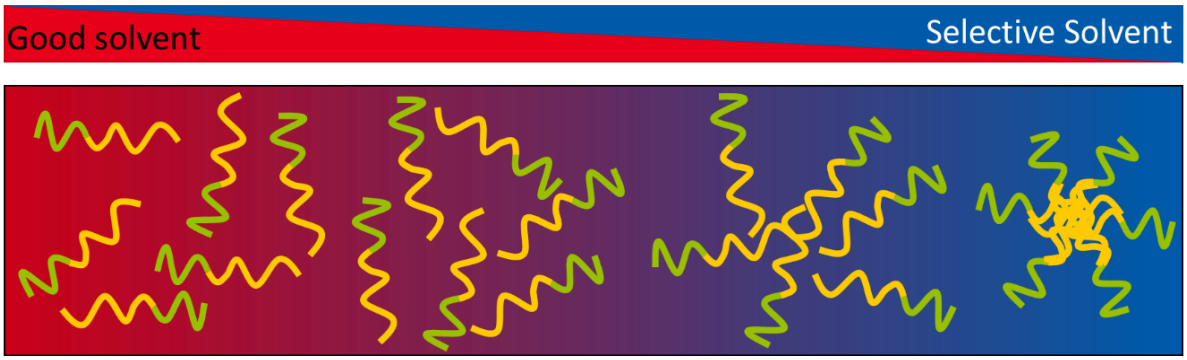

Figure 10: General strategy employed to form micelles where a selective solvent gradient is added to a solution of a block copolymer containing an insoluble segment (yellow) in a good or non-selective solvent.

For micellisation of the prepared amphiphilic block copolymers, a simple approach was adopted here. First, the block copolymer is dissolved in THF, a good solvent for both segments, before water is added until the mixture appears slightly turbid. Afterwards, a small amount of THF is added, the vial is then closed, and the solution stirred overnight to redissolve completely. During this time, the copolymers pre-organise, and since the organisation of block copolymers takes more time than the self-assembly of small molecules due to the chain length of the copolymer, this procedure is repeated until the correct amount of water is added to obtain the desired micellar concentration. As the polarity of the solution increases, the hydrophobic segment arranges to form the core of the micelle, which is then shielded from the more polar environment by the hydrophilic segment that forms the micelle corona. In the final step, the vial containing the THF/water mixture is left open under ambient conditions with vigorous stirring to allow the volatile THF to evaporate. Upon evaporation of the good solvent, the insoluble segment collapses, leading to the formation of stable aggregates in solution. These micellar systems possess interesting physico-chemical properties but are not stimuli-responsive on their own. To form stimuli-responsive micelles, a stimuli-responsive block copolymer needs to be utilised.

3.5.2 Strategies towards Stimuli-Responsive Micelles

The stimuli-responsive unit of a linear block copolymer can be located at three positions in a micelle: within the core, within the corona, or at the junction between segments, to result in different micellar

behaviour (Figure 11). Upon a certain stimulus, the corona of a micelle can collapse to expose a catalyst beneath, or the micelles disassemble close to cancer cells due to the changed local pH-value and a collapsing of the corona. Breaking the junction between the two segments releases the water-soluble segment, resulting in the precipitation of the cores, which may be applied for drug delivery. A stimuli-responsive unit located within the core can similarly lead to swelling or even disruption of the micelle to release a cargo, which is predominantly suited to drug delivery applications. The manifold of possible responses of block copolymer compartments in solution are copious and cannot possibly all be depicted here. Furthermore, reversible crosslinking of the core or corona can alter the permeability of a micelle, permitting loading and unloading of the desired cargo, as well as improving the stability of the formed assembly in various media including organic solvents.

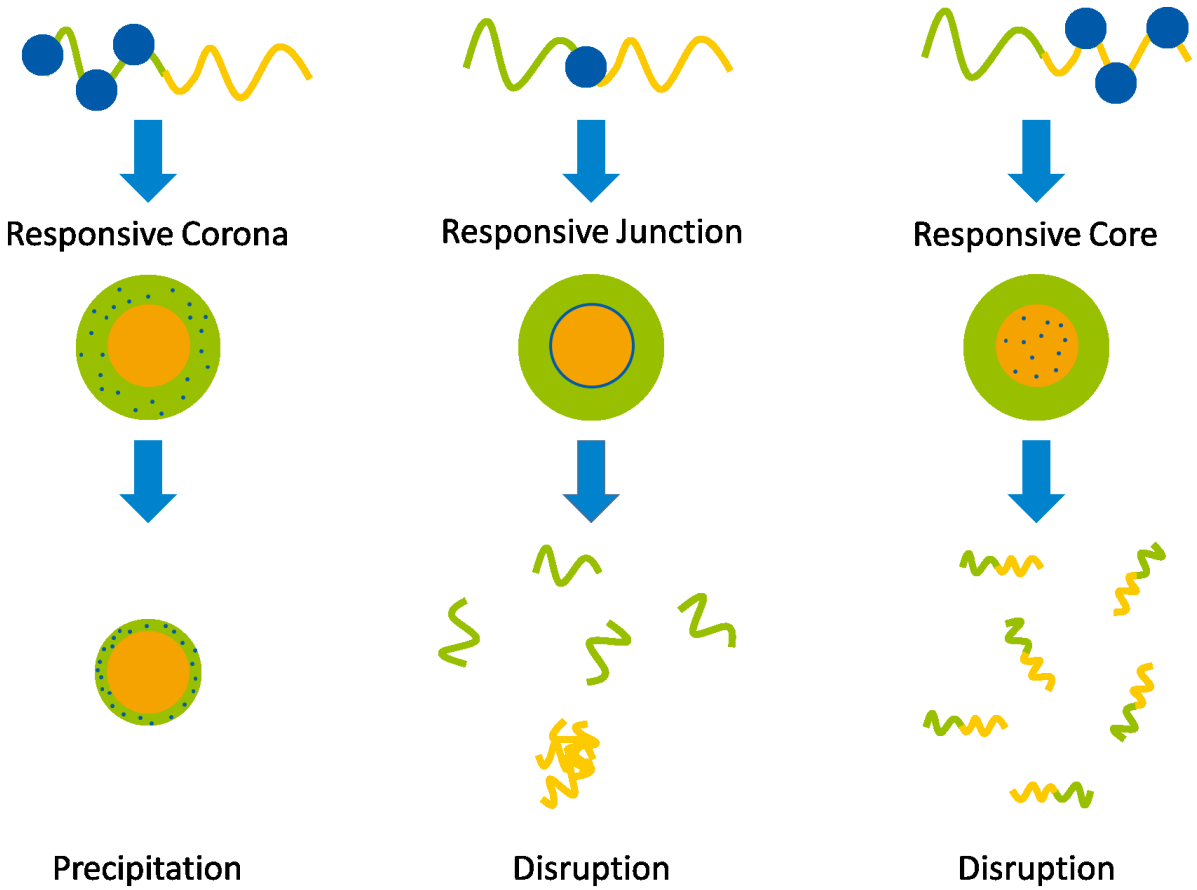

Figure 11: Schematic overview of the three possible positions of a stimuli-responsive moiety in a block copolymer micelle, and the subsequent responsive behaviour.

As mentioned above, the hydrophobic segment of a micelle collapses in a selective solvent. This makes further exchange of block copolymers from one compartment to another impossible. Such micelles are termed “frozen”.[168-169] To defreeze such micelles, the polarity of the core must be adjusted. This can be achieved, for example, by varying the solution pH. Micelles possessing such stimuli-responsive cores are attractive candidates for application in drug delivery.[170] Upon the application of a stimulus, the micelle swells or disrupts to release the cargo. Similarly to a responsive core, severing the blocks at the junction also results in the cores to precipitate, whilst the hydrophilic segment simply dissolves. In most cases reported, this disruption is achieved using light as a stimulus.[171-172] However, when the stimuli-responsive unit is present within the corona, activation generally leads to the collapse of the corona. This leads to a change in the hydrodynamic radius of the micelle, and also further destabilises the assemblies in aqueous media. The closer proximity of polymer chains within micellar assemblies

versus in solution can also affect their responsive behaviour, *e.g.*, the thermo-response of a PNIPAAm corona is broadened compared to free PNIPAAm chains.[173] Furthermore, the transition temperature also decreases with the addition of a hydrophobic comonomer, such as spiropyrans.

Research concerning responsive systems predominantly focusses on the incorporation of one stimuli-responsive moiety. Although there are several examples of block copolymers featuring both a light- and temperature-responsive segment.[1] For example, block copolymer micelles featuring a poly(*N*-isopropylacrylamide) corona and a polystyrene core have been demonstrated by various groups.[173-175] Kim and Cheong reported a light- and temperature-responsive corona in a block terpolymer for reversible polymeric vesicle formation.[176] In another case, the addition of a fluorescent end group enabled the use of such systems as a logical switch.[177] Quite recently, Jin and co-workers showed that PTEGA-*b*-PSPA block copolymers can be used to form micellar structures in different selective solvents.[137]

3.6 Self-Assembly of Block Terpolymers into Membranes

A membrane is a selective barrier between two compartments that separates objects based on size, charge or shape. The smallest objects that can be separated by a membrane are single gas molecules or salts. However, the upper size limit is not really defined, and the separation of different objects demands different membrane architectures (Figure 12).

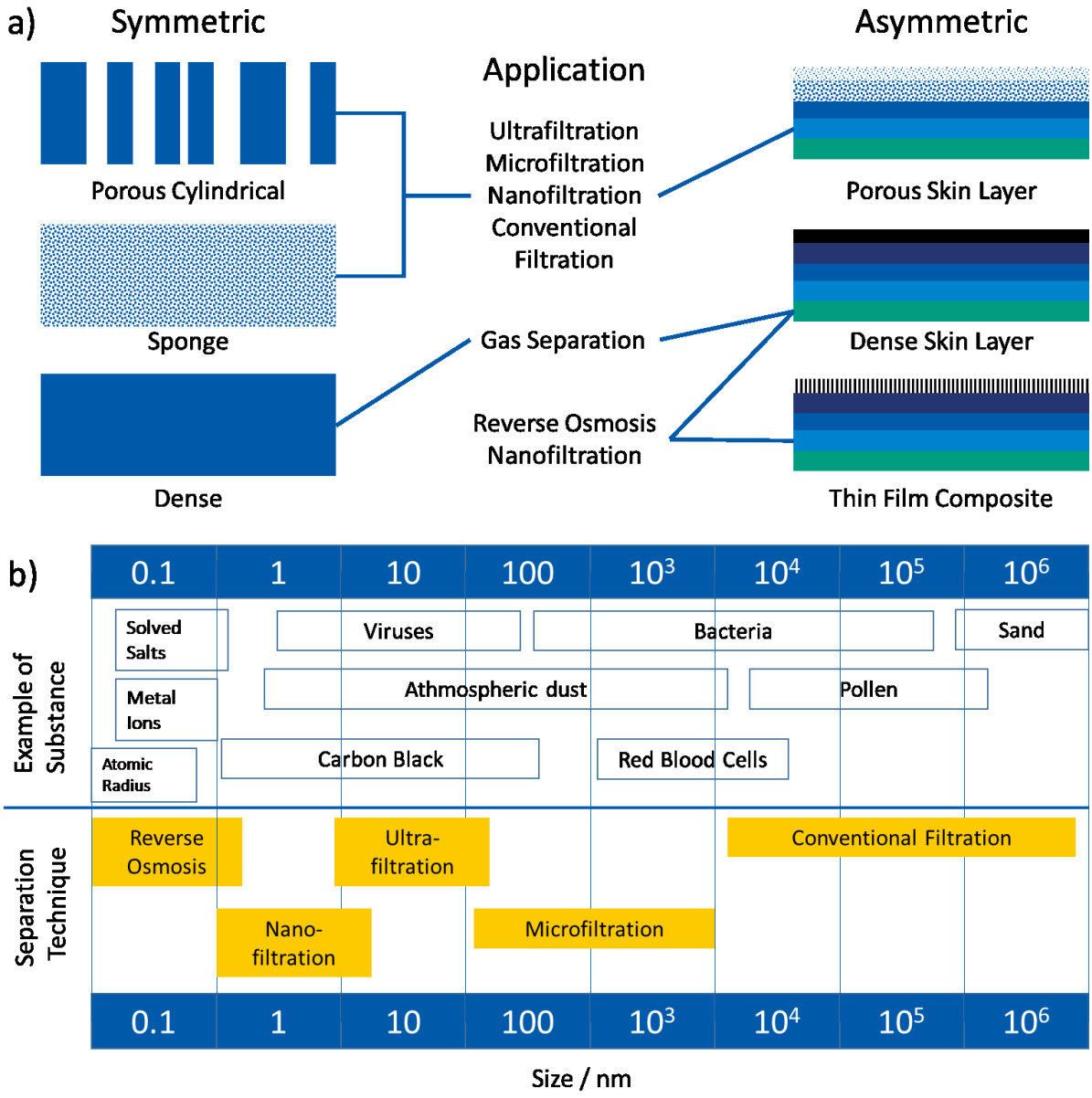

Figure 12: Overview of particle size and filtration methods: a) examples of particle sizes and appropriate filtration methods, and b) various membrane architectures used in different filtration methods.[178]

Typical objects that are separated using reverse osmosis membranes are gas molecules and metal ion salts, which require a dense filtration layer. Slightly bigger objects like carbon black or viruses are separated from solution using nano- or ultra-filtration techniques.

Upon closer inspection, two main membrane architectures can be identified: symmetric or asymmetric. Symmetric membranes are characterised by a uniform porosity or composition along the length of the membrane cross-section, whilst asymmetric membranes differ along the cross-section.

The change in pore-size along the cross-section length endows these membranes with a higher filtration performance, typically manifesting in a higher water-flux and lower clogging compared to the symmetric equivalent. In an ideal model asymmetric membrane, a particle that approaches the small pores on the top is either retained or passes through the pores. Since the pores only get bigger along the membrane, pore-clogging is suppressed. Naturally, such thin separation layers are mechanically unstable, this is why the material is stabilised through the porous volume phase.

The physical state of membrane materials can also vary from the solid-state, soft matter, and to liquids.[178] Solid-state refers to more rigid materials, *e.g.*, zeolites[179] or alumina.[180-181] At the other extreme of liquid membranes we have, *e.g.*, a water barrier between two oil compartments. Both materials have certain advantages depending on their specific field of application; however, for a broad variety of applications, soft matter is preferred. Soft matter membranes often consist of biomolecules (*e.g.*, cellulose esters),[182-183] or synthetic polymeric materials.

3.6.1 Polymer-Based Membranes

Polymeric membranes offer numerous advantages; *e.g.*, they are easy to modify and are mechanically robust.[184] Pore formation within such membranes is generally achieved in one of two possible ways: (i) *via* a top-down approach, *e.g.*, by injection moulding of polysulfones; or (ii) *via* a bottom-up approach, *e.g.*, by the self-assembly of polymers to form a pore and a surrounding polymer matrix. The self-assembly of polymers requires the use of a block copolymer with two distinct blocks. These block copolymers can then organise into different membrane architectures, which are discussed in the following section. The block copolymers can be pre-assembled into micelles, and then subsequently utilised in a thin film to form a membrane.[185] Jenekhe and Chen synthesised various poly(phenylquinoline)-*block*-polystyrene copolymers, and demonstrated their hierarchical self-assembly into coil-rod morphologies, spherical micelles, and further into column-like membranes.[186] Without any pre-organisation, a block copolymer solution can be cast into a thin film and self-assembles upon solvent evaporation leading to the formation of symmetric porous structures.[184] Polystyrene-*block*-polylactide spin-coated onto a silicon wafer from organic solvents will eventually self-assemble into a dual continuous phase. The polylactide can then be removed using aqueous NaOH to result in a sponge-like porous membrane.[187-188] In order to include stimuli-responsive moieties into such porous membranes after cleaving or dissolving one block, a new hydrophilic segment can then be attached using various chemistries, *e.g.*, a click-reaction,[155] grafting-from, or grafting-to. For filtration purposes, the thin and mechanically unstable filtration layer needs an additional layer to provide sufficient mechanical support. In order to achieve a final more mechanically robust material, the block copolymer films can be kinetically frozen during the self-assembly process by immersing the structure into a non-solvent to obtain an asymmetric porous structure.[189]

3.6.2 Integral Asymmetric Membranes from Stimuli-Responsive Block Copolymers

The asymmetric porous structures can be accessed using the self-assembly non-solvent induced phase separation (SNIPS) process.[189-190] This procedure is typically performed in aqueous media; hence, the block copolymer should consist of a hydrophilic and hydrophobic segment. The hydrophilic segment extends into the pores, whilst the hydrophobic segment forms the membrane polymer matrix. The requirements for the formation of asymmetric polymer membranes are simple and can be fulfilled by a large range of polymers. First of all, the amphiphilic block copolymers used need a molar mass above 50,000 g/mol with a hydrophilic content of approximately 25 mol%.[190] They also should be relatively

well-defined with a low dispersity in order to self-assemble.[191] However, while a low dispersity is generally considered crucial for self-assembly, recent evidence suggests it is not essential for the process. It was shown by Urbas et al.[192] that a PS homopolymer mixed with a PS-*b*-PI block copolymer still shows lamellar self-assembly in bulk. Furthermore, it was revealed by Hillmyer that polymers with a dispersity above 1.5 still exhibit self-assembly,[193] and Noro et al.[194] further showed that PS-*b*-P2VP block copolymers exhibit self-assembly with dispersities up to 1.6.[195]

The general procedure involved in the SNIPS process does not vary significantly throughout literature reports. The amphiphilic copolymer is first dissolved in a solvent mixture, cast onto a glass slide, and after a specific waiting time, the film is immersed into a non-solvent, which is in most cases water (Figure 13).

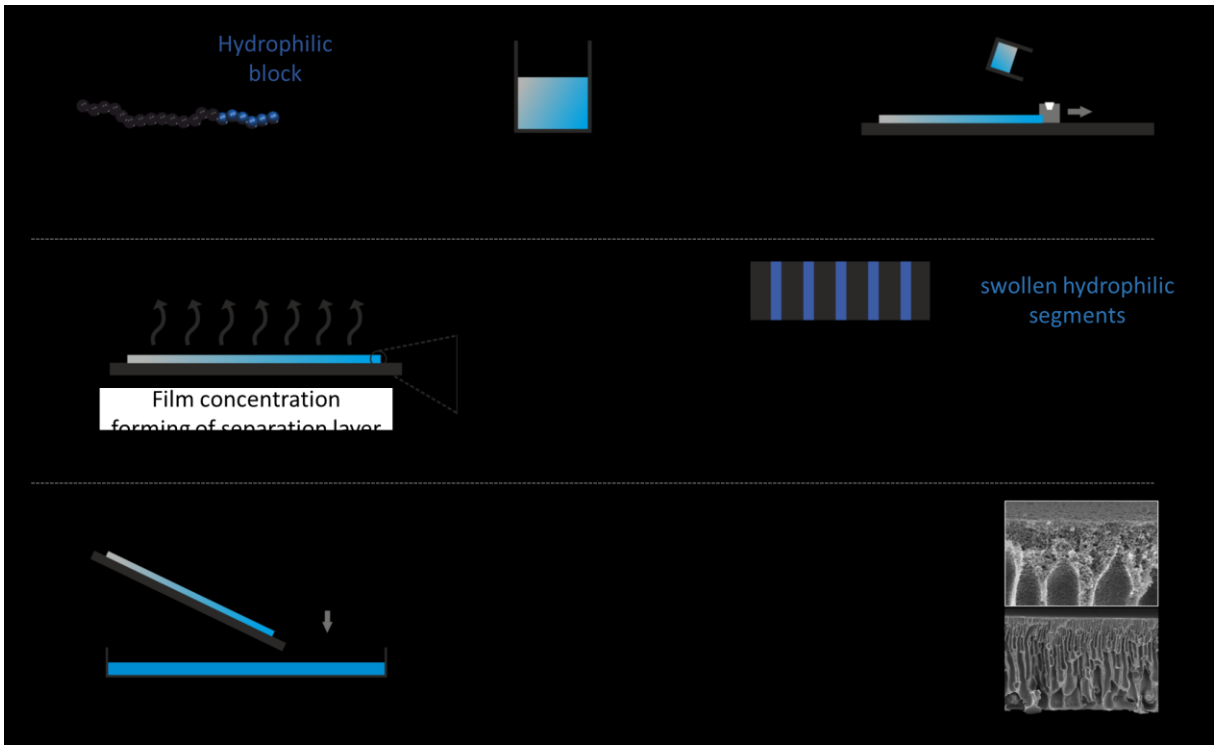

Figure 13: Schematic depiction of the SNIPS process: a) dissolution of the amphiphilic block copolymer and subsequent film-casting; b) open-time, which creates phase-separated layers; and c) immersion into a precipitation bath to create an asymmetric membrane.[196-197]

First, the block copolymer is dissolved in a solvent mixture that must fulfil the following requirements: (i) both solvents must be able to dissolve both blocks of the block copolymer at low polymer concentrations (Figure 13a); (ii) upon increasing the polymer concentration, the two solvents must preferentially dissolve one distinct block; and (iii) upon immersion into a water bath, both solvents must be miscible with water. Naturally, one of the solvents evaporates faster than the other after film-casting, and this causes microphase separation in the upper parts of the film (Figure 13b). In this upper part, self-assembly of the block copolymer occurs; due to steric hindrance, the shorter hydrophilic segments decorate the pore surface, while the hydrophobic segment forms the surrounding matrix. It is possible to form micellar structures within the pores that are later washed out during the immersion step. This causes the cavities to be larger than the path length of the hydrophilic segment. This self-assembled layer is termed the separation layer of the later formed membrane; and its thickness, as well as the thickness of the whole membrane, depends on the evaporation of the hydrophobic

solvent.[189] Below this pre-organised layer, the remaining polymer is arranged in an unorganised manner (Figure 13b).

After a certain waiting time where the block copolymers have self-assembled, the polymer film is immersed into a non-solvent for the block copolymer, and this causes the hydrophobic segment to precipitate (Figure 13c). Consequently, we immerse our glass slide into a water bath at an approximate angle of 30 °, resulting in a precipitate with a finger-like structure. In this way, a free-standing integral asymmetric membrane is obtained.

The membrane is then characterised according to its macroscopic properties such as thickness, asymmetry, pore-size, and water-flux. The impact of the processing parameters used in the membrane formation process and subsequent membrane properties has also been extensively studied using several polymer combinations.[198-200]

3.6.3 Stimuli-Responsive Membranes

The broad variety of block copolymers that can be used makes the SNIPS process very attractive for the formation of stimuli-responsive membranes. A responsive hydrophilic segment, which collapses upon a certain stimulus, offers a broad variety of possible applications from catalytically active membranes to the stimuli-responsive adjustment of pore-size for filtration systems. For the formation of amphiphilic block copolymers with a stimuli-responsive hydrophilic segment, a variety of protocols have been established in recent years. We want to use a dual stimuli-responsive hydrophilic copolymer within a block terpolymer to form asymmetric membranes. In a similar manner to micellar systems, the hydrophilic segment dissolves in aqueous media and collapses upon irradiation and/or heating (Figure 14). Ideally, the hydrophilic segment fills the cavities, whilst the water-insoluble block forms the matrix. The pore, in the context of asymmetric polymeric membranes, consists of the opening seen from the top, but also the cavities inside the membrane. This means that the pore-size of an asymmetric membrane varies over the cross-section of the membrane.

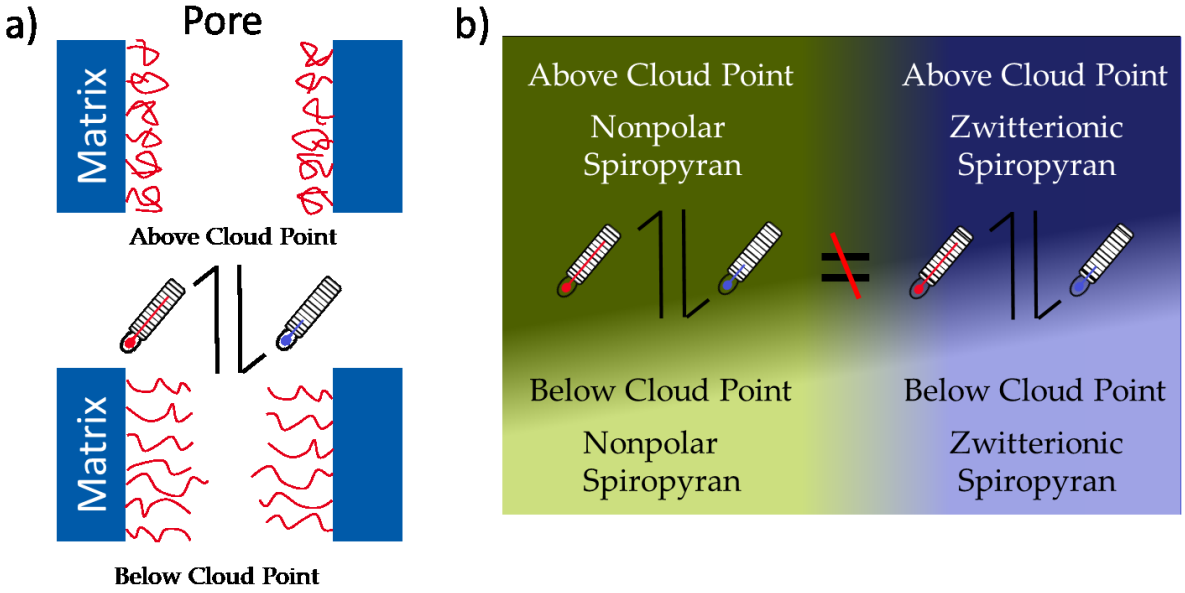

Figure 14: Expected behaviour of membranes formed from an amphiphilic block terpolymer with a photo- and thermo-responsive hydrophilic segment: a) collapse of the hydrophilic segment in the pores upon heating; b) different switching states of the hydrophilic segment consisting of a spiro- and a thermo-responsive moiety.

The collapse of the hydrophilic segment within the pore results in the formation of a bigger cavity, and therefore a higher water-flux is expected.[201-202] Since the hydrophilic segment consists of a thermo-responsive moiety and a photo-responsive spiropyran compound, four different states are possible. The spiropyran moiety can be switched upon irradiation from the spiropyran-form to the merocyanine-form; and during both irradiation states, heating leads to the hydrophilic segment collapsing, but at different temperatures. For temperatures between these two extremes the collapse of the hydrophilic segment can be triggered by a change in irradiation wavelength.

4 Motivation for the Investigation of Dual Photo- and Thermo-Responsive Polymers

We introduced various responsive moieties that have been used to prepare light- or temperature-responsive polymers in the previous chapter. The application of both stimuli in the pores of a polymeric membrane, for example, can endow these materials with various and tuneable properties where multiple applications can be envisioned. Of particular interest, and which has not yet been addressed in the literature, is the ability to adjust the pore-size and/or surface properties of a membrane in filtration processes through the application of orthogonal stimuli. For instance, the same membrane could be used to separate different proteins based on size and properties.

The formation of polymeric membranes is a complex process, with many variables affecting the pore-size obtained. This challenge could indeed be circumvented if the pore-size of the membrane can be tuned post-fabrication. As discussed in the introduction, only a few examples of stimuli-responsive membranes with a tuneable pore-size have been reported so far.[201] The main benefit of light as an external stimulus over pH or temperature is that light does not require physical contact with the membrane and can be applied with high local resolution. Although conformational changes of a photo-responsive polymer upon irradiation may not be enough to cause remarkable changes in pore-size, the coil-to-globule transition of thermo-responsive polymers could induce a very large change in pore-size. As such, the combination of both stimuli (light and temperature) into one material is a promising strategy to form porous membranes that can be highly tuned depending on the desired application.

The combination of two stimuli naturally leads to rather complex behaviour, and this has yet to be comprehensively studied in the literature. However, by restricting the dual-responsive behaviour to the hydrophilic segment localised within the pore of the membrane, we can restrict the possible behaviour, and can further study the dual-responsive behaviour using analogous copolymers in solution. The schematic responsive behaviour of the respective dual responsive copolymer upon stimulation of one stimulus alone and the resulting behaviour if combined in one material is depicted in Figure 15.

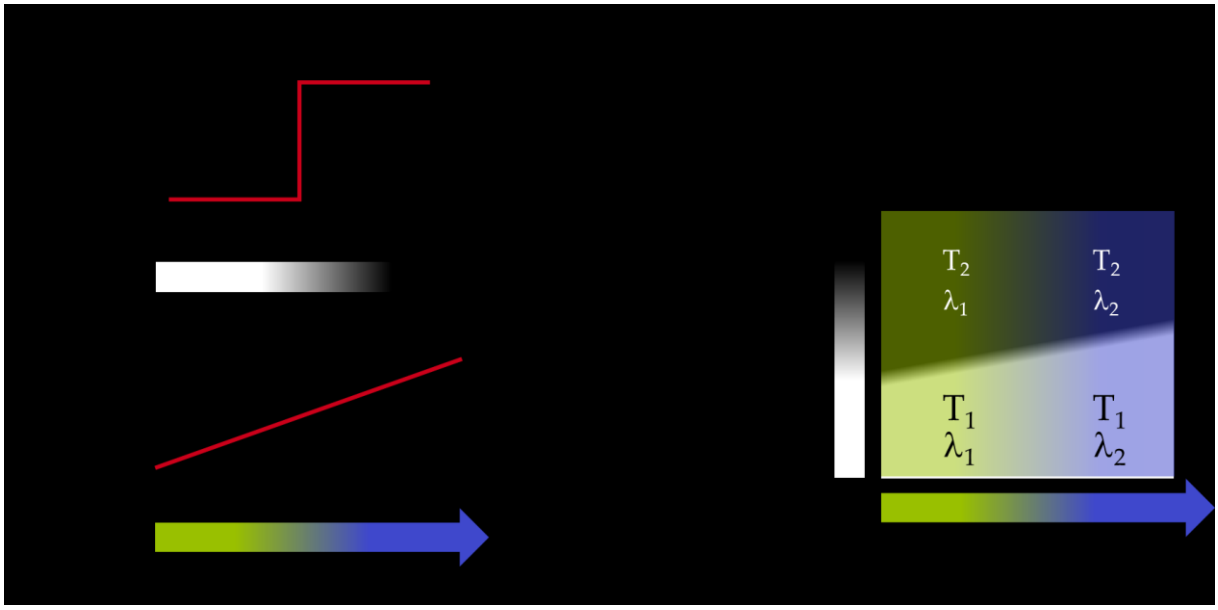

Figure 15: Schematic depiction of the combination of a spontaneously changing thermo-responsive polymer and a continuously changing photo-responsive polymer to give a dual-responsive material with four defined states.

The dual responsive copolymer can be investigated for their response towards each stimulus separately, and also the combination of both simultaneously. The thermo-response of, for example, a PNIPAAm segment-containing copolymer occurs at one distinct temperature, which results in a spontaneous change from soluble to insoluble. On the other hand, a spiropyran-containing copolymer can change their polarity continuously from unipolar to zwitterionic upon irradiation. This change in polarity will ultimately alter the thermo-response of the copolymer, and the aim of this work is to find the limits of this dual-responsive behaviour. We will determine the coil-to-globule transition temperatures of dual-responsive copolymers in both irradiation states; that is, when the spiropyran is solely in the non-polar or zwitterionic state. The transition temperature of the thermo-responsive moiety should be tuneable between these two limits by irradiation, which results in a copolymer that collapses upon irradiation when at an intermediate temperature between the two extremes.

A broad variety of photo-responsive spiropyrans have been reported and used in single-molecule experiments.[131] Many of them can be modified with polymerisable groups to permit the formation of dual-responsive copolymers. As mentioned in the introduction, some of these spiropyran moieties have been incorporated into photo- and thermo-responsive copolymers. Sadly, most of these reports rely on one single copolymer composition to exhibit such dual-responsive behaviour. In order to gain a deeper understanding of the conditions required for this dual-responsive behaviour to manifest, a set of photo- and thermo-responsive copolymers are synthesised within this work and their dual-responsive behaviour intensively investigated.

Upon the self-assembly of these block terpolymers into membranes, the dual-responsive moieties are brought in closer proximity than in the dissolved copolymers. This close proximity can affect the change in polarity originating from the photo-responsive behaviour of the spiropyran moieties in the hydrophilic segment. A well-suitable model for the investigation of spiropyrans in close proximity are micellar compartments, containing the dual-responsive copolymer moiety in the hydrophilic corona. Comparable block terpolymers can then further be used for the formation of dual-responsive polymeric membranes.

The thermo-response of such materials can be tuned between two distinct temperatures by applying light as an external stimulus. While the coil-to-globule transition can be triggered by light irradiation if a temperature between these two extremes is chosen. In this way, the void within a membrane can be tuned by irradiation at a specific temperature, and the water-flux through the membrane adjusted. Such a membrane does not currently exist and is highly attractive due to ease and local control afforded by light as an external trigger.

We will begin by synthesising dual photo- and thermo-responsive copolymers with different compositions of both moieties to systematically investigate their dual-responsive behaviour (chapter 5). We will then synthesise amphiphilic block terpolymers with comparable hydrophilic compositions to form micelles, and compare their behaviour to the dissolved copolymers in the first section (chapter 6). In the final part of this thesis, the optimal conditions to form membranes from amphiphilic block terpolymers will be investigated, and the suitability of these dual-responsive block copolymers to form tuneable water-flux membranes will be investigated (chapter 7). We will show that it is indeed possible to form a dual-responsive membrane, and further investigated its photo- and thermo-responsive behaviour.

5 Thermo- and Light-Responsive Copolymers

Parts of this chapter have been published:

Grimm, O.; Schacher, F., Dual Stimuli-Responsive P(NIPAAm-*co*-SPA) Copolymers: Synthesis and Response in Solution and in Films. *Polymers* **2018,** *10* (6), 645-661.[203]

Grimm, O.; Maßmann, S. C.; Schacher, F. H., Synthesis and solution behaviour of dual light- and temperature-responsive poly(triethylene glycol-*co*-spiropyran) copolymers and block copolymers. *Polymer Chemistry* **2019,** *10* (21), 2674-2685.[204]

In this chapter, water-soluble dual-responsive materials are synthesised, and their physico-chemical behaviour in aqueous systems investigated. Their dual-response to light and temperature is a convenient combination because the stimuli and resulting response of the material can be measured independently from each other. The combination of two stimuli-responsive moieties within one material is easily accessed by combining two monomers together in one copolymer chain. One monomer is photo-responsive and the other one forms a thermo-responsive polymer, considering that both moieties combined in one material can exist in two states each, the copolymer can react to either light or temperature, resulting in the existence of four distinct states that are depicted in Figure 16.

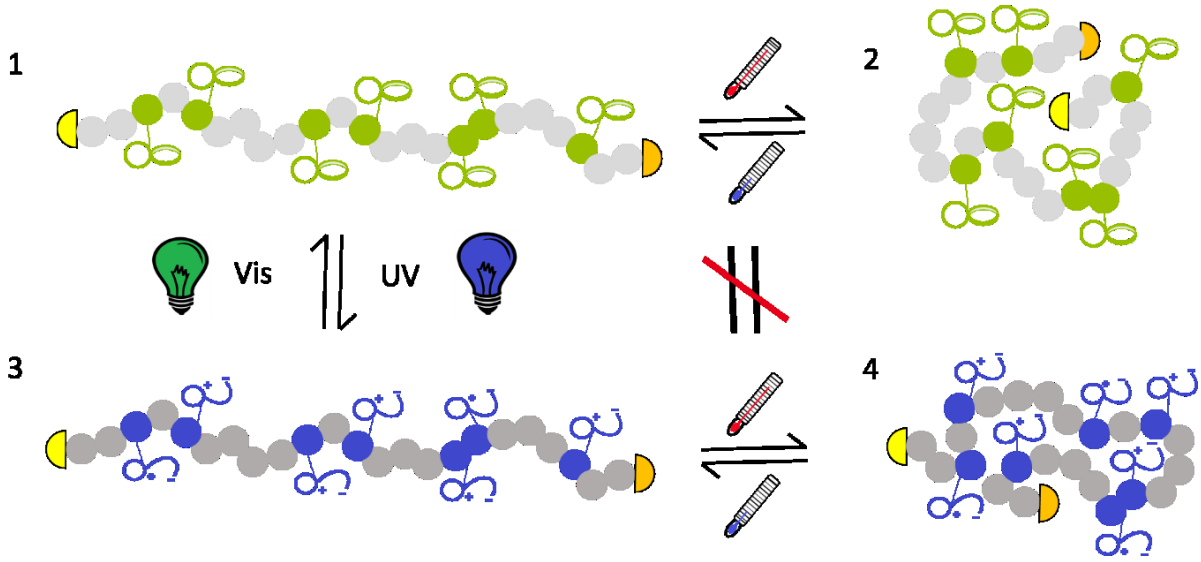

Figure 16: Schematic behaviour of a dual-responsive copolymer with a thermo-responsive moiety (grey) and a photo-responsive moiety (green or blue).

Both stimuli, temperature and light, can be applied independently from each other; and the copolymer response to each stimulus can be measured independently. Upon irradiation, the copolymer switches from a less polar to a more polar form (1 to 3), and upon heating both states (1 and 3), the polymers precipitate. Naturally, the non-polar form precipitates at lower temperatures (1 to 2) than the more polar form (3 to 4). As described previously in the introduction, the copolymer consists of a thermo- and a photo-responsive moiety. Two different thermo-responsive moieties will be introduced and investigated: *N*-isopropylacrylamide (NIPAAm) and monomethyl-triethylenglycolacrylate (TEGA). The copolymer further consists of a photo-responsive moiety; the potential structures of which will be introduced at the beginning of this chapter. A large variety of spiropyrans have been synthesised with varying substitution patterns;[32, 205-206] from those reported, we synthesised several candidates and tested their photo-response.

The focus of this chapter is the investigation of the copolymerisation of a photo-responsive spiropyran with thermo-responsive NIPAAm or TEGA units. Free radical copolymerisation was first applied to indicate the general ability of the monomers to form a copolymer in both combinations. Controlled radical polymerisation was then utilised to permit the preparation of block terpolymers, which is presented in later chapters. Therefore, a unimolecular initiator for nitroxide-mediated polymerisation (NMP) was mixed with the two stimuli-responsive monomers in order to optimise the reaction conditions and to permit block extension with polystyrene and polyisoprene. Utilising these optimal conditions, two sets of copolymers were prepared, and their stimuli-response investigated in detail. Since some literature indicates that the photo-response of spiropyran molecules is pH-dependent, this needs to be investigated thoroughly.[32] Therefore, preliminary investigations to determine the optimal pH-value of the aqueous solution were performed, and these conditions used to determine the photo-response in aqueous solution for both sets of copolymers. Afterwards, the thermo-response upon irradiation was measured to assess how the transition temperatures of the copolymers varied due to irradiation. The effects are then compared between the two sets of dual-responsive copolymers.

5.1 Synthesis of Responsive Monomers

The formation of copolymers *via* a chain-growth polymerisation requires a polymerisable group, which is a substituted double bond in most cases. Acrylates are particularly well suited for nitroxide-mediated polymerisation, and stimuli-responsive acrylate-based monomers for the formation of dual-responsive copolymers have already been described comprehensively in the literature.[25] From the thermo-responsive monomers investigated here, NIPAAm is commercially available, and the synthesis of TEGA is briefly described in the following section.

The synthesis of the photo-responsive moiety used in this study is well-documented and described in detail in literature reports.[123] A broad variety of spiropyran monomers are used to endow polymers with a photo-response. Hence, three example monomers were synthesised, and their photo-response tested in isopropanol and acetonitrile.

5.1.1 Synthesis of Thermo-Responsive Monomers

For the synthesis of the thermo-responsive monomer, monomethyl triethylene glycol was dissolved in dichloromethane and mixed with triethylamine. Acryloyl chloride dissolved in dichloromethane was then added dropwise to the -20 °C solution. The crude product was purified by column chromatography in tetrahydrofuran (Figure 17). The purified monomer was obtained as a colourless oil, which was then stored in the refrigerator until required.

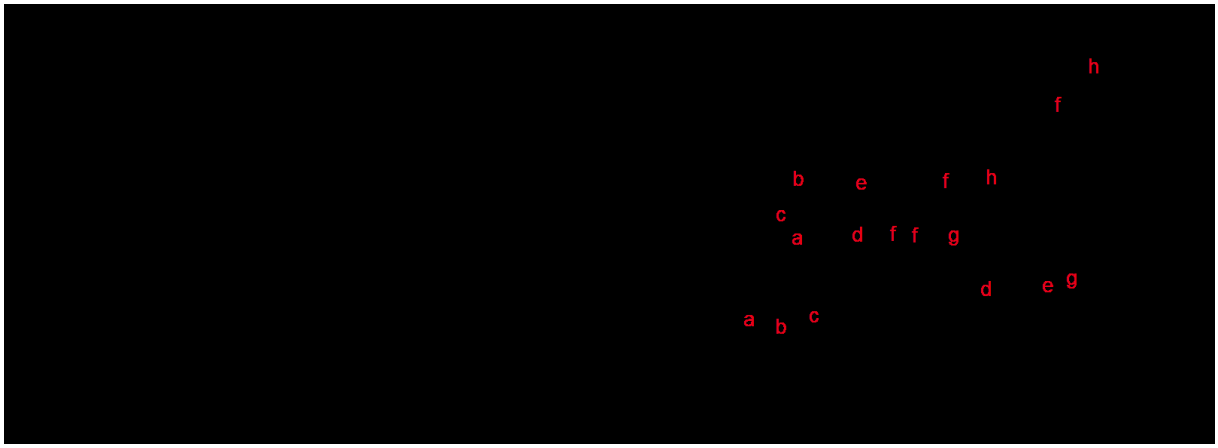

Figure 17: a) Scheme showing the synthesis of TEGA and the corresponding b) ^{1}H-NMR spectra of the purified product in $CDCl_3$.

5.1.2 Synthesis of the Photo-Responsive Monomers

From the numerous examples of photo-responsive spiropyran molecules previously reported, we have a whole host of photo-responsive moieties available to us that have or that can be incorporated within polymers, and most of the combinations have also been used in aqueous systems. The spiropyran moiety, in particular, is expected to exhibit a large change in polarity upon photo-switching based on previous reports.[206] In most cases, the photo-responsive spiropyran molecule is linked covalently to a polymerisable unit. Three different spiropyran-based monomers were selected and synthesised to test their behaviour upon irradiation. The three monomers all possess a benzo-spiropyran moiety as the photo-responsive group, and an acrylate as the polymerisable group, only varying in the position and length of the linker. The structures and assigned abbreviations are given in Figure 18.

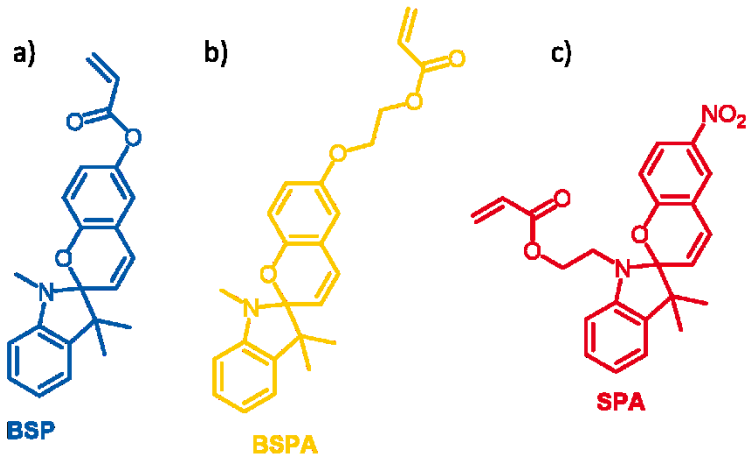

Figure 18: Structures of the three synthesised spiropyran monomers: a) benzo-spiropyran acrylate (BSP), b) BSPA, and c) nitro-benzo-spiropyran acrylate (SPA).

For the 2-((3′,3′-dimethylspiro[chromene-2,2′-indolin]-6-yl)oxy) acrylate (BSP, Figure 18a), the "smallest" monomer, the benzo-spiropyran is directly linked to the acrylate group. The spiropyran acrylates with a linker can either be attached to the oxygen in the para position as in 2-((3′,3′-dimethylspiro[chromene-2,2′-indolin]-6-yl)oxy) ethylacrylate (BSPA, Figure 18b), or at the nitrogen at the para-position as in 2-(3′,3′-dimethyl-6-nitrospiro[chromene-2,2′-indolin]-1′-yl)ethyl acrylate (SPA, Figure 18c). As mentioned previously, the substitution pattern is crucial for the observed photo-response of the molecule. In particular, the bond between the oxygen and quaternary carbon must be relatively weak for good switching behaviour. This is depicted in a simplified way in Figure 22, and in more detail in Scheme 3. We expect that the BSPA (Figure 18b) presents the strongest C-O bond due to its substitution pattern, followed by a slightly weaker bond in BSP (Figure 18a). The best photo-switching results are expected for SPA (Figure 18c), which has an electron-withdrawing nitroxide group at the para-position with a flexible C_2-spacer.

5.1.2.1 Synthesis of Various Spiropyran-Containing Monomers

In this section, the detailed synthesis of the three spiropyran-based monomers is discussed. The benzo-spiropyran with a hydroxyl end group is commercially available. This was combined with acryloyl chloride under water-free conditions to obtain the monomer BSP through nucleophilic addition (Figure 19).

The crude product was purified by column chromatography (silica gel 60; ethyl acetate:*n*-hexane = 2:1 v/v). Interestingly, the column was coloured intensely red, but the product-containing solute and the product itself is colourless. ^{1}H-NMR spectroscopy indeed confirmed that the desired product was obtained. This indicates the typical solvatochromic behaviour of spiro compounds is present in the monomer BSP. When eluting through the column, the BSP is in close proximity to silica OH-groups; this polar environment leads to the observed intense red colour since the solvatochromic behaviour is environment-dependent.[126]

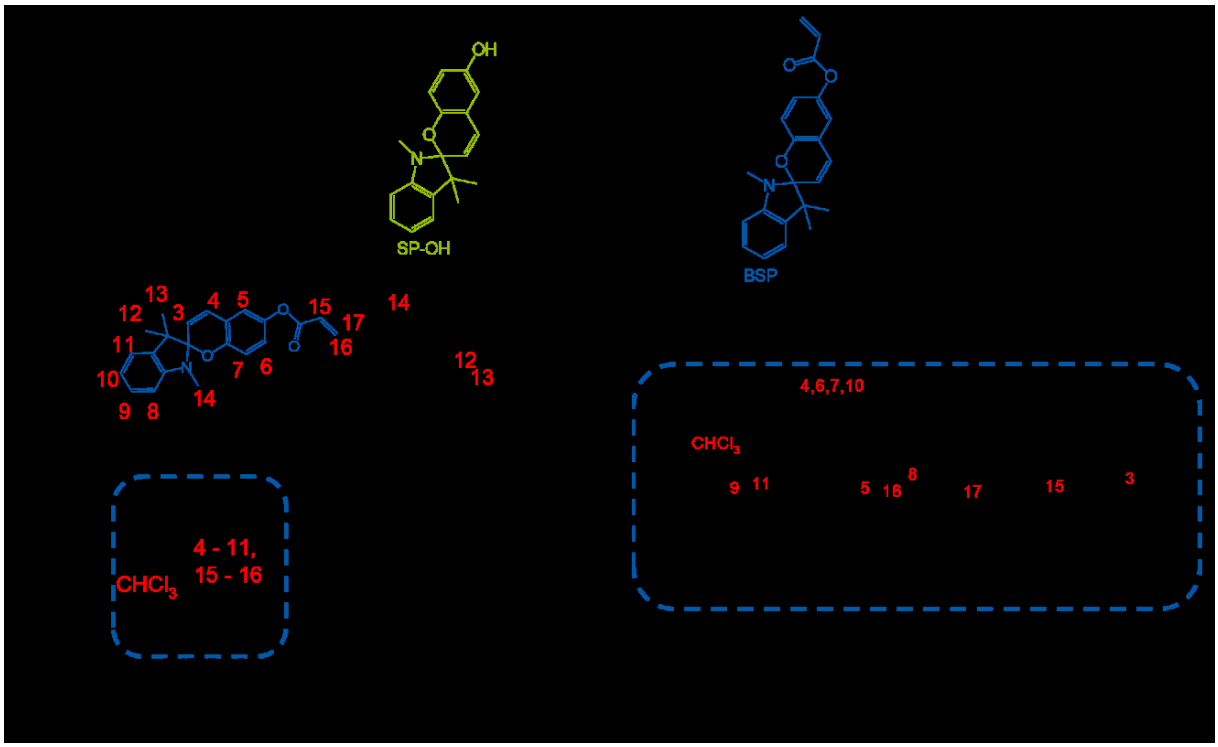

Figure 19: a) Scheme showing the synthesis of BSP, b) ^{1}H-NMR spectra of BPS in $CDCl_3$, and c) detailed ^{1}H-NMR spectra of the aromatic region for BSP.

We then synthesised BSPA, a monomeric spiropyran with a C_2-linker from the oxygen in the para position (Figure 18b). The C_2-linker was first introduced onto acryloyl chloride before being attached to the spiro moiety (see Figure 20a).

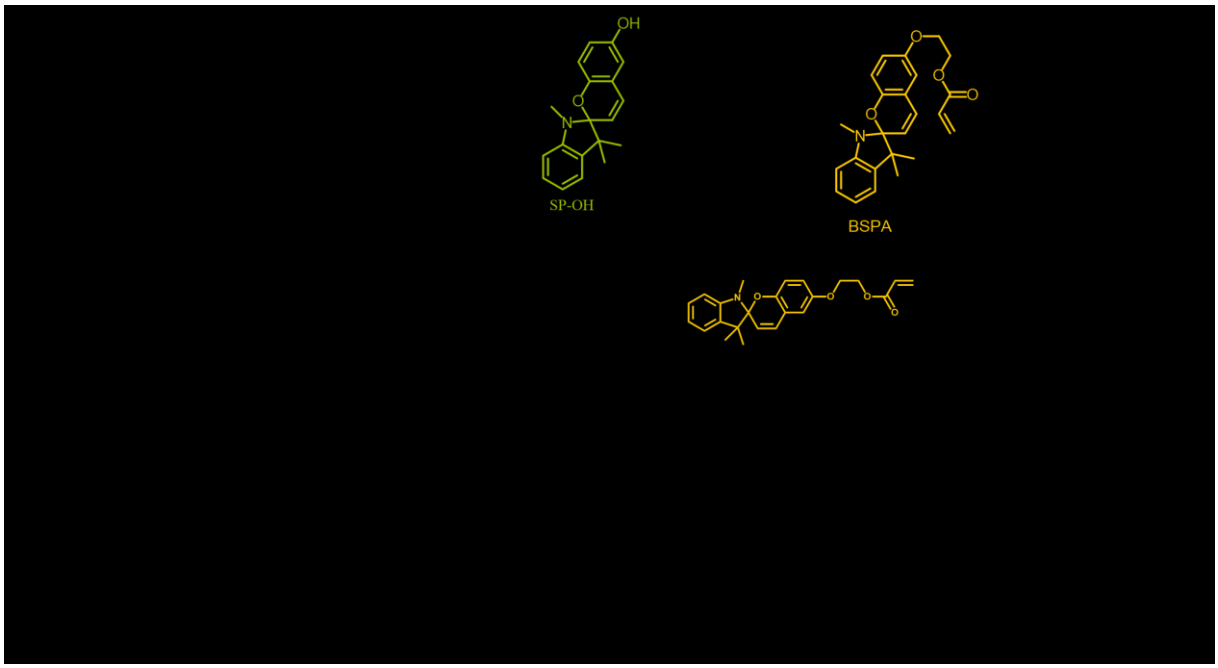

Figure 20: a) Scheme showing the synthesis of BSPA, b) ^{1}H-NMR spectra in $CDCl_3$ of the precursor 2-bromoethylacrylate, and c) ^{1}H-NMR spectra of crude BSPA in $CDCl_3$.

The successful attachment of the spacer was confirmed by ^{1}H-NMR spectroscopy, with the appearance of two additional signals observable in Figure 20c labelled d and e. In addition, the signals associated with the spiropyran moiety are comparable with BSP. In this case, a clear colour change of the

monomer BSPA was visible during purification by column chromatography and after the removal of solvent.

To access SPA (Figure 18c) required more synthetic effort compared to the previous monomers. The reaction pathway is outlined in Scheme 2. 9,9,9a-Trimethyl-2,3,9,9a-tetrahydrooxazolo[3,2-a]indole (compound 1) was obtained as a yellow oil without any intermediate purification steps. After refluxing in ethanol with 3-nitrosalicylic acid for 3 h, SP-NO_2 was obtained as purple crystals after cooling in the refrigerator overnight. The crystals were collected by filtration, and then under dry conditions acylated using acryloyl chloride to obtain the monomer SPA. The crude product was purified by column chromatography (silica gel 60; chloroform). The synthesised monomeric spiropyrans were characterised *via* ^{1}H-NMR.

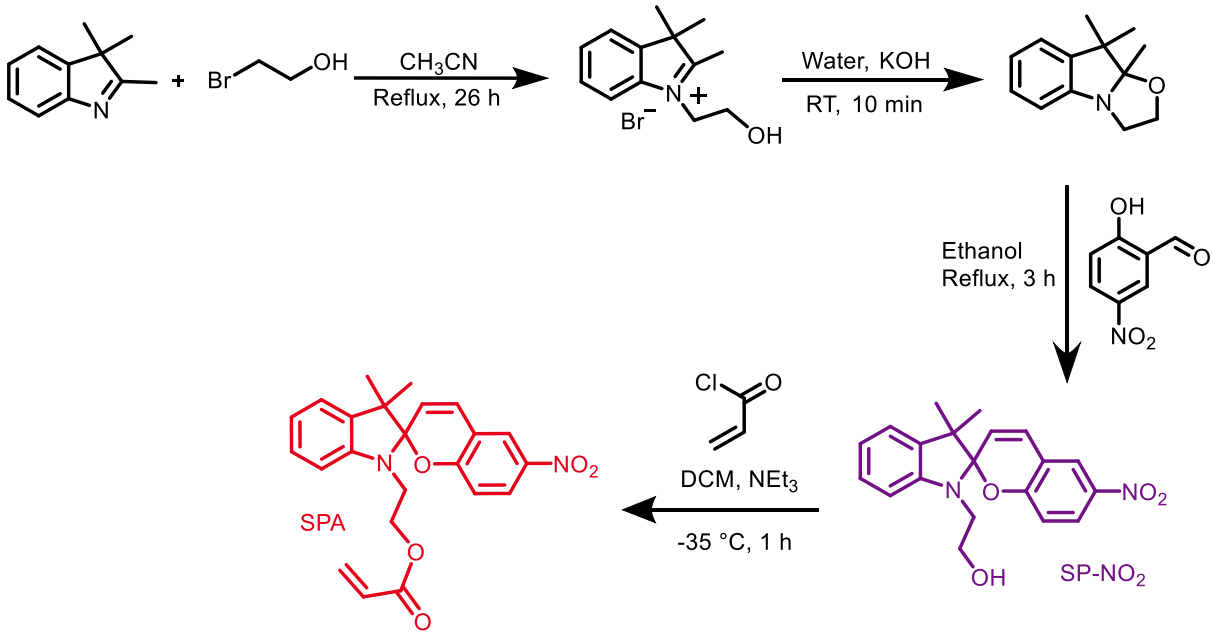

Scheme 2: Scheme showing the synthesis of SPA.

The first two reaction steps in Scheme 2 were performed without isolating the intermediate. All other products were purified and characterised *via* ^{1}H-NMR before subsequent use. The results are given in Figure 21.

From ^{1}H-NMR spectroscopy (Figure 21), the products were all relatively pure with no significant side products observed. On comparing the proton signals of Figure 21b and Figure 21c, some differences are apparent: the most obvious being the additional signals associated with the acrylate group (Figure 21c, proton d, f and g), but also the linker protons b and c change. Comparing the spectra of the monomer to the previous monomers: the aromatic protons of the spiropyran group are shifted to higher chemical shifts; proton 3 of BSPA in Figure 19 is shifted from 5.7 ppm to 6.1 ppm for SPA (Figure 21c, proton e). The protons adjacent to the nitro-group (Figure 21c, proton m and n) are also shifted to above 8 ppm from 6.7 ppm (Figure 19, protons 5 and 6). All protons of the acrylate are shifted compared to the other spiropyran-based monomers.

The SPA monomer was purified *via* column chromatography in chloroform; during this work-up, almost all colours of the rainbow appeared. The product appeared red on the silica column but eluted green. This green colour then intensified upon solvent removal to a dark blue oil, which further solidifies overnight to a yellowish solid. The collected product was then stored in the dark.

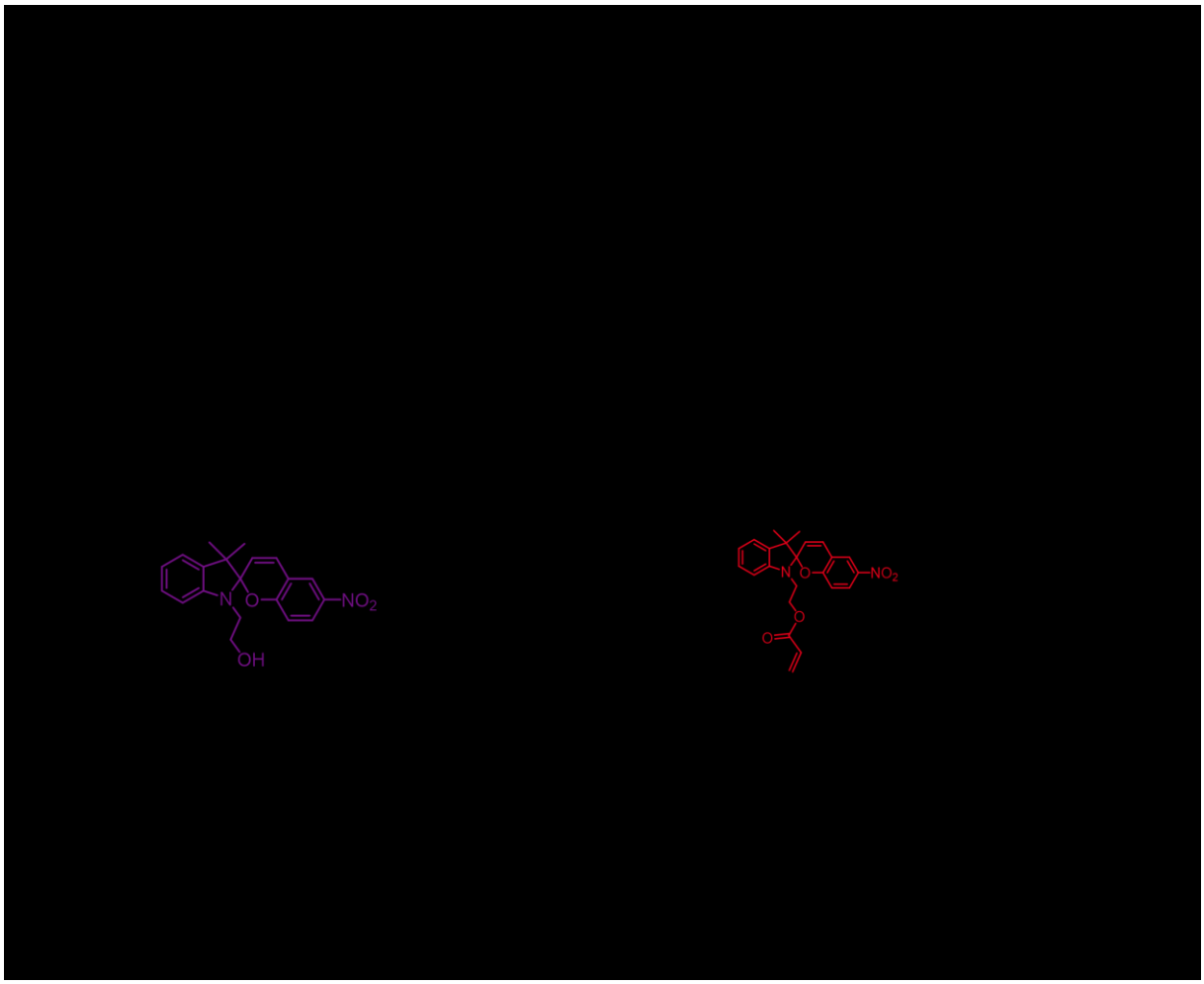

Figure 21: ^{1}H-NMR spectra of the separated intermediates and product SPA. Spectra a was measured in $CDCl_3$; spectra b and c were measured in DMSO-d_6.

The photo-responsive behaviour of the three synthesised spiropyran monomers was investigated. In the following sections, we will explore how the substitution pattern of the monomers influence the behaviour upon light exposure using absorption spectroscopy.

5.1.2.2 Photo-Response of the Spiropyran-Containing Monomers

The photo-response of the three synthesised monomers was then investigated. The switching behaviour of spiropyrans is complex, in general, and has been exhaustively studied for various spiropyran derivatives.[93, 206] The previously synthesised monomers can be switched upon irradiation with UV light from the closed spiropyran- to the open merocyanine-form. Depending on the pH-value, both forms can be protonated; in addition, the open form can also undergo hydrolysis at high pH-values.[32] This behaviour, specifically for the SPA monomer, is depicted in Scheme 3.

This highly complex behaviour makes the investigation of the benzo-spiropyran molecule in aqueous media challenging. In preliminary investigations, the photo-response of each photo-responsive functional unit was explored in the absence of the polymerisable group, and the system was further simplified by probing their response in an organic solvent. Since the molecule switches from non-polar to zwitterionic, a solvent must be chosen that stabilises both forms. Isopropanol is a polar protic solvent with a dipole moment of 5.54×10^{-30} C*m. This is not as high as water, which has a dipole moment of 6.07×10^{-30} C*m, but is in a comparable range. Whilst the dipole moment of a solvent alone

cannot predict whether a molecule will dissolve in it, it is a good indicator. The effect of protonation in isopropanol of the spiropyran can be neglected; however, protonation must be considered in the aqueous-based systems explored later. A further advantage of isopropanol is the low UV cut-off wavelength of 210 nm. This low cut-off wavelength makes isopropanol an ideal solvent for use in irradiation experiments.

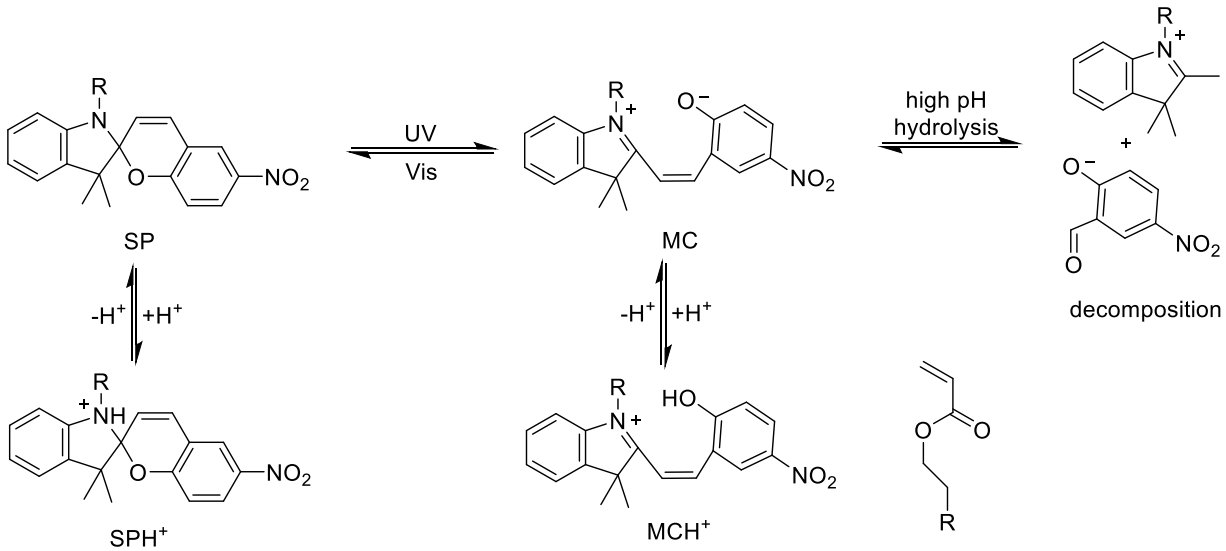

Scheme 3: Expected switching behaviour of the SPA monomer upon irradiation at different pH-values.[207]

From the three synthesised spiro derivatives, two substituents were explored at the para position (a hydroxyl- and a nitro-group). Both SP-OH and SP-NO_2 were dissolved in isopropanol and both solutions were irradiated at 365 nm for 30 min before being irradiated at 525 nm for 30 min, and this cycle was repeated three times. The switching behaviour between the SP and MC is indicated by a change in the absorption spectra (Figure 22).

Both molecules, SP-OH and SP-NO_2, exhibit a reversible photo-switching upon irradiation at 365 nm or 525 nm. The conformational changes expected for both molecules is depicted on the right-hand side of Figure 22. The MC-form exhibits an absorption maximum at approximately 550 nm; whilst the absorption maximum of the SP-form lies within the UV region and is not shown in the current spectra.

Upon irradiation at 365 nm, the absorption at 550 nm is observed to increase; and following subsequent irradiation at 525 nm, the absorption at 550 nm decreases again irrespective of the spiropyran para substituent. Furthermore, this process is reversible for both molecules over at least three irradiation cycles. No significant change in the absorption spectra was observed throughout the three irradiation cycles, which means we can exclude decomposition during the experiment. The main difference between the two spiropyran derivatives is the relative change in intensity upon irradiation; the SP-OH molecule exhibits a small change in absorbance of approximately 0.008 a.u., whilst the SP-NO_2 molecule experiences a change in absorbance of 0.6 a.u.

Since the SP-NO_2 experiences a greater change in absorbance upon irradiation, we expect this photo-responsive unit to show a higher response when incorporated within polymeric materials. As mentioned previously, the addition of the polymerisable group may influence the photo-responsive behaviour. Therefore, the monomeric forms of SP-NO_2 and SP-OH, denoted BSP and SPA, were tested in a similar manner to determine whether the photo-switching behaviour varies. The monomers were dissolved in isopropanol and irradiated for 30 min each with 365 and 525 nm, and repeated for several

cycles. The solvatochromic behaviour that was observed during the synthesis and work-up reveals that the solvent used may affect the overall switching behaviour. Hence, in addition to isopropanol, acetonitrile was also tested as an alternative polar aprotic solvent, which also displays a low UV cut-off wavelength, and a higher dipole moment than isopropanol of 11.48 × 10^{-30} C*m.

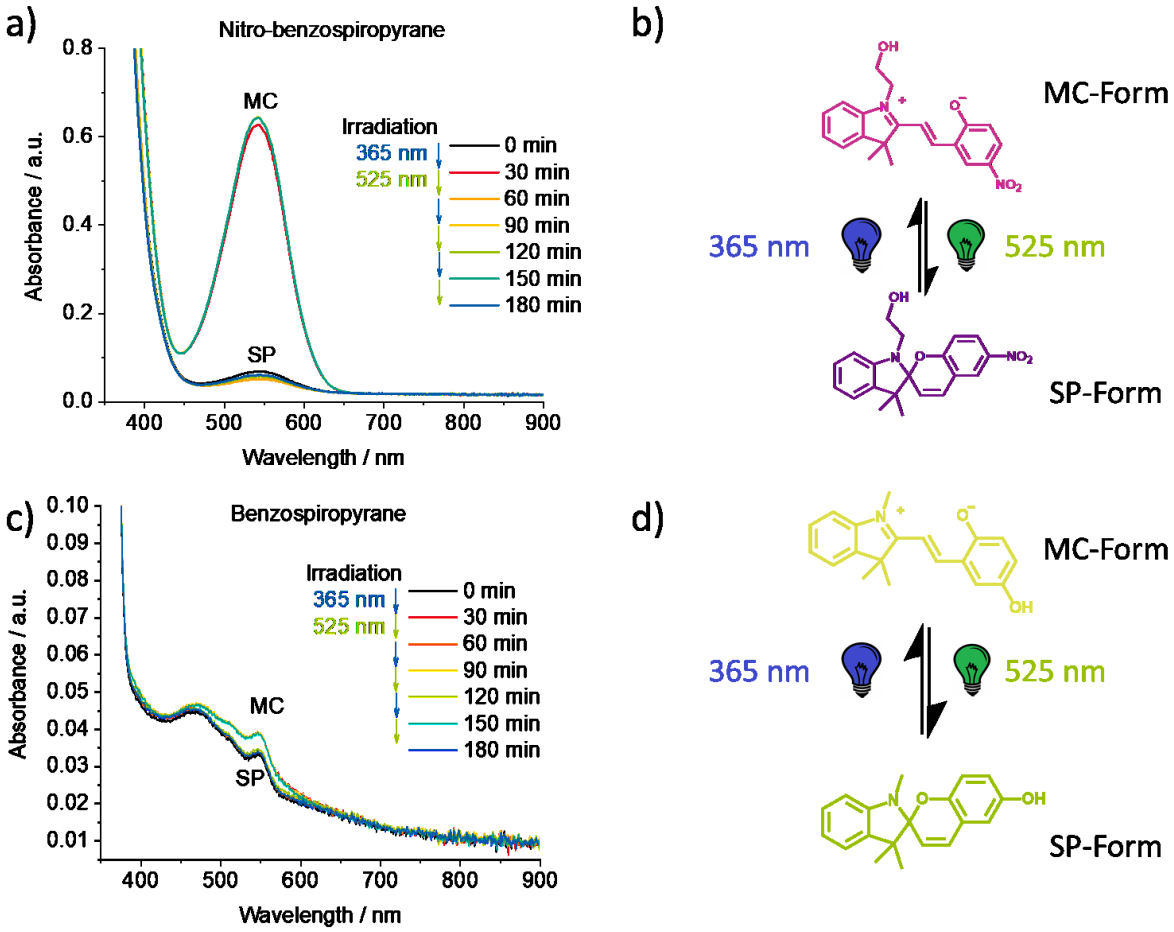

Figure 22: Absorbance spectra showing the photo-response of a) SP-NO_2 and c) SP-OH after irradiation at 365 nm for 30 min and 525 nm for 30 min over three cycles. The expected conformational changes upon irradiation for b) SP-NO_2 and d) SP-OH.

For simplicity, the change in intensity of the maximum absorbance for each molecule is plotted over time. The wavelength maximum differs for each molecule and is given in parentheses after the molecule name. A spectrum was recorded every 30 s to monitor the switching behaviour over the course of the irradiation cycles. The behaviour in both isopropanol and acetonitrile are shown in Figure 23.

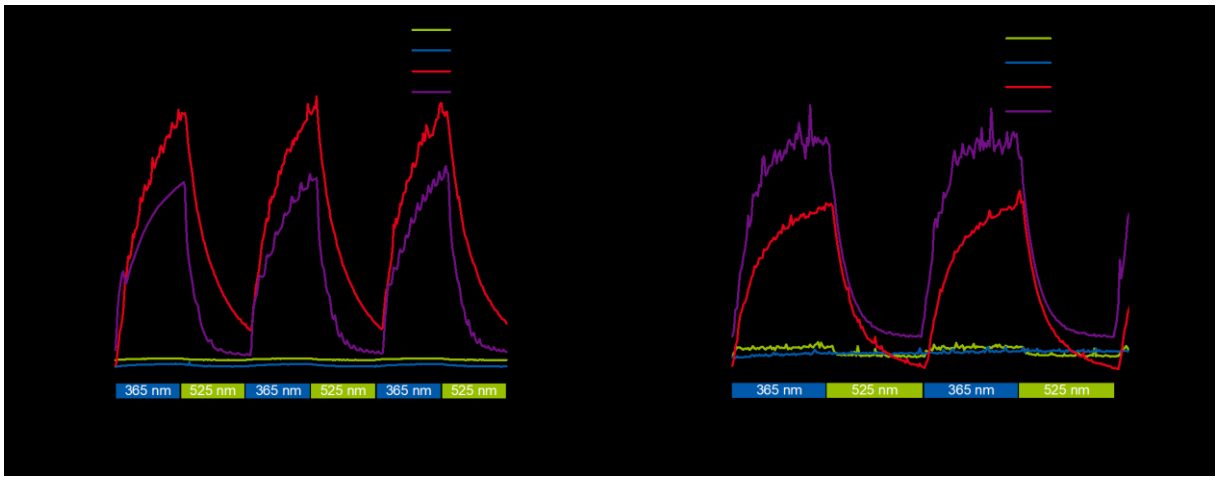

Figure 23: Different photo-responsive molecules irradiated with 365 and 525 nm light for 30 min each over three switching cycles in isopropanol (a), and two switching cycles in acetonitrile (b). The wavelength of maximum absorbance is given in parentheses.

Irrespective of the solvent used, the nitro-functionalised compounds (SP-NO_2 and SPA) show a higher response than the corresponding hydroxyl-functionalised compounds (SP-OH and BSP). In most cases, the monomer presents a lower and slower response than the corresponding photo-responsive molecule alone. One exception is BSP in isopropanol, which exhibits a slightly higher response than SP-OH. The photo-response switching speed of SP-NO_2 in isopropanol is also not the same speed in both directions, which is attributed to different wavelengths or intensities between the two used LEDs. One LED wavelength fits better to the absorption maximum than the other one, which should be addressed for further experiments on polymers. A further observation, especially for high absorption values, is a decreasing signal-to-noise ratio. This may arise from the experimental setup used where the samples were irradiated directly in the UV-Vis device. This means that only a fraction of the cuvette was irradiated by the LED (a photograph of a similar setup is shown in Figure 55). Spiropyran molecules are known to also exhibit switching behaviour in the absence of irradiation based on a thermal equilibrium.[208] In our irradiation experiments, an equilibrium state is not reached, and this is clearly observed for SPA in isopropanol, where a plateau is not reached during the 30 min irradiation increments. To obtain a homogeneous mixture, the cuvette was stirred, which resulted in the poorer signal-to-noise ratio.

These experiments were predominantly used to determine the optimal monomer to prepare photo-responsive polymers. According to the previous observations and results, the best photo-response was obtained using the nitro-compound SPA. It shows a much more intense response and was therefore chosen for further experiments as a photo-responsive moiety. The copolymerisation of this monomer with the two mentioned thermo-responsive moieties is explored in the following sections.

5.2 Free Radical Copolymerisation

The copolymerisation of two monomers *via* radical chain-growth was first tested using free radical polymerisation. This robust and poorly controlled technique was performed as a preliminary test to investigate the general compatibility of both thermo-responsive moieties with the photo-responsive SPA monomer. The two monomers were mixed with azobis(isobutyronitrile) (AIBN) using a molar ratio of 800 to 1. The initiator (2 mg) was mixed with different compositions of the two monomers dissolved in 1,4-dioxane (4 mL) before deoxygenating the mixture by purging with argon for 20 min. The reaction mixtures containing either 0, 25, 50, 75, or 100 mol% of SPA in the monomer mixture were heated to 80 °C for 24 h. The crude reaction mixture was analysed *via* size exclusion chromatography (SEC) for the formation of copolymer and ^{1}H-NMR to determine the relative monomer composition incorporated.

5.2.1 Synthesis of P(NIPAAm-*co*-SPA) by Free Radical Copolymerisation

The monomers NIPAAm and SPA were mixed, and the reaction performed similarly as discussed above (Scheme 4).

Scheme 4: Free radical polymerisation of NIPAAM with SPA in 1,4-Dioxane at 80 °C initiated using AIBN.

A colour change for the SPA-containing mixtures was observed during the polymerisation from dark green to dark red. After the crude mixture cooled to ambient temperature, it appeared dark blue. The first colour change from green to red is likely due to the transformation of the monomer to a polymer. Previous investigations of the absorbance spectra shown in Figure 23 indicate a slight change in the absorbance maximum between the monomer SPA and the SP-NO_2. The close proximity of the spiropyran units in the copolymer can also affect their electronic structure, and therefore their colour. The second colour change to blue is attributed to the well-known thermo-chromatic behaviour of spiropyrans.[120, 209]

As mentioned previously, the crude product was analysed *via* size exclusion chromatography in THF and by NMR spectroscopy (Figure 24). Here, diffusion coupled ^{1}H-NMR (DOSY) is an appropriate method to probe the composition of different molecules in the solution.

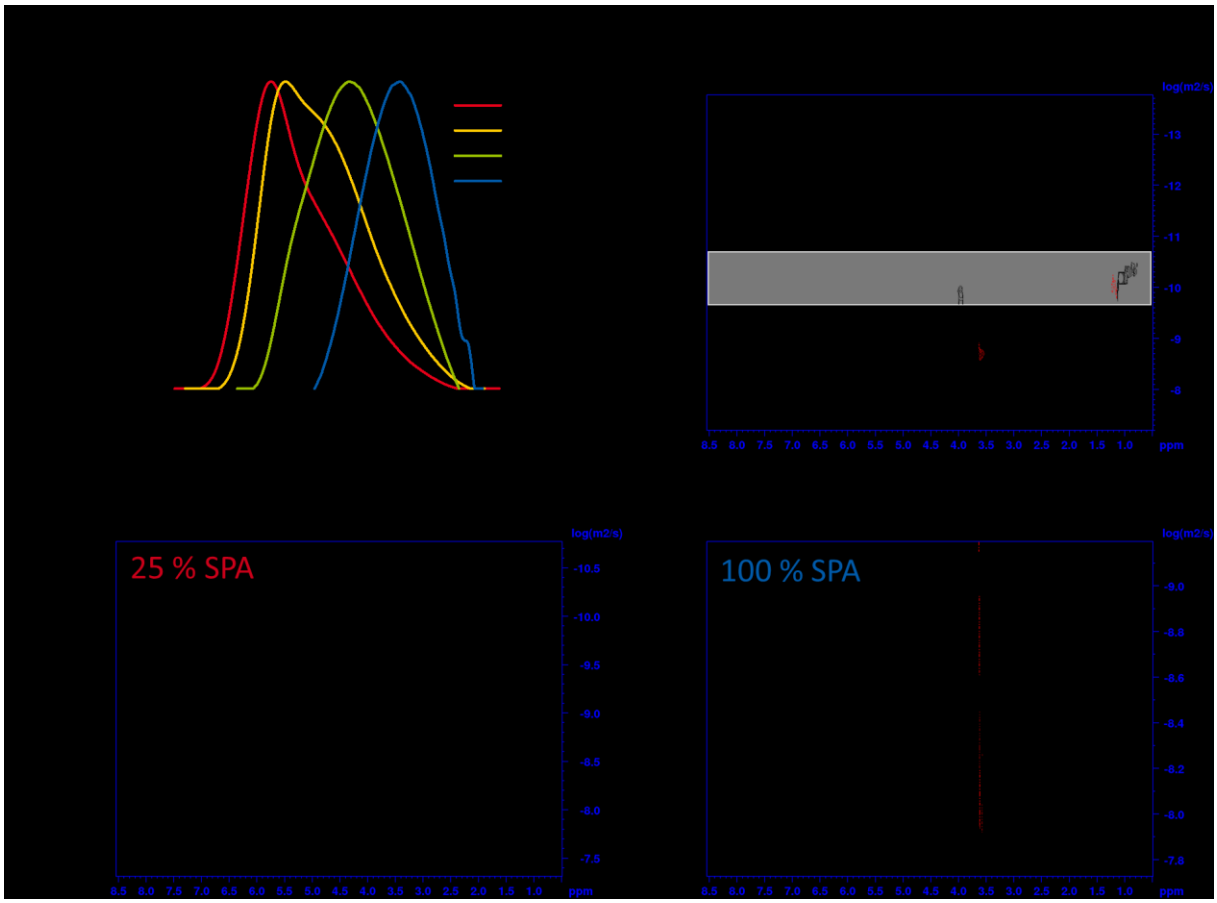

Figure 24: a) Elution traces of P(NIPAAm-co-SPA) in THF prepared by FRP. DOSY spectra of the reaction mixtures with 0 % (b), 25 % (c) and 100 % (d).

The results from SEC show that it is possible to obtain objects with a larger hydrodynamic radius than the bare monomers NIPAAm and SPA *via* radical copolymerisation. The SEC RI traces show monomodal distributions for all reactions, with the elution volume decreasing with increasing SPA in the initial monomer mixture. A selection is given from the measured diffusion ordered spectroscopy (DOSY) spectra. With this specialised technique, the translatoric diffusion coefficient of a molecule can be determined in an inhomogeneous magnetic field. A DOSY spectrum is a two-dimensional method showing the ^{1}H-NMR spectra on the x-axis and the diffusion coefficients on the y-axis. Small particles show a much higher diffusion coefficient than polymers, which appear above the monomers in the spectra. The results indicate that in all cases a copolymer formed as the diffusion signals occur in a region that is not the diffusion coefficient of a single molecule or the solvent itself. Overall, the conversion of the reaction appears to be lower for increasing amounts of SPA in the monomer mixture. The reaction with 0 % SPA shows almost complete conversion, whilst for the 25 % SPA mixture, the formation of a copolymer is less obvious, and the formation of a polymer in the 100 %-sample is only visible by SEC. The signals obtained from these spectra are not sufficient to determine the final copolymer composition, and the yield too low to be purified. However, these results clearly indicate that a radical copolymerisation of NIPAAm and SPA is possible, and the copolymerisation process can be further improved to form dual stimuli-responsive materials.

5.2.2 Synthesis of P(TEGA-*co*-SPA) by Free Radical Polymerisation

The copolymerisation of TEGA with SPA *via* free radical polymerisation is explored in the following section. The reaction is depicted in Scheme 5.

Scheme 5: Free radical polymerisation of TEGA with SPA in 1,4-dioxane at 80 °C initiated using AIBN.

The monomers (TEGA and SPA) and thermal initiator (AIBN) were dissolved in 1,4-dioxane. After deoxygenating the reaction mixture, the polymerisation was initiated by heating to 80 °C for 24 hours. Comparable colour changes were observed as for the previous copolymerisation with NIPAAm (section 5.2.1). It is plausible that the reaction also progressed in a similar fashion. To verify this, the crude product was subjected to SEC and diffusion coupled NMR (Figure 25).

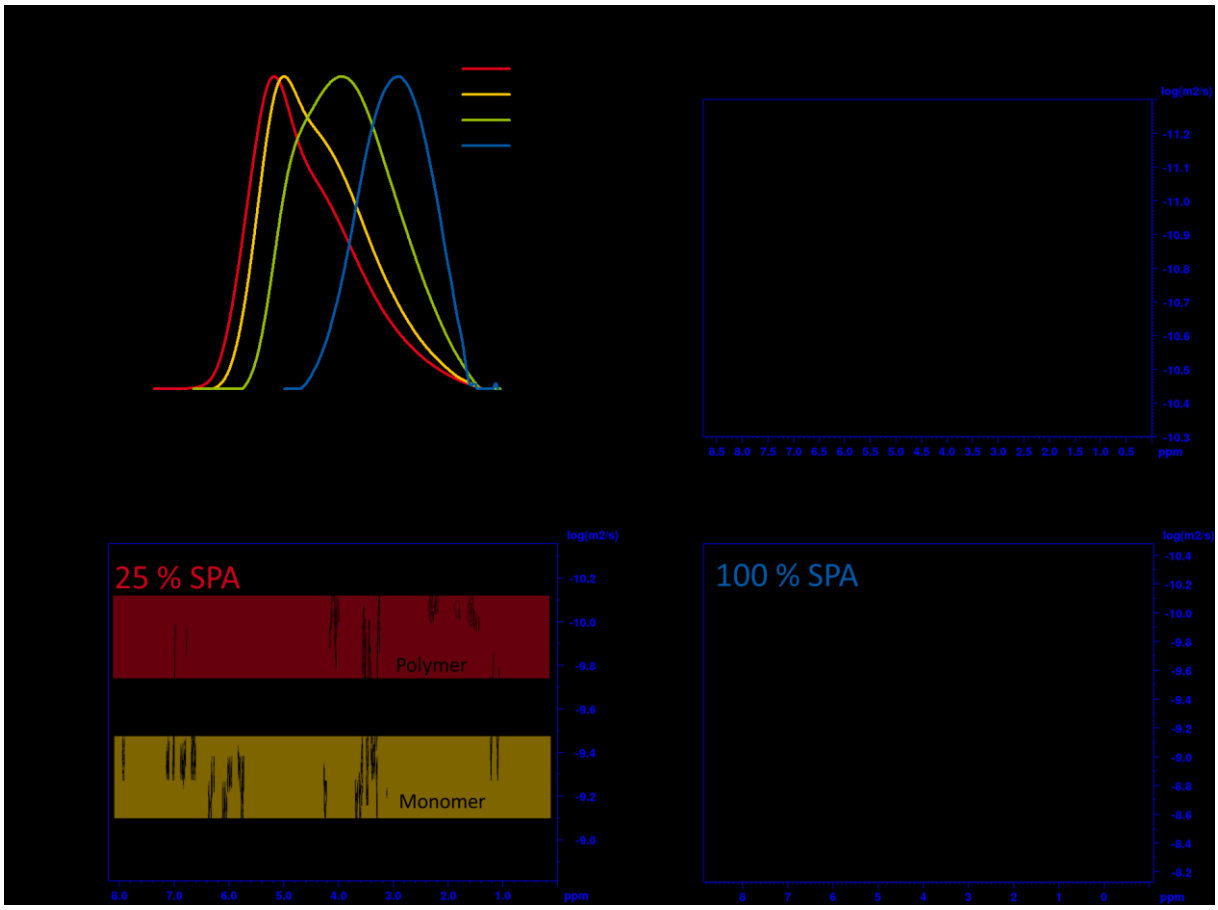

Figure 25: a) Elution traces of P(TEGA-co-SPA) in THF polymerised by FRP. DOSY spectra of the reaction mixtures with 0 % (b), 25 % (c) and 100 % SPA (d). The given percentages refer to the molar ratio of SPA used in the monomer mixture.

At first sight, the free radical polymerisation of TEGA with SPA does not appear to significantly differ from that of NIPAAm with SPA. Similarly, the copolymer appears to become smaller at increasing SPA amounts in the monomer feed. The NMR analysis indicates a decreasing conversion with increasing mol% of SPA in the monomer mixture. However, the conversion is generally higher than for the copolymerisation of NIPAAm and SPA; *e.g.*, on comparing Figure 24c with Figure 25c for the 25 % SPA sample, a clear separation of the polymer from the remaining monomers is possible. Unfortunately,

these spectra do not permit the composition of TEGA and SPA in the final copolymer to be determined. The 100 % SPA sample in both reactions show a comparable SEC trace, but the diffusion coupled NMR varies slightly, which is attributed to the experimental error of the instrument.

In summary, we showed that radical copolymerisation of either NIPAAm and SPA or TEGA and SPA is possible. Increasing amounts of SPA in the monomer mixture leads to decreasing conversions and lower molecular weight polymers according to SEC analysis. The copolymerisation of two acrylates (TEGA and SPA) appears to be more effective than the copolymerisation of an acrylamide and an acrylate (NIPAAm and SPA). With the free radical copolymerisation working in general for both combinations, a controlled radical polymerisation will be applied. This enables us to form more complex polymer architectures such as block copolymers that are capable of forming micelles or membranes.

5.3 Nitroxide-Mediated Copolymerisation

Controlled radical polymerisation (CRP) offers numerous advantages over free radical polymerisation, affording more well-defined polymers characterised by lower dispersities, and the possibility of re-initiation to form block copolymers. In general, all monomers that are polymerisable by free radical polymerisation can also be used in controlled radical polymerisation. Nitroxide-mediated polymerisation (NMP) is a robust polymerisation method that can proceed using unimolecular initiators, and this simplifies the synthetic effort required drastically. This method is well-known for the polymerisation of styrene and acrylate derivatives, which further justifies its use here. However, the synthesis of the unimolecular initiator is crucial, and in the following sections, two different unimolecular initiators are synthesised to prepare dual stimuli-responsive copolymers. The synthesis of P(NIPAAm-*co*-SPA) and P(TEGA-*co*-SPA) was first optimised, followed by the synthesis of a set of copolymers for each combination that was then intensively characterised to determine their degree of polymerisation and composition. The dual-responsive behaviour of both sets of copolymers was then investigated.

5.3.1 Synthesis of Different Unimolecular NMP Initiators

For the synthesis of dual-responsive copolymers, NIPAAm can be considered the most critical monomer. PNIPAAm has been accessed using two different NMP initiators: the SG-1 radical was used by Gibbons et al.,[210] and 2,2,6,6-tetraethyl-1-(1-phenylethoxy)piperidin-4-ol was used by Schulte and coworkers.[211] The latter unimolecular initiator is similar to 1-*tert*-butyl-3,3-dipropyl-5,5-diethyl-4-(1-phenylethoxy)-piperazin-2-one both structurally and in terms of reactivity, which is available in our working group. Additionally, protocols to synthesise macroinitiators using this initiator have already been established,[212] reducing the workload towards preparing micellar systems, or suitable macroinitiators for the formation of membranes. The SG-1 radical was synthesised following a protocol reported by Harrisson and coworkers.[213] Both unimolecular initiators were later used to polymerise NIPAAm.

5.3.1.1 Synthesis of 1-tert-butyl-3,3-dipropyl-5,5-diethyl-4-(1-phenylethoxy)-piperazin-2-one

Our working group already has experience working with 1-*tert*-butyl-3,3-dipropyl-5,5-diethyl-4-(1-phenylethoxy)-piperazin-2-one as a unimolecular NMP initiator.[196] The stable radical, 1-*tert*-butyl-5,5-dipropyl-3,3-diethyl-2-piperazinon-4-oxyl was synthesised according to a protocol reported by Miele and coworkers[214] before the unimolecular initiator was synthesised using a protocol reported by Harrisson and coworkers.[213] The six-step reaction pathway followed is depicted in Scheme 6.

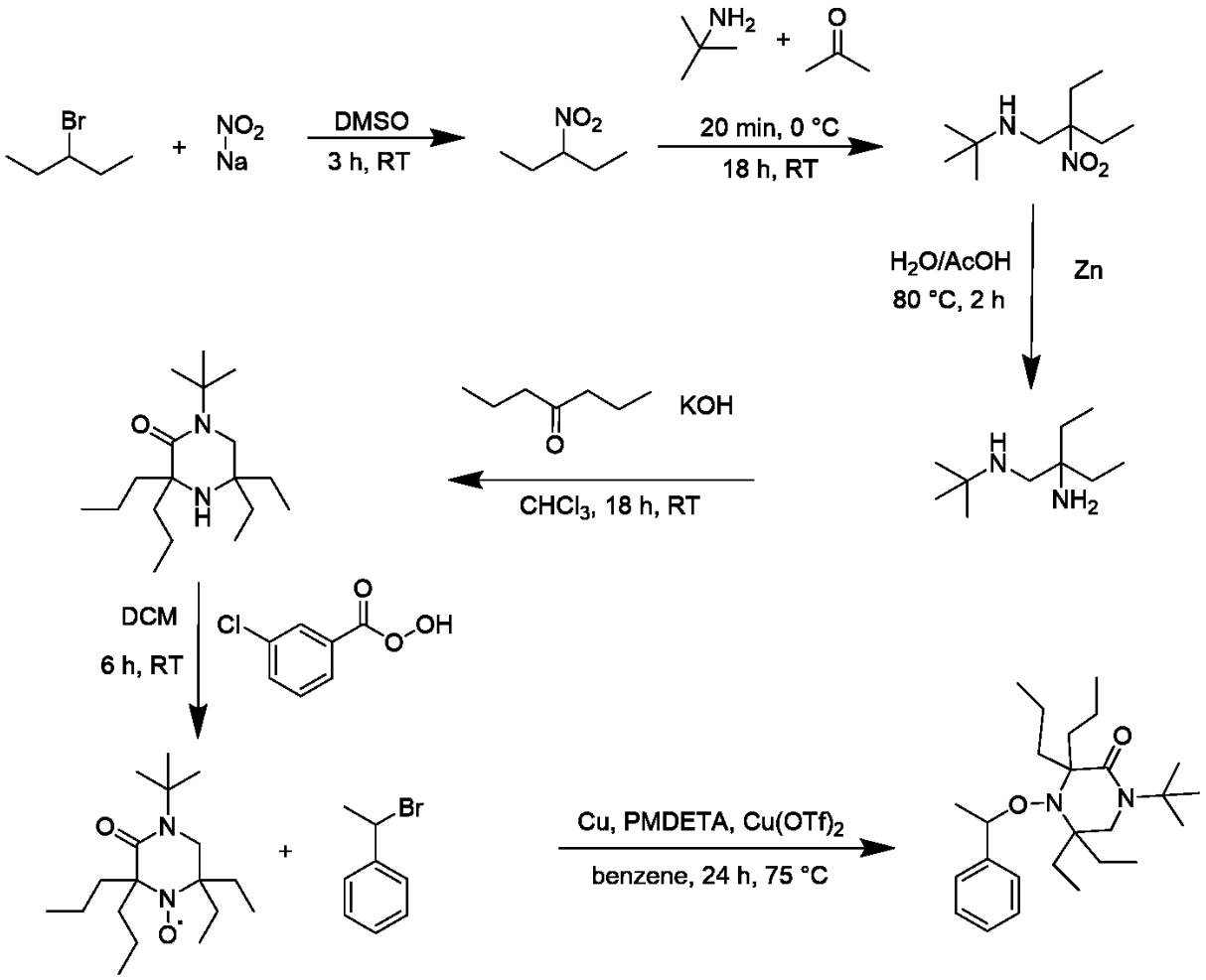

Scheme 6: Synthetic approach followed to synthesise 1-tert-butyl-3,3-dipropyl-5,5-diethyl-4-(1-phenylethoxy)-piperazin-2-one, a unimolecular NMP initiator.

3-Bromopentane was first substituted with sodium nitride to form 3-nitropentane. After which, *N-tert*-butyl-(2-ethyl-2-nitrobutyl)amine was formed from a solution of 2-amino-2-methylpropane and formaldehyde. In a zinc-catalysed reaction, the nitro function was reduced to an amino function before a ring closure was performed using heptane-4-one to form *1-tert*-butyl-3,3,5,5-tetraethyl-2-piperazone. With 3-chloro benzoperoxoic acid, a nitroxide is formed at the secondary nitrogen to yield an orange solid. The monomolecular initiator was then formed in a copper-catalysed reaction with 1-bromo-1-phenyl ethane as a white powder. The success of each step was followed by NMR spectroscopy, and the corresponding spectra are shown in Figure 26.

The expected signals are visible by ^{1}H-NMR at each step, and all products are of high purity. The nitroxide radical itself cannot be measured by NMR. Therefore, the nitroxide radical was captured using hydrazine before performing the NMR measurement. This spectrum revealed the persistent radical was also obtained with high purity. The unimolecular initiator was obtained as a white powder and stored in the refrigerator until use.

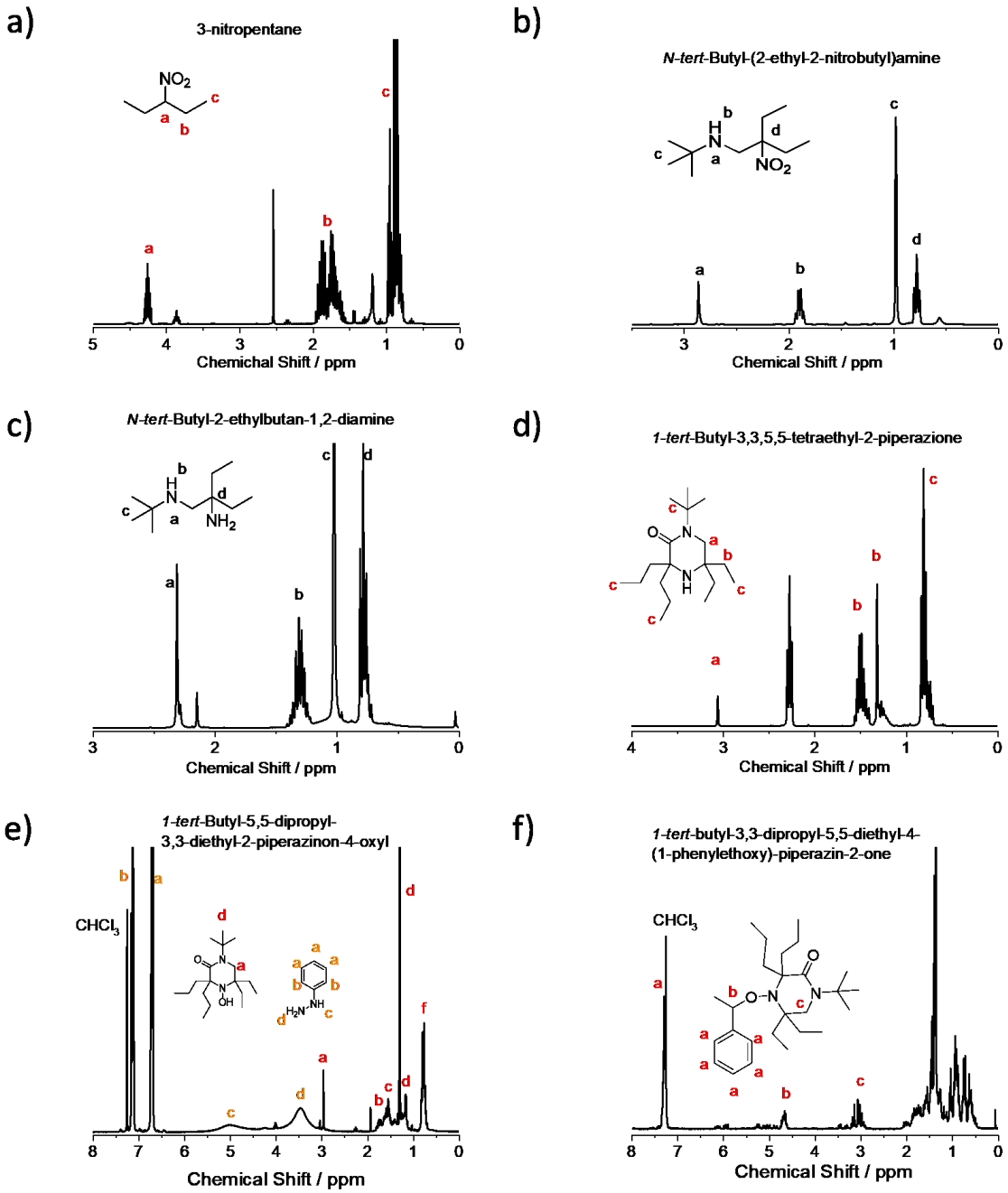

Figure 26: ^{1}H-NMR spectra of the different synthetic steps to prepare 1-tert-butyl-3,3-dipropyl-5,5-diethyl-4-(1-phenylethoxy)-piperazin-2-one for subsequent use as a unimolecular NMP initiator. All spectra were acquired on a 300 MHz Bruker spectrometer using deuterated chloroform as solvent. The nitroxide, 1-tert-butyl-5,5-dipropyl-3,3-diethyl-2-piperazinon-4-oxyl (e), was measured with added phenylhydrazine.

5.3.1.2 Synthesis of BlocBuilder-MA

Whilst the second unimolecular initiator used, BlocBuilder-MA, is commercially available, the synthesis is relatively straightforward following a protocol reported by Harrisson and coworkers.[213] The reaction pathway is depicted in Scheme 7.

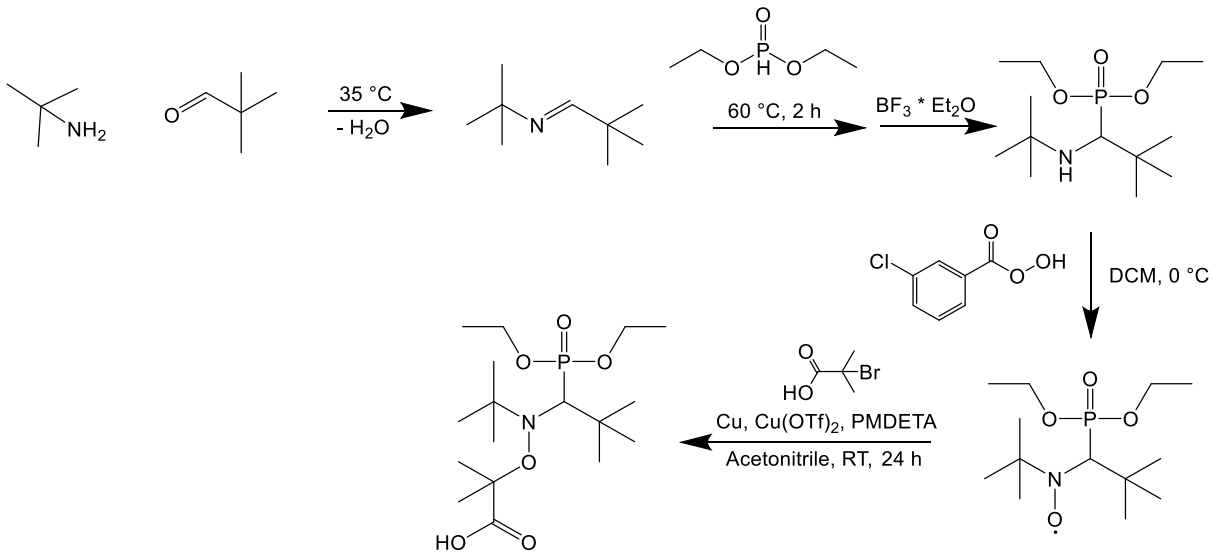

Scheme 7: Synthetic approach followed to synthesise BlocBuilder-MA for use as an NMP initiator.

The unimolecular initiator is synthesised in four steps. First, the *tert*-butyl amine and pivalaldehyde react to form azomethimine, which reacts subsequently with diethylphosphite and boron trifluoride diethyl etherate to form α-aminophosphonate in a Mannich-type reaction. The unimolecular initiator was then formed in a similar reaction as used for the previous unimolecular initiator through a copper-catalysed reaction with 2-bromo-2-methylpropanoic acid to form a white powder. The reactions were followed by ^{1}H-NMR, and these are shown in Figure 27.

Figure 27: ^{1}H-NMR spectra of the a) α-aminophosphonate and b) BlocBuilder-MA unimolecular NMP initiator. Both spectra were recorded in $CDCl_3$.

Both spectra shown in Figure 27 show the expected signals. Furthermore, the chiral nature of the molecule is clearly visible by the doublet of the tertiary proton labelled “b”. This signal further indicates that both enantiomers exist in equal ratios. The prepared unimolecular initiator was then utilised to form water-soluble copolymers.

5.3.2 Synthesis of Water-Soluble Copolymers

The major requirement of the dual-responsive copolymers is that they are water-soluble. So far, our experiments indicate that it is possible to copolymerise both monomers, but that further optimisation is required. In the following section, the copolymerisation optimisation will be detailed. The free radical

polymerisation indicates that the copolymerisation of both combinations to form P(NIPAAm-*co*-SPA) and P(TEGA-*co*-SPA) is possible. The controlled radical polymerisation method NMP is well-known for acrylate and styrene derivatives, but the polymerisation of NIPAAm has not been comprehensively studied, although it is possible.[210-211] As such, first the polymerisation of NIPAAm was optimised before a set of water-soluble P(NIPAAm-*co*-SPA) copolymers were synthesised before a set of P(TEGA-*co*-SPA) copolymers were prepared. Upon synthesis of both P(NIPAAm-*co*-SPA) and P(TEGA-*co*-SPA) copolymer sets, their behaviour upon heating and irradiation was investigated.

5.3.2.1 Synthesis of P(NIPAAm-co-SPA) via Nitroxide-Mediated Polymerisation

The monomers NIPAAm and SPA were copolymerised using the synthesised unimolecular initiator to form water-soluble copolymers. Since this exact monomer combination is not literature known, optimisation was necessary to find the most suitable conditions to form well-defined copolymers before a set of copolymers was prepared to permit a systematic investigation of their stimuli-response.

5.3.2.1.1 Optimisation of the NMP Process for NIPAAm

As mentioned previously, the polymerisation of NIPAAm *via* NMP is known but has not been comprehensively studied. In order to compare both initiators, 1-*tert*-butyl-3,3-dipropyl-5,5-diethyl-4-(1-phenylethoxy)-piperazin-2-one and BlocBuilder-MA, styrene and NIPAAm were homopolymerised using both initiators and the resulting products compared *via* SEC (Figure 28).

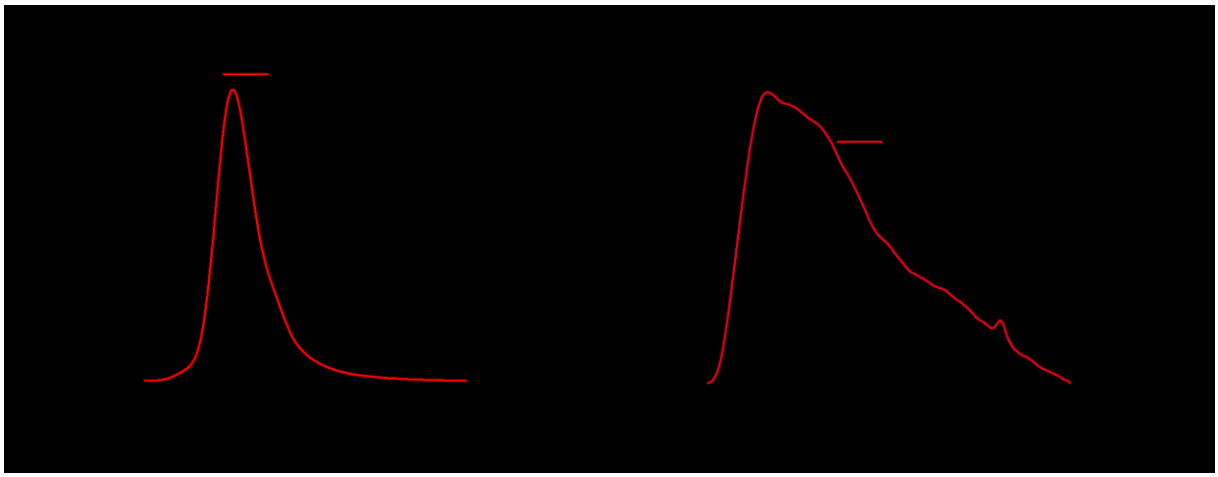

Figure 28: Identical polymerisations performed using different initiators to prepare a) polystyrene and b) PNIPAAm. The normalised RI traces were obtained by SEC in DMAc with 0.21 % LiCl.

The analysis of the crude reaction mixture reveals that, in both cases, a polymer is formed with similar maxima independent of the initiator used, BlocBuilder-MA (red) or 1-*tert*-butyl-3,3-dipropyl-5,5-diethyl-4-(1-phenylethoxy)-piperazin-2-one (black), or monomer. While the peak maximum is similar irrespective of the initiator used, the level of control over the polymerisation differs. For both monomers, styrene and NIPAAm, 1-*tert*-butyl-3,3-dipropyl-5,5-diethyl-4-(1-phenylethoxy)-piperazin-2-one results in better control yielding lower dispersities and more symmetrical molecular weight distributions.

Nevertheless, the results indicate that it is possible to polymerise NIPAAm with both initiators, but 1-*tert*-butyl-3,3-dipropyl-5,5-diethyl-4-(1-phenylethoxy)-piperazin-2-one was chosen to further optimise the reaction conditions, and later for the copolymerisation of NIPAAm and SPA. Since all reagents used (monomers and the unimolecular initiator) are solid, a suitable solvent is required to perform the

copolymerisation. The formation of block copolymers and even triblock terpolymers later further restricts the solvent choice. A suitable solvent to prepare block copolymers should stabilise the radical of the nitroxide and dissolve all blocks. Possible candidates are anisole,[215] dioxane[216] and toluene,[217] since NMP can be performed in all of these solvents, and they also dissolve both polystyrene and PNIPAAm. To simplify the determination of the degree of polymerisation, a macroinitiator (PS_{288}) initiated with 1-*tert*-butyl-3,3-dipropyl-5,5-diethyl-4-(1-phenylethoxy)-piperazin-2-one was dissolved in different solvents and 250 equivalents of NIPAAm was added. The clear solution was degassed by purging with argon before being heated at 110 °C for 16 h. The unreacted monomer was removed *via* precipitation in hot water. The successful block extension of the macroinitiator was then proven by SEC, and the degree of polymerisation determined by ^{1}H-NMR in $CDCl_3$ (Figure 29).

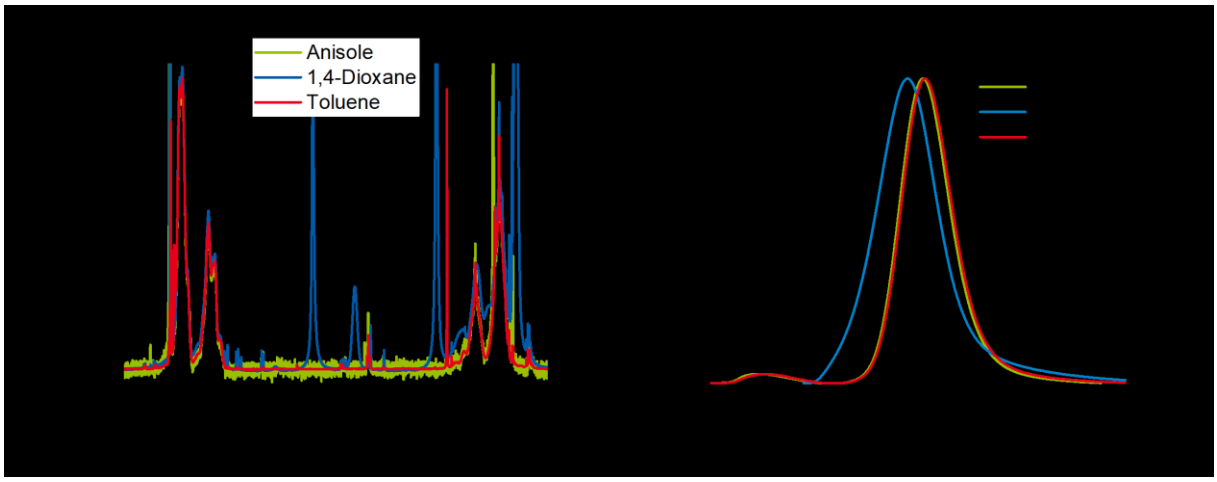

Figure 29: Block extension of PS_{288} via NMP in different solvents: a) ^{1}H-NMR in $CDCl_3$ and b) SEC in DMAc + 0.21 % LiCl.

The shift in the SEC traces to higher elution volumes reveals the macroinitiator was successfully block extended, with the largest shift observed using 1,4-dioxane as solvent. Furthermore, the ^{1}H-NMR spectra only show a noticeable PNIPAAm signal for the reaction performed in 1,4-dioxane. The final composition of the different block copolymers are summarised in Table 1. The molar mass of the polymers was calculated using a combination of SEC and NMR, whereas the dispersity is obtained from SEC using PS standards.

Table 1: Block extension of a PS macroinitiator with NIPAAm in different solvents.

Solvent	M_n[a] / g/mol	$Đ$[a]	Composition[b]	x_{NIPAAm}[c] / %
	30,700	1.19	PS_{288}	-
Toluene	33,900	1.09	PS_{288}-*b*-$PNIPAAm_{21}$	6.7
1,4-Dioxane	37,700	1.24	PS_{288}-*b*-$PNIPAAm_{142}$	33.1
Anisole	35,400	1.08	PS_{288}-*b*-$PNIPAAm_{20}$	6.5

a) SEC in DMAc + 0.21 % LiCl using PS standards, b) calculated from ^{1}H-NMR, c) ^{1}H-NMR in $CDCl_3$.

The reaction in toluene and anisole only resulted in a block extension of approximately 20 repetition units, whilst 1,4-dioxane lead to the addition of 140 repetition units. This block extension equates approximately to a monomer conversion of 50 %. In a subsequent reaction, different monomer to macroinitiator ratios were tested in 1,4-dioxane. The macroinitiator was then changed to polystyrene-*b*-polyisoprene, since this structure is more convenient for the formation of membranes, and which will be discussed later. After being deoxygenated by three consecutive freeze-pump-thaw degassing cycles, the polymerisation was allowed to proceed for 24 h at 110 °C. The resulting polymer was

separated from the unreacted monomer by precipitation in water, redissolving the precipitate in THF followed by a second precipitation in water to remove the remaining monomer completely. The purified product was analysed *via* ^{1}H-NMR to determine the composition (Figure 30).

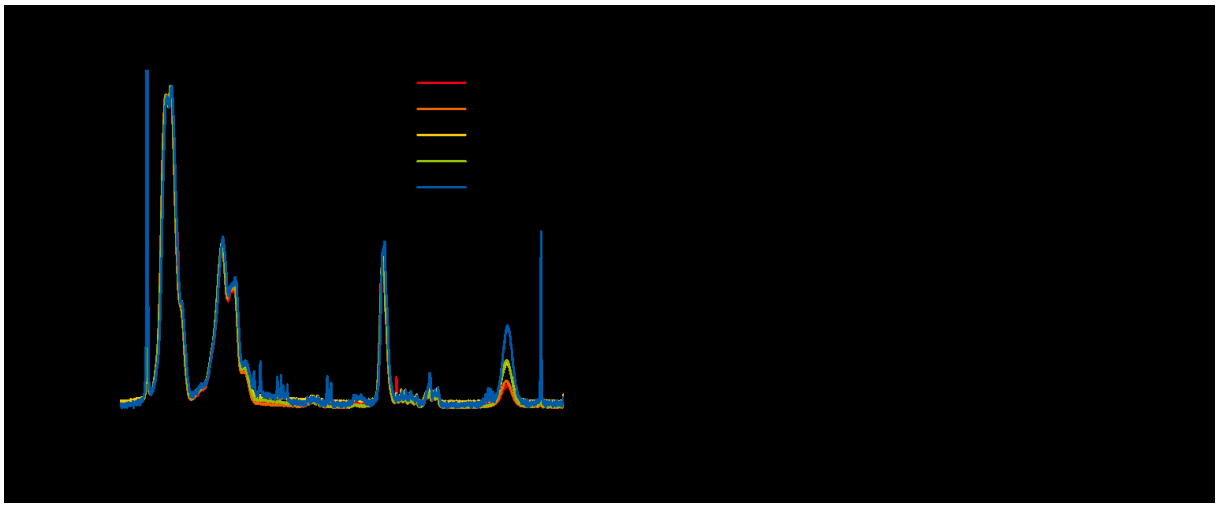

Figure 30: a) ^{1}H-NMR spectra of PS-b-PI-b-PNIPAAm prepared using different M/I ratios in $CDCl_3$, and b) M/I ratio plotted against the amount of NIPAAm incorporated in the final polymer (the line is included to guide the eye).

Increasing the NIPAAm to PS-*b*-PI macroinitiator ratio leads to higher amounts of NIPAAm incorporated into the final structure according to NMR analysis (Figure 30). The NIPAAm units added upon block extension are given in Table 2. The molar mass of the polymers is calculated from a combination of SEC and NMR, whereas the dispersity is obtained from SEC using PS standards.

Table 2: Number of repetition units added by block extension of the macroinitiators using different NIPAAm feed ratios.

Polymer	M_n / g/mol	$Đ$[a)]	x_{NIPAAm}[b)] / %	M/I ratio
PS_{495}	51,600[a]	1.18	-	-
PS_{495}-*b*-PI_{269}	82,000[c]	1.79	-	-
PS_{495}-*b*-PI_{269}-*b*-$PNIPAAm_{59}$	103,400[c]	1.90	7.4	200/1
PS_{495}-*b*-PI_{269}-*b*-$PNIPAAm_{57}$	99,100[c]	1.95	7.4	300/1
PS_{495}-*b*-PI_{269}-*b*-$PNIPAAm_{155}$	144,700[c]	2.13	16.9	400/1
PS_{495}-*b*-PI_{269}-*b*-$PNIPAAm_{129}$	128,800[c]	2.26	15.4	500/1
PS_{495}-*b*-PI_{269}-*b*-$PNIPAAm_{255}$	185,400[c]	3.46	25.0	600/1

a) Determined *via* SEC in DMAc using PS standards, b) determined *via* ^{1}H-NMR in $CDCl_3$, c) calculated from the ratio using the absolute molar mass of the styrene macroinitiator.

The increasing content of NIPAAm within the polymer indicates that the chain length of the hydrophilic segment can be easily adjusted by changing the monomer to initiator ratio. Overall, the previous results show that it is possible to polymerise NIPAAm *via* NMP and that the chain length can be adjusted to a certain extent. The copolymerisation of two monomers, however, can be more challenging, and therefore the copolymerisation of NIPAAm and SPA was then investigated and will be discussed in the following section.

In a similar manner to the previous homopolymerisation of NIPAAm, the monomers NIPAAm and SPA were mixed with a unimolecular initiator in a molar ratio of 400 to 1 dissolved in 1,4-dioxane. The amount of SPA in the monomer mixture was 0, 1 and 5 mol%. The reaction mixture was then deoxygenated by purging with argon before being heated at 110 °C. Samples were taken under argon

protection after different reaction times. The overall monomer conversion was determined *via* ^{1}H-NMR, and the amount of unreacted NIPAAm and SPA in the reaction mixture determined *via* gas chromatography (Figure 31).

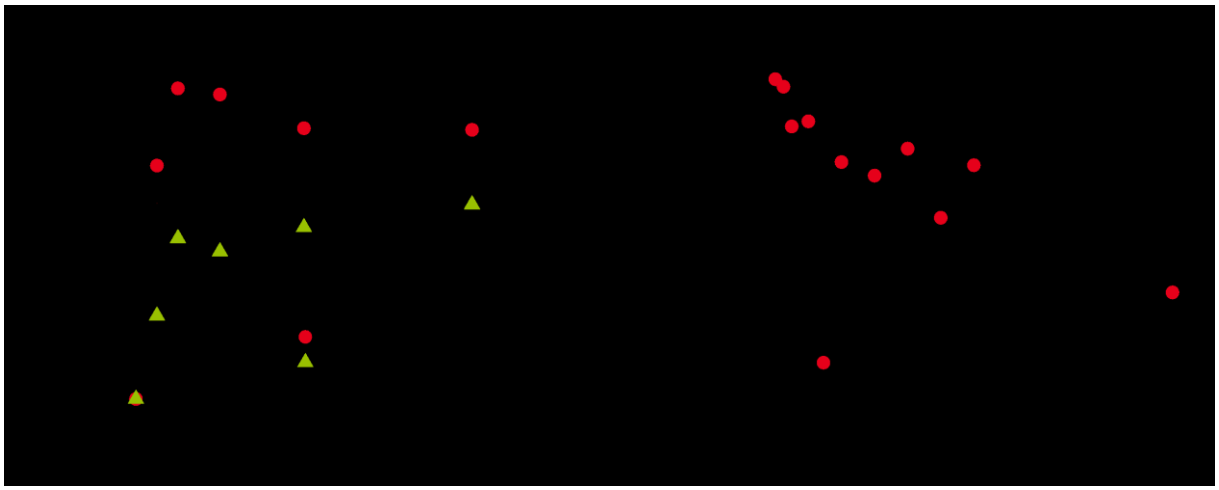

Figure 31: a) Overall monomer conversion with 0, 1 and 5 mol% SPA in the initial monomer feed, and b) the amount of SPA and NIPAAm in the reaction mixture with time determined by gas chromatography for an initial feed of 5 mol% SPA.

The overall monomer conversion is lower when NIPAAm is copolymerised with SPA; as such, the higher the SPA feed ratio, the lower the overall conversion. This was already observed in the free radical copolymerisation in the previous section. We attribute this to the steric hindrance of the bulky SPA monomer. By ^{1}H-NMR analysis, it is only possible to determine the overall monomer conversion, and not how both monomers are consumed over the course of the polymerisation. We therefore used gas chromatography to monitor the consumption of both monomers since they present different retention times. Figure 31b shows the monomer consumption for the reaction mixture containing 5 mol% SPA, which provides a sufficient signal-to-noise ratio. Both monomers are consumed linearly over the 24 h monitored, and approximately 80 % of the initial monomer remains unreacted after this time. Furthermore, the amount of unreacted SPA is lower than unreacted NIPAAm, which indicates NIPAAm is incorporated preferentially into the copolymer. Since it is indeed possible to copolymerise NIPAAm and SPA, these conditions were used to synthesise a set of copolymers with varying amounts of NIPAAm and SPA to systematically investigate how the composition alters the material response towards an external stimulus.

5.3.2.1.2 Preparation of Water-Soluble Dual-Responsive P(NIPAAm-*co*-SPA) Copolymers

The previously found conditions were deemed suitable to prepare copolymers of NIPAAm and SPA for systematic investigation of the composition on the stimuli response, and should further be appropriate for the block extension of a hydrophobic macroinitiator to form amphiphilic block terpolymers later on. To investigate the influence of the composition of the copolymer on stimuli-responsive behaviour, a set of copolymers was prepared. The well-characterised copolymers were then used to investigate how the composition influences their dual-responsive behaviour. Preliminary work showed that P(NIPAAm-*co*-SPA) copolymers with more than ~10 % SPA are not soluble in water, restricting the amount of SPA that can be incorporated into the copolymers, and hence also the monomer mixture to below 10 %. Accordingly, the composition of the monomer mixture consisted of 0, 1, 2, 3, 4, 5, and 6 mol% SPA. The reaction pathway is depicted in Scheme 8.

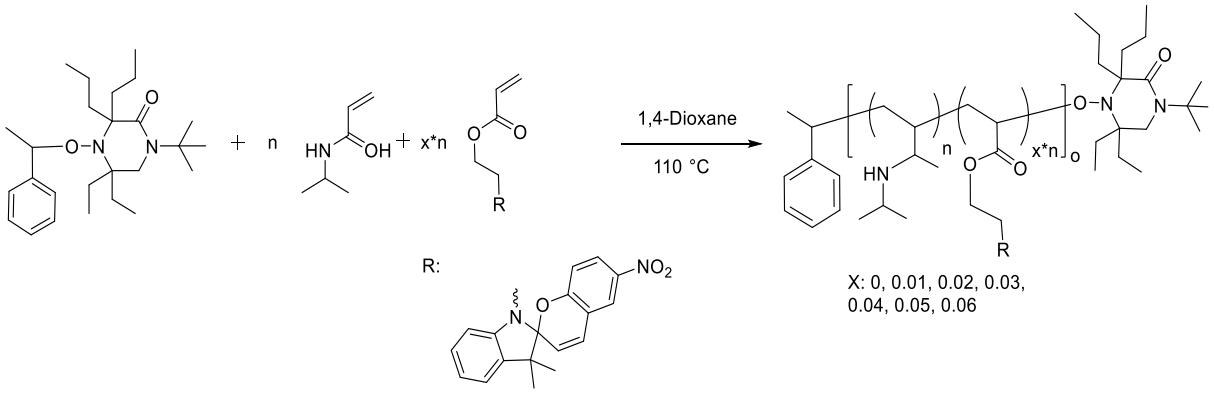

Scheme 8: Synthesis of a set of water-soluble copolymers of NIPAAm and SPA via NMP.

The slightly green solution was deoxygenated by three consecutive freeze-pump-thaw cycles before being heated for 24 h at 110 °C. During the reaction, the colour of the SPA-containing reaction mixture changed from green to red, and further to a dark blue after cooling the vial to ambient temperature. The change in colour is in good agreement with the colour changes observed during the free radical copolymerisation. The crude mixture was precipitated twice in diethyl ether, and the obtained red powder analysed *via* SEC and NMR (Figure 32).

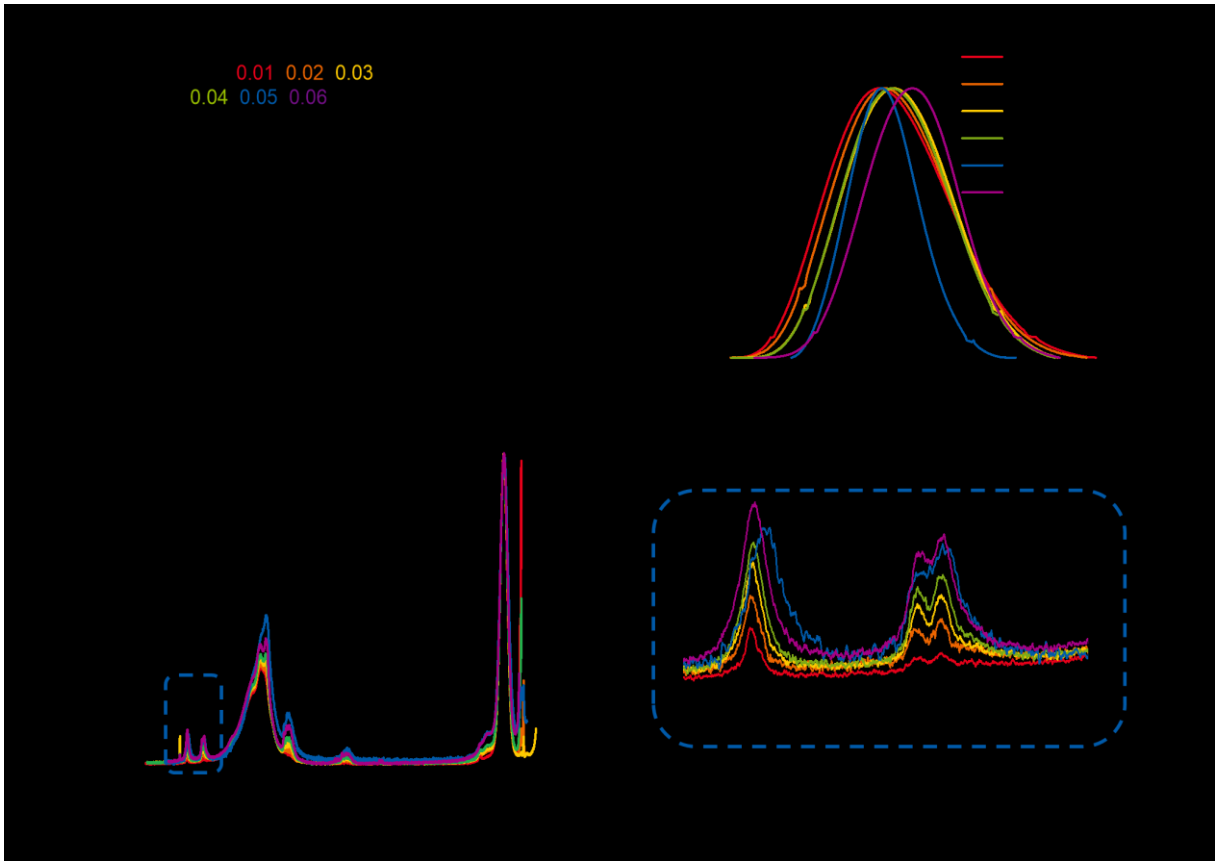

Figure 32: a) Composition of the synthesised set of P(NIPAAm-co-SPA) copolymers determined using ^{1}H-NMR; b) normalised RI SEC elution traces of the copolymers using DMAc as eluent; c) ^{1}H-NMR signals of different P(NIPAAm-co-SPA) copolymers in DMSO-d_6 normalised to the signal at 4 ppm assigned to NIPAAm; and d) detailed view of the ^{1}H-NMR signal at ~8 ppm. Numbers and colours refer to the amount of SPA in the monomer mixture and the resulting copolymer.

The normalised RI SEC traces in DMAc are monomodal, and copolymers containing higher amounts of SPA result in higher elution volumes. The corresponding dispersity also typically decreases for copolymers containing higher amounts of SPA. The ^{1}H-NMR spectra in DMSO were normalised to the

NIPAAm signal at 4 ppm, and the integral of the SPA signal at 8 ppm was used to determine the composition of the copolymer. Further relevant assignments of the protons in the ^{1}H-NMR spectra and assignment are given in Figure 32a and c. The ^{1}H-NMR spectra reveal an increasing amount of SPA in the monomer mixture also leads to increasing amounts of SPA in the copolymer. However, we are not able to determine the degree of polymerisation from these results, and the absolute molar mass could not be determined *via* the RI trace obtained from SEC. To determine the absolute molar mass by static light scattering, the refractive index increment (dn/dc) is required. The results for all seven copolymers are summarised in Table 3.

Table 3: Characteristics of the set of P(NIPAAm-co-SPA) copolymers obtained from varying amounts of SPA in the initial feed.

Composition[b,d]	SPA / %	M_n[a] / g/mol	$Đ$[a]	M_w[b] / g/mol	Yield / %	dn/dc[c] / mL/g
$PNIPAAm_{418}$	0	22,900	2.47	47,280	91.6	0.0975 ± 0.0019
$P(NIPAAm_{311}$-*co*-$SPA_1)$	1	25,700	1.86	35,800	80.7	0.0966 ± 0.0021
$P(NIPAAm_{282}$-*co*-$SPA_2)$	2	25,800	1.76	32,700	70.7	0.0878 ± 0.0012
$P(NIPAAm_{383}$-*co*-$SPA_4)$	3	25,500	1.58	44,800	59.1	0.0984 ± 0.0006
$P(NIPAAm_{538}$-*co*-$SPA_6)$	4	26,300	1.55	63,400	49.7	0.0998 ± 0.0010
$P(NIPAAm_{617}$-*co*-$SPA_7)$	5	19,300	1.47	72,700	45.2	0.1035 ± 0.0007
$P(NIPAAm_{1108}$-*co*-$SPA_{17})$	6	22,600	1.41	124,000	39.8	0.1038 ± 0.0003

a) DMAc SEC, PS standards; b) SLS in THF; c) refractive index increment; d)^{1}H-NMR analysis (not shown here).

The detailed analysis of the prepared copolymers (Table 3) confirmed most of our assumptions. All copolymers are characterised by comparable molar masses according to SEC analysis against PS standards, with lower dispersities obtained at higher amounts of SPA in the initial monomer mixture. The absolute molar mass obtained *via* SLS, however, increases drastically when higher amounts of SPA are used in the initial monomer mixture. The yield of the copolymerisation decreases for increasing amounts of SPA in the monomer mixture, which aligns with the decreasing conversion for increasing amounts of SPA in the initial feed. The refractive index increment, dn/dc, also scales with the amount of SPA incorporated within the copolymer, which is attributed to the higher refractive index increment of the SPA monomer.

One of the potentially more interesting parameters, the copolymer composition, can be determined *via* ^{1}H-NMR. However, due to the poorer signal-to-noise ratio for low amounts of SPA in the copolymer, another method was used. The extinction coefficient of the copolymers should scale with the number of photo-responsive molecules per polymer chain. The copolymer was dissolved in HPLC-grade THF at different concentrations and the absorbance of the solution at 330 nm measured in triplicate. The results were then graphed using two x-axis units. A plot of the concentration in mg/mL is easier to apply since the absolute molar mass of the copolymer is not needed. The plot showing the concentration in g/mol requires the absolute molar mass of the copolymers but enables the extinction coefficients for each sample to be compared. For both cases, the slope changes dependent on the amount of SPA in the solution, hence why the expected trends are comparable. In Figure 33, both plots are shown for the P(NIPAAm-*co*-SPA) copolymers.

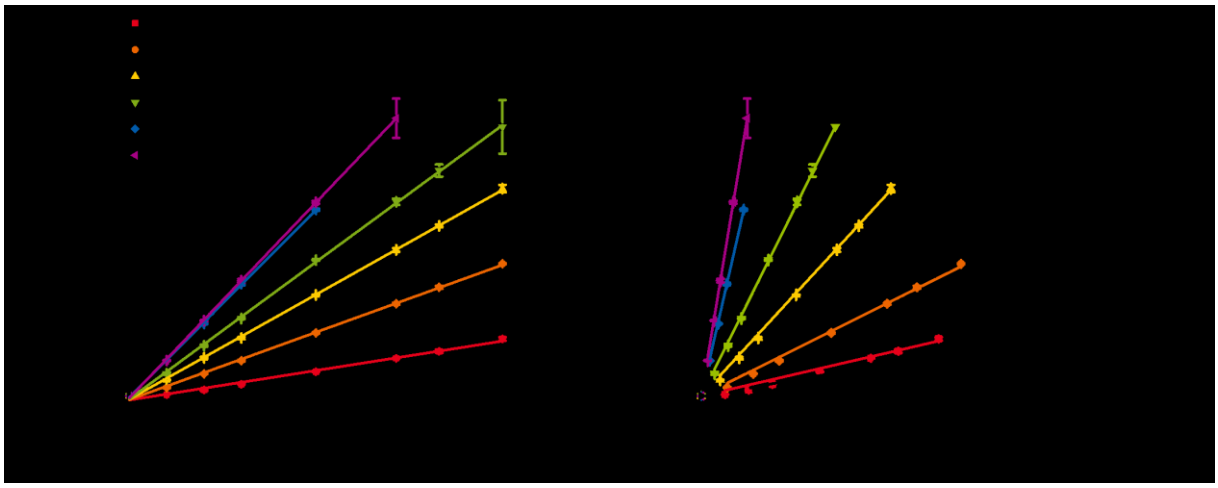

Figure 33: Absorbance of various copolymers of P(NIPAAm-co-SPA) and SPA monomer at different concentrations at 330 nm in THF for the determination of the extinction coefficient with increasing concentration in a) mg/mL and b) g/mol.

The overall observed trend in both plots are comparable. If the concentration of the solution is plotted in mg/mL the monomer naturally has the highest slope, whilst the lowest slope possible is zero for polymers containing no SPA. Increasing amounts of SPA in the copolymers leads to an increase in the slope theoretically until a PSPA homopolymer is obtained, and the slope is then identical to the monomer. If the concentration is plotted in g/mol, the slope for the monomer is the lowest. The number of SPA units in the copolymers was determined by dividing the slope of the copolymer by the slope of the monomer. The slopes of each were further used to determine the extinction coefficient of the copolymers (Table 4).

Table 4: Characterisation of the synthesised P(NIPAAm-co-SPA) copolymers with varying amounts of SPA by NMR and UV-Vis spectroscopy.

Composition[a),b)]	**SPA in monomer mixture / %**	**SPA[b)] / %**	**Extinction coefficient[c)] / mol*mL^{-1}*cm^{-1}**	**SPA[c)] / %**
$PNIPAAm_{418}$	0	0	10,000	0
$P(NIPAAm_{311}\text{-}co\text{-}SPA_1)$	1	1.57	13,000	1.1
$P(NIPAAm_{282}\text{-}co\text{-}SPA_2)$	2	2.49	29,000	2.2
$P(NIPAAm_{383}\text{-}co\text{-}SPA_4)$	3	3.31	63,000	2.3
$P(NIPAAm_{538}\text{-}co\text{-}SPA_6)$	4	3.96	116,000	2.6
$P(NIPAAm_{617}\text{-}co\text{-}SPA_7)$	5	4.05	253,000	2.9
$P(NIPAAm_{1108}\text{-}co\text{-}SPA_{17})$	6	5.28	350,000	3.1

a) Absolute molar mass, b) 300 MHz ^{1}H-NMR from Bruker in $CDCl_3$, c) UV-Vis in THF at 330 nm.

According to both methods, ^{1}H-NMR and UV-Vis spectroscopy, the amount of SPA incorporated within the copolymer increases as the amount of SPA in the monomer feed increases. While the amount of SPA determined *via* ^{1}H-NMR is in close agreement to the amount in the initial monomer mixture, the amount determined using the extinction coefficient only agree at low SPA amounts, *i.e.*, less than 2 mol%. The higher the amount of SPA in the initial feed, the higher the difference between both methods, ^{1}H-NMR and UV-Vis. This difference can be attributed to the close proximity of the SPA moieties in the copolymers, which leads to the absorbance being quenched. The determination of the composition *via* ^{1}H-NMR is also in agreement with observations from gas chromatography, indicating that the consumption of both monomers is comparable.

To summarise, the copolymerisation of SPA and NIPAAm with a unimolecular NMP initiator was investigated. First, we optimised the polymerisation conditions to prepare a PNIPAAm homopolymer before testing the same conditions to form copolymers with SPA. Similar conditions were then used to prepare a set of copolymers and their compositions determined by several methods. ^{1}H-NMR revealed that the six copolymers prepared have a composition ranging from 0 to 5.28 mol%. This set of copolymers will later be used to investigate the influence of the switching state of SPA on the thermo-response of the NIPAAm moiety.

5.3.2.2 Synthesis of P(TEGA-co-SPA) via Controlled Radical Copolymerisation

The second thermo-responsive moiety to be investigated in this thesis is TEGA. PTEGA provides numerous advantages over PNIPAAm including a higher cloud-point temperature[155] and the same polymerisable group as the SPA monomer, an acrylate. A further advantage exists relating to the thermo-response of the copolymers: the thermo-response of PNIPAAm depends on the chain length, which leads to a certain blurring of the thermo-response in statistical copolymers. This effect may be reduced for copolymers containing TEGA since the thermo-response originates from the side chain. In the following section, the monomer TEGA (synthesised in section 5.1.1) is polymerised using nitroxide-mediated polymerisation, and a set of copolymers prepared to investigate their dual-responsive behaviour in aqueous solution.

5.3.2.2.1 Optimisation of the NMP Process for TEGA

From our previous results copolymerising NIPAAm and SPA, similar conditions were tested for the copolymerisation of TEGA and SPA. In our first attempt, a macroinitiator was mixed with both monomers with an M/I ratio of 1333/1 dissolved in 1,4-dioxane. The polymerisation mixture was then deoxygenated before being heated to 110 °C for 8 h (Scheme 9).

Scheme 9: Nitroxide-mediated polymerisation of TEGA and SPA in 1,4-dioxane at 110 °C.

The crude product was purified to remove any unreacted monomer by dialysis in THF, and the block extension of the macroinitiator assessed *via* ^{1}H-NMR and SEC (Figure 34). Here, a different unimolecular initiator was employed than for the copolymerisation NIPAAm and SPA. From our preliminary investigations, we observed that it was not crucial whether 1-*tert*-butyl-3,3-dipropyl-5,5-diethyl-4-(1-phenylethoxy)-piperazin-2-one or BlocBuilder-MA was used. Hence, due to the fewer synthetic steps required, BlocBuilder-MA was used.

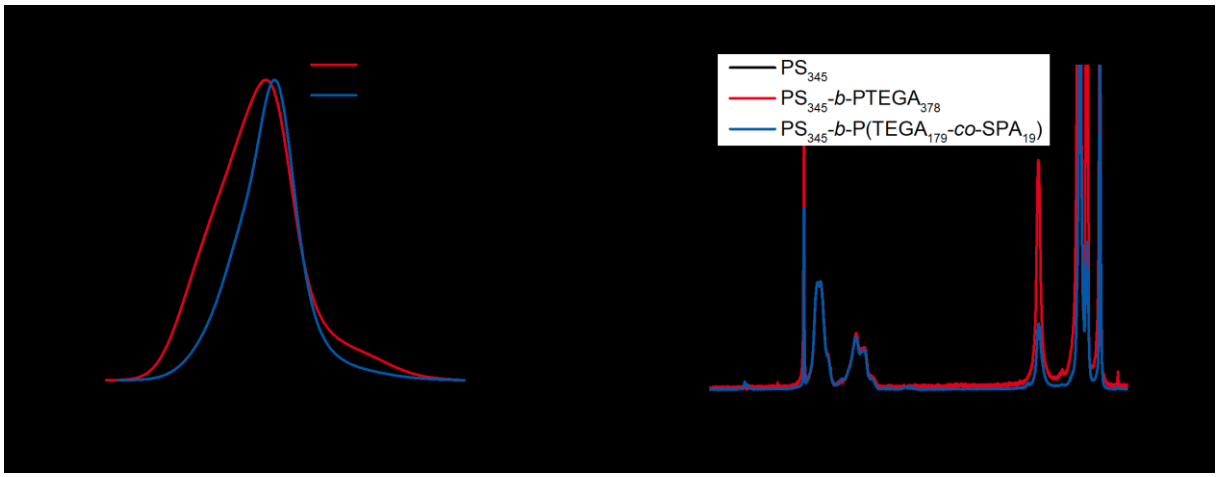

Figure 34: Analysis of the block extension of a polystyrene macroinitiator with TEGA or with TEGA and 5 mol% SPA by a) SEC in DMAc and b) ^{1}H-NMR in $CDCl_3$.

The SEC traces in Figure 34 reveal that the block extension of polystyrene with TEGA is possible, with the expected signals for the macroinitiator and incorporated TEGA observed by ^{1}H-NMR, and with no unreacted monomer present following purification. The monomer to initiator ratio in this reaction is higher than for the previous experiments to permit a clearer and observable shift to be observed upon block extension by SEC. The low degree of polymerisation may originate from the generally lower reaction speed of block extensions due to restricted end group accessibility of the macroinitiator. To investigate the consumption of both monomers (TEGA and SPA) simultaneously, both were mixed with the unimolecular initiator BlocBuilder in 1,4-dioxane. The reaction mixture was deoxygenated by purging with argon before being heated to 110 °C for 8 h. During the polymerisation, samples were taken and analysed *via* gas chromatography to determine the conversion of each monomer starting from different monomer feed ratios or compositions in a similar manner as previously presented for NIPAAm and SPA in Figure 31. The comonomer SPA was added in varying amounts of 0, 1 and 5 mol% to investigate the consumption of both monomers *via* gas chromatography (Figure 35).

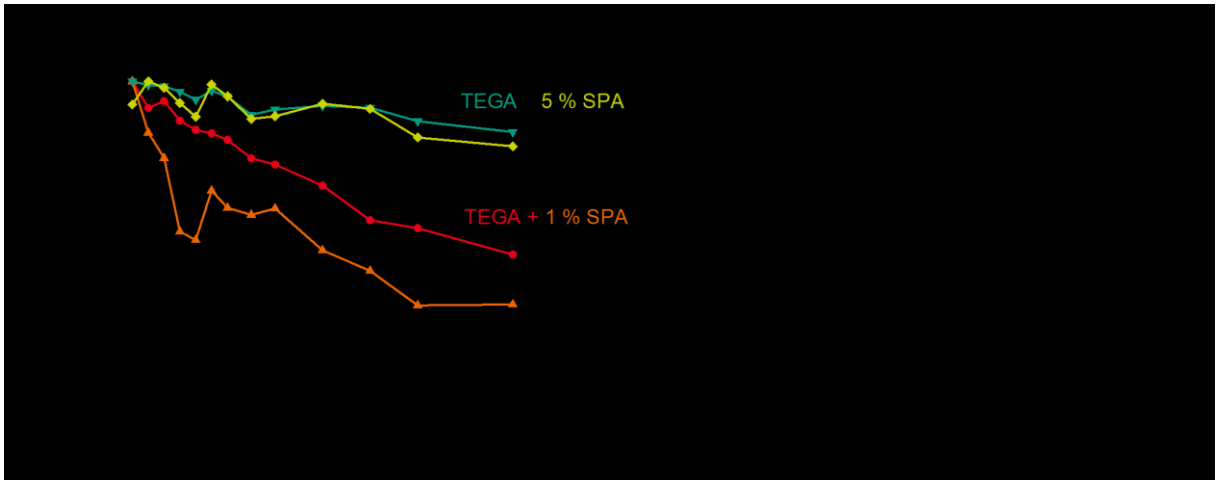

Figure 35: Gas chromatographic analysis of the a) nitroxide-mediated copolymerisation of TEGA with varying amounts of SPA; and an b) exemplary chromatogram showing the retention times for each component in the reaction mixture.

The GC signals were normalised to the solvent (1,4-dioxane), and the relevant monomer signals integrated to determine the monomer conversion at various time points during the polymerisation. In general, the results obtained for the copolymers P(TEGA-*co*-SPA) do not differ significantly from the previous investigations of P(NIPAAm-*co*-SPA); with the only exception that when TEGA is used as a comonomer, complete conversion is achieved after 8 h. Similarly, to the previous copolymerisations

with SPA, the polymerisation proceeds more slowly as the amount of SPA in the initial monomer mixture increases; and both monomers are consumed at approximately the same rate, with SPA being consumed at a slightly higher rate than TEGA. With these promising initial results for the copolymerisation of TEGA and SPA, a set of copolymers was synthesised to investigate their dual-response systematically.

5.3.2.2.2 Preparation of Water-Soluble Dual-Responsive P(TEGA-*co*-SPA) Copolymers

Here, we present the synthesis and characterisation of a set of P(TEGA-*co*-SPA) copolymers containing varying amounts of SPA to investigate the effect of the SPA content on the transition temperature. Therefore, the two monomers SPA and TEGA were mixed in different ratios with the unimolecular NMP initiator Blocbuilder-MA in an 800 to 1 ratio in 1,4-dioxane. The mixture was deoxygenated and then heated at 110 °C overnight. After the reaction, the copolymer was precipitated twice in diethyl ether and dried under reduced pressure (Scheme 10).

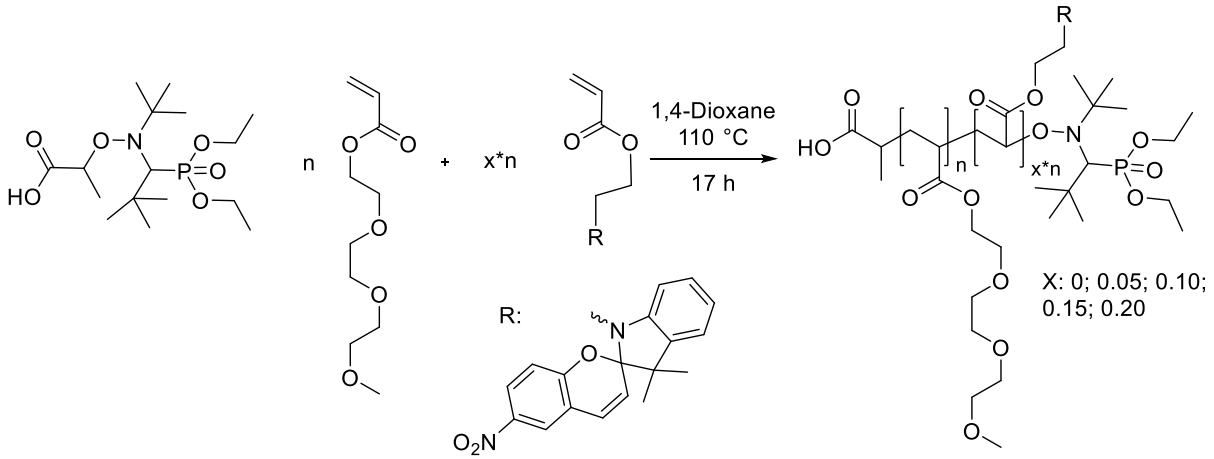

Scheme 10: Synthesis of a set of water-soluble copolymers containing TEGA and SPA via NMP in 1,4-dioxane at 110 °C.

The colour changes observed during the reaction were in good agreement with the changes observed in the free radical polymerisation (section 5.2.2). PTEGA was obtained as a colourless oil, while the SPA-containing copolymers were obtained as red oils, which were more intense with increasing amounts of SPA. The copolymers were analysed by SEC and ^{1}H-NMR (Figure 36).

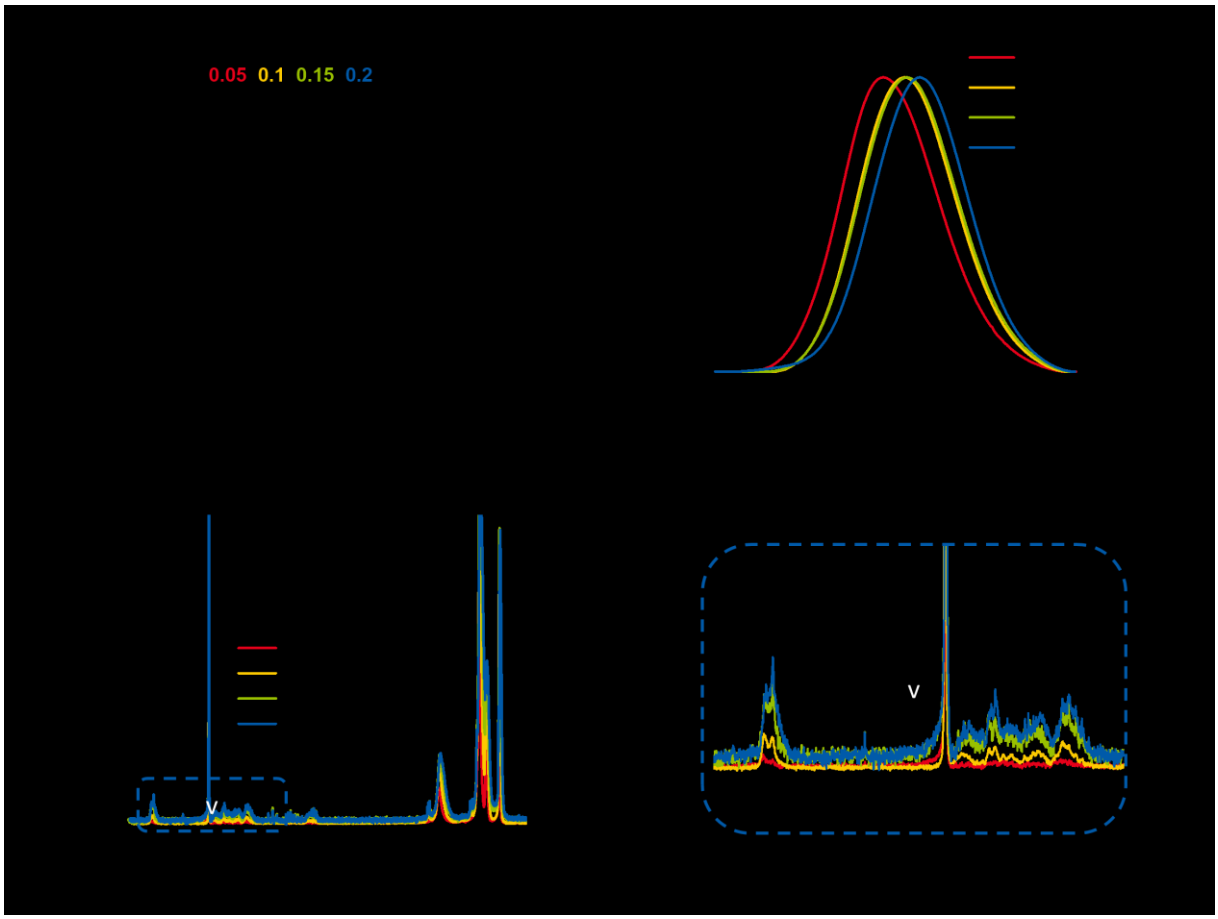

Figure 36: Characterisation of the prepared set of water-soluble P(TEGA-co-SPA) copolymers. a) Structure and ^{1}H-NMR assignment. Numbers and colours refer to the amount of SPA in the initial monomer mixtures. b) RI SEC traces of the copolymers in THF. c) ^{1}H-NMR spectra in $CDCl_3$, and d) corresponding detailed view of the aromatic region.

This set of copolymers presents a higher SPA content compared to the previously investigated P(NIPAAm-*co*-SPA) copolymers, which increases the signal-to-noise ratio in the NMR. Consequently, the SPA content within the copolymer could be determined by ^{1}H-NMR, and the absolute molar mass was determined *via* SEC triple detection (Table 5). Triple detection refers to three different detectors being used in combination: refractive index, viscometry, and multi-angle light scattering. When the change of refractive index increment (dn/dc) is known, it is possible to combine the results from these three detectors and obtain the absolute molar mass.

Table 5: Molecular weights and compositions of the prepared set of P(TEGA-co-SPA) copolymers.

Composition[c)]	x_{SPA} (Monomer) / %	x_{SPA}[a)] (Polymer) / %	M_n[b)] / g/mol	$Đ$[b)]	dn/dc / mL/g
$PTEGA_{266}$	0	0	58,000	1.4	0.0588 ± 0.0019
$P(TEGA_{202}$-*co*-$SPA_5)$	5	4	46,000	1.3	0.0704 ± 0.0010
$P(TEGA_{175}$-*co*-$SPA_9)$	10	9	42,000	1.3	0.0832 ± 0.0028
$P(TEGA_{194}$-*co*-$SPA_{16})$	15	13.5	49,000	1.2	0.0951 ± 0.0015
$P(TEGA_{142}$-*co*-$SPA_{15})$	20	16	37,000	1.3	0.1158 ± 0.0037

a) Determined *via* ^{1}H-NMR in $CDCl_3$, b) MALLS triple detection in THF, c) degree of polymerisation determined from M_n and x_{SPA}.

The amount of SPA in the monomer mixture is in good agreement with the final copolymer composition, but is generally slightly lower than expected from the feed ratio used. The absolute molar mass of the copolymers decreases with increasing SPA amount, ranging from 58,000 to 37,000 g/mol.

The dispersity does not vary significantly with copolymer composition. The degree of polymerisation for each copolymer was determined from the composition obtained by ^{1}H-NMR and the absolute molar mass.

The higher amount of SPA in the copolymer increases the signal-to-noise ratio of the ^{1}H-NMR, improving the accuracy of this method to determine the composition for the P(TEGA-*co*-SPA) copolymers compared to the P(NIPAAm-*co*-SPA) copolymers. Nevertheless, the extinction coefficient of the copolymers was also determined to calculate the amount of SPA incorporated within the copolymer. To compare the results to the previous investigations shown in Figure 33, the absorbance of the copolymers was plotted in mg/mL, as well as in g/mol (Figure 37).

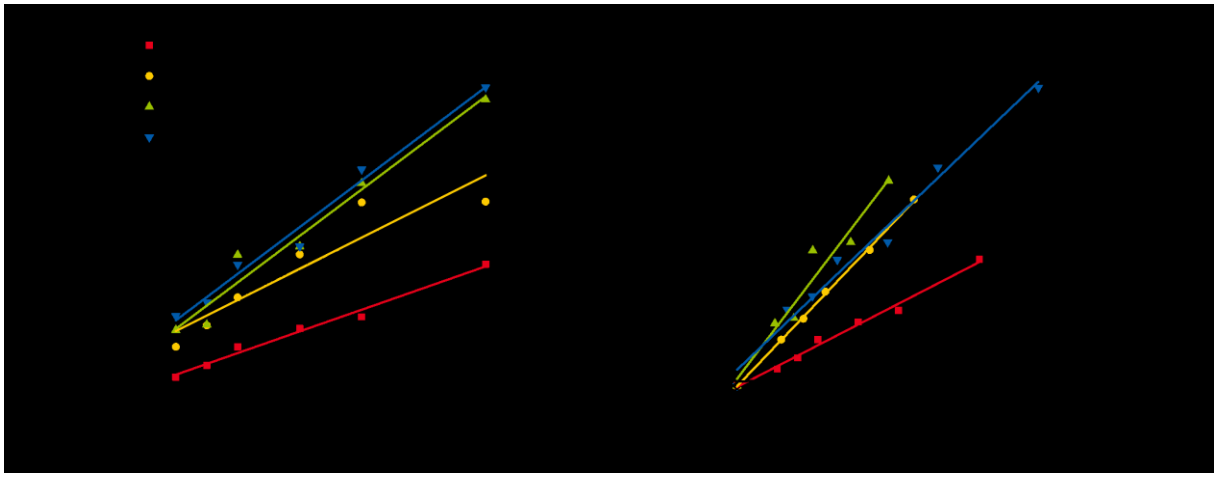

Figure 37: Absorbance of various copolymers of P(TEGA-co-SPA) and SPA monomer at different concentrations at 330 nm in THF for the determination of the extinction coefficient with increasing concentration in a) mg/mL and b) g/mol.

The overall trend observed in both plots is comparable: increasing amounts of SPA in the copolymer lead to an increasing extinction coefficient. However, the slopes are not as ordered as for the previously investigated copolymers of NIPAAm and SPA. The extinction coefficient of the copolymers does not scale linearly with the amount of SPA in the copolymer, as already previously observed for the P(NIPAAm-*co*-SPA) copolymers. The quenching of the absorbance due to the close proximity of the photo-responsive moieties to each other is even increased in the copolymers investigated here. All extinction coefficients and resulting copolymer compositions are shown in Table 6.

Table 6: Comparison of the compositions determined by ^{1}H-NMR analysis and from the extinction coefficient for P(TEGA-co-SPA) copolymers.

Composition	SPA / %	SPA[a] / %	ε [b] / mol/(mL*cm)	SPA[b] / %
$PTEGA_{266}$	0	0	-	0
$P(TEGA_{202}$-*co*-$SPA_5)$	5	4	6,300	1.2
$P(TEGA_{175}$-*co*-$SPA_9)$	10	9	9,200	2.8
$P(TEGA_{194}$-*co*-$SPA_{16})$	15	13.5	15,100	5.2
$P(TEGA_{142}$-*co*-$SPA_{15})$	20	16	11,600	12.8

a) Amount of SPA determined *via* ^{1}H-NMR, b) amount of SPA determined *via* UV-Vis.

Again we see that absorption spectroscopy is only suitable for the determination of low SPA concentrations. The close proximity of the photo-responsive moieties to each other affects the absorption, and which may also affect their photo-responsive behaviour. In addition, the absorbance

of the different thermo-responsive moiety affects the extinction coefficient. All of the drawbacks mentioned make this method even less suitable for the determination of the composition.

In summary, the copolymerisation of P(TEGA-*co*-SPA) was optimised according to our previous results in the copolymerisation of NIPAAm and SPA. Subsequently, a set of P(TEGA-*co*-SPA) copolymers was synthesised *via* NMP for the systematic investigation of their dual-responsive behaviour in aqueous media. The five copolymers are characterised by an average molar mass of 45,000 g/mol with 0 to 16 % SPA with a step-width of ~4 %. After the synthesis of these two sets of dual-responsive copolymers, P(NIPAAm-*co*-SPA) and P(TEGA-*co*-SPA), their response towards both light and temperature was investigated.

5.4 Dual Thermo- and Photo-Responsive Behaviour of Copolymers

The formed copolymers consist of a photo-responsive moiety and a thermo-responsive moiety, such that a dual-response to both stimuli should be observed. The response of the copolymer towards irradiation is expected to be more of a continuous change, whereas the response towards heating is expected to be more spontaneous (Figure 38).

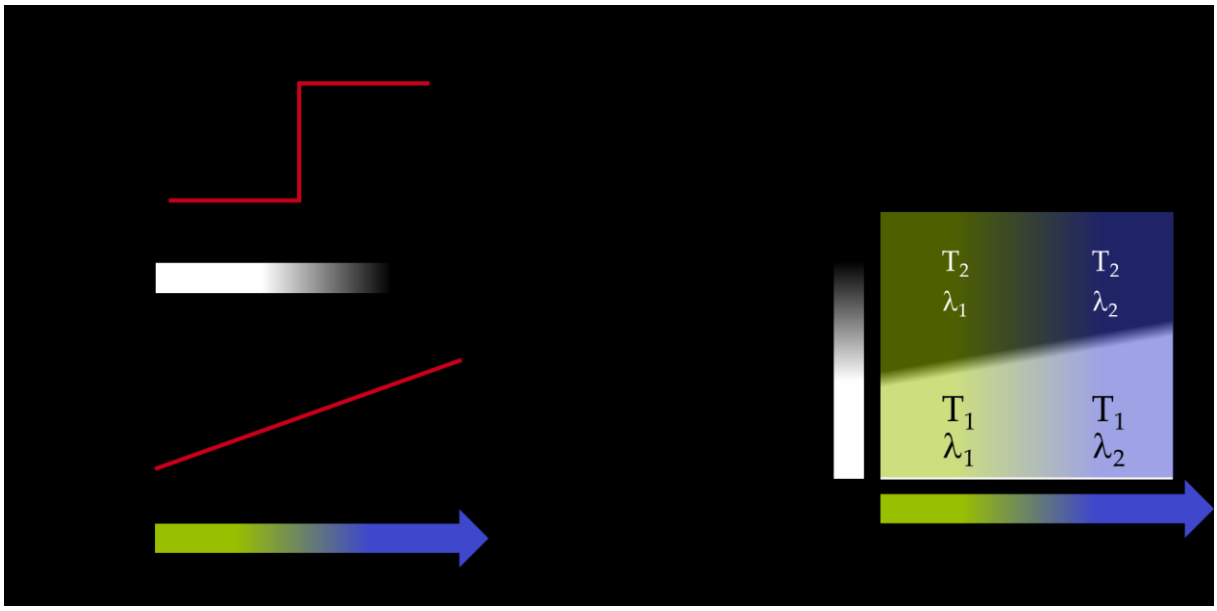

Figure 38: Response of thermo- and photo-responsive materials to an external stimulus in separate materials and in a combined material.

In the given system, the water-soluble copolymer responds to both stimuli simultaneously, which results in four states, with two extremes for each stimulus. The response to temperature can differ between the two distinct extremes of soluble and insoluble. The response to light can differ between the two extremes of the spiropyran- and merocyanine-form. These two distinct states only exist in a single localised molecule. The copolymers, however, consist of many photo-responsive molecules, which leads to a statistical distribution of molecules existing in one of two extreme states, rather than all existing in a specific state. To investigate the complex behaviour in an aqueous solution, some preliminary investigations were first performed before investigating the responses independently from each other. First, the thermo-response of PNIPAAm was probed, which is known to be dependent on additives, which result in different transition temperatures.[145, 148] The photo-responsive SPA moiety is known to also react to the pH-value of the solution, and the effect of the pH on the photo-response needs to be determined.[207, 218] Therefore, the optimal conditions to perform the measurements needs to be determined where the copolymer exhibits a response to both stimuli.

The photo-response of both sets of copolymers will be subsequently tested in aqueous solution. The P(NIPAAm-*co*-SPA) copolymers are solid, which permits their photo-response in the solid-state to also be investigated. The thermo-response of the dissolved copolymers in relation to the irradiation state is then investigated. For these experiments, the samples are irradiated constantly and heated above the transition temperatures. Due to the formation of two sets of copolymers consisting of different thermo-responsive moieties, we compared the results for both systems.

5.4.1 Preliminary Investigation of Copolymers in Aqueous Solution

The dual-response of the copolymers in solution is affected by the surrounding media. As we will later investigate these structures in more complex systems including membranes prepared from block terpolymers, it is important we first assess and understand their responsive behaviour in solution. For the investigation of membranes containing NIPAAm, an aqueous environment with a high viscosity is advantageous for measurements performed later in this thesis. The photo-response of spiropyrans in aqueous solutions depend on the pH-value, hence why this behaviour is also expected for copolymers and needs to be investigated in detail to find the optimal pH for the observation of their photo-responsive behaviour.

All the previous considerations rely on the simultaneous investigation of both stimuli. The dual-response needs to be determined in dissolved copolymers as well as in micelles or membranes. This complicates the analysis and also excludes many techniques, which are only capable of the determination of only one stimulus-response at any given time. In aqueous media, both stimuli (light and temperature) can be applied separately without influencing each other, so they can be considered orthogonally. The response of the polymeric material to one external stimulus can be measured by a large variety of specialised methods. However, most of these methods suffer from several drawbacks when investigating an orthogonal response. Upon heating, the polymer will precipitate, and this behaviour is commonly measured by turbidity or light scattering techniques. On the other hand, upon irradiation, the polymer will change polarity, and this is often probed by cyclic voltammetry. All the methods mentioned up until now can only be applied to measure the response to one stimulus alone. Methods that provide structural information can provide information when both stimuli are applied, but these methods typically require a complex experimental setup. The photo-response of spiropyran moieties[208] and the thermo-response of PNIPAAm[148-149] have been studied *via* NMR and IR spectroscopy.[219-220] The major drawback of these methods is the extensive effort for the experimental setup. The switching of the photo-responsive spiropyran does not only result in a different polarity of the molecule, but also in a different electronic structure. This manifests as a different absorbance profile in the UV-Vis wavelength range (see Figure 6). Therefore, the change in polarity of the spiropyran moiety is directly linked to its absorbance and/or fluorescence. Absorbance and/or fluorescence measurements could provide information on the response to both stimuli simultaneously.

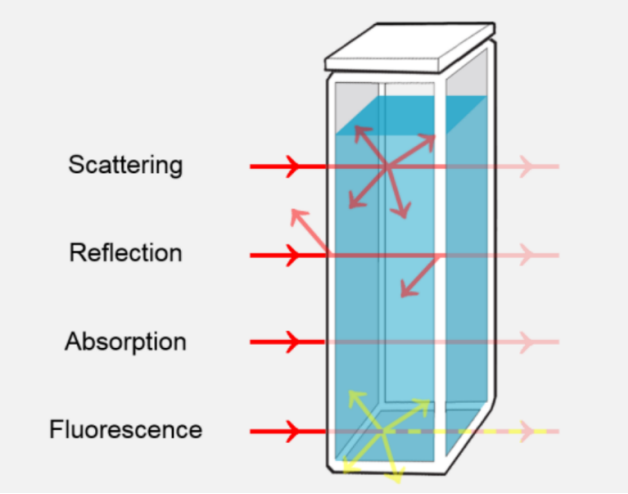

Figure 39: Possible mechanisms resulting in a decrease in light intensity in UV-Vis spectroscopy.[221]

Absorption spectroscopy, a rapid and very robust method, measures the difference in light intensity with (I) or without (I_0) a sample between 190 and 1100 nm. Upon irradiation, the absorption profile of a spiropyran-containing polymer changes since the non-polar spiropyran-form and the zwitterionic merocyanine-form have different electronic structures. In this case, the absorbance of light follows the Beer-Lambert Law:

$$Abs = lg\left(\frac{I}{I_0}\right) = \varepsilon_\lambda * c * d \quad (1)$$

The absorbance of a sample is linearly-dependent on the molar extinction coefficient (ε_λ), the concentration of the molecule (c), and the path-length (d). The molar extinction coefficient depends on the measured wavelength, which means for the spiropyran example, that the molar extinction coefficient of the SP-form at 550 nm is significantly lower than the extinction coefficient of the MC-form at 550 nm.[207] For simplification the concentration of the MC-form in a solution is directly linked to the absorbance at 550 nm. This law, however, only holds at low concentrations. However, the change in light intensity reaching the detector in the wavelength range from 300 to 650 nm can be completely attributed to elastic scattering of the spiropyran moiety.

On the other hand, the polymer precipitates upon heating, which results in the formation of insoluble aggregates in solution. The resulting elastic scattering of photons from these larger particles reduces the light intensity at the detector, and can be calculated according to the Rayleigh Scattering Equation:

$$T\,(\%) = \frac{I}{I_0} = \frac{1+cos^2\theta}{2R^2}\left(\frac{2\pi}{\lambda}\right)^4\left(\frac{n^2-1}{n^2+2}\right)^2\left(\frac{d}{2}\right)^6 \quad (2)$$

The transmittance of a sample containing solid spherical particles is calculated from the diameter of the particles (d), their refractive index (n), the distance of the particles (R), the scattering angle (ϑ), and most importantly the wavelength of the unpolarised beam (λ). At a wavelength of 700 nm, the absorbance of the spiropyran molecules can be neglected so the change in light intensity here can be completely attributed to inelastic scattering. To summarise, both effects lead to a reduced light intensity reaching the detector, but due to different reasons. This enables us to follow both responses simultaneously. To clarify the difference between both responses, the absorbance of the photo-response is measured; whereas, the transmission of the thermo-response is measured. In order to trigger both responses, *i.e.*, to light and to temperature, the sample must be heated and irradiated simultaneously.

5.4.1.1 Testing the Experimental Setup

For the irradiation of the samples, two systems are used in this thesis: LEDs and a Hg(Xe)-Lamp equipped with different filters. The emission wavelengths of the LEDs and the transmission of the filters are shown in Figure 40.

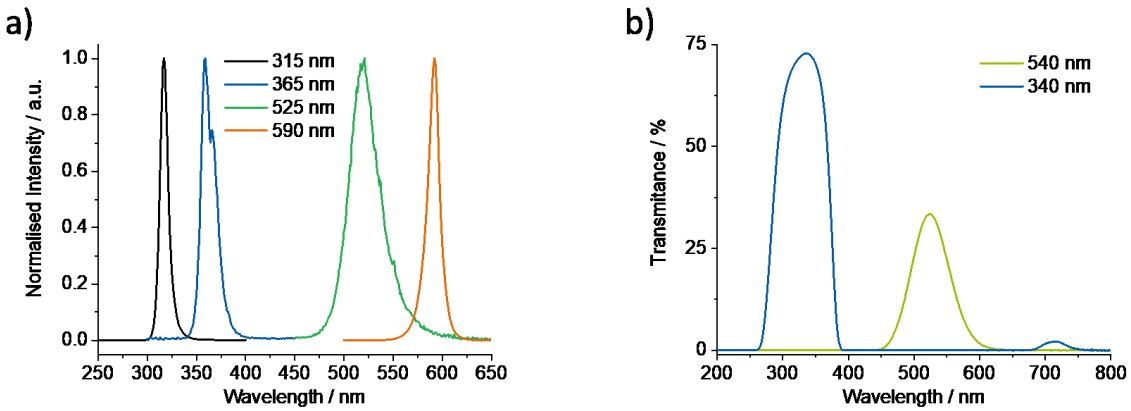

Figure 40: a) Normalised emission spectra of the 315, 365, 525, and 590 nm LEDs used here, and the b) absorption spectra of the filters used to filter the light of the fibre-coupled 200 W Hg(Xe)-lamp system. The colours refer to the colour of the LEDs and filters.

The normalised intensities of the LEDs used show a sharp intensity maximum for all investigated wavelengths. The broadest source, the LED with a maximum at 525 nm, has a variation of ± 30 nm, while the other LEDs show a variation of only ± 15 nm. On the other hand, the filters allow a broad range of wavelengths to pass and irradiate the sample. While the maximum itself is still in a comparable range, it is significantly broadened to ± 60 nm. However, the location of the irradiation wavelength can be considered less important, if the irradiation energy is higher in general. Therefore, the irradiation energy was determined for each device (Table 7).

Table 7: Irradiation intensity of the used irradiation sources.

Irradiation source	Irradiation energy / mW / cm²
LED 315 nm	8.2
LED 365 nm	3.4
LED 525 nm	2.4
LED 590 nm	4.5
Hg (Xe) 340 nm	10.6
Hg (Xe) 540 nm	10.6

Both irradiation sources permitted the intensity to be modulated. However, the highest intensity was used for all experiments. Furthermore, irradiation of the samples in the UV-Vis absorption spectrophotometer could interfere with the detection. Therefore, a sample polymer was irradiated with the Hg(Xe) lamp using both filters (Figure 41).

All three absorption spectra of the same polymer show no significant variation. We can therefore conclude that stray light from irradiating the sample does not interfere with the UV-Vis measurements.

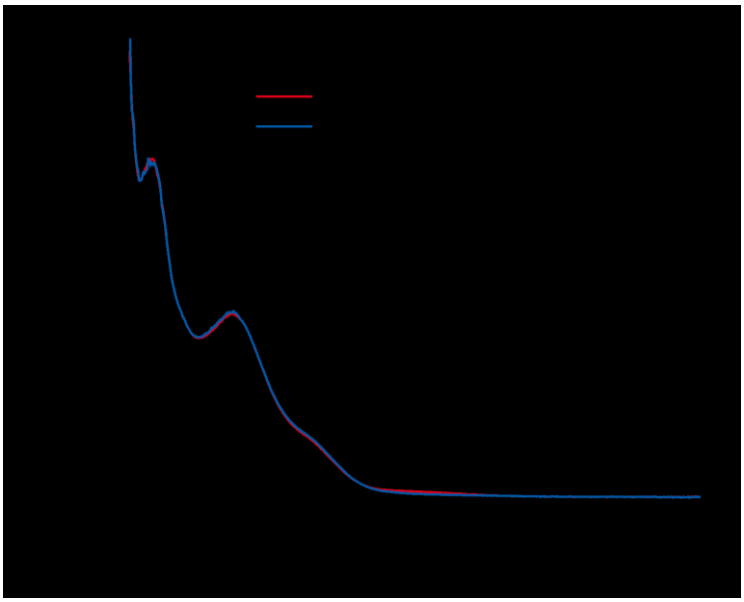

Figure 41: P(NIPAAm$_{383}$-co-SPA$_4$) with and without irradiation at 340 and 540 nm.

Although heating the sample is relatively straightforward, the stability of the device was also examined. The heating protocol consists of an equilibration time of 30 min before the first measurement is recorded (not shown here). At each temperature, there is an additional waiting time of 10 min before the spectra is measured (Figure 42).

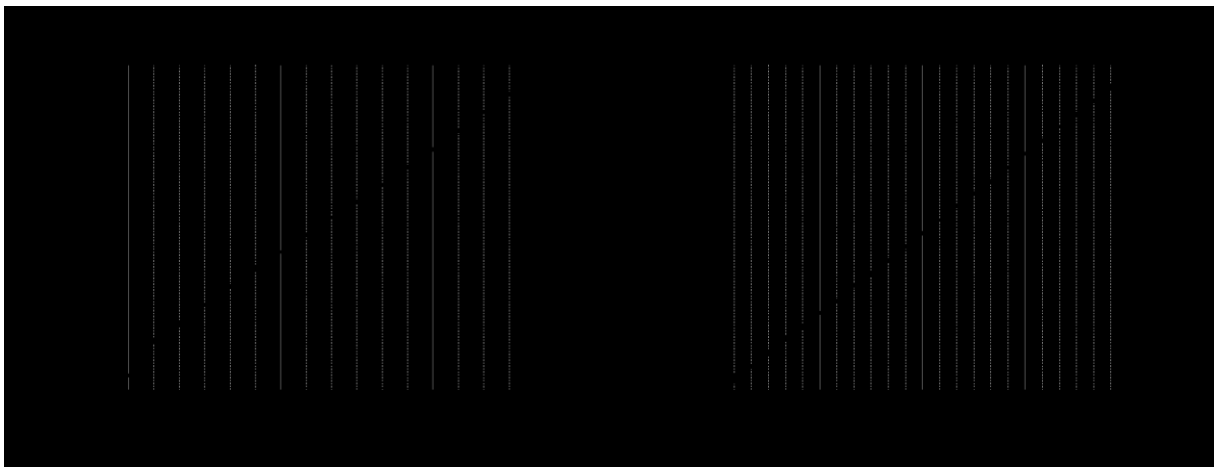

Figure 42: Temperature measured during the heating protocols: a) heating from 15 to 30 °C in 1 °C steps, averaged over 15 measurements, b) heating from 5 to 50 °C in 2 °C steps.

The temperature is stable until a new temperature is set and once a new temperature is set, the desired temperature is reached within 10 min. The device takes some time to reach the desired temperature, particularly for temperatures below room temperature where the device overheats slightly (compare Figure 42a). But even at high temperatures, the desired temperature is reached before the measurement is performed.

5.4.1.2 Investigation of the Transition Temperature with Various Additives

The thermo-response of PNIPAAm depends on the complex interactions between the polymer, the solvent, and any additives. These interactions can shift the transition temperature higher or lower. Low concentrations of salt or different pH-values do not have an effect on the transition temperature.[143] In fact, salt buffer solutions with an ionic strength of ~50 mM were not found to have

a measurable effect on the transition temperature. Increasing amounts of additive in an aqueous solution, however, tend to have an effect, and this can increase with concentration. The addition of additives to a thermo-responsive PNIPAAm solution can also be beneficial for some measurements, *e.g.*, by increasing the viscosity and therefore also decreasing the movement speed of single particles tracked inside a membrane (see chapter 0). Suitable additives to achieve higher viscosity include sugars such as glucose or other organic solvents such as thiodiethanol (TDE). The latter is further advantageous, presenting a high refractive index, which increases the signal-to-noise ratio of a measurement.

Aqueous solutions of $PNIPAAm_{418}$ (1 g/L) with varying amounts of glucose or TDE were prepared. These solutions were then heated from 20 to 40 °C and the transmission at each temperature measured (Figure 43). The amount of glucose ranges from 0 to 40 wt%, and the amount of TDE ranges from 0 to 20 vol%.

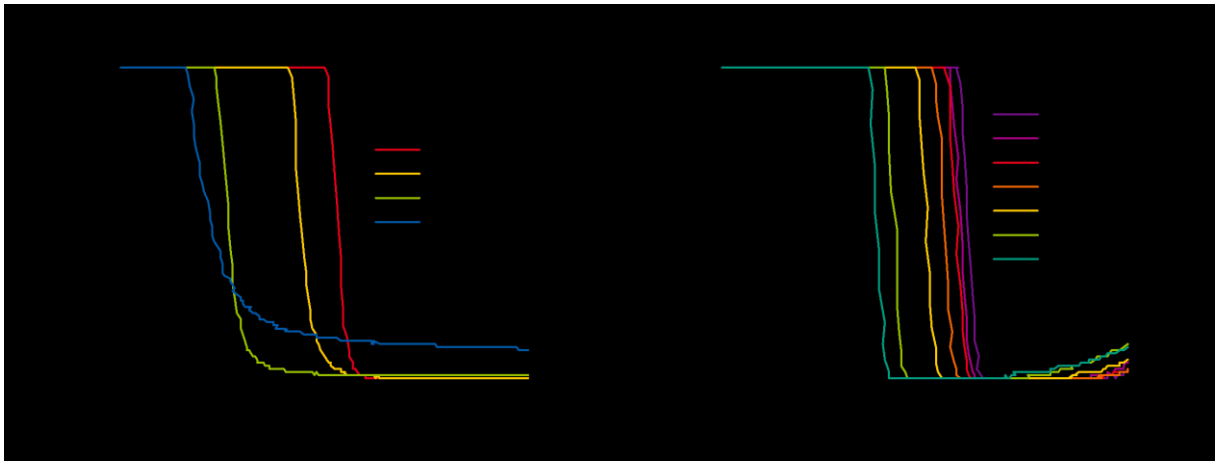

Figure 43: Determination of the cloud point in water with varying amounts of glucose (a) and thiodiethanol (b).

Heating a solution of PNIPAAm above the transition temperature leads to precipitation and reduced transmission. The transition temperature is the temperature where the measured temperature reaches halfway between the maximum and the minimum transmission. The addition of additives leads to a decrease in the transition temperature of PNIPAAm, and the effect scales linearly with the amount of additive. With increasing amounts of glucose, the transition temperature becomes less sharp, and at a glucose concentration of 40 %, the minimum cannot be determined, resulting in a higher uncertainty in the actual transition temperature. The transmission of the TDE-containing samples appears to increase again at increasing temperatures due to aggregation and precipitation of the insoluble polymer. However, the transition temperature remains sharp irrespective of the amount of TDE. To compare both additives more precisely, the transition temperatures were fitted using a linear fit; the intercept, slope, as well as the R^2 value, are given in Table 8.

Table 8: Linear fit of the transition temperatures of PNIPAAm dissolved in aqueous solution with different amounts of glucose or thiodiethanol.

Additive	Intercept	Slope	R^2
Glucose	32.04	-0.196	0.929
Thiodiethanol	32.27	-0.240	0.996

The linear fits have a certainty (R^2) of 92.9 % (glucose) and 99.6 % (TDE), which allows the transition temperatures to be predicted based on the amount of additive added. The slope is higher for TDE-

containing solutions, which means TDE effects the transition temperature more than glucose. So, one can adjust the transition temperature precisely using lower quantities of TDE than glucose. The transition temperature of PNIPAAm in a solution containing glucose further shows a blurring of the transition temperature, which is not observed for TDE. The advantages of using TDE as an additive over glucose prompted the use of TDE as a cosolvent in our tracking experiments later on in chapter 0.

5.4.1.3 Investigation of the Photo-Response at Different pH-Values

The solution pH has a significant effect on the photo-response in our single-molecule experiments for spiropyran in aqueous solutions.[207] Hence why the effect of the pH on the photo-response of the copolymers needs to be determined. The expected behaviour of SPA upon irradiation in aqueous solution is shown in Scheme 11 according to previous literature reports.[32, 218]

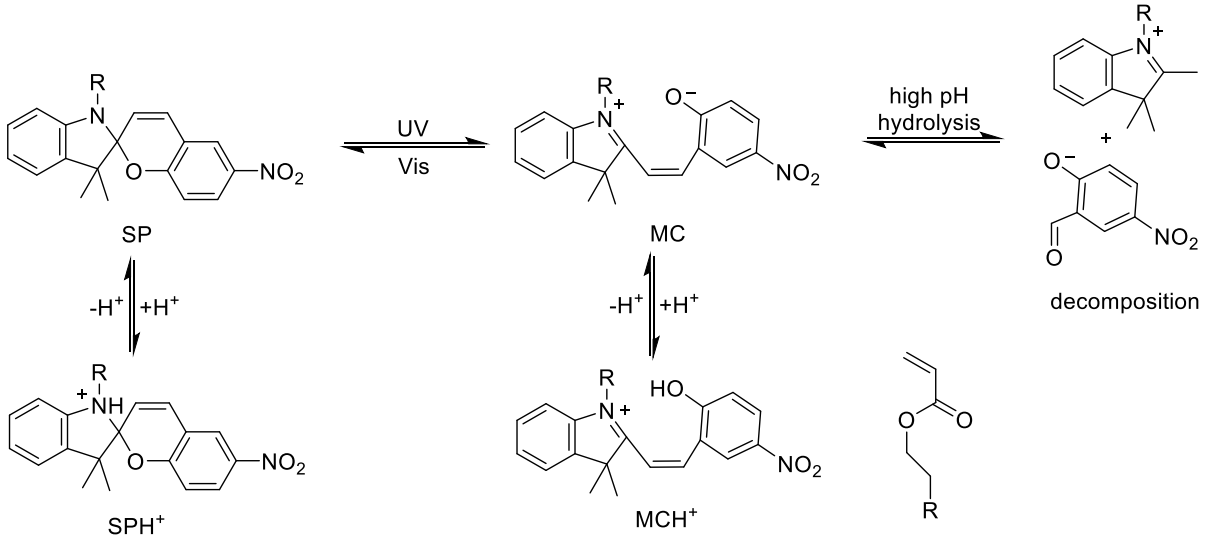

Scheme 11: Simplified expected behaviour of the SPA moiety in copolymers upon irradiation at various pH-values.[207]

The SPA can be switched from the spiropyran (SP) to the merocyanine (MC) form upon irradiation with UV light and back again by irradiation with green light. Both forms can be protonated, which is indicated in the structure by the H^+. Naturally, the protonation of the two positions exhibits a different pK_a-value, and the protonation of the merocyanine has a pK_a of ~4, whereas the protonation of the spiropyran has a pK_a of ~1. The merocyanine-form is also known to hydrolyse and decompose at high pH. Single-molecule experiments have shown that all five forms have a different absorption maximum, which makes it possible to distinguish them separately by UV-Vis spectroscopy. In order to compare the single-molecule experiments to SPA-containing copolymers, a 1 g/L solution of P(NIPAAm$_{538}$-*co*-SPA$_6$) at different pH-values were prepared. The measurements were performed at 15 °C to separate the photo-response of the polymer from the potential thermo-response. The absorption spectra measured for different pH-values are shown in Figure 44.

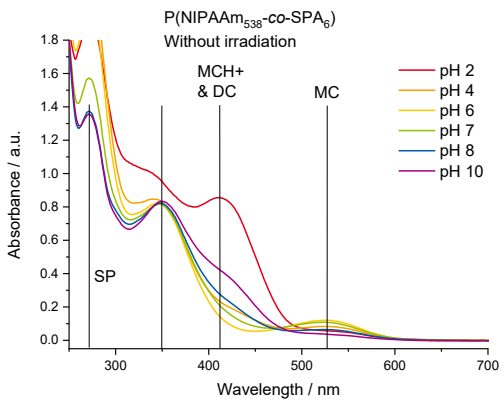

Figure 44: Absorption spectra of P(NIPAAm$_{538}$-co-SPA$_6$) in aqueous solution at varying pH-values at 15 °C. Lines refer to the literature known absorbance maxima of the respective states (for structure abbreviations, refer to Scheme 11).

The absorbance spectra of the copolymer, P(NIPAAm$_{538}$-*co*-SPA$_6$), varies with the solution pH, and the maxima correspond to that of the single molecules. All copolymers show the absorption at 270 nm, which corresponds to the SP-form but is also partially associated with the copolymer itself due to the NIPAAm units. The highest absorbance in that region appears at acidic pH because of the higher absorbance of the protonated SPA moiety in this region compared to the unprotonated equivalent. For most samples, a small quantity of the MC-form was observed at 540 nm, and at around 400 nm the protonated SP- and MC-form were found, as well as the potentially decomposed spiropyran moiety. The decomposition of spiropyrans upon irradiation is highly discussed in the literature. In aqueous solutions, we expect decomposition to occur *via* hydrolysis as well as by oxidation. The signals that appear around 420 nm are highest at pH 2 where all species are protonated, and at pH 10 where the SPA moiety is vulnerable to hydrolysis. The samples were subsequently irradiated with 340 nm light for 30 min (Figure 45a), and then with 540 nm light for 30 min directly afterwards (Figure 45b). An absorption spectrum was recorded after each irradiation process.

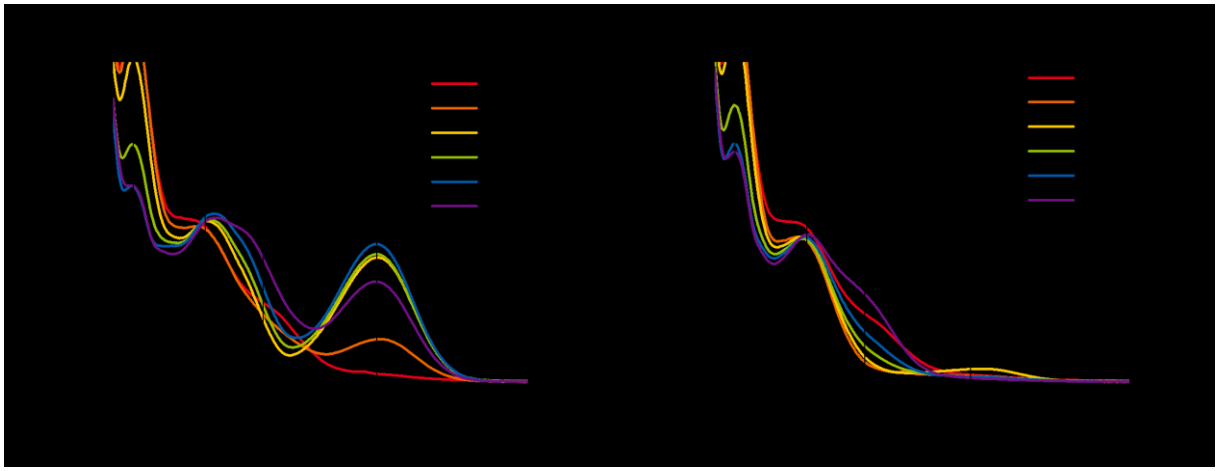

Figure 45: Absorption spectra of P(NIPAAm$_{538}$-co-SPA$_6$) at different pH-values after irradiating at a) 340 or b) 540 nm for 30 min at 15 °C. The vertical lines indicate the absorbance maxima of each respective SPA state.

Comparing Figure 45a to b, the most apparent difference is the decreased absorbance at 540 nm. This absorbance is attributed to the amount of merocyanine in solution and is also pH-dependent. The intensity of the merocyanine signal at 540 nm after irradiation at 340 nm appears to decrease as the pH decreases, resulting in no apparent change at pH 2. Whilst the absorbance at 270 nm exhibits the reverse behaviour, but to a lower extent, and is attributed to the spiropyran-form. This is why the signal at 540 nm is used to monitor the change in concentration of merocyanine upon irradiation in all

future investigations. We also see variations in the absorbance spectra at 420 nm after the first irradiation at 340 nm, and subsequent irradiation at 540 nm. This signal is attributed to the protonated merocyanine, as well as to the decomposition products, and shows a significant increase at pH 10 due to decomposition.

The transition from the spiropyran- to merocyanine-form can be easily illustrated by plotting the absorbance at 540 nm with time for both irradiation experiments: 340 nm for 30 min, and 540 nm for 30 min (Figure 46).

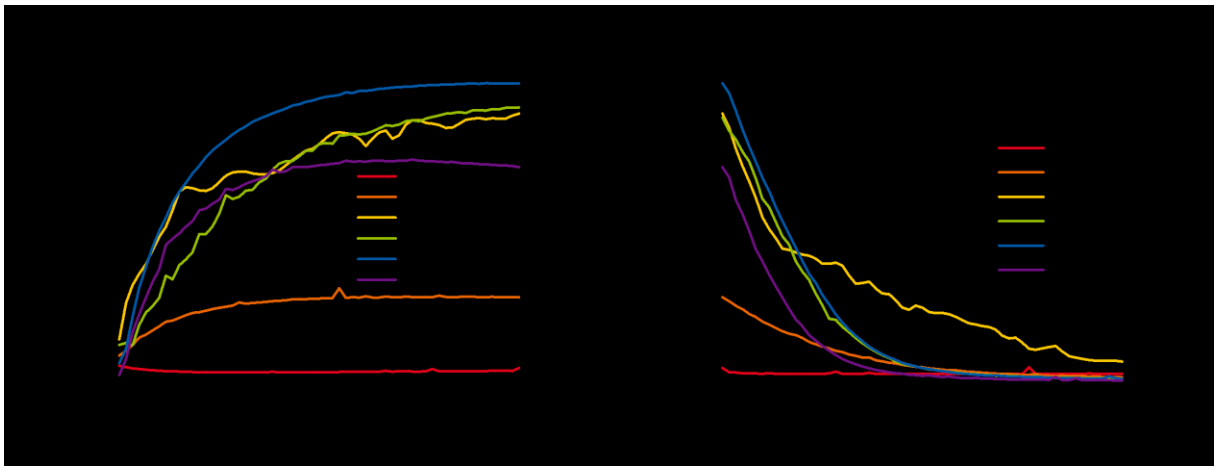

Figure 46: Change in absorbance at 550 nm of P(NIPAAm$_{538}$-co-SPA$_6$) at different pH-values during irradiation with a) 340 nm and b) 540 nm light at 15 °C.

As we already expected, at pH 2 the absorbance at 540 nm does not vary significantly since the SPA moiety is protonated and the photo-response can be neglected. At pH 10, the absorbance increases at first but then decreases again upon further irradiation. This behaviour can be attributed to the decomposition of the photo-responsive moiety. The response speed also increases with pH, with pH 10 showing the fastest response. This can be attributed to less protonated species being present at higher pH-values. The observations made for the transition from the SP- to MC-form reverse upon irradiation with 540 nm light. All pH-values lead to the same minimum absorbance at 540 nm, which means that the SPA moiety is switched to the least possible number of merocyanine. The minimum absorbance after irradiation at 540 nm is even lower than the absorbance at 540 nm for some of the samples before irradiation. This observation indicates the copolymer exists in a thermal equilibrium that is not shifted completely to the SP-form of the SPA moiety.[208] To better understand the kinetics of the response, the change in absorbance at 540 nm over time was fitted using first-order kinetics (Figure 47). First-order kinetics was chosen since excitation of the photo-responsive moiety only depends on one molecule. The signal intensity of a sample predominantly depends on the concentration of the SPA moiety in solution, whereas the transition speed depends on the probability a photon excites an SPA moiety, and therefore on the intensity of the light source.

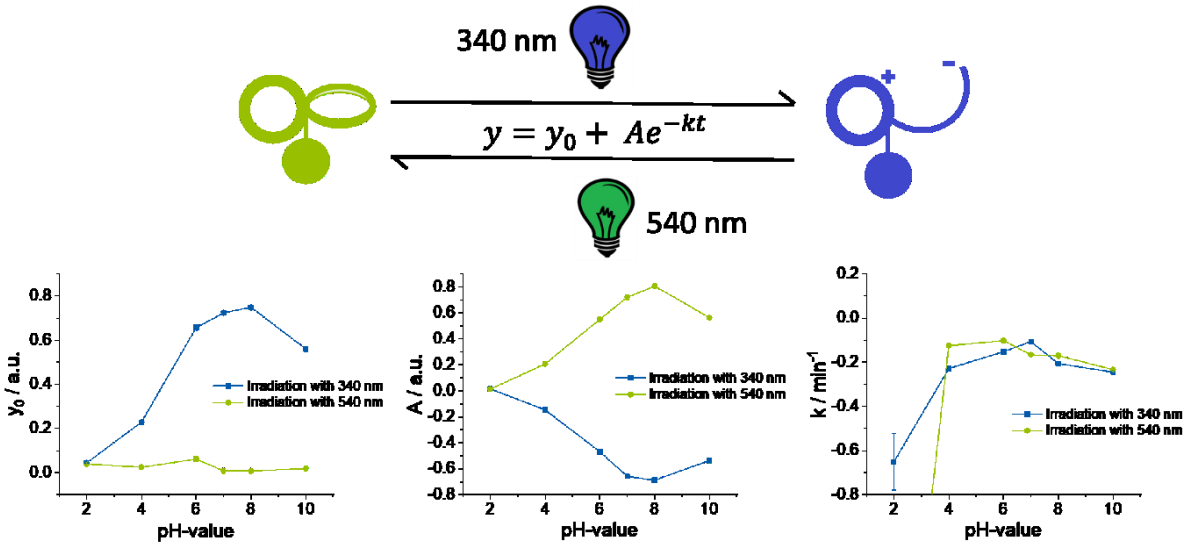

Figure 47: Switching of the SPA moiety between the SP- to MC-form. The y-axis refers to the fitted parameters using first-order kinetics ($y = y_0 + Ae^{-kt}$), which are also given in Table 9.

The first-order kinetics equation used to plot the change at 540 nm upon irradiation consists of three variables: "y_0", "A", and "k". "y_0" indicates the threshold of every experiment and naturally it is higher for the experiments irradiated with 340 nm than for the irradiation with 540 nm. Furthermore, the absorbance at 340 nm increases with increasing pH, before decreasing again at pH 10. For the experiments irradiated at 540 nm, no trend is observed. The second variable "A" determines the difference between the "end-point" and the "start" of the measurement. Naturally, these numbers are negative upon irradiation at 340 nm and positive upon irradiation at 540 nm. The most interesting factor, "k", represents the speed of the reaction, and which is not obvious from the graphs presented in Figure 46 alone. The more negative this value is, the faster the material responds. Here, we observe as expected that the reaction speed increases with pH, with the fastest response is observed at pH 10. The first order parameters with pH are summarised in Table 9.

Table 9: Calculated reaction constants for P(NIPAAm$_{538}$-co-SPA$_6$) at different pH-values.

pH	$[y_0]$(green)	A(green)	k(green)	$[y_0]$(UV)	A(UV)	k(UV)
2	0.03916	0.01365	-2.31773	0.04404	0.0147	-0.65091
4	0.02433	0.20678	-0.12487	0.22833	-0.14654	-0.22859
6	0.06154	0.55109	-0.10243	0.65712	-0.46856	-0.15204
7	0.00812	0.72066	-0.16587	0.72326	-0.6591	-0.10682
8	0.00714	0.80662	-0.17001	0.74883	-0.68844	-0.20607
10	0.01888	0.56278	-0.23346	0.56007	-0.53651	-0.24484

Fitting the irradiation experiments enables a more in-depth analysis and understanding of the photo-response of the SPA moiety at various pH-values. Else the response speed is only accessible by a qualitative comparison. To summarise, pH 8 appears to be the most suitable pH to measure the photo-response of the copolymers in aqueous solution. The copolymer exhibits a fast response to irradiation and shows no decomposition upon irradiation at 340 nm for 30 min at this pH-value. Furthermore, the change upon irradiation is maximised at this pH. Consequently, all subsequent measurements are performed at pH 8.

5.4.2 Photo-Responsive Behaviour of SPA-Containing Copolymers

All sets of copolymers prepared previously were dissolved in pH 8 TRIS buffer solution and their photo-response investigated. The dissolved copolymer sets of P(NIPAAm-*co*-SPA) and P(TEGA-*co*-SPA) were irradiated at 340 nm for 30 min followed by irradiation at 540 nm for 30 min for one switching cycle. For all copolymers, three consecutive switching cycles were performed at 15 °C to neglect any effect of the thermo-responsive moiety. Since the set of P(NIPAAm-*co*-SPA) copolymers is solid, their photo-response was also investigated in the solid-state.

5.4.2.1 Photo-Response in Basic Aqueous Media

All copolymers were dissolved in a pH 8 TRIS buffer solution before being irradiated according to the previously described protocol of 340 nm for 30 min and then 540 nm for 30 min to form one switching cycle. Three switching cycles were carried out in total. Exemplary absorbance spectra of P(NIPAAm$_{1108}$-*co*-SPA$_{17}$) and P(TEGA$_{142}$-*co*-SPA$_{15}$) at the very beginning and the end of each irradiation step are shown in Figure 48.

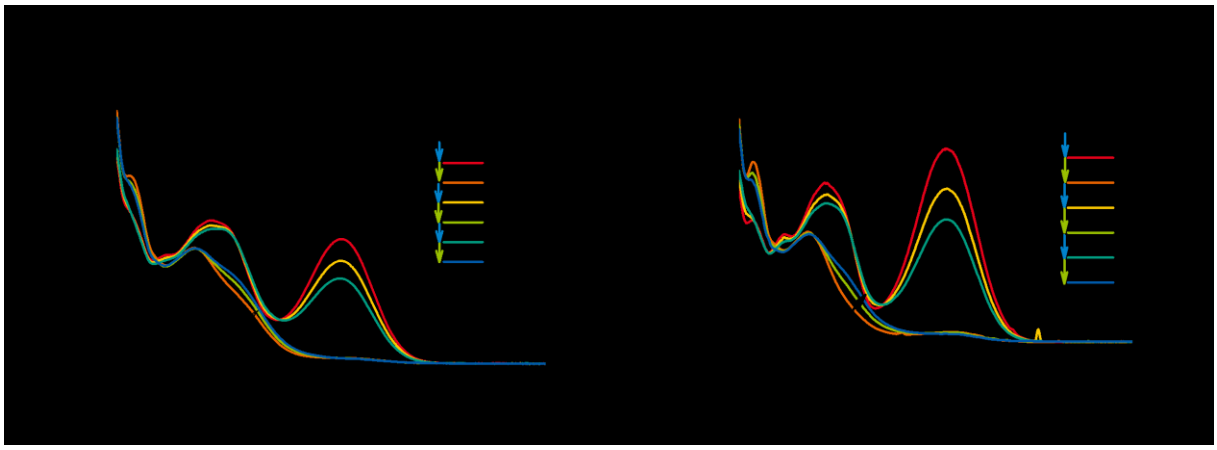

Figure 48: Absorption spectra of P(NIPAAm$_{1108}$-co-SPA$_{17}$) (a) and P(TEGA$_{142}$-co-SPA$_{15}$) (b) in pH 8 TRIS buffer solution at 15 °C over three irradiation cycles. Signals at 270 nm are assigned to the spiropyran-form (SP), signals at 540 nm are assigned to the merocyanine-form (MC), and the decomposition (DC) products are assigned to 400 nm.

As expected for both copolymers, the signal at 540 nm attributed to the merocyanine-form increases upon irradiation with UV light and decreases again upon irradiation with green light. For both P(NIPAAm$_{1108}$-*co*-SPA$_{17}$) and P(TEGA$_{142}$-*co*-SPA$_{15}$), the maximum absorbance observed at the beginning before irradiation is never reached again. This loss in intensity after every cycle appears to scale with the increased intensity at 400 nm, which is assigned to the decomposition and/or protonation of the merocyanine-form. In both cases, we see that some of the SPA moieties do not switch back to the spiropyran-form upon irradiation. This effect is more apparent for the TEGA-containing copolymers than for the NIPAAm-containing copolymers. This trend may be attributed to the higher quantity of SPA moieties incorporated in the P(TEGA-*co*-SPA) copolymers. In addition to the signal at 540 nm, a signal at 380 nm appears and undergoes the same increase and decrease as the signal at 540 nm, which is assigned to the spiropyran/merocyanine transition. This absorption band has also been assigned to the merocyanine-form in previous literature reports.[222] The previously described behaviour is observed for all copolymers examined irrespective of the amount of SPA present within the copolymer, but for simplicity, we have only shown the spectra for the two copolymers containing the highest amount of SPA. As the most noticeable change for all copolymers occurs at a wavelength of 540 nm, the absorbance at this wavelength was selected and plotted over time for all copolymers (Figure 49).

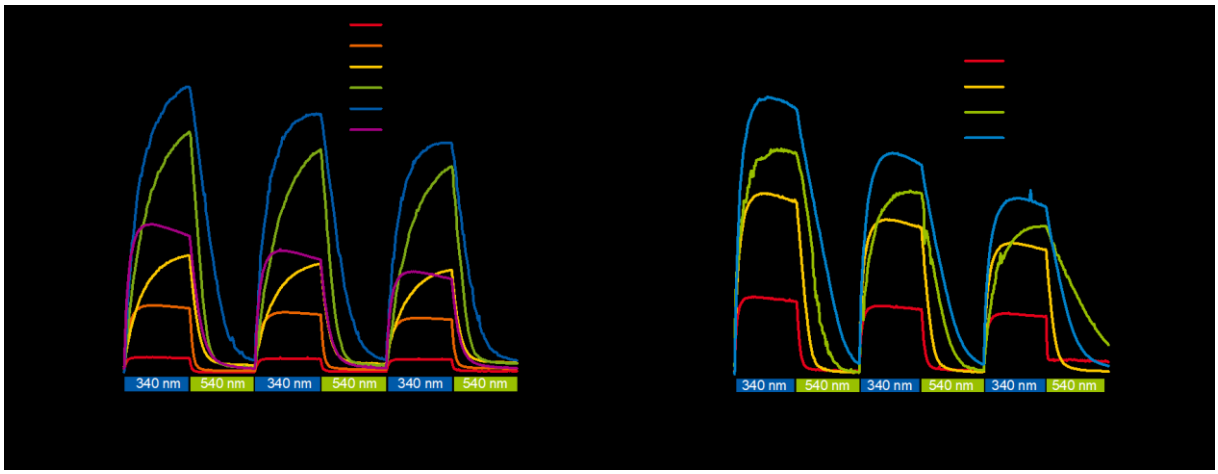

Figure 49: Absorbance of the copolymers containing SPA moieties after irradiation with a 200 W Hg(Xe) lamp. Three cycles were performed alternating between a 340 and 540 nm filter for 30 min each at 15 °C. The concentration of the copolymers in a pH 8 TRIS buffer is given in parentheses. For the P(TEGA-co-SPA) copolymers the concentration is fixed to 0.125 g/L.

The absorbance of all copolymers increases at 540 nm upon irradiation at 340 nm and decreases again upon irradiation at 540 nm. This irradiation cycle can be repeated at least three times without an appreciable loss in intensity. Although all samples see a decrease in their intensity over these three cycles, which can be attributed to decomposition processes and/or protonation of the SPA moiety. Naturally, the overall absorbance intensity is linked to the amount of SPA units in solution, which results in an increased absorbance for the P(TEGA-*co*-SPA) copolymers. However, the P(NIPAAm-*co*-SPA) copolymers were examined at various concentrations, to increase the signal-to-noise ratio for the copolymers containing low amounts of SPA. Hence, the absorbance is not comparable for all samples.

Another notable observation is the differing shape of the above time traces between Figure 30a and b; for the NIPAAm-containing copolymers, the absorbance generally increases rapidly, whilst for the TEGA-containing copolymers, the absorbance increases to a threshold. To better understand this effect, the first cycle of both sets of copolymers was normalised, and the results are shown in Figure 50.

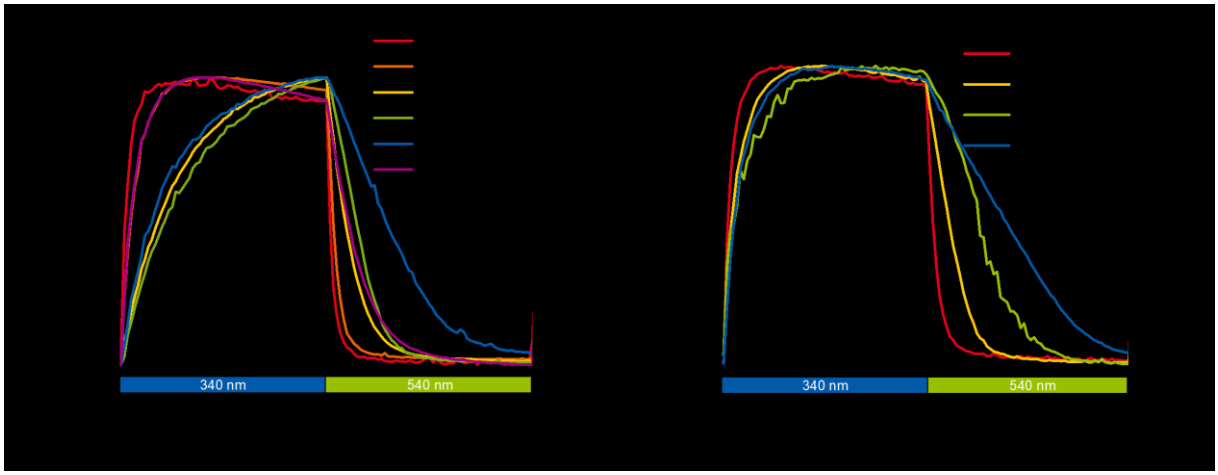

Figure 50: Normalised photo-response of the first switching cycle of (a) P(NIPAAm-co-SPA) and (b) P(TEGA-co-SPA).

Normalising the intensity reveals that some copolymers reach a maximum rapidly and then slowly decrease again, while others increase to a certain threshold. There is no obvious trend to explain this observation, which is only visible upon irradiation with 340 nm. At this wavelength, the majority of SPA moieties are present in the merocyanine-form. From here, the molecule can decompose or be

protonated (Scheme 11), and in both cases the absorbance at 540 nm changes. The normalised plots also make it easier to compare the speed of the photo-response of the copolymers. Unfortunately, the normalised plots of the P(NIPAAm-*co*-SPA) copolymers are not really comparable to each other because they were recorded at different concentrations for high amounts of SPA, which also affects the speed of the response. The P(TEGA-*co*-SPA) copolymers are better comparable and show an interesting trend. As the amount of SPA incorporated within the copolymer decreases, the molecule switches faster. During irradiation experiments, the concentration of the copolymers is kept constant, and therefore the number of SPA moieties in solution is less for copolymers with smaller amounts of SPA. The irradiation, on the other hand, is the same for all copolymers and the amount of photons per photo-responsive moiety is higher for copolymers with a smaller amount of SPA. Hence why the copolymers with a smaller amount of SPA respond faster to irradiation. To visualise this, all traces were plotted using first-order kinetics (compare to Figure 47). In Figure 51 all three cycles were fitted, resulting in an average value with the corresponding error.

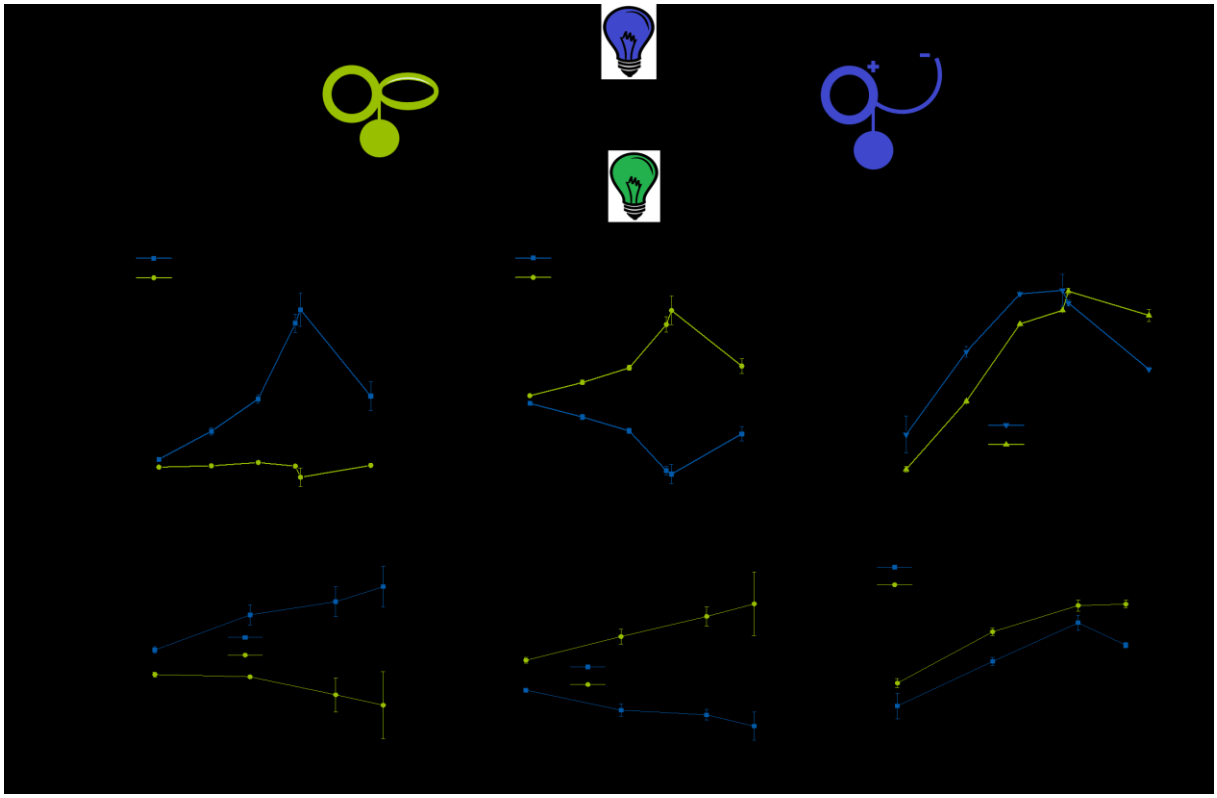

Figure 51: Switching of the SPA moiety between the SP- to MC-form. Different P(NIPAAm-co-SPA) (Top) and P(TEGA-co-SPA) (bottom) copolymers were dissolved in pH 8 buffer solution and sorted after the amount of SPA. The y-axis refers to the fitted parameters using first-order kinetics ($y = y_0 + Ae^{-kt}$), which are also given in Table 10.

The plots of the fits show similar patterns as shown before for the photo-response of the copolymer at different pH-values. On the left, the threshold y_0 of each fit is given. Irradiation at 340 nm leads to an increase in the threshold absorbance y_0 for increasing amounts of SPA in solution, which appears to follow a linear trend with increasing amount of SPA in the copolymer. For all P(NIPAAm-*co*-SPA) copolymers, irradiation at 540 nm results in a threshold absorbance y_0 around 0, whilst for the P(TEGA-*co*-SPA) copolymers the threshold absorbance y_0 decreases below zero for increasing amounts of SPA in the copolymers. This is a mathematical issue since the waiting time at the threshold is reached for a short time, hence why these results are not further discussed. The difference between the end and start (A) also reflects the previous observation: increasing amounts of SPA increase the change in absorbance at 550 nm between the end and start point. The value of A increases linearly as the number

of SPA moieties in the solution increases. This effect can be seen more clearly for the P(TEGA-*co*-SPA) copolymers since all the copolymers here were dissolved at the same concentration. All trends discussed so far for the threshold value (y_0) and the difference between the final and initial absorbance (A) are accompanied by an increase in the associated error, which is attributed to a higher amount of SPA potentially being protonated or decomposed during the measurement. Naturally, this effect is less apparent for the P(NIPAAm-*co*-SPA) copolymers, since they contain less SPA than the P(TEGA-*co*-SPA) copolymers. If we now look at the reaction speed (k), a linear trend is observed; increasing amounts of SPA in the copolymer lead to a slower reaction speed for both sets of copolymers. Furthermore, the reaction speed upon irradiation at 340 nm (blue trace) is always faster than with irradiation at 540 nm (green trace). This is attributed to a higher overlap in the emission of the irradiation source and the absorption of the copolymers, and further to a different reaction speed of the single SPA moiety itself. Comparing both sets of copolymers, the photo-responsive behaviour of the SPA moiety is not significantly affected by the copolymerised thermo-responsive moiety, neither NIPAAm nor TEGA. The overall trends described above apply for both thermo-responsive units, but the values themselves are not comparable since the irradiation experiments were performed at different concentrations. The higher concentrations, especially for the P(NIPAAm-*co*-SPA) copolymers with small amounts of SPA, were used to improve the signal-to-noise ratio obtained. The averaged fitted parameters (y_0, A, and k) shown in Figure 51 are summarised in Table 10.

Table 10: Calculated first-order reaction constants for the P(NIPAAm-co-SPA) and P(TEGA-co-SPA) copolymers upon irradiation in aqueous solution.

Polymer	$[y_0]$(green)	A(green)	k(green)	$[y_0]$(UV)	A(UV)	k(UV)
P(NIPAAm$_{311}$-*co*-SPA$_1$)	0.024	0.072	-1.166	0.099	-0.075	-0.957
P(NIPAAm$_{282}$-*co*-SPA$_2$)	0.037	0.323	-0.757	0.365	-0.332	-0.460
P(NIPAAm$_{383}$-*co*-SPA$_4$)	0.068	0.601	-0.293	0.672	-0.596	-0.114
P(NIPAAm$_{538}$-*co*-SPA$_6$)	0.034	1.420	-0.212	1.388	-1.352	-0.095
P(NIPAAm$_{617}$-*co*-SPA$_7$)	-0.071	1.689	-0.098	1.517	-1.414	-0.168
P(NIPAAm$_{1108}$-*co*-SPA$_{17}$)	0.041	0.634	-0.242	0.698	-0.652	-0.566
P(TEGA$_{202}$-*co*-SPA$_5$)	0.051	0.336	-0.684	0.398	-0.365	-0.863
P(TEGA$_{175}$-*co*-SPA$_9$)	0.018	0.894	-0.281	0.893	-0.837	-0.514
P(TEGA$_{194}$-*co*-SPA$_{16}$)	-0.236	1.369	-0.074	1.080	-0.948	-0.210
P(TEGA$_{142}$-*co*-SPA$_{15}$)	-0.383	1.665	-0.064	1.291	-1.217	-0.386

In the previous sections, the photo-response of P(NIPAAm-*co*-SPA) and P(TEGA-*co*-SPA) copolymers in solution were investigated. The copolymers were dissolved, irradiated according to a defined irradiation protocol, and during the irradiation, the absorbance was recorded. The changes occurring during irradiation were shown on one exemplary example for both copolymer combinations, and the most interesting spectral changes occurred at 540 nm. This wavelength is linked to the merocyanine-form of the SPA moiety, and an increase in absorbance at this wavelength is attributed to an increase in merocyanine present in solution. The absorbance at 540 nm is plotted over time, and the absorbance traces compared. Increasing amounts of SPA in the copolymers lead to a slower but more intense photo-response. A first-order kinetics fitting of all irradiation traces results in linear trends for the maximum absorbance and reaction speed for varying amounts of SPA independent of the thermo-responsive comonomer used.

5.4.2.2 Photo-Response in the Solid-State

The photo-response of the copolymers does not only occur in solution but is also visible in the bulk material. As mentioned above, the P(NIPAAm-*co*-SPA) copolymers are solid and show a photo-response in the powdered state. In order to investigate this effect in more detail, a thin film of the copolymer was prepared on a microscope slide, and the films irradiated in a comparable manner to the previous investigations in solution. Each P(NIPAAm-*co*-SPA) copolymer was dissolved in THF at a concentration of 25 wt%. The solution (2 mL) was then cast onto the surface of a glass microscope slide using a 120 µm doctor blade to form a thin film (Figure 52). After the solvent evaporated, the film thickness was determined *via* profilometry (Figure 53).

Figure 52: Film casting procedure used to prepare thin polymer films to investigate their photo-response in the solid-state.

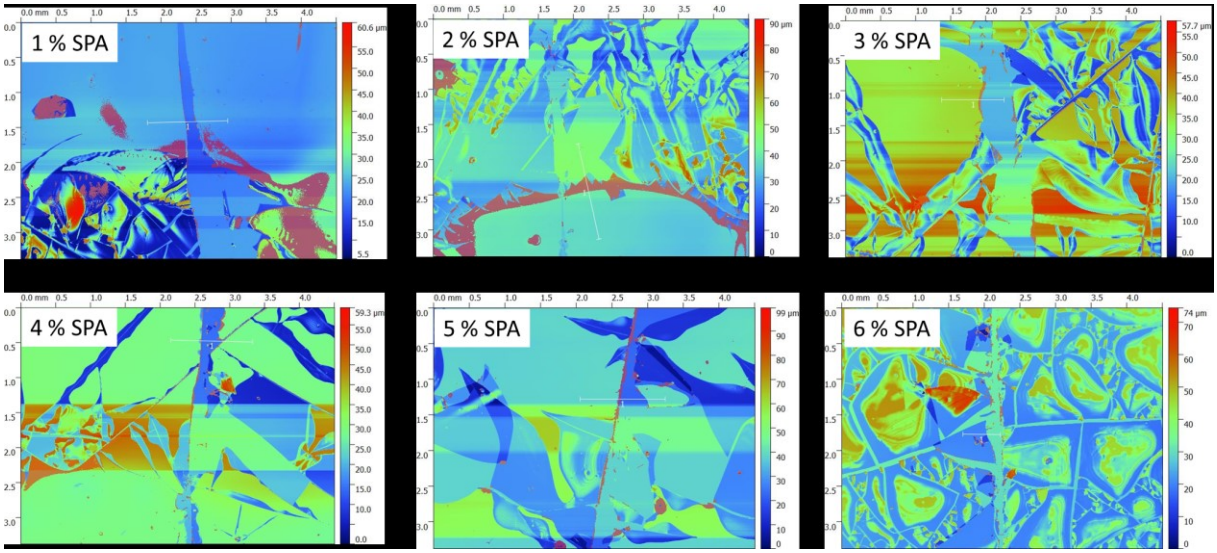

Figure 53: False-colour images of scratches in the prepared polymer films on glass substrates for thickness determination. White bars indicate the measured area.

As visible from the false colour images, the films are very brittle, resulting in a lot of cracks on the surface. The white bar in each image indicates the region used to determine the film thickness. From the height profiles, the film thickness was determined to be between 11 and 17 µm with no visible trends (Table 11).

Table 11: Summary of the thickness of the thin films prepared using a 120 µm doctor blade for subsequent investigation of their solid-state photo-response.

Polymer	Thickness / µm
P(NIPAAm$_{311}$-*co*-SPA$_1$)	16
P(NIPAAm$_{282}$-*co*-SPA$_2$)	11
P(NIPAAm$_{383}$-*co*-SPA$_4$)	16
P(NIPAAm$_{538}$-*co*-SPA$_6$)	14
P(NIPAAm$_{617}$-*co*-SPA$_7$)	17
P(NIPAAm$_{1108}$-*co*-SPA$_{17}$)	11

The colour of the copolymers in the solid-state differs slightly from the colour in solution, indicating a different absorbance maximum compared to the dissolved copolymers. To adjust the experimental setup, a quick preliminary irradiation experiment for P(NIPAAm$_{311}$-*co*-SPA$_1$) was performed with different irradiation sources to determine the most suitable irradiation source. The MC-form of the SPA moiety in the solid-state is characterised by a different absorbance maximum, and its photo-response is much slower than in solution. The application of a higher intensity light source did not result in further improvements in the speed of the photo-response (Figure 54).

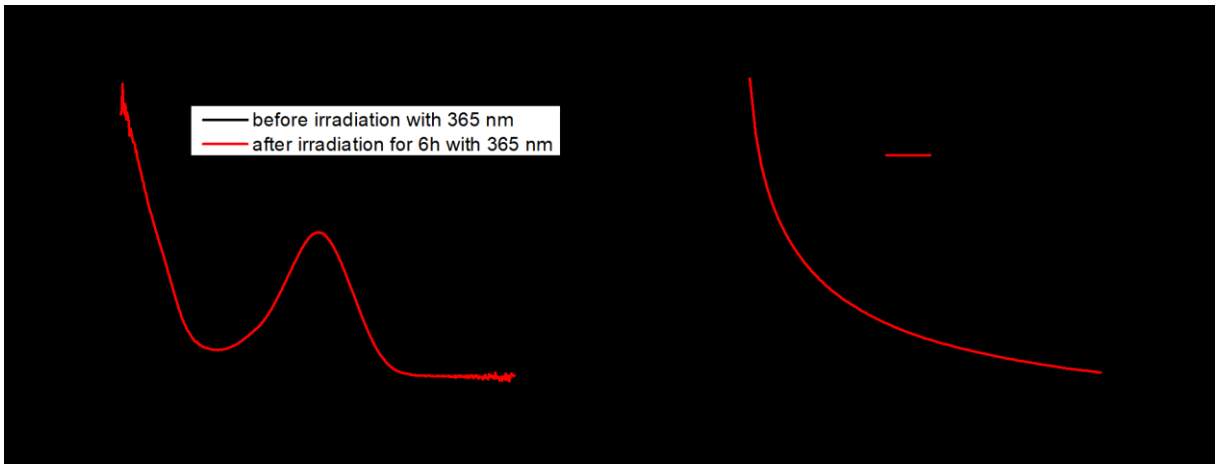

Figure 54: Absorption spectra of a P(NIPAAm$_{311}$-co-SPA$_1$) thin film on a microscope slide a) before and after irradiation at 365 nm for 6 h, and an b) irradiation time trace at 590 nm using different light sources.

Irradiation of the copolymer film with UV light reveals a shift in the absorbance maximum from 540 nm in solution to 590 nm in the solid-state. This is attributed to the different environment of the SPA moiety. Irradiation at 540 nm, as used before, does not reveal any significant changes. Hence why the light source was changed to a 590 nm LED, where the absorbance overlaps better with the LED emission. The same effect is observed for the UV irradiation: the reaction speed upon irradiation with 340 nm from before do not significantly differ from the photo-response speed by irradiation with 365 nm LED. This is why the irradiation source was changed from Hg(Xe)-lamp to two LEDs with either 365 or 590 nm. From these preliminary results, the copolymer films were subjected to irradiation at 365 nm for 6 h, followed by irradiation at 590 nm for 6 h. This cycle of irradiation was repeated for three consecutive cycles similar to the previous experiments. To conduct these irradiation experiments of the copolymer films, a customised sample holder was built, and it is shown in Figure 55.

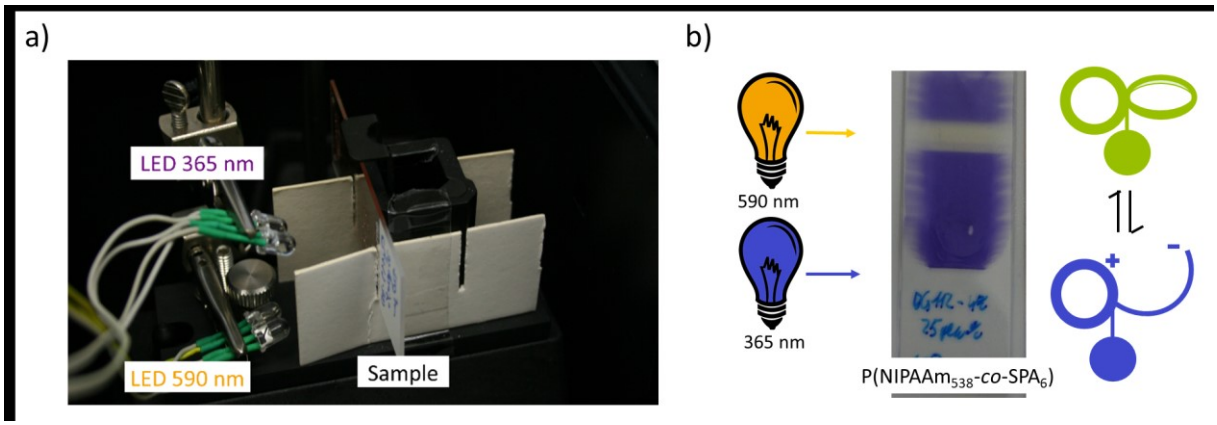

Figure 55: a) Experimental setup for the irradiation of thin polymer films of P(NIPAAm-co-SPA) on a microscope slide and the b) copolymer film before and after irradiation.

The set of P(NIPAAm-*co*-SPA) copolymers was irradiated for at least three switching cycles, which consisted of 6 h of irradiation at 365 nm followed by 6 h of irradiation at 590 nm. The spectral changes were in good agreement with our previous studies in solution, as exemplified by plotting the absorbance at 550 nm over time in Figure 56.

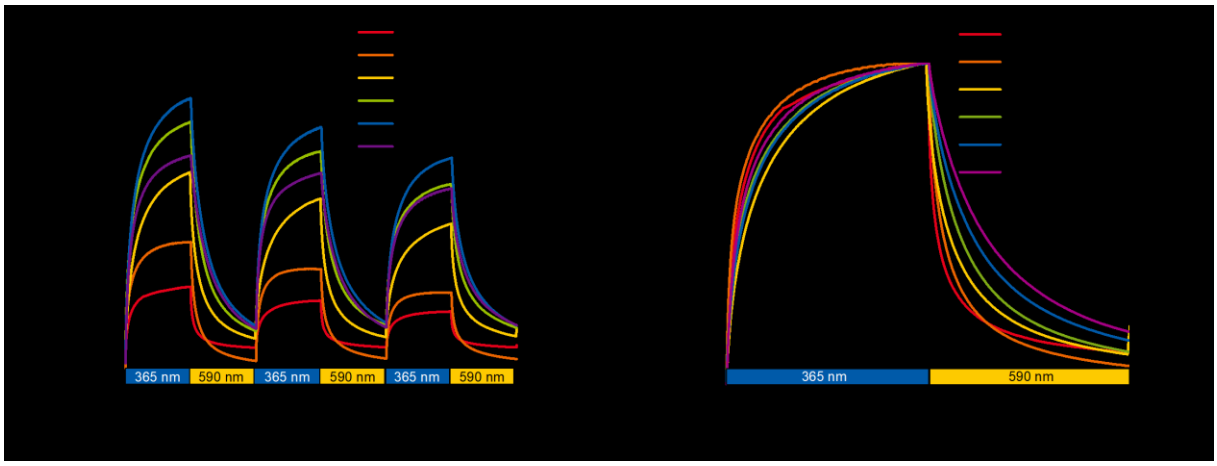

Figure 56: Change in absorbance at 550 nm for different polymer films supported on a microscope slide with in-situ irradiation at 365 or 590 nm for 6 h each over three irradiation cycles.

Irradiation of the copolymer films with UV light (365 nm) leads to an increase in the absorbance at 550 nm, whilst irradiation with visible light (590 nm) results in a subsequent decrease in the absorbance at 550 nm. Increasing the SPA content within the copolymer leads to an increase in the absorbance as expected from the irradiation experiments performed in solution. Although we should point out here that the maximum absorbance decreases throughout the irradiation experiment similar to the observations in solution. We attribute this reduction in absorbance to oxidative decomposition in this case, since protonation can be neglected in the solid-state. To confirm our hypothesis, the irradiation experiment was repeated under argon. The absorbance still decreases during the irradiation cycles, and the formation of cracks in the film were noticed. The switching of the spiropyran to the merocyanine results in mechanical stress, which leads to the formation of cracks in the copolymer film. This mechanical damage of the copolymer film results in the observed decrease in absorbance upon irradiation at 365 nm. The minimum absorbance observed fits to the thickness of the copolymer film itself, which also can have a slight influence on the maximum or the change in absorbance during irradiation. The previous investigations of the photo-response suggested that the amount of SPA in the copolymer also influences the speed of the photo-response. To elucidate whether

this is still the case in the solid-state, the absorbance of the first cycle was normalised and plotted against time (Figure 56b). In agreement with the P(TEGA-*co*-SPA) copolymers in solution, the copolymer with the lowest amount of SPA shows the fastest response upon irradiation in the solid-state. Similarly, to our previous experiments in solution, it is also possible to quantify this effect by fitting all three irradiation cycles. The results are shown in Figure 57.

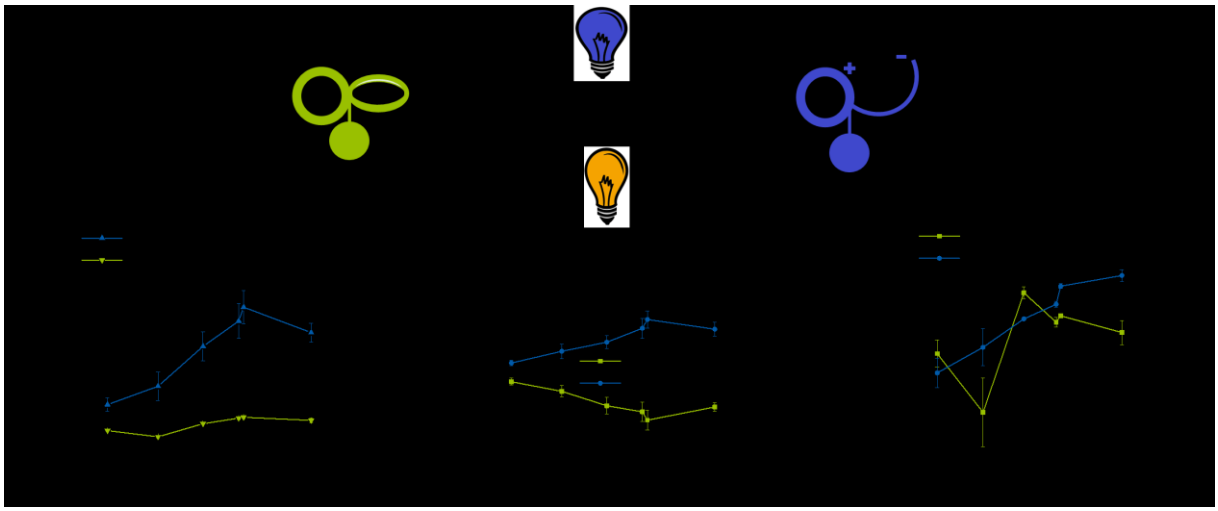

Figure 57: Plot of calculated reaction constants from irradiation experiments in the solid-state fitted over three switching cycles. The variables of the fitted equation are indicated on the corresponding y-axis.

The fitted parameters shown in Figure 57 are in close agreement to the previous switching kinetics observed previously for the photo-response of copolymers in solution. Increasing amounts of SPA lead to an increased absorbance upon irradiation at 365 nm, and also to a higher change in absorbance. The reaction speed decreases for increasing amounts of SPA in the copolymers. The value for "k" determined here is approximately one-tenth of the reaction speed of the copolymers in solution, because of the higher restriction in the solid-state for the opening and closing of the SPA moiety, which is, in fact, a mechanical movement. The fitted parameters are given in Table 12.

Table 12: Calculated reaction constants for the set of P(NIPAAm-co-SPA) copolymers upon irradiation in the solid-state.

Polymer	$[y_0]$(green)	A(green)	k(green)	$[y_0]$(UV)	A(UV)	k(UV)
P(NIPAAm$_{311}$-*co*-SPA$_1$)	0.075	0.158	-0.022	0.333	-0.214	-0.0194
P(NIPAAm$_{282}$-*co*-SPA$_2$)	0.014	0.390	-0.019	0.515	-0.403	-0.0267
P(NIPAAm$_{383}$-*co*-SPA$_4$)	0.144	0.569	-0.015	0.909	-0.689	-0.0119
P(NIPAAm$_{538}$-*co*-SPA$_6$)	0.200	0.845	-0.013	1.157	-0.810	-0.0155
P(NIPAAm$_{617}$-*co*-SPA$_7$)	0.207	1.019	-0.011	1.297	-0.973	-0.0147
P(NIPAAm$_{1108}$-*co*-SPA$_{17}$)	0.177	0.827	-0.010	1.045	-0.713	-0.0168

To summarise, the photo-response of SPA-containing polymers is also visible in bulk materials and could be demonstrated for P(NIPAAm-*co*-SPA) copolymer films ranging from 11 to 17 µm in thickness. The photo-response in the solid-state reveals the same trends as already observed in solution, but occur approximately ten times slower.

5.4.3 Simultaneous Response to Temperature and Light

The photo-response of the dual-responsive copolymers was intensively studied in the previous sections, but the investigation of the thermo-response is still pending. It is expected, that the

switching-state of the SPA moiety, SP- or MC-form, affects the thermo-response of the copolymer, and the difficulties associated with the investigation of both stimuli simultaneously were described previously. First, a suitable protocol to probe both stimuli simultaneously for both copolymers was established. This protocol was then applied to determine the transition temperatures for both sets of copolymers.

5.4.3.1 Protocol used to assess the Thermo-Responsive Behaviour of the Copolymers

Upon heating above a certain temperature, the copolymer will become insoluble and precipitate, and the precipitation temperature can be determined *via* absorption spectroscopy. For the determination of the transition temperature, absorbance spectra were recorded at increasing temperatures during irradiation with 540 nm light. The two copolymers, P(NIPAAm$_{617}$-*co*-SPA$_7$) and P(TEGA$_{194}$-*co*-SPA$_{15}$), are dissolved in a pH 8 TRIS buffer solution at a concentration of 0.5 g/L and irradiated with 540 nm light. The temperature is increased in 1 or 2 °C steps with a waiting time of 10 minutes at each step to reach thermal equilibrium. The absorbance spectra for both copolymers are shown in Figure 58.

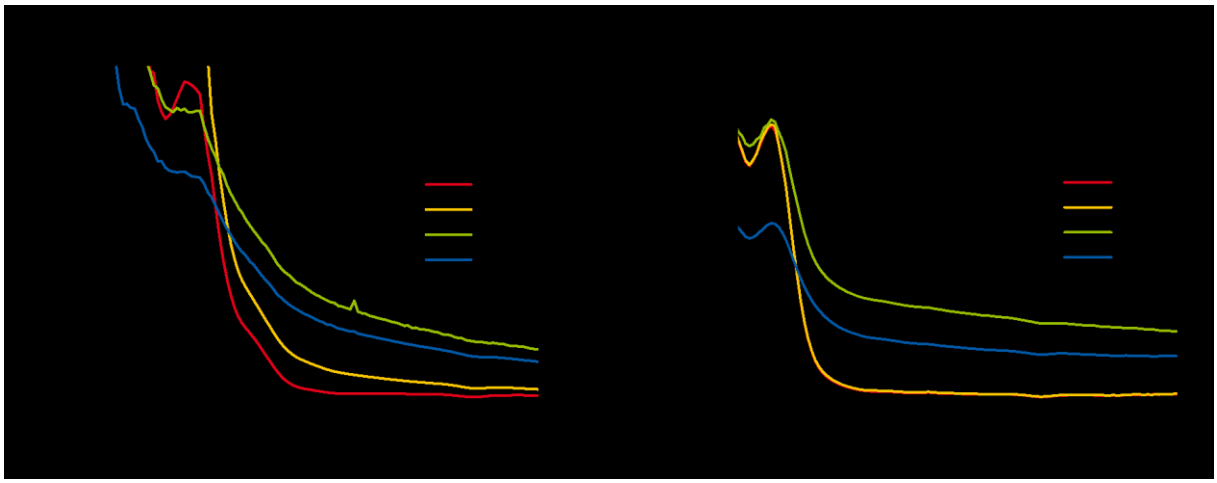

Figure 58: UV-Vis absorbance spectra of (a) P(NIPAAm$_{617}$-co-SPA$_7$) and (b) P(TEGA$_{194}$-co-SPA$_{15}$) in a pH 8 buffer with in situ irradiation at 540 nm at different temperatures.

Upon heating, two distinct spectral changes are observed: first, the absorbance increases in the visible range from 400 nm to 800 nm; and second, the absorbance decreases in the UV range below 400 nm. Both effects originate from the soluble to insoluble transition of the copolymer in solution. As mentioned in the introduction, the absorbance measured is simply a decrease in the amount of light that reaches the detector. The soluble to insoluble transition of the copolymer leads to an increase in elastic scattering of light, which decreases the amount of light that reaches the detector. The reason for light not reaching the detector is now different than before in the dissolved state. In the dissolved state, the copolymer absorbs light and scatters light inelastically, which can be described by the Beer-Lambert Law, whereas the insoluble copolymer scatters light elastically. The inelastic scattering of a particle scales with $1/\lambda^4$, which means that higher wavelengths get scattered less than lower wavelengths. This can be observed for high temperatures when the absorbance spectrum is almost reduced to a line. A further observation is a decrease in the absorbance after the transition temperature, which is attributed to aggregation of the insoluble copolymer particles. The difference between the transition temperature of both copolymers is the higher transition temperature of the TEGA-containing copolymer, which also results in a higher transition temperature for the respective copolymer. However, the transition temperature itself is lower than the homopolymer due to the hydrophobic character of the SPA moiety.

After performing the measurement, both copolymers were stored in the dark at 6 °C overnight before being subjected again to a similar experiment where both copolymers were irradiated at 340 nm and heated to investigate the thermo-response (Figure 59).

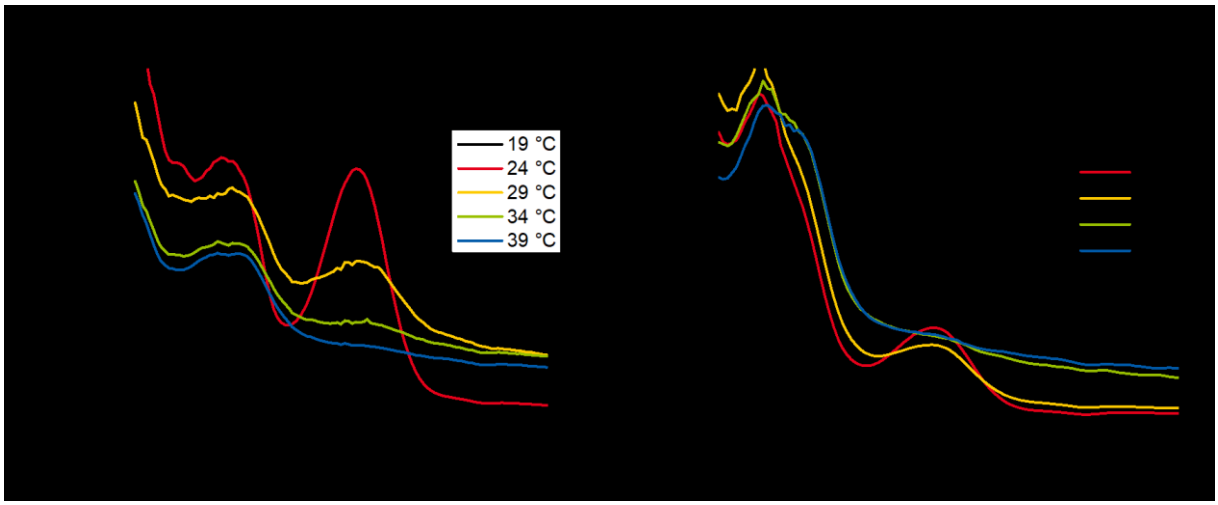

Figure 59: UV-Vis spectra of (a) P(NIPAAm$_{617}$-co-SPA$_7$) and (b) P(TEGA$_{194}$-co-SPA$_{15}$) in pH 8 buffer while being irradiated in situ at 340 nm at different temperatures.

In general, both copolymers show the same behaviour as in the previous experiment in terms of the increase in absorbance in the visible range from 400 to 800 nm and decrease in absorbance in the UV range below 400 nm. The most obvious difference in the absorbance spectra when going from irradiation at 540 nm to irradiation at 340 nm is the absorbance of the merocyanine at 540 nm is increased for both copolymers. This absorption band decreases during the heating process, and the absorbance spectra flatten out as already observed in the previous experiment (Figure 58) irradiated at 540 nm since the sample precipitates. This observation is the most noticeable at an absorbance of 540 nm, which is attributed to the absorption of the merocyanine-form, because the insoluble copolymer cannot absorb light at this specific wavelength.

In order to compare the heating experiments with different irradiation wavelengths, the soluble to insoluble transition of the copolymers can be followed at 700 nm, independent of the irradiation state. Consequently, the transmittance at 700 nm is plotted for both irradiation experiments to determine the transition temperature for both heating experiments of both copolymers (Figure 60). Transmittance, over absorbance, was used here to indicate the difference in the thermo-responsive behaviour of the copolymers compared to the photo-responsive behaviour.

Both copolymers, P(NIPAAm$_{617}$-*co*-SPA$_7$) and P(TEGA$_{194}$-*co*-SPA$_{15}$), exhibit a different transition temperature depending on the irradiation state. As expected, the transition temperature is higher while irradiating at 340 nm than the transition temperature while irradiating at 540 nm. This can be attributed to the change in polarity of the SPA moiety upon irradiation, which leads to a higher water-solubility of the copolymer, and therefore the thermo-responsive moiety remains dissolved at higher temperatures.

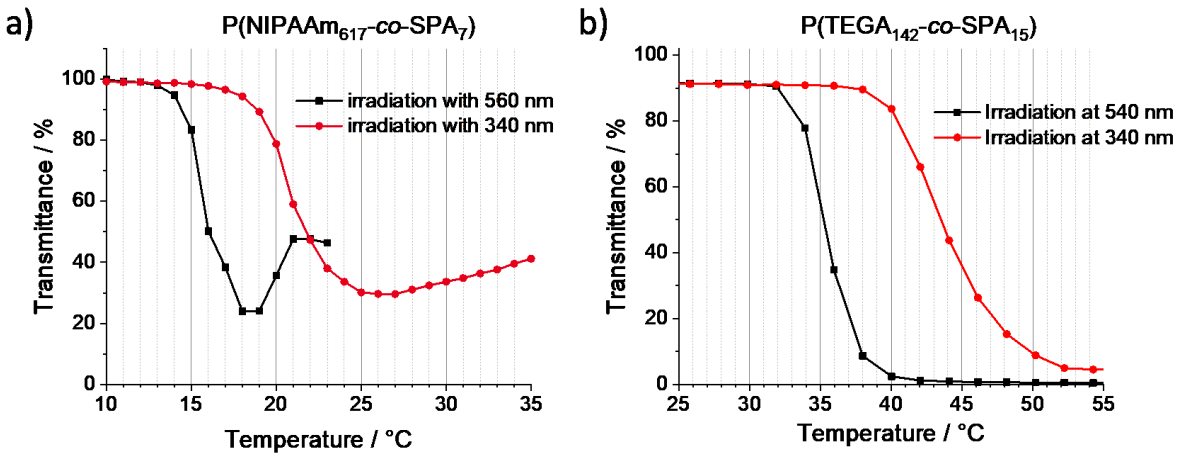

Figure 60: Transmittance of (a) P(NIPAAm$_{617}$-co-SPA$_7$) and (b) P(TEGA$_{194}$-co-SPA$_{15}$) at 700 nm with increasing temperature.

To confirm the importance of the surrounding medium, P(NIPAAm$_{617}$-*co*-SPA$_7$) was dissolved in deionised water and heated above the transition temperature with no change in transmittance. Heating of the same copolymer in a 50 mM NaCl solution, which resembles the ionic strength of the buffer itself, exhibits the same transition temperature as the copolymer when irradiated at 340 nm (see Figure 62e). Here, the transition temperature of the sample irradiated at 540 nm while being heated is in the same range as the sample irradiated at 340 nm when dissolved in pH 8 buffer solution. The absorbance spectra confirmed that in a 50 mM NaCl solution the SPA moiety within the copolymer is in the merocyanine-form despite being irradiated at 540 nm. The salt in the solution stabilises the zwitterionic merocyanine-form well and leads to a loss of the photo-responsive behaviour of the SPA moiety in the copolymer. In a second experiment, the P(NIPAAm$_{617}$-*co*-SPA$_7$) copolymer was dissolved in pure water, which leads to no thermo-responsive behaviour at all. This can be attributed to the different pH-value of deionised water, which protonates the SPA moiety to result in a polyanion, which naturally shows no thermo-response. Further experiments revealed that the concentration of the copolymer in solution effects the transition temperature. Concentrations ranging from 0.5 to 2 g/L were tested three times, and the dual-responsive behaviour investigated. The results are shown in Figure 61.

The thermo-response of the copolymer during irradiation at 540 nm does not depend on the concentration, with the transition occurring at ~40 °C at all concentrations tested. Upon irradiation at 340 nm, a clear concentration dependence is observed with the transition shifting to higher temperatures as the copolymer concentration decreases. This increase in transition temperature is also accompanied by a broadening. We did not expect a clear measurable transition at lower concentration, hence why no lower concentrations were investigated. This effect occurs because of a combination of the measurement method and a broader transition temperature of the copolymer because of longer and shorter thermo-responsive sequences in the copolymer.

TEGA as a comonomer was chosen predominantly because the effect of a broadened transition temperature of copolymers is reported to be less intense than for the NIPAAm equivalents. Unfortunately, the broadening of the thermo-responsive behaviour indicates that the transition temperature of PTEGA is also dependent on the number of repetition units between two SPA moieties in the copolymer. While the chain length-dependent thermo-response of PNIPAAm is well-known, we also observed this dependence for the P(TEGA-*co*-SPA) copolymers. Upon heating, the randomly distributed thermo-responsive segments precipitate at different temperatures, resulting in a

broadening of the thermo-response of the copolymers (Figure 60) when compared to the PNIPAAm homopolymer (Figure 43). Insoluble segments of the copolymer already scatter light, while other segments of the same copolymer are still dissolved. The precise transition temperature is difficult to determine due to this broadening. Additionally, the precipitated long segments overlap with the signal of the precipitation of the short segments which are not visible anymore. This is still the case even when the transmittance is not at zero. The measured change in transmittance here is more a loss in light intensity at the detector, which occurs due to inelastic scattering. As mentioned earlier, the inelastic scattering decreases for longer wavelengths, and the path length may not be sufficient to measure lower light intensities. The formation of larger aggregates, on the other hand, can then lead to increased scattering, resulting in the transmittance approaching zero.

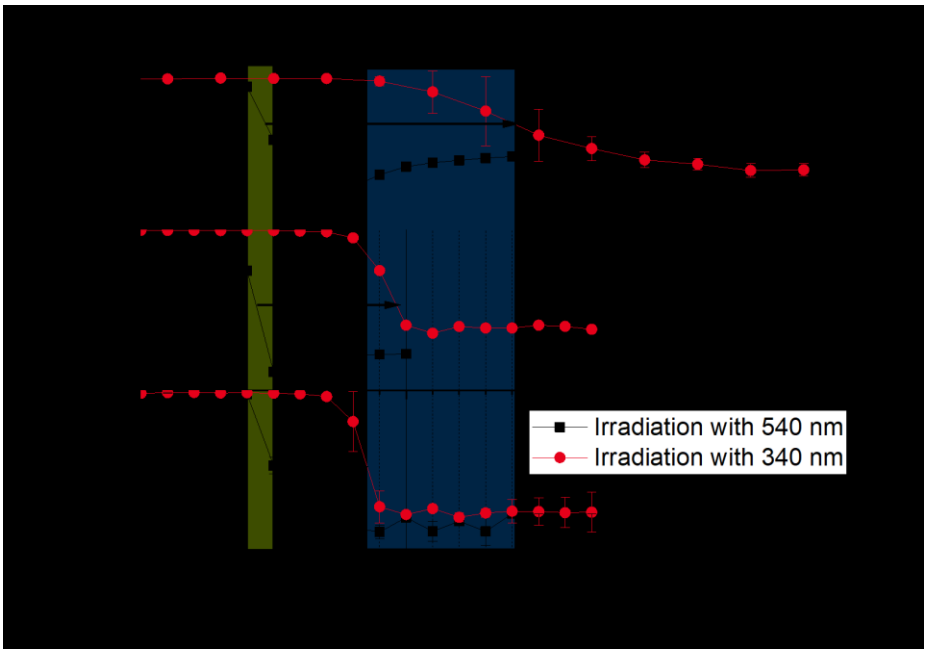

Figure 61: P(TEGA$_{194}$-co-SPA$_{19}$) dissolved in a pH 8 TRIS buffer at different concentrations. The absorbance was measured at 700 nm, and the error bars result from 3 measurements.

In summary, a measurement protocol was established to determine the transition temperatures for dual stimuli-responsive copolymers, which permits the change in transition temperature in various irradiation states (540 or 340 nm) to be determined. The conditions found are suitable to apply to investigate how the irradiation state influences the thermo-response for the remaining sets of copolymers.

5.4.3.2 Summary of the Thermo-Responsive Behaviour of the Prepared Copolymers

Similarly to the P(NIPAAm$_{617}$-*co*-SPA$_7$) and P(TEGA$_{194}$-*co*-SPA$_{15}$) measured in the previous section, the transition temperatures were determined for all other copolymers from the previously synthesised copolymer sets. The copolymers were dissolved in a pH 8 TRIS buffer solution at a concentration of 0.5 g/L and stored in the refrigerator before use. The copolymers were first irradiated with 540 nm light whilst being heated. The precipitated copolymers were then redissolved in the refrigerator overnight before being irradiated with 340 nm light whilst being heated. At every set temperature, a waiting time of 10 min was employed to ensure the copolymer is in thermal equilibrium. After which time an absorbance spectrum was measured. The transmittance at 700 nm was extracted from these spectra and plotted at each temperature for the set of P(NIPAAm-*co*-SPA) copolymers (Figure 62) and P(TEGA-*co*-SPA) copolymers (Figure 64).

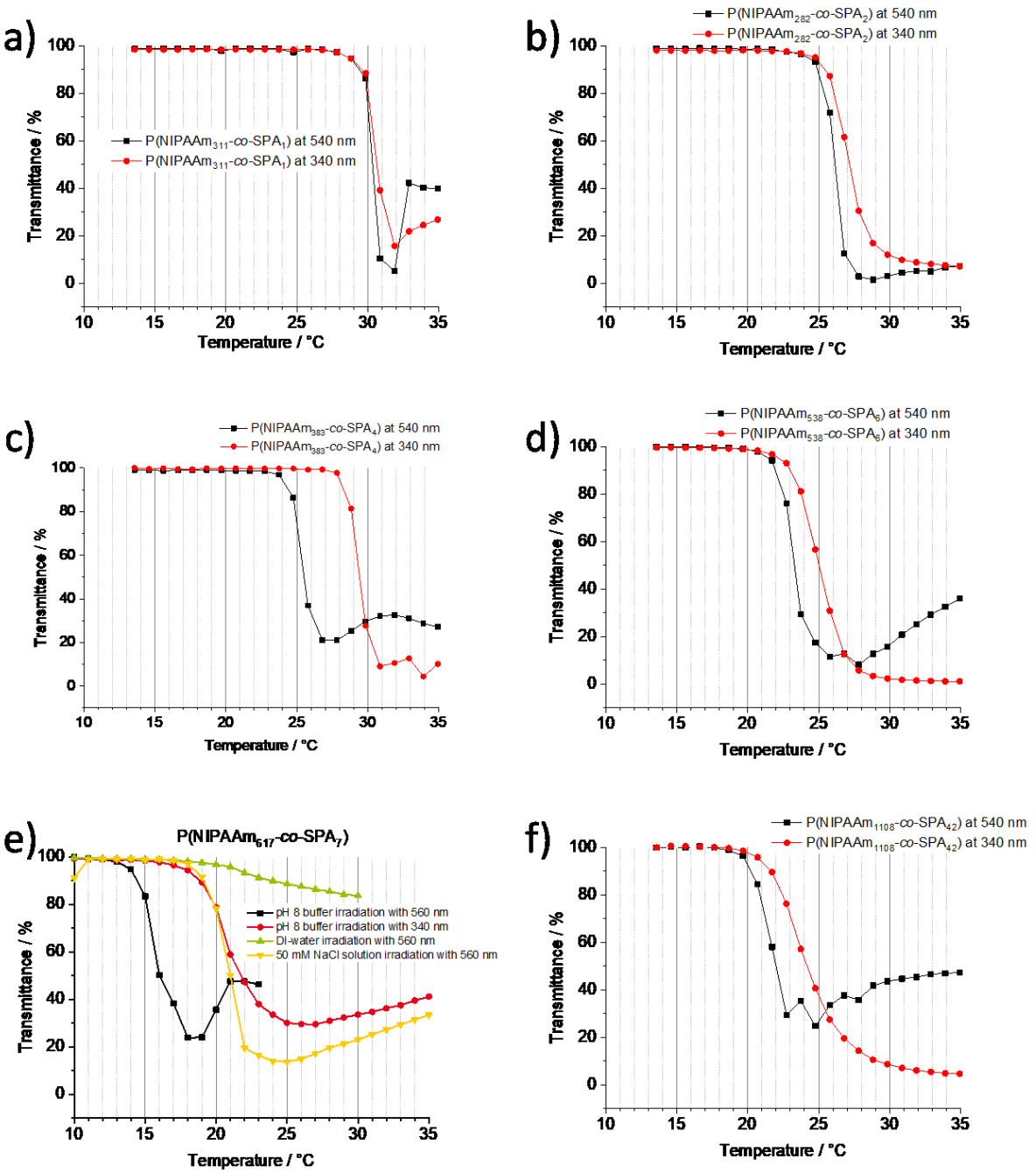

Figure 62: Transmittance at 700 nm of copolymers dissolved in a pH 8 TRIS buffer at different temperatures while irradiating with a 200 W Hg(Xe) lamp using different wavelength filters. The polymer containing 5 % SPA (e) was also measured in deionised water (green) and NaCl aqueous solution (yellow) while irradiating at 540 nm.

All six SPA-containing copolymers are characterised by different transition temperatures upon irradiation at 540 or 340 nm. The transition temperature is the temperature at which the transmittance reaches halfway between the maximum and minimum transmittance, similar to the transition temperature determined for the homopolymers in different solutions (section 5.4.1.2). The transition temperatures for all copolymers are summarised in Table 13.

Table 13: Transition temperatures of the different P(NIPAAm-co-SPA) copolymers while irradiating with UV (340 nm) or green light (540 nm). The temperature at which precipitation occurs was determined as the temperature where the transmission was halved from Figure 62.

Polymer	Transition temperature under irradiation with 540 nm / °C	Transition temperature under irradiation with 340 nm / °C
P(NIPAAm$_{311}$-*co*-SPA$_{1}$)	30	31
P(NIPAAm$_{282}$-*co*-SPA$_{2}$)	26	28
P(NIPAAm$_{383}$-*co*-SPA$_{4}$)	25	29
P(NIPAAm$_{538}$-*co*-SPA$_{6}$)	23	25
P(NIPAAm$_{617}$-*co*-SPA$_{7}$)	19	25
P(NIPAAm$_{1108}$-*co*-SPA$_{17}$)	21	24

Increasing amounts of SPA lead to a lower transition temperature in general, but also the temperature difference between both transition temperatures increases. To visualise the transition temperature or the temperature difference, both are plotted against the amount of spiropyran in the copolymer (Figure 63).

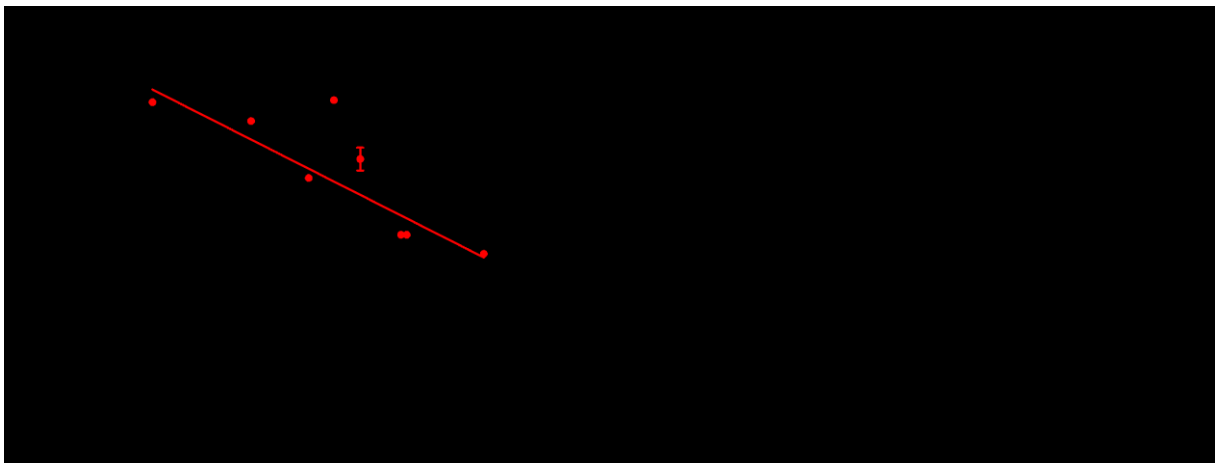

Figure 63: a) Determined transition temperatures between the soluble SP- and insoluble MC-form for P(NIPAAm-co-SPA) copolymers containing different amounts of SPA, the red and black line are just a guide for the eye; b) temperature difference plotted against the amount of SPA in the copolymer.

The transition temperature decreases linearly with increasing amounts of SPA in the copolymers. The slopes of both curves vary, which indicates there is an increasing effect on the thermo-response for increasing amounts of SPA. The lowest measured value is at 19 °C, which is slightly below room temperature. Higher amounts of SPA in P(NIPAAm-*co*-SPA) copolymers are synthetically possible, but result in an insoluble copolymer at room temperature, complicating the measurement. The transition temperature of PNIPAAm$_{418}$ was determined six times in the described setup and always resulted in a transition temperature of 32 °C. This confirms an overall stability of the measurement setup, but some minor effects could affect the polarity of the SPA moiety, and therefore also the transition temperature of P(NIPAAm-*co*-SPA) copolymers. The transition temperature of P(NIPAAm$_{386}$-*co*-SPA$_{10}$) was measured three times to determine the error associated with this method. The transition temperatures vary by ~1 °C, which corresponds to the step-width of these measurements.

The same experiments were also performed with the set of P(TEGA-*co*-SPA) copolymers, but due to the higher temperature of the transition, the step-width was increased from 1 to 2 °C. The remaining experimental conditions were kept constant. The results are summarised in Figure 64.

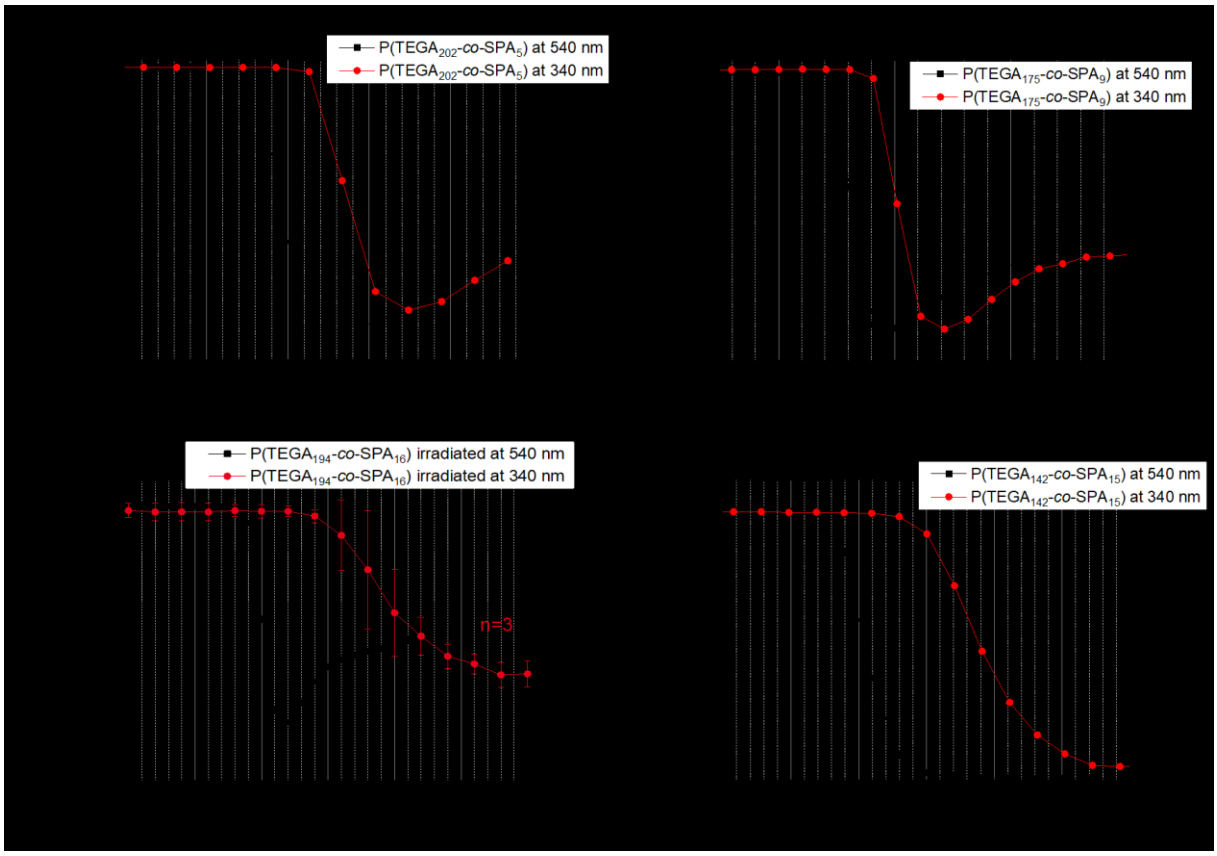

Figure 64: Transmittance at 700 nm of P(TEGA-co-SPA) copolymers dissolved in a pH 8 TRIS buffer at different temperatures while irradiating with a 200 W Hg(Xe) lamp using different wavelength filters. P(TEGA$_{194}$-co-SPA$_{16}$) (c) was measured three times.

The transition temperatures of the P(TEGA-*co*-SPA) copolymers were determined similarly to the previous set of P(NIPAAm-*co*-SPA) copolymers. The transition temperature again differed depending on the irradiation wavelength. All transition temperatures are summarised in Table 14.

Table 14: Transition temperatures of the different P(TEGA-co-SPA) copolymers while irradiating with UV (340 nm) or green light (540 nm). The temperature at which precipitation occurs was determined as the temperature where the transmission was halved from Figure 64.

Composition	Transition temperature under irradiation at 540 nm / °C	Transition temperature under irradiation at 340 nm / °C
PTEGA$_{266}$	66	66
P(TEGA$_{202}$-*co*-SPA$_5$)	54	58
P(TEGA$_{175}$-*co*-SPA$_9$)	47	53
P(TEGA$_{194}$-*co*-SPA$_{16}$)	40	49
P(TEGA$_{142}$-*co*-SPA$_{15}$)	35	44

The overall transition temperature decreases depending on the increasing amount of SPA in the copolymer, whilst the temperature difference between the two transition temperatures increases as the amount of SPA increases. To better compare how the SPA content influences the transition temperature and the temperature difference between the two irradiation wavelengths, the results are presented graphically in Figure 65.

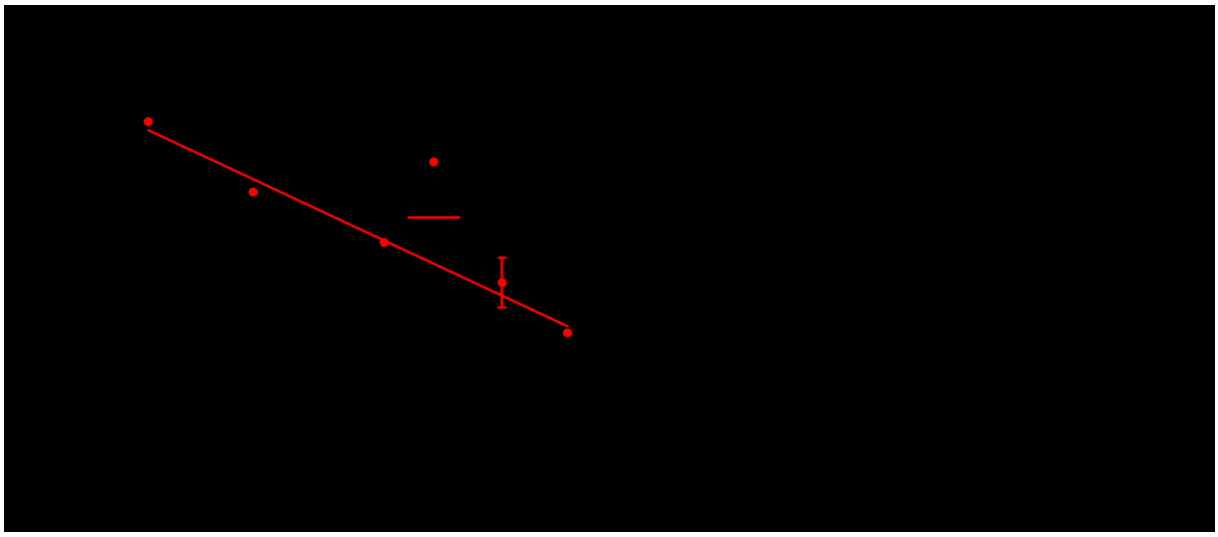

Figure 65: a) Determined transition temperatures between the soluble SP- and insoluble MC-form for P(TEGA-co-SPA) copolymers containing different amounts of SPA, the red and black line are just a guide for the eye. b) Temperature difference plotted against the amount of SPA in the copolymer.

Here, the transition temperature also decreases linearly with the amount of SPA incorporated within the copolymer, and the slope of the linear fit depends on the irradiation wavelength. The results for the P(TEGA-*co*-SPA) copolymers are better represented by a linear fit than for the P(NIPAAm-*co*-SPA) copolymers. We attribute this to the lower chain length dependence of the thermo-responsive behaviour to the TEGA-containing copolymers. The reproducibility of the measurements was assessed by repeating the irradiation of P($TEGA_{194}$-*co*-SPA_{16}) three times, which results in a variation of ~3 °C, which is higher than the step-width used, but still allows a clear difference between the individual copolymers to be discerned. The amount of SPA in the copolymer again appears to influence the temperature difference between the two irradiation states. According to the previous plot (Figure 63b), a linear fit cannot describe the temperature difference as well as for the P(NIPAAm-*co*-SPA) copolymers, indicating that the temperature difference between the two irradiation wavelengths is independent of the thermo-responsive moiety used. The spiropyran-containing thermo-responsive copolymers undergo changes in polarity upon irradiation which affect the solvent hull around the copolymer. This change in polarity results in the varying temperature response observed in aqueous solutions. This consideration makes the temperature difference caused by the change in polarity of the SPA moiety independent from the thermo-responsive moiety used. This can be seen clearly by plotting both temperature differences in the same graph (Figure 66).

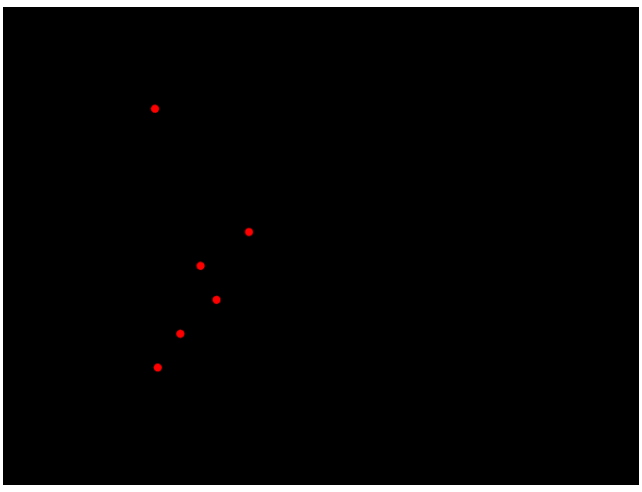

Figure 66: All temperature differences of P(NIPAAm-co-SPA) and P(TEGA-co-SPA) copolymers plotted together.

The effect of the amount of SPA on the temperature difference between both irradiation states is clear. Nevertheless, during previous experiments, some basic trends are observed. Increasing the amount of SPA in the copolymer leads to a decrease in the transition temperature in general due to the non-polarity of the photo-responsive group. Photo-switching from the SP-form to the zwitterionic MC-from increases the transition temperature due to the higher polarity of the SPA-group in this state. This effect naturally occurs for both thermo-responsive moieties investigated, and also the change in polarity depends solely on the amount of built-in SPA.

During this chapter, the synthesis of two different sets of dual-responsive copolymers was presented, P(NIPAAm-*co*-SPA) and P(TEGA-*co*-SPA), using unimolecular NMP initiators. Both sets of copolymers were then used to investigate the photo- and thermo-response systematically with variations in the SPA content. The seven P(NIPAAm-*co*-SPA) copolymers contained 0 to 5.28 mol% SPA with a step-width of ~1 %, whereas the five P(TEGA-*co*-SPA) copolymers contained 0 to 16 mol% of SPA with a step-width of ~4 %. The optimal pH for the photo-response was found to be pH 8. The photo-response of the SPA-containing copolymers was probed at 550 nm, and assigned to the spiropyran-merocyanine transition, was found to depend on the amount of SPA in the copolymer; with lower amounts leading to faster but less intense responses, and which are independent of the thermo-responsive comonomer used. The photo-response in the solid-state of the P(NIPAAm-*co*-SPA) copolymers in thin films present similar behaviour; however, the response in the solid-state is slower than in solution. The insolubility upon heating was also investigated *via* absorption spectroscopy at a higher wavelength of 700 nm where the copolymer precipitation can be probed unaffected by the absorbance of the SPA moieties. Irradiating a copolymer with 340 nm light leads to a higher precipitation temperature than irradiating the same copolymer with 540 nm light. This effect depends on the incorporated amount of SPA in the copolymer and is also independent of the comonomer used. Increasing amounts of SPA lead to a lower transition temperature in general, but also to a higher temperature difference between the two transition temperatures up to 9 °C. The effect of SPA on the dual-responsive behaviour is independent of the used thermo-responsive comonomer. This effect would be interesting to investigate using more complex architectures such as block copolymers that form micelles. The close proximity of the dual-responsive chains could yield different dual-responsive behaviour.

6 Thermo- and Light-Responsive Block Terpolymers

Parts of this Chapter have been published in Grimm, O.; Maßmann, S. C.; Schacher, F. H., Synthesis and solution behaviour of dual light- and temperature-responsive poly(triethylene glycol-co-spiropyran) copolymers and block copolymers. Polymer Chemistry 2019, 10 (21), 2674-2685.[204]

Within this chapter, the findings concerning the dual stimuli-responsive behaviour investigated in the previous chapter will be utilised in stabilised compartments. These compartments consist of a hydrophobic core-forming segment and a hydrophilic corona-forming segment. The core consists of a PS macroinitiator, whereas the corona consists of the previously investigated dual stimuli-responsive copolymer. We, therefore, expect that the compartments will exhibit similar dual stimuli-responsive behaviour as for the thermo- and photo-responsive copolymers investigated previously. These structures and their expected dual-response are depicted with a spherical core in Figure 67.

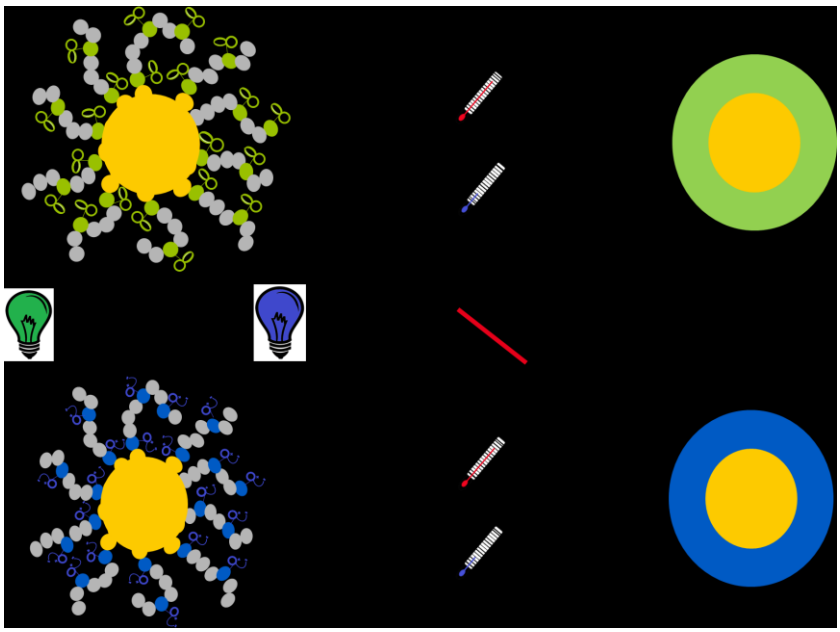

Figure 67: Expected behaviour of micelles consisting of an amphiphilic block terpolymer.

Similarly to the previously investigated copolymers, the compartment corona is also photo- and thermo-responsive, consisting of both a thermo-responsive moiety (NIPAAm or TEGA) and a photo-responsive moiety (SPA). This means that the corona can also change in polarity upon irradiation, and precipitate upon heating. Furthermore, the precipitation temperature of the corona should vary depending on the irradiation state of the photo-responsive moiety, similar to the previous copolymers investigated.

In this chapter, the preparation of various macroinitiators is first presented before the effect of several input parameters on the block extension is investigated to prepare PS-*b*-PNIPAAm. Following the optimisation of this simple system, SPA is added as a comonomer with either NIPAAm or TEGA to prepare dual-responsive block terpolymers. The prepared amphiphilic block terpolymers are then used in micellisation experiments, and the particle size investigated by dynamic light scattering (DLS) and cryo-TEM. The stable compartments are then investigated in terms of their dual-responsive behaviour upon irradiation, heating, and both stimuli simultaneously *via* UV-Vis spectroscopy. The results are then compared to the dual-responsive copolymers presented earlier.

6.1 Synthesis of Amphiphilic Block Terpolymers

The formation of micellar systems in aqueous media from amphiphilic block copolymers requires some synthetic effort. The amphiphilic block copolymer consists of a hydrophobic and a hydrophilic segment. The hydrophilic segment contains the dual-responsive moieties introduced in the previous chapters. The hydrophobic segment is formed from a water-insoluble polymer that is well-known in NMP: styrene. Styrene is commercially available, and within the working group, various protocols have been developed allowing the chain length to be controlled using NMP. Besides the length of the macroinitiator, the ratio between the hydrophobic and hydrophilic blocks is crucial. Therefore, after the synthesis of various macroinitiators, the block extension was optimised for PS-*b*-PNIPAAm. After which, the comonomer SPA was added to form dual-responsive micelles. We will then apply and compare our findings for the NIPAAm-containing block terpolymers to TEGA-containing block terpolymers.

6.1.1 Macroinitiator Formation

Three different polystyrene macroinitiators were used in the preparation of dual stimuli-responsive block terpolymers in this work. To prepare the PS macroinitiators, destabilised styrene was mixed with a unimolecular macroinitiator in bulk, deoxygenated by purging with argon, and the reaction mixture heated at 110 °C for 12 to 24 h (Scheme 12).

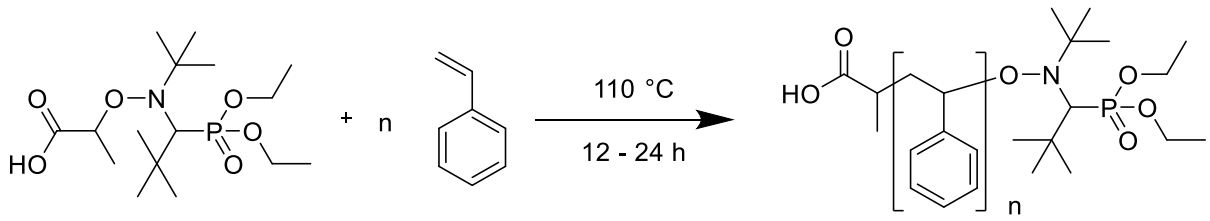

Scheme 12: Formation of different PS macroinitiators achieved using different reaction times.

By varying the reaction times, macroinitiators with different chain lengths can be accessed. After the necessary reaction time, the mixture was cooled to room temperature and the highly viscose reaction mixture precipitated in methanol and stirred overnight to obtain a fine white powder. The chain length and dispersity were determined *via* SEC using PS standards (Figure 68 and Table 15).

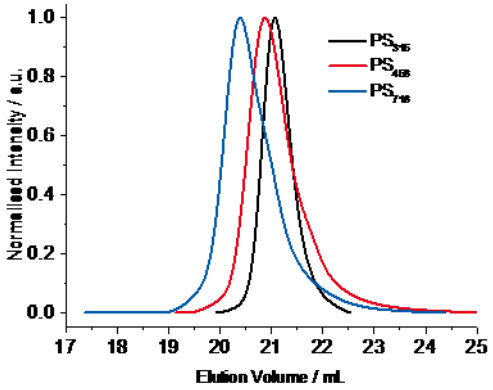

Figure 68: THF-SEC traces of the prepared PS macroinitiators used and synthesised in this chapter. The degree of polymerisation was determined using PS standards.

Table 15: Molecular weights and dispersities of the prepared PS macroinitiators.

Macroinitiator	M_n / g/mol	$Đ$
PS_{315}	39,900	1.23
PS_{456}	56,600	1.23
PS_{716}	74,600	1.20

The prepared PS macroinitiators have an SG-1 end group that can be removed upon heating back to their original reaction temperature of approximately 110 °C, permitting their block extension by NMP. Following the synthesis of the PS macroinitiators, amphiphilic block terpolymers were synthesised.

6.1.2 Optimisation of the Block Extension

Amphiphilic block terpolymers consist of two segments of a defined ratio, and a defined overall length is desired. In literature, most PS-*b*-PNIPAAm micellar systems contain 70 mol% NIPAAm units with an overall molecular weight above 15,000 g/mol.[223-224] For the block extension, the optimised conditions used previously to synthesise the P(NIPAAm-*co*-SPA) copolymers were applied from the prepared PS macroinitiator to access dual-responsive block copolymers. In order to maintain a hydrophilic segment ratio of 70 %, the PS_{315} macroinitiator requires approximately 600 repetition units of NIPAAm to be added. The NMP of NIPAAm with BlocBuilder depends on the monomer to initiator ratio, hence why different ratios were investigated (Scheme 13)

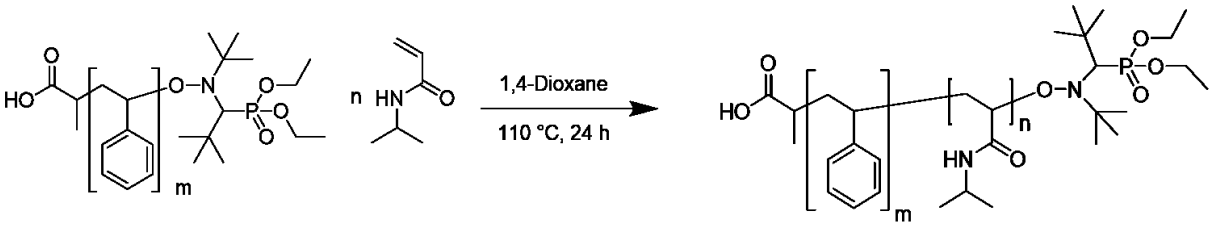

Scheme 13: General reaction scheme for the block extension of a nitroxide end-capped PS-macroinitiator with NIPAAm.

The PS_{456} macroinitiator was dissolved in 1,4-dioxane with varying amounts of NIPAAm ranging from a monomer to initiator ratio of 1000/1 to 2000/1. The reaction mixture was then deoxygenated by purging with argon for 20 min before being heated at 110 °C for 20 h. The crude product was purified by precipitation into diethylether twice to remove all unreacted monomer. To determine whether the block extension was successful, as well as the ratio between blocks, SEC in DMAc and ^{1}H-NMR in $CDCl_3$ was performed, and the results are given in Figure 69.

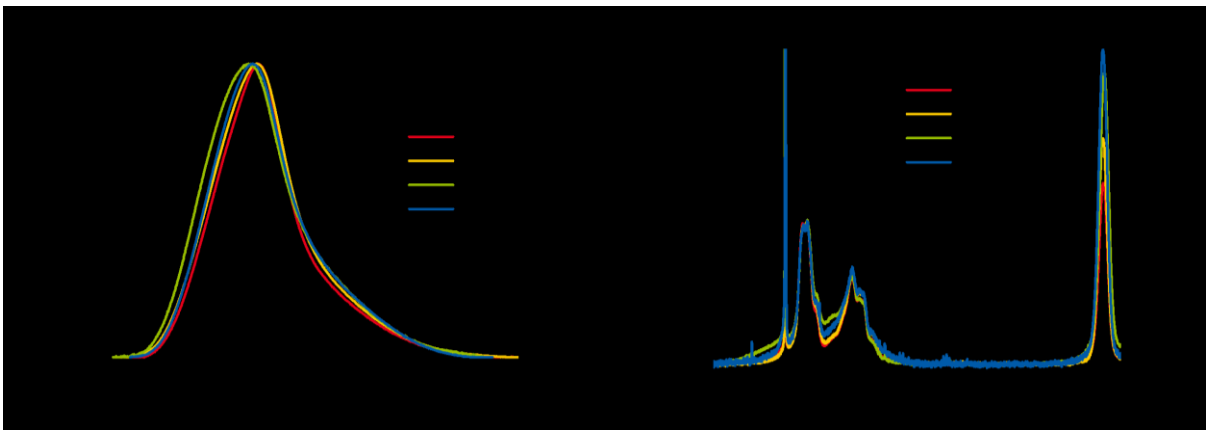

Figure 69: Block extension of PS_{456} with varying amounts of NIPAAm in the monomer mixture: a) RI traces of SEC in DMAc and b) ^{1}H-NMR in $CDCl_3$.

The block copolymers shift to lower elution volumes compared to the PS macroinitiator according to SEC measurements, indicating the block extension has been successful. However, a broadening of the SEC trace is observed. The shoulder that appears at higher elution volumes may indicate the formation of homopolymer or unreacted macroinitiator. To assess the degree of block extension, the block copolymers were characterised by ^{1}H-NMR in deuterated chloroform. The characteristic signals of polystyrene (~7 ppm) and PNIPAAm (4 ppm) were integrated to determine the block ratio. Similarly to the previous investigations, the degree of polymerisation of the block copolymer could be determined using the block ratio and the absolute molar mass of the macroinitiator (Table 16). To determine the effect of the macroinitiator used, the same experiments were repeated with a lower molecular weight macroinitiator, PS_{315}.

Table 16: Degree of polymerisation for the block extension of two different macroinitiators with comparable monomer to initiator ratios.

Macroinitiator	Copolymer	M/I ratio	M_n[c] / g/mol	$Đ$[a]	x_{NIPAAm}[b] / %
PS_{315}	PS_{315}-*b*-$PNIPAAm_{660}$	1000/1	107,500	1.88	67.6
	PS_{315}-*b*-$PNIPAAm_{847}$	1333/1	128,700	1.85	72.9
	PS_{315}-*b*-$PNIPAAm_{941}$	1666/1	139,400	2.07	74.9
	PS_{315}-*b*-$PNIPAAm_{1077}$	2000/1	154,700	2.00	77.4
PS_{456}	PS_{456}-*b*-$PNIPAAm_{948}$	1000/1	154,800	1.44	67.5
	PS_{456}-*b*-$PNIPAAm_{1053}$	1333/1	166,700	1.44	69.8
	PS_{456}-*b*-$PNIPAAm_{1464}$	1666/1	213,100	1.47	76.2
	PS_{456}-*b*-$PNIPAAm_{1478}$	2000/1	214,700	1.57	76.4

a) THF-SEC using a PS standard, b) ^{1}H-NMR in $CDCl_3$, c) composition determined from a combination of both methods.

In all cases, the macroinitiator is successfully block extended with a hydrophilic to hydrophobic ratio of ~70/30 obtained in most cases. The hydrophilic ratio is slightly higher for the block copolymers formed using the lower molecular weight macroinitiator (PS_{315}). The number of repetition units added, depending on the macroinitiator used, is shown in Figure 70.

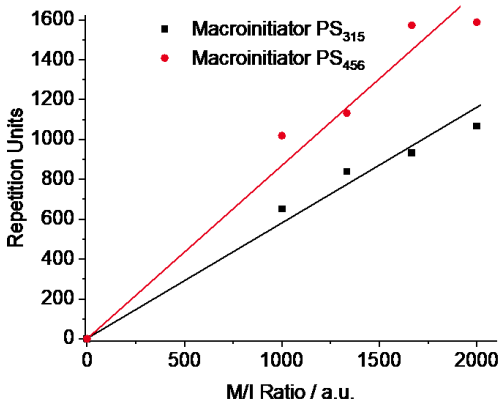

Figure 70: Comparison of the added NIPAAm units to different PS macroinitiators using varying monomer to initiator ratios.

Comparing the block extension from different macroinitiators, the lower molecular weight macroinitiator (PS_{315}) adds less NIPAAm units than the higher molecular weight macroinitiator (PS_{456}). These results are counter-intuitive, with higher molecular weight macroinitiators generally presenting poorer end group accessibility. On the other hand, the SEC traces from Figure 69 indicate that some

PNIPAAm homopolymer is formed. The homopolymer is indistinguishable from the block extended block copolymer by ^{1}H-NMR. The potential presence of PNIPAAm homopolymer will result in an overestimation of the number of NIPAAm units added during the block extension according to ^{1}H-NMR. The formation of homopolymer originates from the transfer of an active chain end to a monomer or polymer backbone. The kinetics of this side reaction is challenging to determine, but side reactions can be suppressed by reducing the radical concentration. This can be achieved in two ways: a) reducing the temperature to result in less frequent cleavage of the CO bond of the nitroxide, and b) reducing the concentration of the macroinitiator. Both adjustments lead to a slower reaction speed, and therefore also a longer reaction time. The previously controlled radical copolymerisations of NIPAAm and NIPAAm with SPA were possible under the same reaction conditions. The copolymerisation, and also the block extension, should proceed similarly. Hence why the addition of SPA to the monomer mixture should result in similar results as previously observed for the block extension with NIPAAm alone. The only notable drawback of the optimisation of the block extension from an SPA-containing monomer mixture is the large demand of monomer. In the following section, the influence of temperature and concentration of the macroinitiator is investigated (Figure 71). First, different reaction temperatures ranging from 100 to 150 °C in 10 °C steps were tested. Second, the concentration of the reaction mixture was changed at 100 and 120 °C. The monomer mixtures were mixed with the PS_{716} macroinitiator using a monomer to initiator ratio of 2000 to 1 containing NIPAAm and 5 mol% of SPA.

The crude reaction mixture shows a clear shift for all reaction temperatures. The RI traces following block extension shift clearly to lower elution volumes, and no formation of homopolymer is observed. The elution traces do not differ significantly with changes in polymerisation temperature, which indicates the temperature does not affect the block extension in the range tested.

For the experiments using different macroinitiator concentrations, the PS_{716} macroinitiator is dissolved in 1,4-dioxane at a concentration of 45 or 90 nmol/L. The respective monomers have the same concentration of 20 wt% or 1.6 mmol/L for both macroinitiator concentrations. The highest change observed for these SEC traces after the reaction is a narrowing of the distribution. The maximum does not shift significantly for any of these changes, with the highest impact on the formed block copolymer being the monomer to initiator ratio.

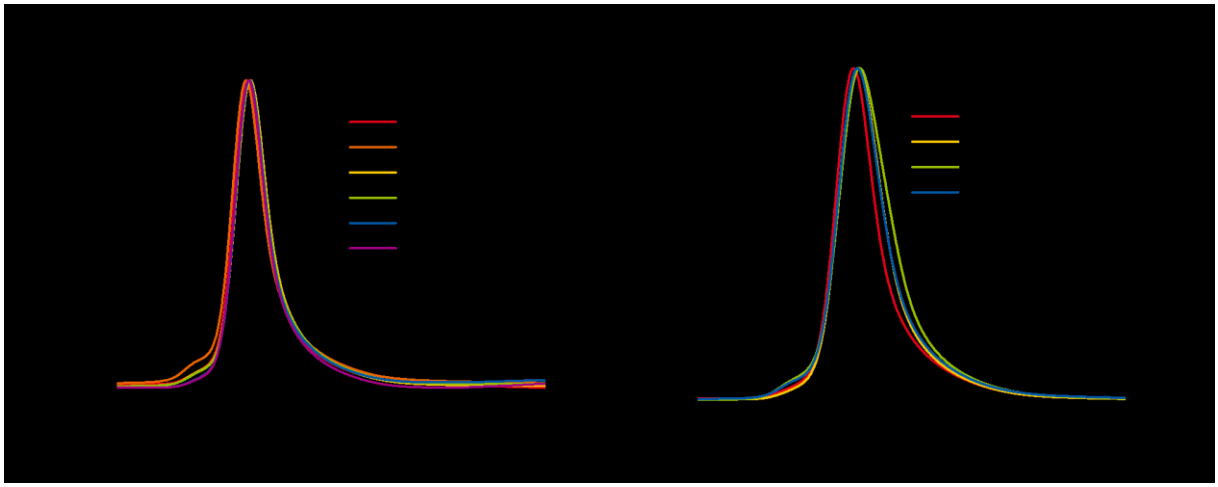

Figure 71: Block extension of PS_{716} dissolved in 1,4-dioxane with NIPAAm and 5 mol% SPA using a monomer to initiator ratio of 2000/1. a) SEC traces of the crude reaction mixtures obtained at different reaction temperatures after 6 h, and b) SEC traces of the same composition at different macroinitiator concentrations. Concentration refers to the macroinitiator in 1,4-dioxane.

6.1.3 Purification of the Crude Amphiphilic Block Terpolymers

In order to determine the degree of polymerisation, the unreacted monomer needs to be separated from the block extended block terpolymer or the unreacted macroinitiator. From the degree of polymerisation of the PS-*b*-P(NIPAAm-*co*-SPA) block terpolymer, the built-in ratio of SPA can be determined. This is important since the amount of SPA incorporated is crucial for the thermo- and photo- dual-responsive behaviour of the micellar systems. The previous investigations on the copolymerisation of NIPAAm and SPA indicate that increasing amounts of SPA in the monomer mixture lead to slower reaction speed. However, the copolymerisation was possible under the same conditions as the controlled radical polymerisation of NIPAAm. The macroinitiator and monomers were dissolved in 1,4-dioxane. A M/I ratio of 1333/1 was used, and the monomer mixture consisted of 0 to 7 mol% of SPA as a comonomer. The mixture was deoxygenated and heated at 90 °C for 24 h.

Scheme 14: Copolymerisation of NIPAAm and SPA in various ratios from a PS macroinitiator.

After the reaction, the block copolymer was purified by precipitation into diethylether to remove the unreacted monomer. The obtained red powder was analysed by SEC and ^{1}H-NMR (Figure 72).

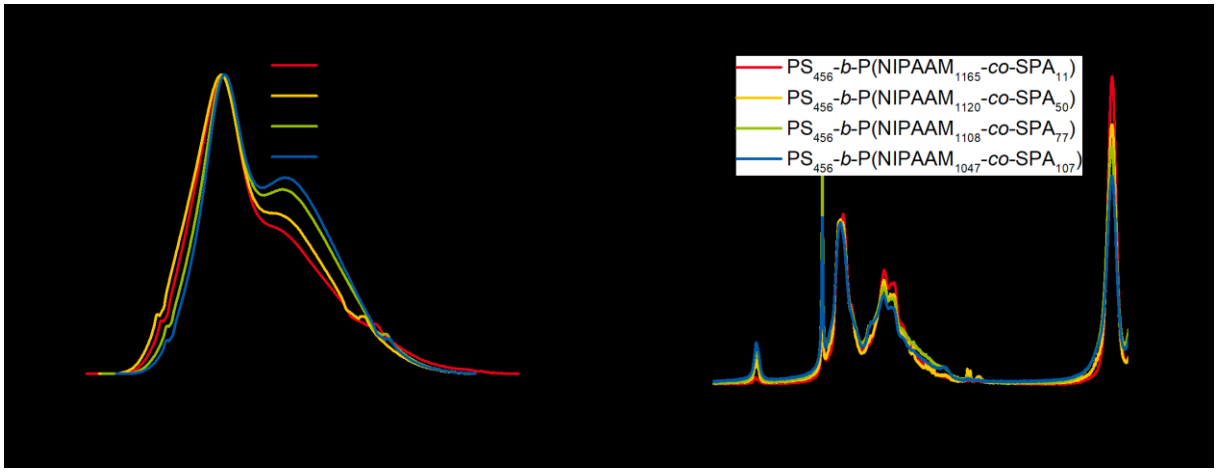

Figure 72: Block extension of PS_{456} dissolved in 1,4-dioxane with NIPAAm and SPA (0 to 7 mol%) using a monomer to initiator ratio of 2000/1: a) SEC traces after precipitation in diethylether and b) ^{1}H-NMR spectra in $CDCl_3$.

The SEC traces of the precipitated samples after block extension are bimodal, and the elution volume of each population strongly suggests a mixture of block copolymer and homopolymer is present. This bimodal distribution was not observed in the crude reaction mixture. Since the reaction mixture contains potentially unreacted macroinitiator, free copolymer, and the desired block terpolymer, it appears the ratio these three polymers have in the actual reaction mixture is not represented after precipitation. It is also apparent that the precipitation of NIPAAm-containing copolymers is favoured in diethylether, which also means that block terpolymers containing a high amount of NIPAAm are also precipitated. This is advantageous for the formation of micelles, but the copolymer needs to be separated from the block terpolymer since it will affect the formation of micelles, and will likely also

alter their dual-responsive behaviour. One simple strategy is the dissolution of the water-soluble P(NIPAAm-*co*-SPA) in pH 8 buffer solution to separate it from the water-insoluble block terpolymer. However, this strategy proved unsuccessful in the current system as some of the copolymer remained undissolved. A potential alternative route is precipitation in methanol since methanol is suitable for the precipitation of the polystyrene macroinitiator. Therefore, we repeated the block extension using NIPAAm alone from the high molecular weight PS macroinitiator. Following the reaction, half of the crude mixture was precipitated in methanol, while the other half was precipitated in diethylether. The resulting products were analysed *via* SEC and ^{1}H-NMR, and the results are shown in Figure 73.

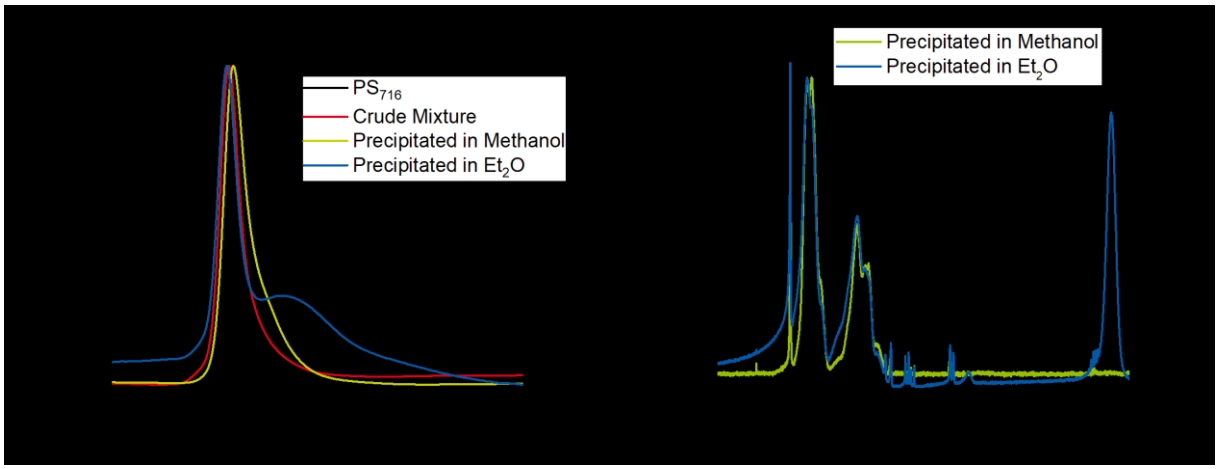

Figure 73: Work-up procedure of crude PS-b-PNIPAAm: a) SEC traces after precipitation in different non-solvents, and b) ^{1}H-NMR spectra in $CDCl_3$ of the precipitate.

The SEC traces of the crude reaction mixture show a shift towards lower elution volumes, which indicates the block extension has been successful. Precipitation of the crude mixture in different solvents results in marked differences in the elution traces observed by SEC. The precipitation in diethylether is bimodal as already observed in previous experiments. The precipitation in methanol leads to a slight shift to lower elution volumes with a peak maximum between that of the crude reaction mixture and the macroinitiator. In order to compare the composition of the white powders, they were dried and dissolved in deuterated chloroform. The ^{1}H-NMR reveals significant differences between the two samples. The sample precipitated in diethylether still contains small amounts of unreacted monomer, but also shows the characteristic signals of polystyrene as well as PNIPAAm. According to the previous experiments, it is not possible to distinguish between the PNIPAAm homopolymer, and the NIPAAm units incorporated into the block copolymer. While precipitation in methanol reveals all monomer is successfully removed, the characteristic signals of PNIPAAm are also not observed, which indicates that methanol is selectively precipitating the unreacted PS macroinitiator. As such, it is clearly challenging to purify this system by simple precipitation. Precipitation in diethylether over-represents PNIPAAm-containing polymers, and precipitation in methanol over-represents PS-containing polymers. We attribute this observation to co-solvency and co-non-solvency effects, as observed for many solvent combinations for PNIPAAm-containing polymers.[142, 225] Co-solvency describes the effect of a polymer being insoluble in two solvents but being soluble in a combination of both. Co-non-solvency describes the mirroring effect, where a polymer is soluble in two separate solvents, but not in the mixture.[141] The solvent mixture of 1,4-dioxane and methanol or diethylether affect the solvency of the polymers and leads to an over or under-representation of the polymer chains in the precipitate.

Another common method to separate unreacted monomer from the polymer is dialysis. To test this approach over precipitation, a PS macroinitiator was dissolved in 1,4-dioxane at a concentration of 45 nmol/L. The monomer mixture was then added such that the monomer to initiator ratio was 1333 to 1 containing 3 or 5 mol% SPA. The mixture was then deoxygenated by purging with argon and heated at 110 °C for 6 h. The reaction mixture was dialysed first against a water/THF mixture and then against pure THF. Afterwards, the reaction mixture was dried, and the red powder obtained following dialysis was analysed *via* SEC and ^{1}H-NMR (Figure 74).

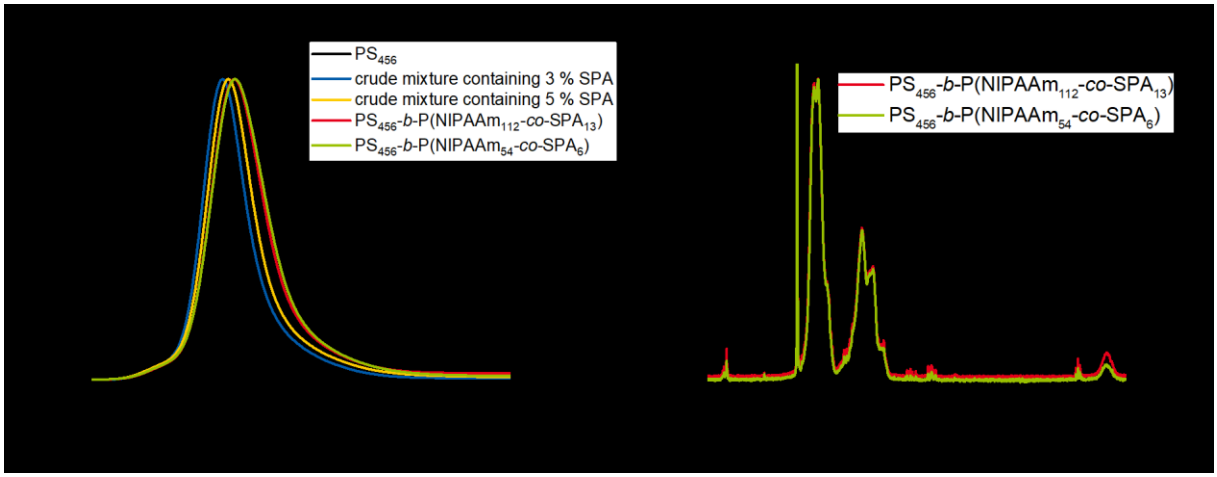

Figure 74: Block extension of PS_{456} dissolved in 1,4-dioxane with NIPAAm and 3 (red) or 5 (green) mol% SPA with a monomer to initiator ratio of 1333/1. The crude block terpolymer was purified by dialysis in THF.

The SEC traces of the crude mixture and purified block terpolymer obtained following dialysis do not differ significantly. This indicates that dialysis is a suitable method to separate the monomer from the block copolymer. The ^{1}H-NMR spectra also show the relevant signals for all repetition units expected in the block terpolymer. The remaining monomer is negligible and could be removed by further extending the dialysis time. However, the composition of the block terpolymers obtained by dialysis differs significantly from the composition of the previous block terpolymers obtained from precipitation. The block extension here is much shorter than observed during the previous precipitation experiments. A summary of the prepared block terpolymers, PS-*b*-P(NIPAAm-*co*-SPA), is given in Table 17.

Table 17: Degree of polymerisation and compositions of the previously synthesised NIPAAm containing block terpolymers.

Polymer Composition[a]	M_n[a] / g/mol	$Đ$[b]	x_{NIPAAm}[c] / %	x_{SPA}[c] / %	Yield / %	x_{SPA} in Monomer / %
PS_{456}	47,500	1.23	-	-	-	-
PS_{456}-*b*-$PNIPAAm_{1478}$	214,700	1.57	76.4	-	62	-
PS_{456}-*b*-P(NIPAAm$_{1165}$-*co*-SPA$_{11}$)	183,900	2.20	71.7	0.7 (0.96)	58	1
PS_{456}-*b*-P(NIPAAm$_{1120}$-*co*-SPA$_{50}$)	194,600	2.03	68.9	3.1 (4.3)	40	2.9
PS_{456}-*b*-P(NIPAAm$_{1108}$-*co*-SPA$_{77}$)	204,200	2.02	67.5	4.7 (6.5)	46	4.7
PS_{456}-*b*-P(NIPAAm$_{1047}$-*co*-SPA$_{107}$)	209,700	1.95	65.0	6.7 (9.3)	36	6.5
PS_{456}-*b*-P(NIPAAm$_{112}$-*co*-SPA$_{13}$)	65,600	1.13	19.4	2.2 (10.4)	-	3
PS_{456}-*b*-P(NIPAAm$_{54}$-*co*-SPA$_{6}$)	56,100	1.14	10.6	1.1 (9.4)	-	5

a) Absolute molar mass and *DP* determined by composition and absolute molar mass of macroinitiator, b) SEC in THF using a PS standard, c) ^{1}H-NMR in $CDCl_3$, number in parentheses refers to the amount of SPA in the hydrophilic segment only.

The block extension of PS with NIPAAm and SPA depends predominantly on the monomer to initiator ratio. However, the amount of built-in SPA in the hydrophilic segment is significantly higher than observed during the synthesis of the copolymers. We attribute this to the formation of free P(NIPAAm-*co*-SPA) copolymer that is not detected by SEC. This undetected copolymer cannot be distinguished from the block extended block terpolymer by ^{1}H-NMR, which results in a higher amount of SPA in the block terpolymer than actually present in the hydrophilic segment. The amount of SPA in the previously formed copolymers did not differ significantly from the amount of SPA in the respective monomer mixture, hence why we presume that also here the amount of SPA in the monomer mixture is represented in the composition of the hydrophilic segment.

In the section above, various PS-*b*-P(NIPAAm-*co*-SPA) block terpolymers were formed. The reaction conditions and purification procedure were optimised. The polymerisation procedure does not need to be adjusted significantly compared to the previous nitroxide-mediated polymerisations to form dual-responsive copolymers. However, precipitation of the terpolymer is challenging due to complex interactions between the reaction solvent and the precipitation solvent. As such, dialysis of the reaction mixture was tested, and lead to the successful removal of the unreacted monomer.

6.1.4 Synthesis of TEGA-containing Block Terpolymers

In the previous section, amphiphilic PS-*b*-P(NIPAAm-*co*-SPA) block terpolymers could be accessed. However, the purification was more challenging compared to the previously prepared set of copolymers. We therefore expect the preparation and purification of PS-*b*-P(TEGA-*co*-SPA) block terpolymers will also require a more complex work-up procedure. Apart from that, the synthesis does probably not need to be modified, since the reaction conditions did not need to be adjusted when switching from NIPAAm to TEGA as the thermo-responsive moiety in copolymers. We, therefore, synthesised amphiphilic PS-*b*-P(TEGA-*co*-SPA) diblock terpolymers using nitroxide-mediated polymerisation (Scheme 15). The macroinitiator was first dissolved in 1,4-dioxane containing TEGA or TEGA and 5 mol% SPA using a monomer to initiator ratio of 1333/1. The reaction mixture was then heated at 110 °C for 6 h.

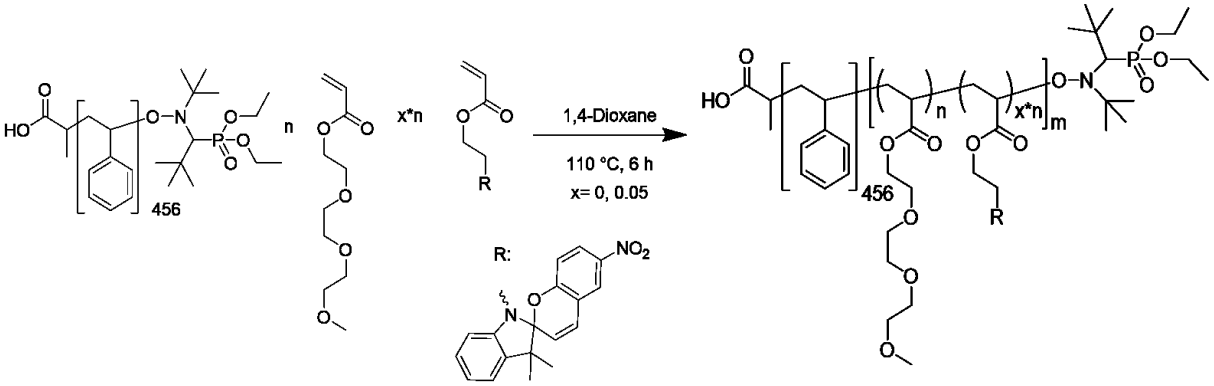

Scheme 15: Copolymerisation of TEGA and SPA in various combinations from a PS_{456} macroinitiator.

After the reaction, the crude product was precipitated into diethylether to remove the unreacted monomer (Figure 75a). As observed before for the NIPAAm-containing polymers, the SEC trace of the precipitate is bimodal, arising from the presence of the desired block terpolymer and free copolymer. In contrast to the block terpolymer, the unwanted copolymer that formed happens to be water-soluble. As such, the precipitated product was dispersed in a pH 8 buffer solution to isolate the remaining insoluble block terpolymer (Figure 75b).

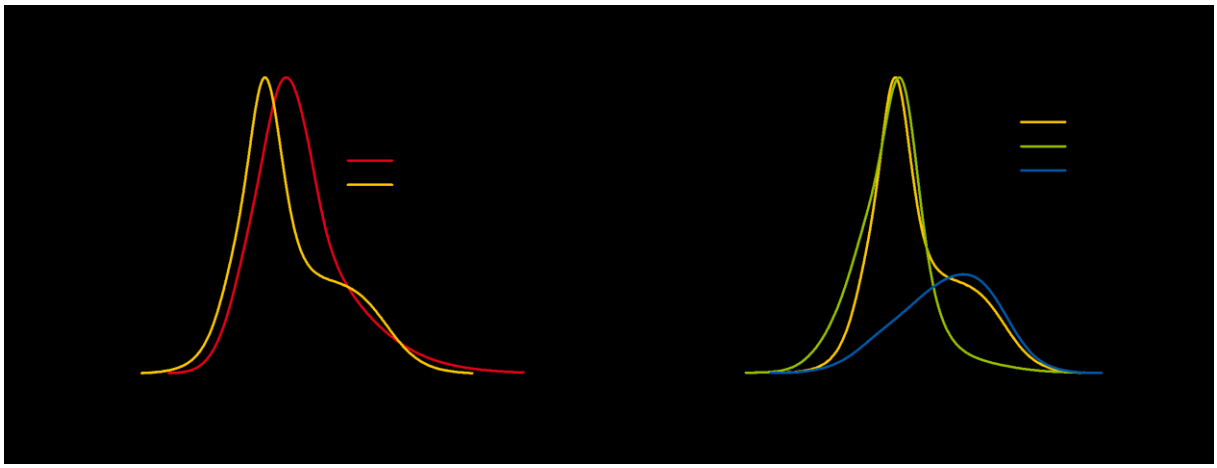

Figure 75: Work-up procedure used to purify crude PS_{456}-b-P($TEGA_{240}$-co-SPA_{31}) block terpolymers: a) polymers separated from unreacted monomer by precipitation, followed by b) dispersion in a pH buffer to precipitate the block terpolymer. SEC traces recorded in THF.

After the reaction, the crude product was analysed *via* SEC in THF. Besides a broadening of the elution trace, no other changes were observed. After precipitation in diethylether to remove unreacted monomer, the distribution appears bimodal due to the presence of PS-*b*-P(TEGA-*co*-SPA) and P(TEGA-*co*-SPA). This observation is in good agreement with the previous NIPAAm-containing polymers following precipitation. In order to separate these populations and isolate the desired PS-*b*-P(TEGA-*co*-SPA) block terpolymer, the polymeric mixture was dissolved in a pH 8 buffer solution. The P(TEGA-*co*-SPA) copolymer is water-soluble and remains dissolved, whilst the block terpolymer is insoluble in water and precipitates. After a certain period of time, the water becomes red, indicating the copolymer has dissolved, and the insoluble precipitate is separated from the solution. The SEC trace shows a clear shift to lower elution volumes for the block extended macroinitiator, and the degree of polymerisation could be determined from ^{1}H-NMR (Figure 76). Unfortunately, as we discussed previously, this purification strategy was not successful for the NIPAAm-containing polymers, as not all the copolymer could be removed. But for the TEGA-containing polymers discussed here, the monomer is completely removed, and no remaining copolymer is visible by SEC. Therefore, this is a suitable and efficient method to prepare a set of PS-*b*-P(TEGA-*co*-SPA) block terpolymers to investigate their micelle formation and dual stimuli-responsive behaviour.

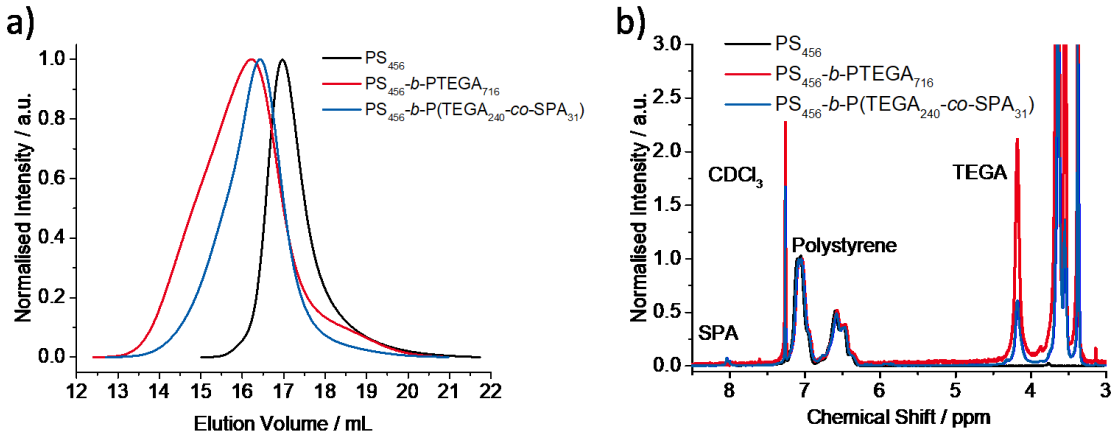

Figure 76: Block extension of PS_{456} dissolved in 1,4-dioxane with a mixture of TEGA and SPA (0 or 5 mol%): a) SEC traces and b) ^{1}H-NMR of the respective block terpolymers in $CDCl_3$ following work-up procedure.

Following the successful block extension of a PS macroinitiator with copolymers of TEGA and SPA, and elucidation of a suitable purification procedure, a set of block terpolymers was synthesised in order to investigate the responsive behaviour systematically. The monomers and PS_{456} macroinitiator were mixed in a molar ratio of 1333 to 1 in 1,4-dioxane. The monomer mixture contained 0, 5, 10, and 15 mol% of SPA. The mixture was degassed by three consecutive freeze-pump-thaw-cycles, heated at 110 °C for 8 h, and precipitated in diethylether. The obtained red powder was stored in a pH 8 buffer solution to dissolve the formed copolymer before subsequent analysis by SEC in THF and ^{1}H-NMR in $CDCl_3$. The results are shown in Figure 77.

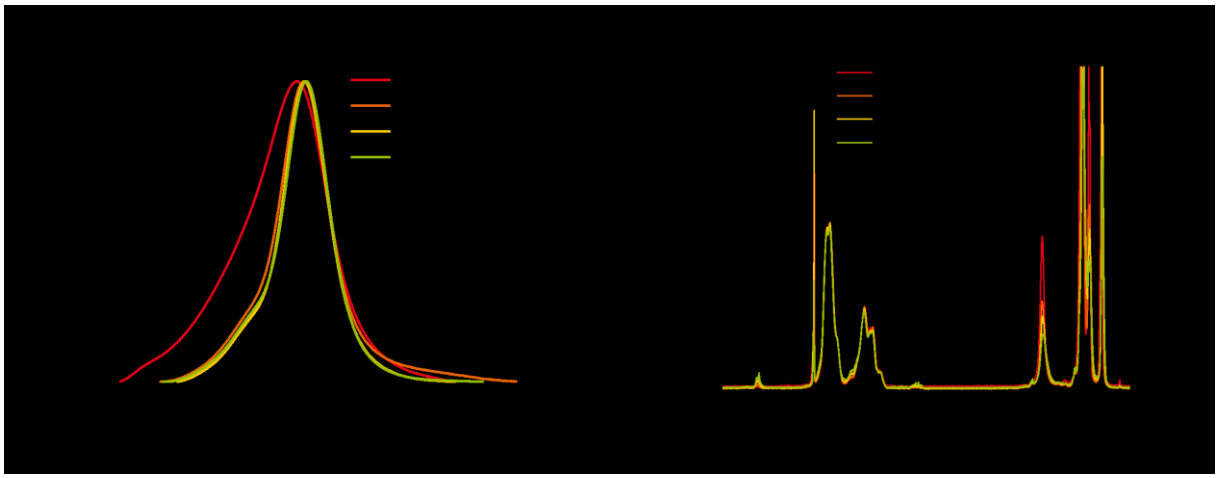

Figure 77: a) SEC traces of the PS macroinitiator in comparison to the block extended polymers with TEGA and SPA with the monomer mixture containing between 0 and 15 % SPA. b) ^{1}H-NMR spectra in $CDCl_3$ of the respective block terpolymers.

The block extension of the PS macroinitiator was performed in a similar manner as the copolymer synthesis described previously. The insoluble material is typically free from copolymer contaminants, and were investigated *via* SEC and ^{1}H-NMR (Table 18).

Table 18: Summarised degree of polymerisation and compositions for each added monomer (TEGA and SPA) of the previously synthesised block terpolymers after purification.

Sample	M_n[a)]	$Đ$[b)]	x_{TEGA}[c)] / %	x_{SPA}[c)] / %
PS_{456}	52,300[a)]	1.23	-	-
PS_{456}-*b*-$PTEGA_{716}$	203,800	2.22	61,1	-
PS_{456}-*b*-$PTEGA_{330}$	115,000	1.54	42.0	-
PS_{456}-*b*-P($TEGA_{203}$-*co*-SPA_8)	92,200	1.29	30.4	1.2 (3.8 %)
PS_{456}-*b*-P($TEGA_{240}$-*co*-SPA_{31})	112,400	1,59	33.0	4.2 (11.4 %)
PS_{456}-*b*-P($TEGA_{195}$-*co*-SPA_{16})	93,900	1.18	29.2	2.4 (7.6 %)
PS_{456}-*b*-P($TEGA_{169}$-*co*-SPA_{27})	93,000	1.19	26.0	4.1 (13.6 %)

a) M_n calculated from a combination of PS macroinitiator and ^{1}H-NMR, b) THF-SEC, RI detector using a PS calibration, c) ^{1}H-NMR in $CDCl_3$, numbers in parentheses refer to $\%_{SPA}$ in the hydrophilic segment only.

The formed PS-*b*-P(TEGA-*co*-SPA) block terpolymers present lower added repeating units of ~200; while it was possible to add ~1000 repeating units for the NIPAAm-containing equivalent block terpolymers. Though, the amount of SPA incorporated in the hydrophilic segment fit better to our previous observations concerning the formation of P(TEGA-*co*-SPA) copolymers. This makes the degree of polymerisation for this set of block terpolymers more plausible when compared to the NIPAAm-containing block terpolymers. A selection of the formed block terpolymers were then applied to form

stable compartments in solution, which we expect to show similar photo- and thermo-responsive behaviour as the previously investigated dual-responsive copolymers in solution.

6.2 Micellisation of Amphiphilic Diblock Terpolymers

The self-assembly of amphiphilic block terpolymers to micellar structures is a crucial step for the investigation of the dual-responsive behaviour of the hydrophilic segments located in the corona of micelles. The procedure to form micellar compartments is similar for all block terpolymers used. First, the block terpolymer is dissolved in THF before pH 8 TRIS buffer is added until the solution turns slightly turbid. The buffer ensures the correct pH-value of the micellar solution as for the copolymers before. To the turbid solution, a few drops of THF are added to redissolve the precipitated block terpolymer. The vial is then sealed and stirred overnight. This procedure is repeated until the desired amount of pH 8 TRIS buffer is added to reach a concentration of 0.5 g/L of block terpolymer in a buffer solution. The vial is then left open to let the volatile THF evaporate.

Dissolving SPA-containing block terpolymers in THF is not always possible without modifications. SPA exists in an equilibrium between the aromatic spiropyran-form and the zwitterionic merocyanine-form. Since both exist at room temperature, it is possible that insoluble polyelectrolyte complexes are formed between the zwitterionic merocyanine units. Constant irradiation at 525 nm leads to a shift in this equilibrium towards the SP-form, resulting in re-dissolution of the block terpolymer. After the formation of micellar structures, they are investigated *via* dynamic light scattering and cryo-TEM to assess the formed morphology in solution.

6.3 Characterisation of Amphiphilic Block Terpolymers Micelles

It is possible to determine the size and shape of the stable compartments in solution *via* various techniques. In most cases, the compartments scatter beams in a specific way, which can be used to gain information about the size of a particle. The beam can be visible light (dynamic light scattering), x-rays (small-angle x-ray scattering), or electrons (transmission electron microscopy). Dynamic light scattering (DLS) determines the particle size of the micelles by the fluctuation in light intensity due to diffusing particles into and out of the irradiated area. This fluctuation can be used to determine the Brownian diffusion coefficient. If the temperature, viscosity and refractive index of the surrounding medium is known, the diffusion coefficient can be used to determine the size of the actual particle. This calculation, however, only holds true for solid spheres that are only interacting with the surrounding solvent. For polydisperse systems, the distribution can be weighted since the scattering intensity increases with the size and number of particles. This manifests in numerous small particles showing a lower scattering intensity than a few large particles.

A selection of block terpolymers were used to form stable assemblies in solution and were analysed *via* DLS. The size distribution of the particles is depicted in Figure 78, indicating the specific block terpolymers selected.

The micellar structures formed from the selected block terpolymers are all characterised by a hydrodynamic radius between 20 and 100 nm, which is fairly typical for micellar solutions.[167] The TEGA-containing block terpolymers increase in size as the amount of SPA incorporated within the hydrophilic segment copolymer block increases. This is attributed to the lower solubility of the hydrophilic segment for increasing amounts of SPA. This trend, however, is not observed for the NIPAAm-containing block terpolymers. Some of the aggregates formed indicate a much larger size of around 500 nm, which most likely indicates the formation of vesicles.

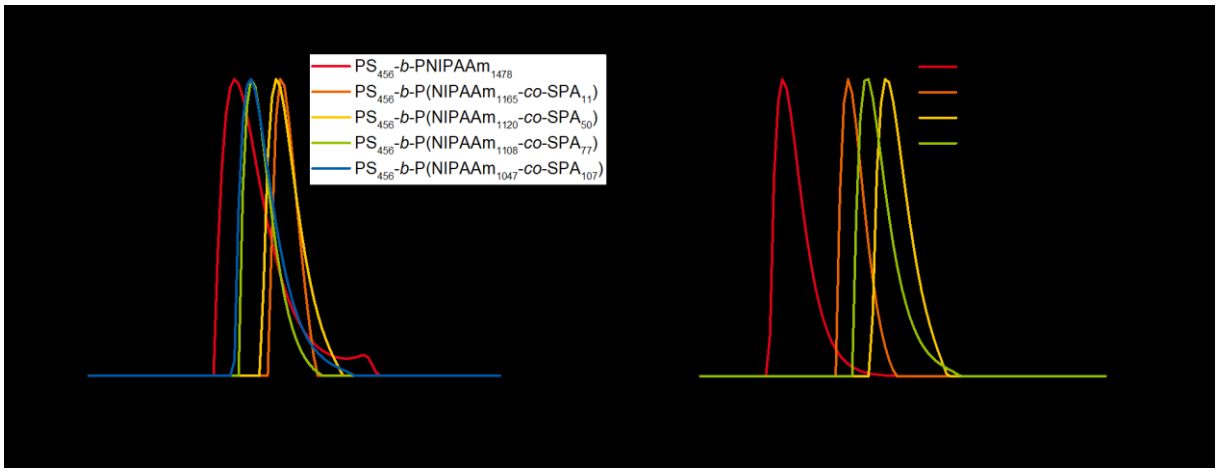

Figure 78: Number-weighted hydrodynamic radii of a) PS-b-P(NIPAAm-co-SPA) and b) PS-b-P(TEGA-co-SPA) block terpolymers determined via DLS in a pH 8 buffer solution.

The DLS results indicate spherical micelles were obtained, which we can verify using cryo-TEM. The general principle of cryo-TEM is similar to standard TEM. Here, an electron beam is also used to interact with the electrons in the analysed structures, which is why areas with a high electron density appear darker. The main difference lies in the sample preparation. In cryo-TEM, the samples are not dried. Drying samples for conventional TEM would destroy the structure of the compartments formed in

solution. So instead, the aqueous solutions are frozen and investigated in the solid-state. The micrographs of select samples are given in Figure 79.

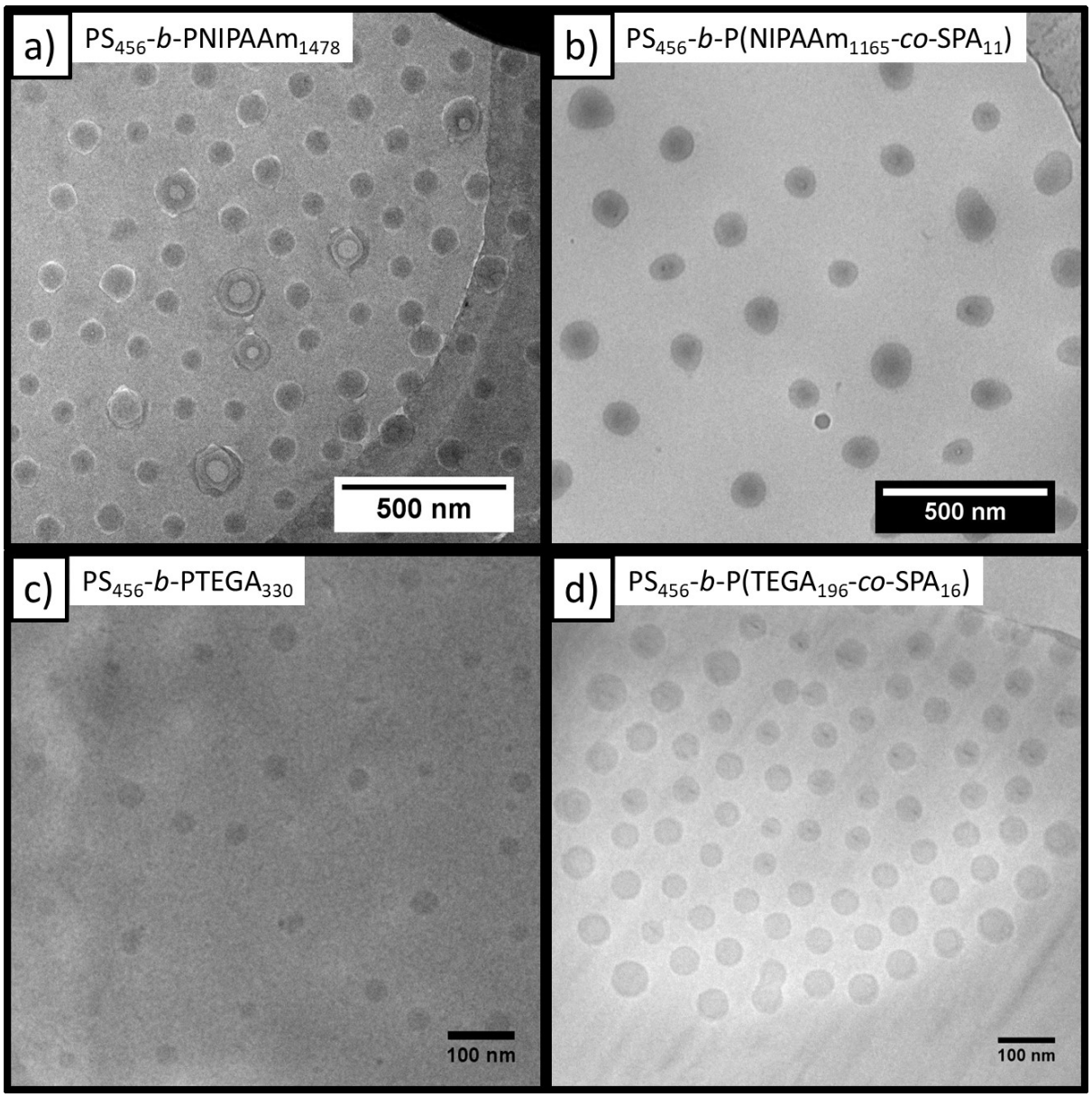

Figure 79: Cryo-TEM micrographs of the aggregates formed from selected block copolymers: a) PS_{456}-b-$PNIPAAm_{1478}$, b) PS_{456}-b-$P(NIPAAm_{1165}$-co-$SPA_{11})$ c) PS_{456}-b-$PTEGA_{330}$, and d) Ps_{456}-b-$P(TEGA_{196}$-co-$SPA_{16})$.

The cryo-TEM micrographs show spherical micelles for all four investigated block copolymers. The micrograph reveals core–shell-like structures for all investigated block copolymers. For PS_{456}-*b*-$PNIPAAm_{1478}$, spherical micelles and spherical vesicles of approximately double the size are visible. This second population was also visible by DLS. Although the PS_{456}-*b*-$P(NIPAAm_{1165}$-*co*-$SPA_{11})$ assemblies are expected to also contain free copolymer, the sample was still capable of forming stable compartments in solution. The particle size of the NIPAAm-containing block copolymers is much higher than the particle size of the TEGA-containing block copolymers, which is predominantly attributed to the larger hydrophilic segment. The size of the structures formed was measured for all given micrographs, and the results summarised in Table 19.

Table 19: Summary of the resulting micelle size formed from various amphiphilic block terpolymers according to DLS and cryo-TEM.

Polymer	$\langle R_h \rangle_{n,app}$ [a] / nm	Diameter[b] / nm
PS_{456}-*b*-$PNIPAAm_{1478}$	51.2	126.3 ± 30.9
PS_{456}-*b*-P($NIPAAm_{1165}$-*co*-SPA_{11})	85.3	154.4 ± 22.7
PS_{456}-*b*-P($NIPAAm_{1120}$-*co*-SPA_{50})	81.4	-
PS_{456}-*b*-P($NIPAAm_{1108}$-*co*-SPA_{77})	61.6	-
PS_{456}-*b*-P($NIPAAm_{1047}$-*co*-SPA_{107})	61.6	-
PS_{456}-*b*-$PTEGA_{330}$	25.5	37.2 ± 7.8
PS_{456}-*b*-P($TEGA_{203}$-*co*-SPA_{8})	53.6	-
PS_{456}-*b*-P($TEGA_{240}$-*co*-SPA_{31})	23.2	-
PS_{456}-*b*-P($TEGA_{195}$-*co*-SPA_{16})	77.7	55.1 ± 9.6
PS_{456}-*b*-P($TEGA_{169}$-*co*-SPA_{27})	67.6	-

a) determined *via* DLS, b) determined *via* cryo-TEM.

The size obtained from both methods for the NIPAAm-containing block copolymer assemblies are in close agreement. Unfortunately, the results obtained for the TEGA-containing block terpolymers are not in agreement. Here, the diameter determined by cryo-TEM resembles the hydrodynamic radius obtained from DLS. Possible reasons for this mismatch could include the lower electron density of the micelle corona, which means it is poorly visible in comparison to the core by TEM without additional staining. Alternatively, it can be presumed that the formed micelles are touching each other which allows the measurement from the centre of one micelle to an adjacent one. Nevertheless, various micelles from both thermo-responsive moieties were formed, and their dual stimuli-responsive behaviour investigated.

6.4 Amphiphilic Block Terpolymer Micelles and their Dual-Response

The dual-responsive behaviour of the micellar systems should not differ significantly from the behaviour of the copolymers investigated previously. The micelles should exhibit photo-responsive behaviour upon irradiation, as well as poorer solubility upon heating. This precipitation upon heating can be tuned by irradiation at either 340 or 540 nm. In order to compare the results of the copolymers with those of the block terpolymers, an identical setup was chosen and is shown in Figure 80.

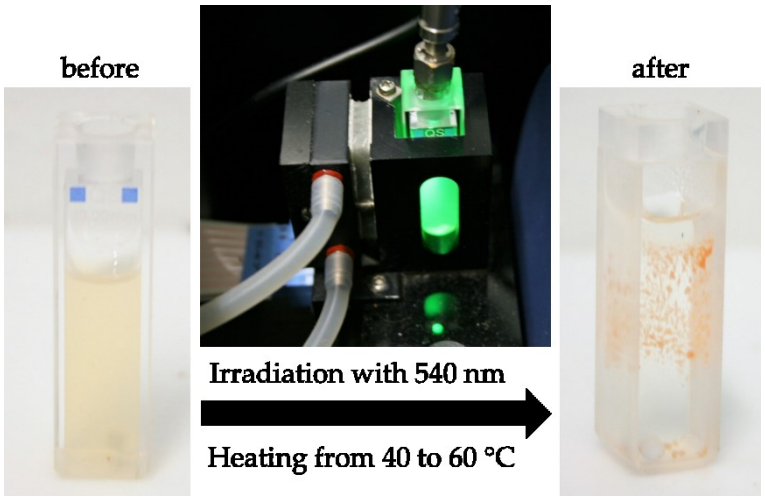

Figure 80: Experimental setup for the measurement of the dual-responsive behaviour of micellar systems in the UV-Vis.

The turbid micellar solution was irradiated at either 340 or 540 nm, and a time-dependent absorbance spectrum measured to investigate the photo-responsive behaviour. In a second experiment, the micelles were heated while being irradiated, and at each temperature, the transmission of the solution determined to show the dual-responsive behaviour. Naturally, the PS-*b*-PNIPAAm and PS-*b*-PTEGA block copolymers do not exhibit any photo-responsive behaviour, which simplifies the investigation of the thermo-responsive behaviour. This is why in our preliminary studies these block copolymer micelles were used to investigate the general behaviour of micellar solutions upon heating *via* UV-Vis spectrophotometry.

6.4.1 Behaviour of Block Copolymer Micelles Upon Heating

The thermo-responsive behaviour of the prepared block copolymer micelles was investigated in a similar manner as for the copolymers (chapter 5.4.3.1). The analyte is heated in the UV-Vis spectrometer, and at each temperature, a transmission spectrum is recorded. To increase the visibility of the transition temperature, the transmittance at 700 nm is plotted against the respective temperature. The micelles formed from PS-*b*-PNIPAAm result from three different reactions and contain 37.2, 37.7, and 43.4 mol% of PNIPAAm in the hydrophilic segment, and the radius of the formed micelles are in a comparable range as the PS_{456}-*b*-$PNIPAAm_{1478}$ micelles. Three samples of PS_{456}-*b*-$PTEGA_{330}$ micelles were heated in the UV-Vis spectrometer, and the averaged results are given in Figure 81.

The transition temperatures were determined in the same way as for the thermo-responsive copolymers. Performing the measurements in triplicate revealed that the method is reliable and reproducible, with the transition temperature not differing more than the step-width used in the heating protocol. When comparing the results to the investigations with the PNIPAA or PTEGA

homopolymer, the most obvious difference is the higher transmittance at low temperatures of ~90 %, which originate from the higher turbidity of the micellar solutions. In addition, a broad variation in the transmittance above the transition temperature was also observed. This originates form micellar aggregates that attach to the cuvette wall similarly to the observations from the respective copolymers. The transition temperature of the PNIPAAm-containing micelles do not differ; whilst the transition temperature of the PS-*b*-PTEGA micelles is 5 °C lower than the transition temperature of the PTEGA homopolymer.

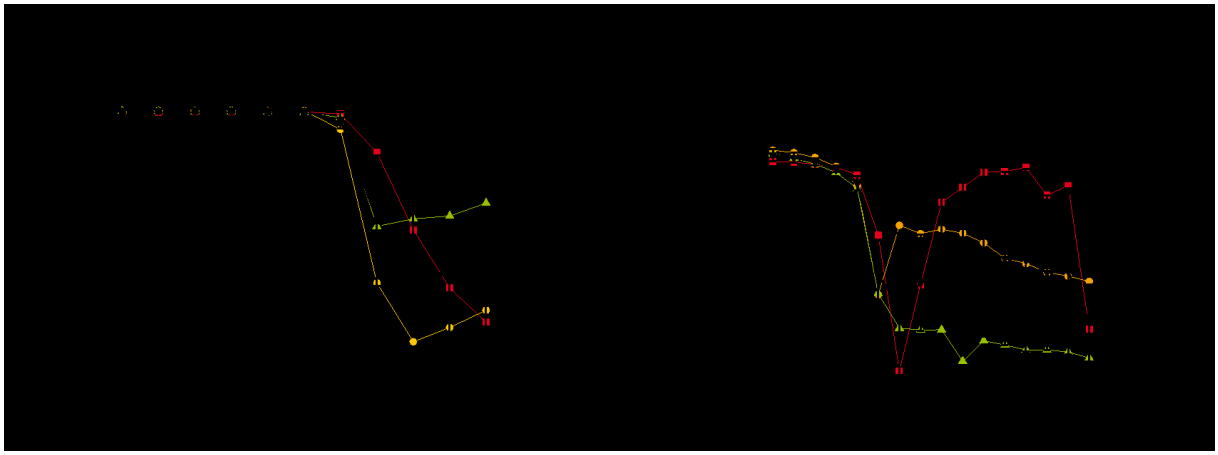

Figure 81: Transmittance at 700 nm of thermo-responsive micelles formed from a) three comparable PS-b-PNIPAAm block copolymers and b) PS_{456}-b-$PTEGA_{330}$. Transition temperature averaged from three measurements.

The transition temperature of the micelles originates from the collapse of the hydrophilic corona, and this behaviour can also be observed *via* dynamic light scattering. Upon coronal collapse, the micelle hydrodynamic radius should decrease. The collapsed PNIPAAm-segments are insoluble in water, which will result in the aggregation of the micelles to form larger compartments that precipitate from solution. This will lead to an increase in particle size, but also to a decrease in the scattering intensity. To investigate these considerations, the micelles formed from PS_{456}-*b*-$PNIPAAm_{1478}$ were heated from 25 to 35 °C, and at each temperature a waiting time of 15 min was used before the particle size was determined. The micelles formed from the PS_{456}-*b*-$PTEGA_{330}$ block copolymer were heated to 70 °C to measure the increase in aggregate size above the transition temperature. Subsequently, the micellar solution was cooled and stored at room temperature for 24 h. This leads to a redissolution of the micellar structures, to show the reversible nature of the thermo-responsive behaviour. The hydrodynamic radii during both experiments are depicted in Figure 82.

The NIPAAm-containing micelles show an increase in hydrodynamic radius upon heating above 30 °C. This originates from the aggregation of the insoluble block copolymer compartments. The transition temperature of 30 °C is approximately 1 °C lower than the transition temperature observed by UV-Vis. This variation between the two methods arises due to the different responses measured. Using the DLS, the aggregation of two or more micelles is measured, which naturally happens at slightly lower temperatures than the precipitation of the micelles as measured by UV-Vis. Longer waiting times at each temperature should narrow the difference between the two methods. The transition temperature was determined *via* DLS for four different PS-*b*-PNIPAAm copolymers and range between 30 and 32 °C. The increase in particle size upon heating is also observed for the micelles formed from the PS_{456}-*b*-$PTEGA_{330}$ block copolymer. After a resting time of 24 h, the micelles return to their original size. This indicates the thermo-response is reversible. The structural changes upon application of an external stimulus is reversible since heating above the transition temperature of PTEGA at ~65 °C only

affects the corona of the micelle. The core consists of PS, which has a much higher T_g than the transition temperature of the corona. This leads to aggregation upon heating, but the structure of a single micelle is not affected by precipitation. A similar behaviour as for the micelles formed from PS_{456}-*b*-$PTEGA_{330}$ was also observed for the micelles formed from PS_{456}-*b*-P($TEGA_{240}$-*co*-SPA_{31}). Unfortunately, it is not possible to observe the photo-response of the micellar systems *via* DLS, since the micellar size does not change upon irradiation. This makes this method unsuitable for the investigation of the dual-responsive behaviour of the prepared micelles.

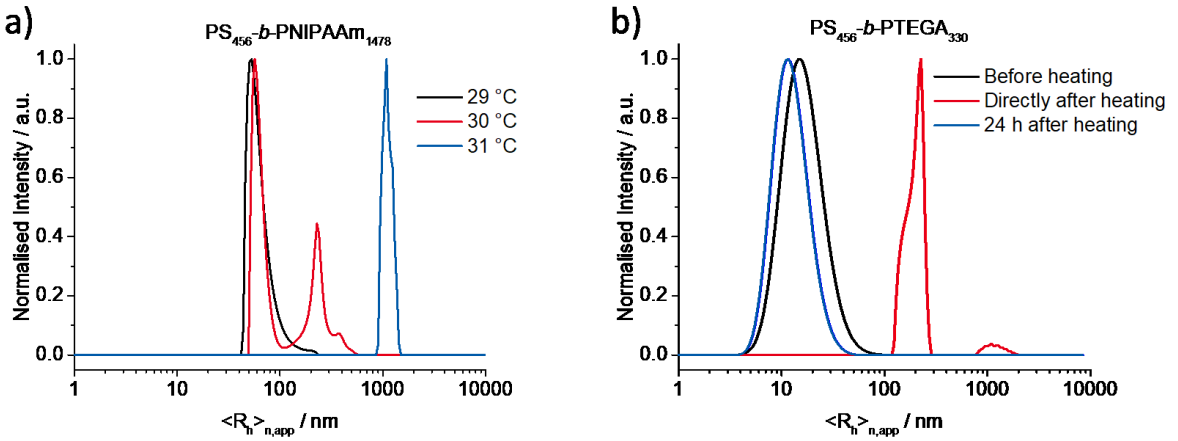

Figure 82: Changes observed by DLS of micelles formed from selected block copolymers upon heating. a) PS_{456}-b-$PNIPAAm_{1478}$ heated to different temperatures, and b) PS_{456}-b-$PTEGA_{330}$ before, directly after heating above the transition temperature, and 24 h after the heating process.

6.4.2 Photo-Responsive Behaviour of Micellar Solutions

The photo-responsive behaviour of the micellar systems could be investigated using the same experimental procedure as the photo-response of the copolymers (see chapter 5.4.2.1). As the photo-response of the SPA moiety was also possible in the solid-state, although it was significantly slower, it is likely that micellar systems react similarly to irradiation.

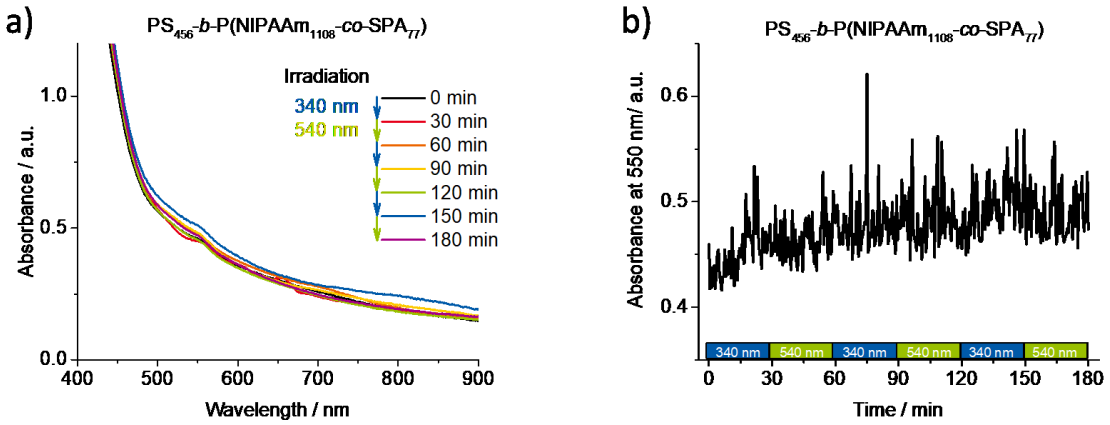

Figure 83: Photo-response of a 0.5 g/L PS_{456}-b-P($NIPAAm_{1108}$-co-SPA_{77}) micellar solution in pH 8 buffer irradiated at 340 and 540 nm for 30 min for three consecutive cycles. a) Absorbance spectra at the beginning and the end of each cycle, and b) absorbance at 550 nm with time.

Similarly to the copolymers investigated earlier, the formed micelles were irradiated at 340 nm followed by irradiation at 540 nm to complete one cycle. This irradiation cycle was then performed three times. Upon irradiation, the turbid solution is expected to undergo spectral changes, particularly

at an absorbance wavelength of 550 nm. An increased absorbance at 550 nm indicates an increasing number of SPA units have switched to the zwitterionic merocyanine-form, whilst a decrease in absorbance indicates an increasing number of SPA units have switched to their aromatic spiropyran-form. The photo-response of the PS_{456}-*b*-P($NIPAAm_{1108}$-*co*-SPA_{77}) micelles were first investigated, and the results are shown in Figure 83.

The absorbance of a micellar solution, in general, differs from the absorbance observed for a dissolved copolymer. The absorbance increases due to the turbidity of the solution caused by elastic scattering of the light from the stabilised compartments. This elastic scattering leads to a low absorbance at long wavelengths, and to higher absorbance at shorter wavelengths. The overlapping effects of elastic and inelastic scattering complicates the interpretation of the photo-response. During the measurements, the absorbance spectra do not change significantly upon irradiation. This is further visualised when plotting the absorbance at 550 nm over time. The lack of an observed effect originates from several factors. First, it is possible that the SPA moiety does not respond to irradiation in micellar systems because of the SPA moieties interfering with each other due to their close proximity. However, this is improbable since the SPA moiety responds to irradiation in the solid-state. It is further plausible that the high scattering of the micellar aggregates leads to an overlapping absorbance of the MC- and SP-form. This will also result in spectral changes that cannot be visualised. A possible solution is increasing the amount of SPA in the micellar corona. A higher SPA content in the micellar corona may lead to a more intense response that may result in an observable photo-response by UV-Vis spectroscopy. Higher amounts of SPA are not possible for the NIPAAm-containing block terpolymers since they may become insoluble in water. The TEGA-containing block terpolymers, on the other hand, can contain higher amounts of SPA. Here the micellar aggregates formed from PS_{456}-*b*-P($TEGA_{240}$-*co*-SPA_{34}) and PS_{456}-*b*-P($TEGA_{196}$-*co*-SPA_{16}) were irradiated following similar irradiation protocols used for the water-soluble copolymer systems. The results are given in Figure 84 and Figure 85 for PS_{456}-*b*-P($TEGA_{240}$-*co*-SPA_{34}) and PS_{456}-*b*-P($TEGA_{196}$-*co*-SPA_{16}), respectively.

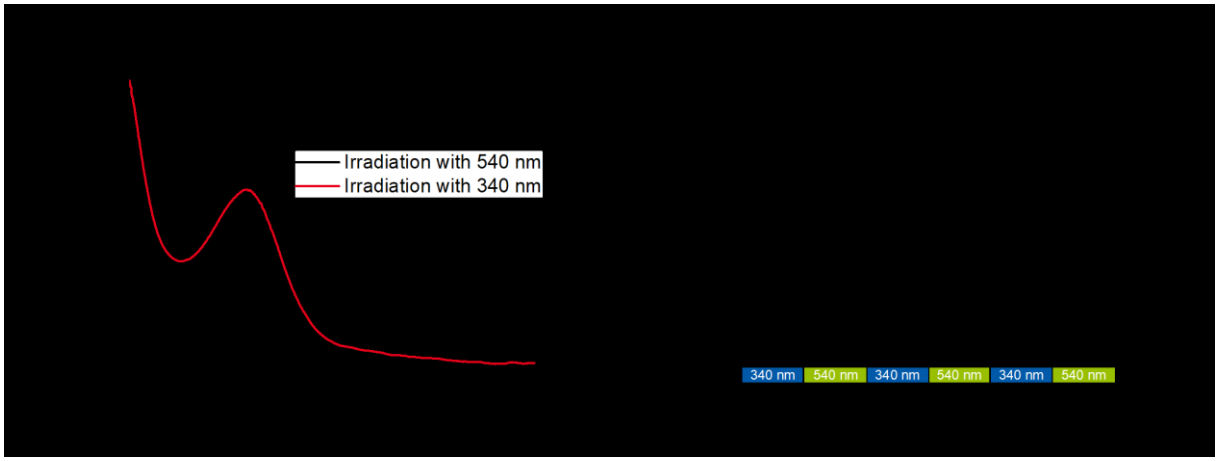

Figure 84: Behaviour of PS_{456}-b-P($TEGA_{240}$-co-SPA_{34}) micelles upon the application of external stimuli. a) Absorbance spectra of the micelles upon irradiation with either 540 or 340 nm light and the b) absorbance at 540 nm over three consecutive switching cycles.

The absorbance spectra of the PS_{456}-*b*-P($TEGA_{240}$-*co*-SPA_{34}) micelles changes upon irradiation as expected: the absorbance increases at 540 nm upon irradiation at 340 nm, and decreases again upon irradiation at 540 nm. This process is reversible (Figure 84b), and the maximum absorbance decreases after every cycle as already observed for the water-soluble copolymers. The photo-response also appears faster than for the free copolymers, since the absorbance at 540 nm reaches a maximum after

20 min of irradiation at 340 nm, indicating a maximum number of SPA units are present in the MC-form. This faster photo-response may originate from the different SPA moieties affecting each other in a kind of chain-reaction and one switched SPA moiety triggers the response of the next SPA moiety in close proximity. As shown in Figure 85, the behaviour of the PS_{456}-*b*-P($TEGA_{196}$-*co*-SPA_{16}) micelles varies slightly from the PS_{456}-*b*-P($TEGA_{240}$-*co*-SPA_{34}) micelles.

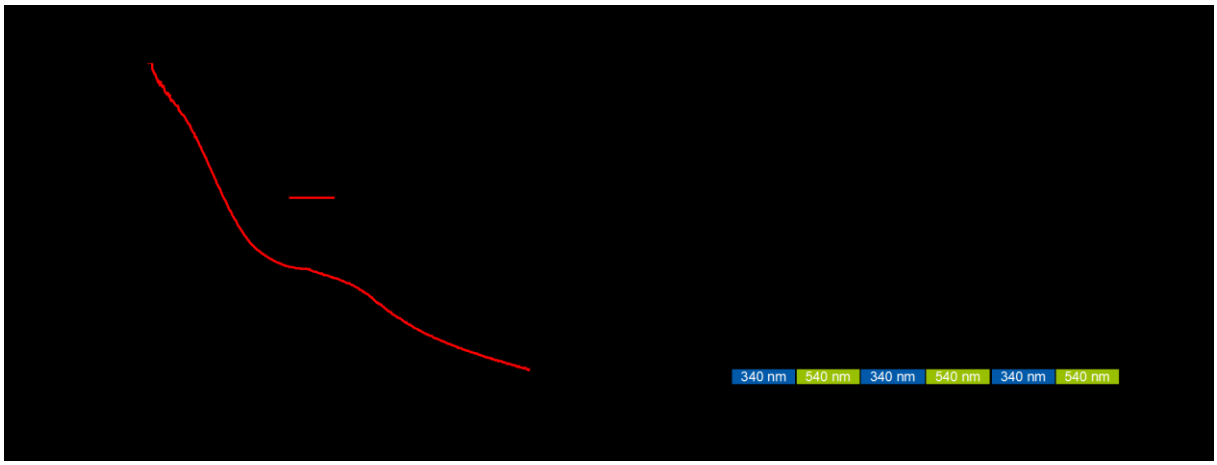

Figure 85: Behaviour of PS_{456}-b-P($TEGA_{194}$-co-SPA_{16}) micelles upon the application of external stimuli. a) Absorbance spectra of the micelles upon irradiation with either 540 or 340 nm light, and b) the absorbance at 600 nm over three consecutive switching cycles.

The absorbance spectra of the PS_{456}-*b*-P($TEGA_{196}$-*co*-SPA_{16}) micelles changes upon irradiation, but the shape differs compared to the previously investigated PS_{456}-*b*-P($TEGA_{240}$-*co*-SPA_{34}). Here, the highest change in absorbance is observed at 600 nm rather than 550 nm. This is attributed to the higher absorbance of the micellar systems due to elastic scattering. Hence why in this case the absorbance at 600 nm is plotted over time. The photo-response upon irradiation at 340 nm is also significantly faster than for the corresponding copolymer containing a comparable amount of SPA. After the fast increase in absorbance at 600 nm, it drops significantly. For the free copolymers, such an observation was assigned to decomposition or protonation of the SPA moiety in the MC-form. Irradiation at 540 nm results in a subsequent decrease in the absorbance at 600 nm back to the initial absorbance before irradiation. This process is reversible over three cycles, but the last cycle does not exhibit a noticeable response. During these measurements, some aggregates formed in the micellar solution, which anyway remained largely turbid, and the formation of these aggregates is clearly visible in the time traces. This manifests in the observed spikes shown in Figure 85b. The close proximity of the SPA moieties in micellar systems clearly affects each other more drastically than for free copolymers, causing micelle precipitation. Nevertheless, the block terpolymer micelles exhibit the expected responsive behaviour in a similar way as the free copolymers in solution.

6.4.3 Simultaneous Response of Block Terpolymer Micelles to Temperature and Light

The dual-responsive behaviour of the prepared micelles was probed in a similar manner as for the water-soluble copolymers. The turbid solution was irradiated at 540 nm and heated in small incremental steps. At each step, an absorbance spectrum was recorded, and the absorbance at 700 nm plotted against temperature. The sample was then irradiated at 340 nm and the heating protocol repeated in the same manner. Since the micelles formed from PS_{456}-*b*-P($NIPAAm_{1108}$-*co*-SPA_{77}) do not exhibit any measurable photo-responsive behaviour, the transition temperature may also be independent of the irradiation state. The measured transition temperature was however blurred,

which complicates its exact determination. The half value of the transmission was reached at approximately 27 °C. Furthermore, no difference was observed upon heating under irradiation with 340 or 540 nm light. A general shift in the transition temperature to lower temperatures with increasing amounts of SPA in the copolymer was already observed for the water-soluble copolymers. However, the investigated block terpolymer contains 6.5 % SPA in the hydrophilic segment, which would lower the transition temperature to approximately 20 °C, which could not be confirmed for the given PS_{456}-*b*-P(NIPAAm$_{1108}$-*co*-SPA$_{77}$) micelles.

The TEGA-containing block terpolymers, on the other hand, did exhibit photo-responsive behaviour in a comparable manner to the P(TEGA-*co*-SPA) copolymers. Here, we repeated the same experiments used for the copolymers using the micellar solutions. The micellar solutions of PS_{456}-*b*-P(TEGA$_{240}$-*co*-SPA$_{34}$) and PS_{456}-*b*-P(TEGA$_{196}$-*co*-SPA$_{16}$) were heated from 35 to 55 °C in 1 °C steps with a waiting time of 10 min at each step to reach thermal equilibrium. For simplicity, only the transmittance of the sample at 700 nm for different temperatures is shown in Figure 86.

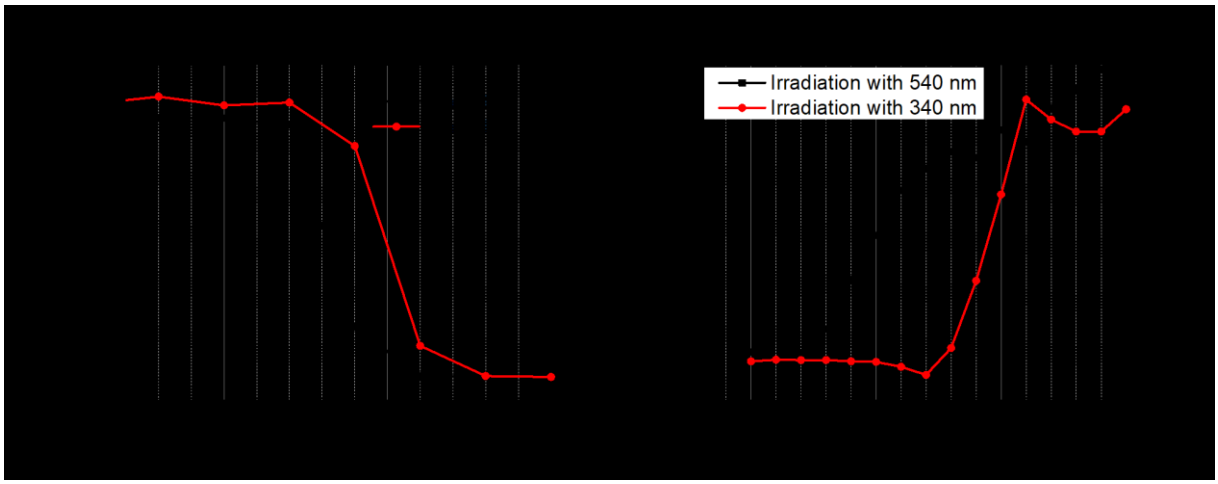

Figure 86: Response of micelles upon irradiation with 540 (black) or 340 nm (red) light and heating. Transmittance at 700 nm of micellar solutions formed from a) PS_{456}-b-P(TEGA$_{240}$-co-SPA$_{34}$) and b) PS_{456}-b-P(TEGA$_{194}$-co-SPA$_{16}$) block terpolymers.

The PS_{456}-*b*-P(TEGA$_{240}$-*co*-SPA$_{34}$) block terpolymer, which already showed similar photo-responsive behaviour as the copolymers, also exhibits the expected decrease in absorbance at 700 nm. The transition temperature varies depending on the irradiation state of the sample, as already observed for the copolymers. However, the transition temperature is significantly lower than for the analogous dissolved copolymer. The corona of PS_{456}-*b*-P(TEGA$_{240}$-*co*-SPA$_{34}$) contains 11.4 % SPA, which should result in a significantly higher temperature difference in the transition temperature with the irradiation state. The PS_{456}-*b*-P(TEGA$_{196}$-*co*-SPA$_{16}$) micelles exhibit contrary behaviour: here the transmittance is initially relatively low at ~20 % before it increases to ~80 % due to precipitation of the aggregates. In both irradiation states, heating leads to coronal collapse and precipitation, and therefore results in a higher transmission. Irradiation at 540 nm leads to a transition temperature of 45 °C, whereas irradiation at 340 nm leads to a transition temperature of 50 °C. In order to better compare the block terpolymer behaviour to the free copolymer, the transition temperatures of the PS_{456}-*b*-P(TEGA$_{196}$-*co*-SPA$_{16}$) micelles were plotted with the transition temperatures of the P(TEGA-*co*-SPA) copolymers (Figure 87).

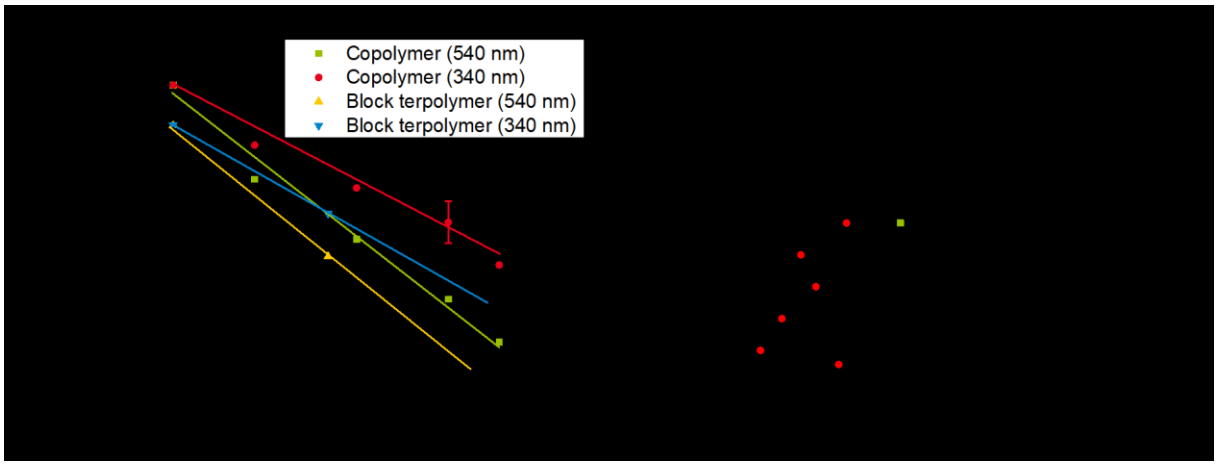

Figure 87: Thermo-responsive behaviour of dual stimuli-responsive micelles compared to the water-soluble copolymers. a) Change in transition temperature for different irradiation states (the lines are just to guide the eye), and b) temperature difference between both irradiation states with varying amounts of SPA in the hydrophilic segment.

The PS_{456}-*b*-P($TEGA_{196}$-*co*-SPA_{16}) block terpolymer contains 7.6 % SPA in the hydrophilic corona-forming segment. However, the thermo-response of the micelles is constantly higher than the thermo-response of a comparable copolymer. In order to describe the relationship between the transition temperature and the amount of SPA in the copolymer or the hydrophilic segment, they were fitted using a standard linear fit: y = m*x + b. The results are summarised in Table 20.

*Table 20: The transition temperature plotted over the amount of SPA in the copolymer, as well as for the terpolymer using the equation y = m * x + b.*

	Irradiation Wavelength / nm	b	m	R^2
Copolymer	540	64.16 ± 0.96	-1.22 ± 0.09	0.9771
	340	63.32 ± 1.30	-1.78 ± 0.13	0.9802
Diblock Terpolymer	540	60.33	-1.36	-
	340	60.33	-2.02	-

The y-intercept (b) for the copolymers does not depend on the irradiation state, and is approximately 64 °C for the copolymers, and approximately 60 °C for the amphiphilic diblock terpolymers. This fits the previous considerations of the polystyrene block as a large hydrophobic end group. The slope for the samples irradiated with 340 nm light is similar for both copolymers and block terpolymers, and a similar trend is observed for the samples irradiated at 540 nm. As shown previously for the P(TEGA-*co*-SPA) copolymers, the switching state of the SPA moiety has a significant effect on the detected cloud point temperature. This effect of the SPA switching state also seems to apply for the described diblock terpolymers, PS-*b*-P(TEGA-*co*-SPA). Considering the overall differences in temperature, it appears that the effect of the incorporated SPA moieties is independent of the sample investigated. This is further confirmed by plotting the temperature difference over the amount of SPA in the copolymer or the corona (Figure 87b). The observed temperature difference fits well with the expected behaviour of a copolymer with the expected amount of SPA.

In this section, dual stimuli-responsive micelles were formed from a polystyrene core and a dual-responsive corona consisting of a thermo- and photo-responsive segment. It was possible to form block terpolymers containing either NIPAAm or TEGA as the thermo-responsive moiety. It was also possible to form stable compartments in water from these block terpolymers, and their size elucidated by DLS and cryo-TEM. The micelles further exhibit thermo-responsive behaviour. PNIPAAm-containing

micelles show a transition temperature of 32 °C; whereas, the PTEGA-containing micelles show a transition temperature of 60 C, which is about 4 °C lower than the PTEGA homopolymer. The TEGA-containing micelles further exhibit photo-responsive behaviour, and their light-dependent transition temperature is also shifted to lower values by 4 °C. This further confirms that the spiropyran moiety influences the thermo-responsive behaviour and that the thermo-responsive behaviour is independent of the thermo-responsive moiety used or the proximity of the dual-responsive copolymer-chains. This preliminary work further confirms that dual-responsive behaviour may be exploited in other aggregate-based systems such as membranes.

7 Light- and Thermo-Responsive Block Terpolymer Porous Membranes

Parts of this chapter have been published in Zalami, D.; Grimm, O.; Schacher, F. H.; Gerken, U.; Köhler, J., Non-invasive study of the three-dimensional structure of nanoporous triblock terpolymer membranes. Soft matter 2018, 14 (48), 9750-9754.[226]

The focus of this chapter is the formation of polymeric membranes, their structures, and the corresponding physical and chemical properties of the block copolymers used. First, an introduction to membranes, in general, is given with a focus on polymeric membranes and the formation of integral asymmetric membranes from amphiphilic block copolymers. The amphiphilic block copolymers used for the formation of membranes have a comparable composition to the block terpolymers utilised in the previous chapter for the formation of micellar structures, and these block terpolymers also exhibit self-assembly. Therefore, membranes formed from these block terpolymers should exhibit the same stimuli-response as observed previously. Similarly to micellar systems, the dual stimuli-responsive segment projects out from the surface and is therefore predominantly found in the pores. This enables the void volume to increase or decrease upon the collapsing or swelling of the hydrophilic segment.

In addition to the methods used to characterise the prepared polymers described previously, scanning electron microscopy (SEM) and water-flux investigations were performed to investigate the prepared integral asymmetric membranes. Furthermore, a cooperation partner introduced 3D single-particle orbit tracking (SPOT) to gain further non-invasive insight into the diffusion path length of different nanoparticles inside the cavities of the prepared membranes. As a final step, a dual stimuli-responsive amphiphilic triblock terpolymer containing spiro- and NIPAAm moieties in the hydrophilic segment was synthesised, and a membrane formed from this triblock terpolymer. The thermo- and photo-response of the prepared membrane was then investigated.

7.1 Synthesis of Block Terpolymers for Membrane Formation

For the method chosen to prepare membranes here, the polymer synthesis is crucial. Here, we exploited our previous optimised systems to form suitable responsive block terpolymers for membrane formation. We will then explore the stimuli-responsive behaviour of the prepared membranes, first addressing one stimulus at a time, *e.g.*, temperature, through the inclusion of PNIPAAm. After the synthesis of a suitable macroinitiator, different hydrophilic chain lengths were added (Figure 88). The well-defined block terpolymers synthesised were then used to prepare porous membranes according to literature conditions.

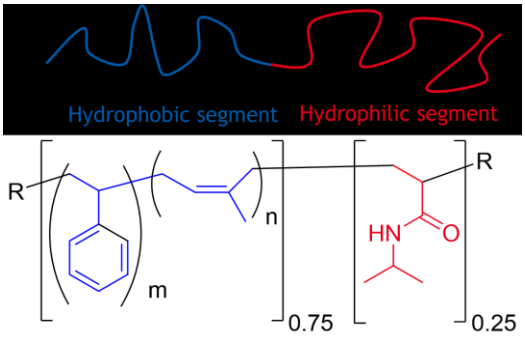

Figure 88: Amphiphilic block terpolymer structure. The fractions shown here refer to the desired block ratios.

7.1.1 Macroinitiators and Building Blocks

Previously, our group showed that a block copolymer of styrene (S) and isoprene (I) is suitable for the hydrophobic segment of stimuli-responsive membranes.[196, 212] Nitroxide-mediated polymerisation (NMP) was used to synthesise the macroinitiator of S and I, as well as for the subsequent block extension with a stimuli-responsive hydrophilic segment.[212] Furthermore, our group showed that the block extension from a block copolymer is more predictable than from a copolymer (results unpublished). The nitroxide group used to initiate and reversibly end-cap growing chains in NMP has a significant impact on the polymerisation. Here, the previously described SG-1 radical (BlocBuilder) exhibits good results and is easier to synthesise than the NMP initiator 1-*tert*-butyl-3,3-dipropyl-5,5-diethyl-4-1(1-phenylethoxy)-piperazin-2-one (chapter 5.3.2). The macroinitiators prepared were characterised *via* SEC to determine the molar mass and dispersity, and by ^{1}H-NMR to determine the composition. Since the synthesis of polystyrene, poly(styrene-*co*-isoprene) and polystyrene-*block*-polyisoprene are well-known, only exemplary SEC traces and NMR spectra are shown here (Figure 89).

The PS and PS-*b*-PI macroinitiators are narrowly distributed with dispersities around 1.1, and are therefore suitable for block extension. In most cases, we expect that block extension will result in an increase in the measured molar mass by SEC, shifting the RI trace to lower elution volumes. The elution volume of an SEC measurement, however, depends on the hydrodynamic radius of the dissolved polymer. Since the hydrodynamic radius depends on complex interactions between the solvent and the polymer, it is possible for block copolymers to appear lower in molar mass than the corresponding macroinitiator, or to show no change at all. If not stated otherwise, the molar mass of the block terpolymers is determined using the molecular weight of the PS macroinitiator and then calculating the mass after block extension from the ratio of the respective blocks determined from ^{1}H-NMR.

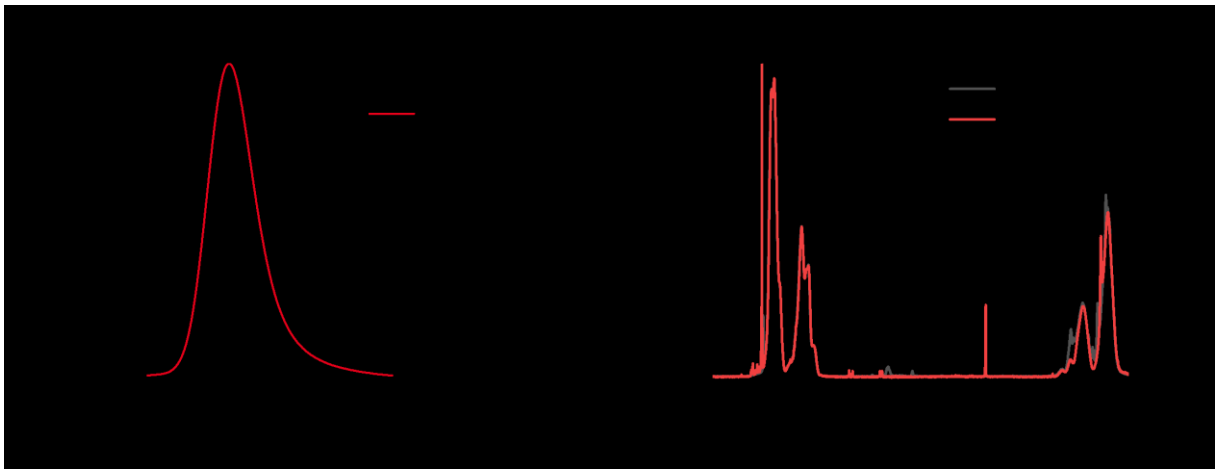

Figure 89: Typical (a) SEC traces and (b) ^{1}H-NMR spectra of the prepared macroinitiators used. The SEC measurements were performed using chloroform as eluent, and the ^{1}H-NMR spectra were recorded in $CDCl_3$.

7.1.2 Macroinitiator Block Extension with a Stimuli-Responsive Hydrophilic Segment

To fabricate stimuli-responsive membranes, the PS-*b*-PI macroinitiator was block extended with PNIPAAm. Here, similar reaction conditions were applied as used for the block extension of the micellar systems (chapter 6.1.2). The PS-*b*-PI macroinitiator was dissolved in 1,4-dioxane and mixed with varying amounts of NIPAAm. After a reaction time of 20 h at 110 °C, the reaction mixture was precipitated; first in methanol, then water, before being dried under reduced pressure. We aimed to prepare triblock terpolymers with a hydrophilic segment accounting for 15 to 25 mol% of the triblock terpolymer, and subsequently analysed the prepared triblock terpolymers *via* SEC and NMR (Table 21).

Table 21: Triblock terpolymers with varying amounts of PNIPAAm.

Polymer	Amount of PNIPAAm[a] / %	M_n[b] / g/mol	$Đ$[d]
PS_{546}	0	49,100[c]	1.14
PS_{546}-*b*-PI_{24}	0	50,500	1.15
PS_{546}-*b*-PI_{24}-*b*-$PNIPAAm_{28}$	15	61,600	1.40
PS_{546}-*b*-PI_{24}-*b*-$PNIPAAm_{168}$	21	77,500	1.46
PS_{546}-*b*-PI_{24}-*b*-$PNIPAAm_{202}$	26	81,400	1.23

a) determined *via* ^{1}H-NMR in $CDCl_3$, calculated from the absolute molar mass of the PS macroinitiator and composition determined from ^{1}H-NMR, c) absolute molar mass determined from SEC in DMAc using a PS calibration, d) PS calibration in DMAc.

All triblock terpolymers synthesised here have a molar mass over 50,000 g/mol with the desired hydrophilic content to form integral asymmetric membranes *via* the SNIPS process. The SEC traces and ^{1}H-NMR spectra show no unexpected results (Figure 90).

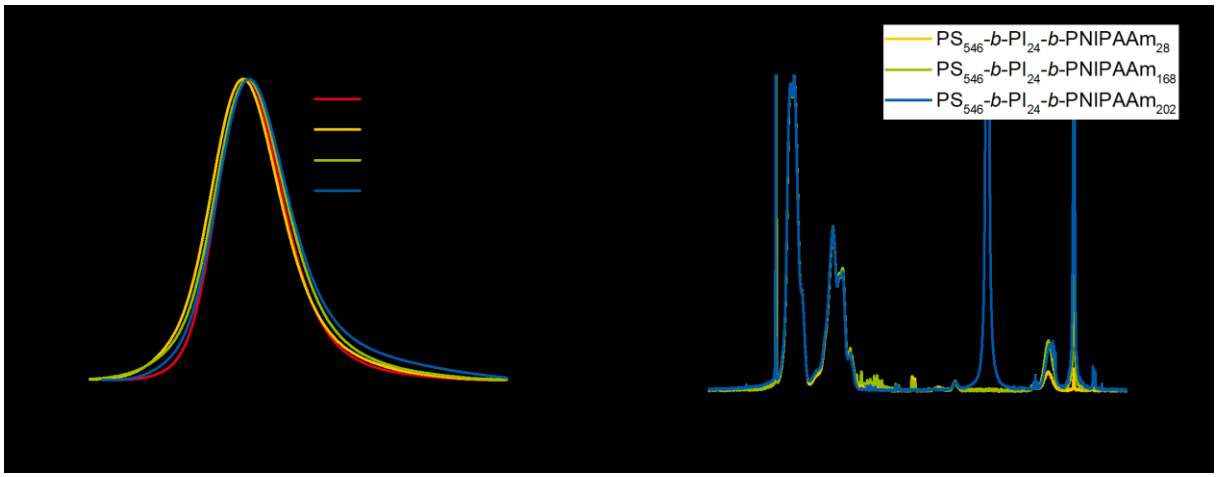

Figure 90: (a) SEC traces in DMAc and (b) ^{1}H-NMR spectra in $CDCl_3$ of the synthesised triblock terpolymers.

All obtained SEC traces are monomodal, and the ^{1}H-NMR spectra show increasing amounts of PNIPAAm are incorporated with increasing amounts of NIPAAm in the monomer mixture. On closer inspection of the SEC traces of the triblock terpolymers (Figure 3a), it is unclear whether the PNIPAAm block is attached to the macroinitiator. The addition of the hydrophilic segment does not change the apparent hydrodynamic radius. However, normalising the ^{1}H-NMR spectra to the PS signal at 7 ppm reveals an increasing amount of PNIPAAm in the block terpolymers at a chemical shift of 4 ppm. The NMR spectra also reveals remaining solvent. In order to confirm a successful block extension, diffusion coupled NMR was performed. In Figure 91, the DOSY spectrum of the triblock terpolymer in DMSO-d_6 is shown.

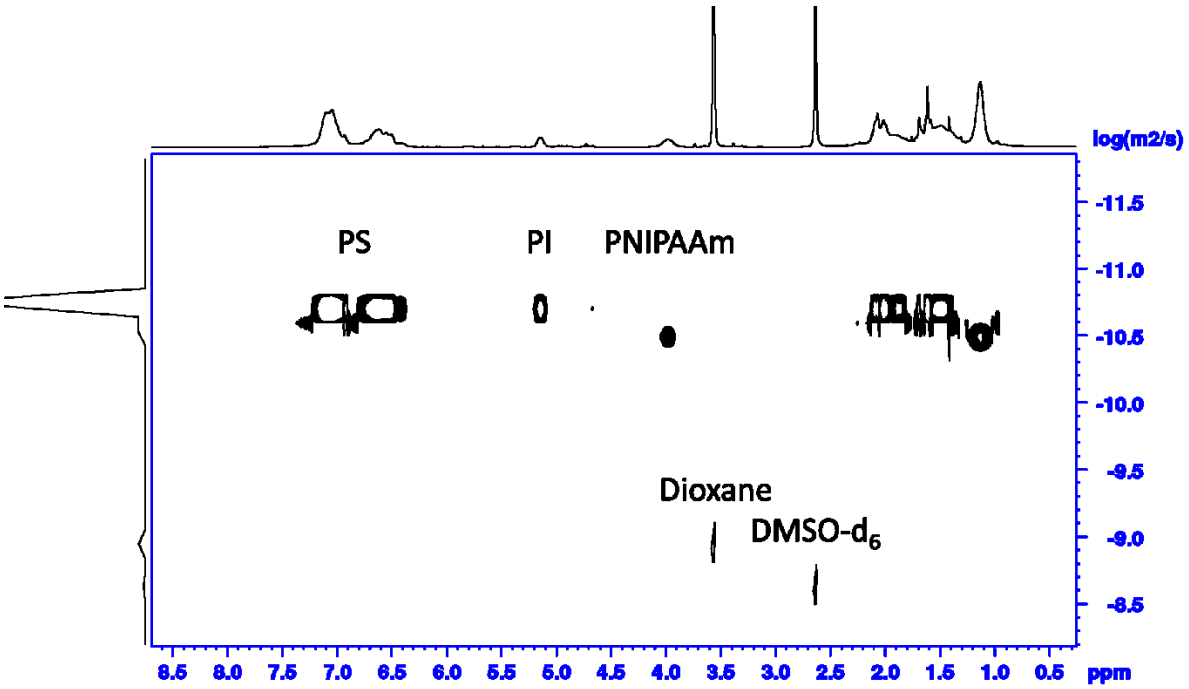

Figure 91: Diffusion coupled ^{1}H-NMR of PS-b-PI-b-PNIPAAm in DMSO-d_6.

In this 2D-NMR, the x-axis shows the ^{1}H-NMR spectra, and the y-axis shows the diffusion coefficient. In this type of 2D-NMR, more negative numbers indicate slower diffusion associated with larger molecules. The lower the diffusion coefficient, the less this ^{1}H-NMR signal diffuses out of the measurement area of the NMR tube. Single molecules such as the NMR solvent (DMSO-d_6) or the reaction solvent (1,4-dioxane) diffuse quickly out of the measurement area of the NMR tube and

appear at the bottom of the 2D-NMR spectra. Polymers diffuse slower and therefore appear further up in the spectrum. The PNIPAAm segment exhibits the same diffusion coefficient as the PS and PI. Therefore, we can assume that the block extension of PS-*b*-PI with NIPAAm was successful. However, there is a slight difference in the diffusion coefficient between the PNIPAAm segment and the PS-*b*-PI segment. This is attributed to a formation of unimeric structures consisting of a PS-*b*-PI core and a PNIPAAm corona. The protons of the corona show faster diffusion than the core due to geometrical considerations. Therefore, the PNIPAAm signal at 4 and 1.2 ppm show slightly faster diffusion than the core. The three synthesised triblock terpolymers were then utilised to form membranes *via* the SNIPS process.

7.2 Investigation of Membrane Formation by Design of Experiments

It is well-understood that membrane formation *via* SNIPS depends on the complex interactions between both blocks with the solvents and non-solvents used.[189] This creates a complex system that is challenging to investigate extensively. In the following section, a collection of predominantly mathematical or statistical techniques are explored and implemented to optimise the processing conditions with minimal experiments, called the Design of Experiments. A brief introduction to these helpful tools is given here as the membrane formation is planned, performed, and analysed. The membranes are characterised *via* scanning electron microscopy (SEM) and temperature-dependent water-flux measurements to investigate the thermo-response of the obtained structures.

7.2.1 Introduction to Design of Experiments

Every chemical reaction consists of various input factors that affect different outputs. In this way, a chemical reaction can be considered a black box that provides, within a certain range, reproducible output factors if the same input factors are chosen. Then a statistical analysis leads to reliable models without understanding the process in detail, but to reproducible results. This approach was first used by James Lind[227] in 1739 to find a treatment for scurvy in British navy hospitals. He gave various sailors different foods in a controlled manner to observe their vulnerability to scurvy. The trials suggested that lemons and oranges added to the meals reduce the negative effects of scurvy the most. This approach was then systematised by Ronald Aylmer Fisherin[228-229] in 1920, increasing its usability. He and his coworkers were working in agriculture at the Rothamsted experimental station where they investigated the growth of crops. The tremendous number of potential parameters that affect the growth lead to a simplification of the Design of Experiments (DoE), as shown in Figure 92.

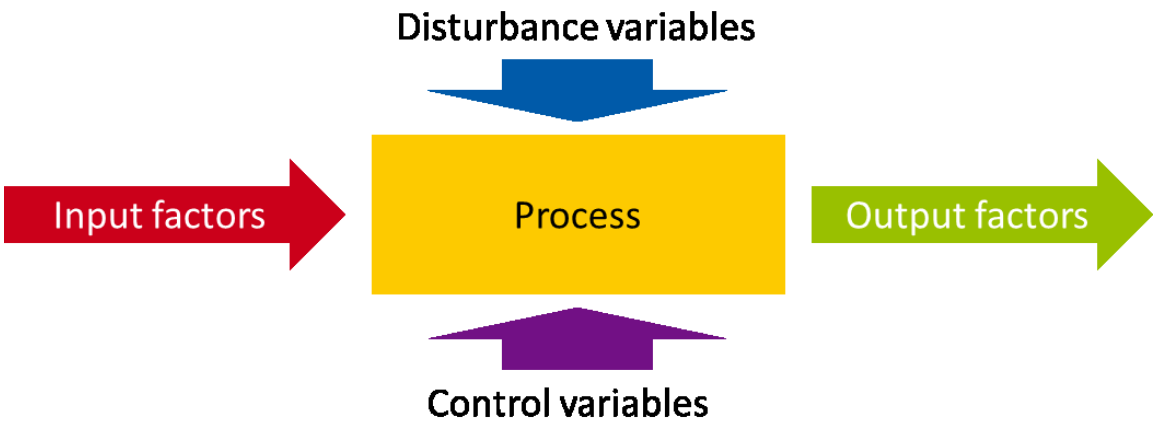

Figure 92: General influences on a process.

This systematic classification of parameters that influence the output, without understanding the details of a process, requires statistical considerations. The analysis of variances (ANOVA), an additional collection of mathematical tools, analyses whether input factors have significant effects on output factors. This separates the mathematical optimisation of experiments into two steps. First, the planning in order to minimise the number of experiments needed to achieve the maximum information; and second, the analysis of variances enables results to be predicted within a confidence interval of 95 % in most cases.

The factors having an effect on input and output can be sorted into quantitative and attributive factors. Quantitative factors are continuous, making these factors the most desired; examples of quantitative factors include temperature and time. Attributive factors have discrete values and are not continuous. Examples of attributive factors include the solvent polarity or the reactivity of a catalyst. It is desirable to adjust discrete factors, for example to yes/no statements, to as continuous as possible, since they contain very little information. A commonly used tool is the Likert-scale, predominantly used for surveys, to weight yes/no answers on a one to ten scale.

7.2.2 Initial Planning of Experiments

The experiments in science are planned in such a way that only one factor at a time (OFAT) is varied in most cases. This is a good strategy if the output factor only depends on this single input factor. These main effects are investigated in a series of experiments and can be described with an equation as linear, exponential, or other models. This strategy reaches its limits if two factors are dependent on each other, such as in the case of saturation for example. The reaction speed of a free radical polymerisation at very high concentrations is different from the same system in very dilute conditions although nothing has changed on a molecular level. These effects are challenging to determine, and even more challenging to quantify.

The approach of Design of Experiment (DoE) is to minimise the number of experiments and maximise the information obtained. If all input factors can be adjusted independently, they are considered orthogonal. For orthogonal reaction plans, the number of necessary experiments can be calculated according to the following equation:

$$n(Exp) = l^{k-p} \tag{3}$$

Where “l” is the number of levels of each factor, “k” is the number of factors used, and “p” describes the size fraction. Usually for each factor investigated, two extreme but reasonable levels are chosen. To further reduce the number of experiments, only a certain size fraction can be investigated. This reduces the experimental effort drastically but also reduces the amount of determinable multi-factor interactions. However, choosing only two factors reduces the significance of the reaction plan between the two extreme values. A centre point, even if it is not exactly in the centre between the two extreme values is beneficial to obtain further information from the centre of the reaction plan.

Therefore, to investigate five factors A, B, C, D and E with 2 steps, 32 experiments are necessary; if all experiments are performed, it is a full factorial plan. If all five input factors are quantitative, it is possible to perform only a half factorial plan (p = 1), which reduces the experiments to 16. This reduction of experiments reduces the resolution of the reaction plan from V to IV (compare Table 22). For the full factorial plan (32 experiments), an output factor could depend on all five input factors. For the partial factorial plan (16 experiments), any output factor can depend on only four input factors. It is, therefore, necessary to find a balance between a reasonable number of experiments and a high enough resolution to quantify the effects (see Table 22).

Table 22: Resolution of reaction plans and their determinable multi-factor interactions.

Resolution	Observed effects	Factor	Relation
III	Only for the main effects	Only A but paired with interactions	ABC
IV	Two-way interactions	Also A*B but paired with interactions	ABCD
V	Three-way interactions	Also A*B*C but paired with interactions	ABCDE
Full	All possible interactions		All

Empiric experience shows that many chemical reactions show multi-factor interactions that originate, for example, from concentration effects. However, the effects that depend on more than three factors are particularly rare. Therefore, it is preferable to investigate many input factors, in a partially factorial reaction plan, which leaves out some experiments, but still results in a reaction plan with a resolution of IV to V. This is where reaction planning with orthogonal factors has the greatest benefit.

7.2.3 Analysis of Variance

The methods used to evaluate any results are summarised in a collection of statistical and mathematical tools, the analysis of variance (ANOVA). The results of ANOVA are summarised in a table consisting of different parameters, the degrees of freedom, the sum of square errors, and the p-test.

The degrees of freedom describe in how many dimensions a system can change. The overall number of degrees is determined by the number of experiments in total minus one, each input factor that affects the output factor has one degree of freedom, and the remaining ones are summarised in “Errors”. The degrees of freedom are used to determine the residuals or the difference between the fit and the measured values. If the residuals of each fit are squared to counterbalance positive and negative errors and summed up, the “sum of squares” is obtained. The smaller the total sum of squares is, the lower the variance of the mathematical fit. The total sum of squares is then separated for every entry in the ANOVA table to indicate its contribution to that number. Higher numbers indicate a higher influence on the mathematical fit. Finally, the p-value, or probability value, is determined in a range from zero to one. This p-value indicates the statistical significance of an input factor on the output factor. For instance, a p-value of zero indicates a 0 % probability that the measured effect is random. In most cases, a p-value of 0.05 indicates a significant effect. A p-value of 0.05 equates to a 5 % chance that the observed effect occurred randomly. This significance value of 0.05 was randomly chosen by Robert Fisher and must be regarded as a soft border.[230]

Second, the output factors can be modelled with an equation, but the type of equation (linear, logarithmic or exponential) should be chosen wisely upon the expected model of the reaction. The confidence of determination of a mathematical fit is expressed by the R^2-value. The closer this value is to 1, the better the experimental results can be explained by the mathematical fit. As before, an R^2 value of 0.95 means that 95 % of the results can be explained using this fit, the remaining 5 % are attributed to experimental or measurement errors. The square difference between the measured and the fitted values are called the residuals. If the residuals exhibit any pattern, this may be an indication that the wrong model was applied to the fitted results.

7.2.4 Effect of Processing Conditions on the Formed Membranes

Several pronounced input factors that impact membrane formation significantly have been well investigated over the last two decades. As already shown by van de Witte and coworkers,[189] the open-

time before immersing the polymer film into water is one of the relevant factors that influence the membrane thickness. Phillip and coworkers[199] showed that the casting solution affects the membrane formation and subsequent water-flux of the resulting membrane. Hahn[231] and Fu[232] showed that the ratio between the hydrophilic and hydrophobic segments influences the pore-size, and consequently the water-flux of the prepared membrane. The three variables mentioned here, which are considered significant in the membrane-forming process, have also been investigated for the previously synthesised triblock terpolymers (see chapter 6.1.2). To further reduce further variation in the preparation procedure, the membrane casting procedure was performed in a climate-controlled chamber with a humidity of 50 % and a temperature of 25 °C.

These three input factors (open-time, casting solution composition, and hydrophilic/hydrophobic ratio) are easily adjusted. Consequently, the synthesised triblock terpolymers (Table 21) were dissolved in a THF/DMF mixture containing 30, 50 or 70 % THF. The solutions were then filtered, cast onto glass slides using a doctor blade with a height of 200 µm, and then the films were left open for either 15, 40 or 60 s before immersing the substrate into a water bath. The membranes were photographed, investigated *via* SEM, and the water-flux measured if possible.

Photographs of the membranes obtained under the same casting conditions; 50 % THF and 40 s open-time, but from different triblock terpolymers; are shown in Figure 93.

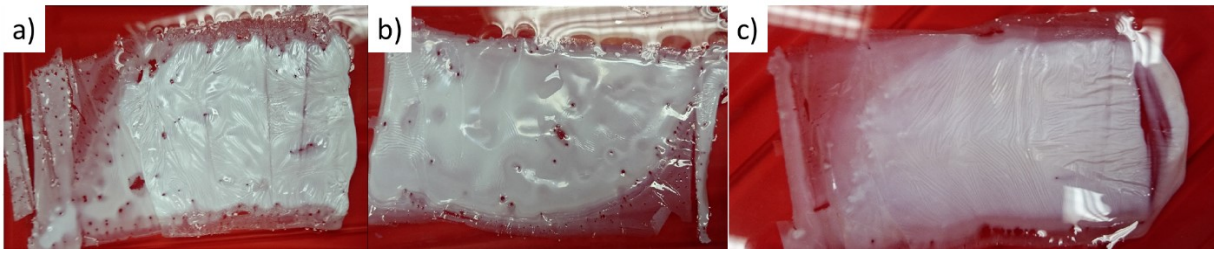

Figure 93: Membranes formed from different triblock terpolymers under similar conditions with a) PS_{546}-b-PI_{24}-b-$PNIPAAm_{28}$, b) PS_{546}-b-PI_{24}-b-$PNIPAAm_{168}$, and c) PS_{546}-b-PI_{24}-b-$PNIPAAm_{202}$.

As seen in Figure 93, a free-standing polymer film with a width of 6 cm and a length of approximately 12 cm is obtained for all polymers shown. However, every polymer film shows similar inhomogeneity over the entire area. On the edges and towards the end, the films are significantly thinner, which originates from the film-casting process where a doctor blade is placed on a glass slide and then pushed over the surface at a constant speed. The polymer solution flows between the glass slide and the doctor blade, resulting in an uneven membrane edge. The doctor blade was also pushed over the whole glass slide such that towards the end of the substrate no polymer solution was left for film-casting. Consequently, the first few centimetres of the cast film result in a uniform membrane. This area was used to prepare 2.4 cm patches for the water-flux measurements. The patches for the SEM micrographs were taken from the same area.

All the investigated mixtures resulted in solid structures that lifted off the glass slide to form free-standing films upon immersion in a water bath. However, some of the polymer films were very holey and do not contain a patch large enough to measure the water-flux. This could be attributed to impurities in the polymer solution or on the glass slide. Holes in the structure could be reduced by filtration of the polymer solution. The most consistent results were obtained using PS_{546}-*b*-PI_{24}-*b*-$PNIPAAm_{202}$. The membranes prepared using triblock terpolymers containing lower hydrophilic contents tended to form less consistent structures, *e.g.*, PS_{546}-*b*-PI_{24}-*b*-$PNIPAAm_{28}$ cast from 70 % THF

after 15 s broke apart, and membranes from PS_{546}-*b*-PI_{24}-*b*-$PNIPAAm_{168}$ cast from 70 % THF after 60 s needed several attempts to obtain a membrane containing a patch big enough for water-flux measurements. To obtain further information about the film thickness and structure asymmetry, SEM measurements of the solid structures were performed. For these measurements, small patches of the prepared membranes were dried under vacuum. Representative micrographs of the films prepared using PS_{546}-*b*-PI_{24}-*b*-$PNIPAAm_{28}$, PS_{546}-*b*-PI_{24}-*b*-$PNIPAAm_{168}$, and PS_{546}-*b*-PI_{24}-*b*-$PNIPAAm_{202}$ are shown in Figure 94, Figure 95 and Figure 96, respectively. Cross-sections, as well as a top-view, were imaged for all membranes.

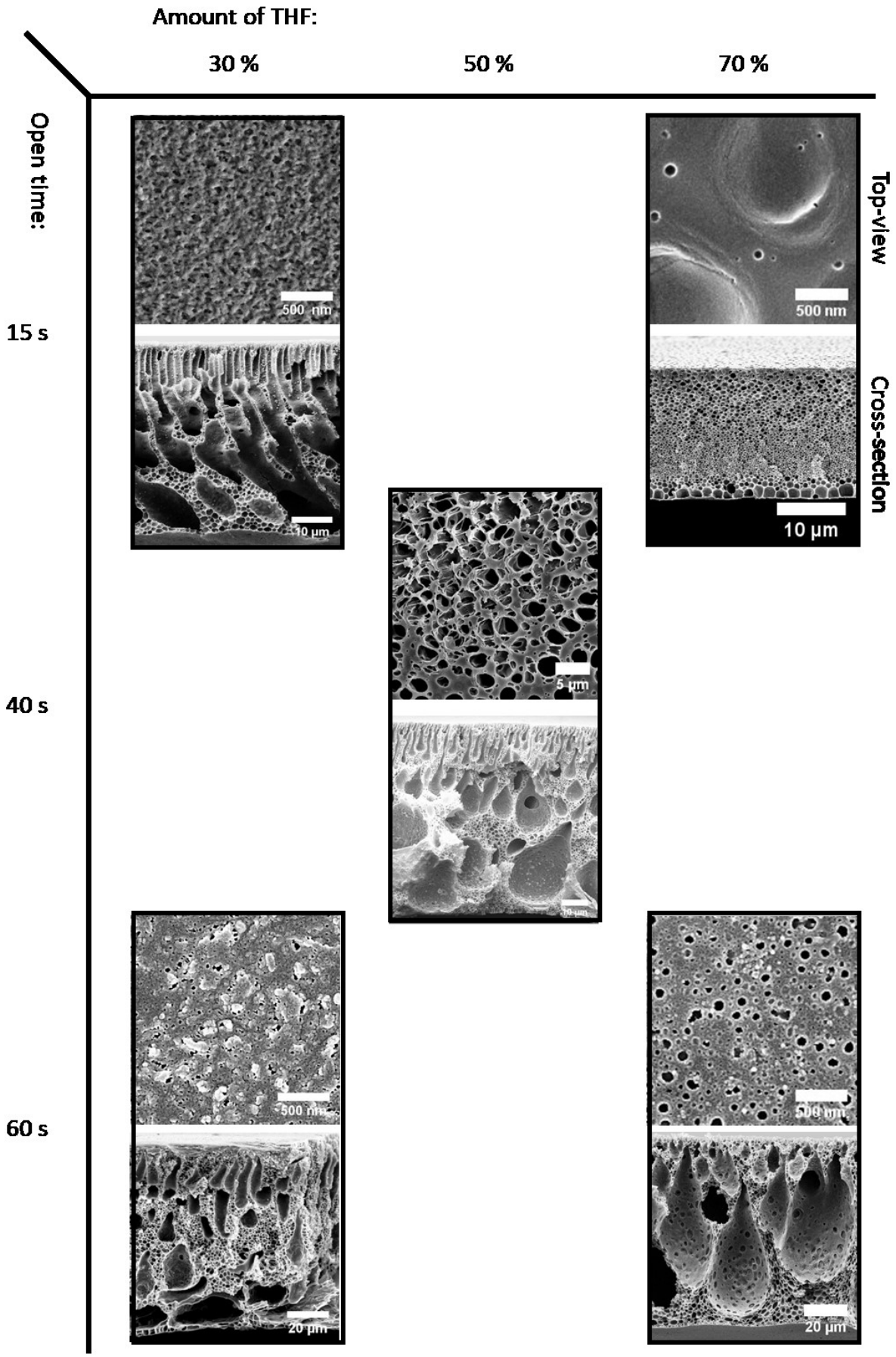

Figure 94: Membranes prepared from PS_{546}-b-PI_{24}-b-$PNIPAAm_{28}$ containing a hydrophilic content of 15 mol%. The open-time for is shown on the left side, and both a top-view and cross-section is shown for each film.

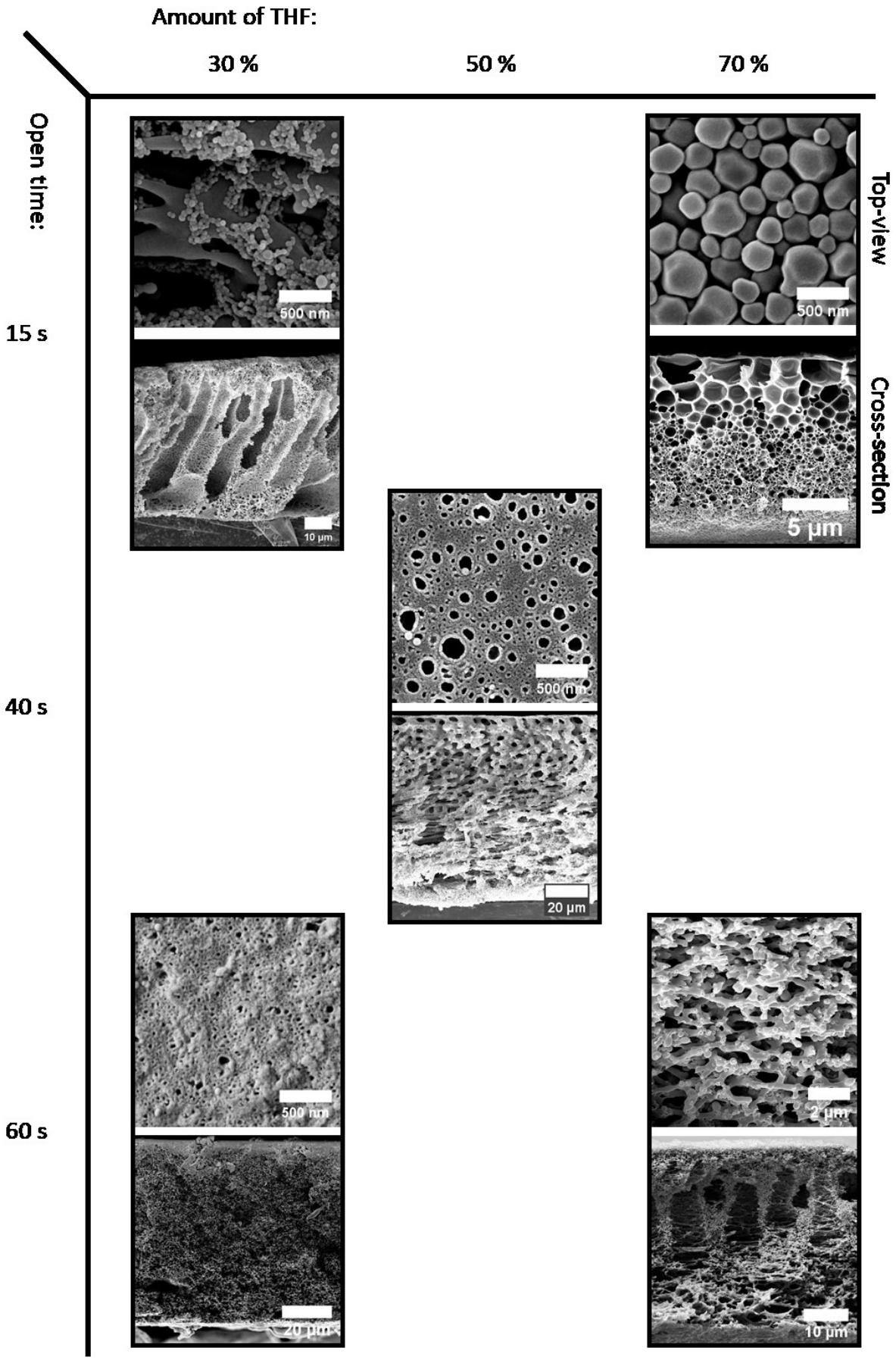

Figure 95: Membranes made from PS_{546}-b-PI_{24}-b-$PNIPAAm_{168}$ containing a hydrophilic content of 21 mol%. The open-time for is shown on the left side, and both a top-view and cross-section is shown for each film.

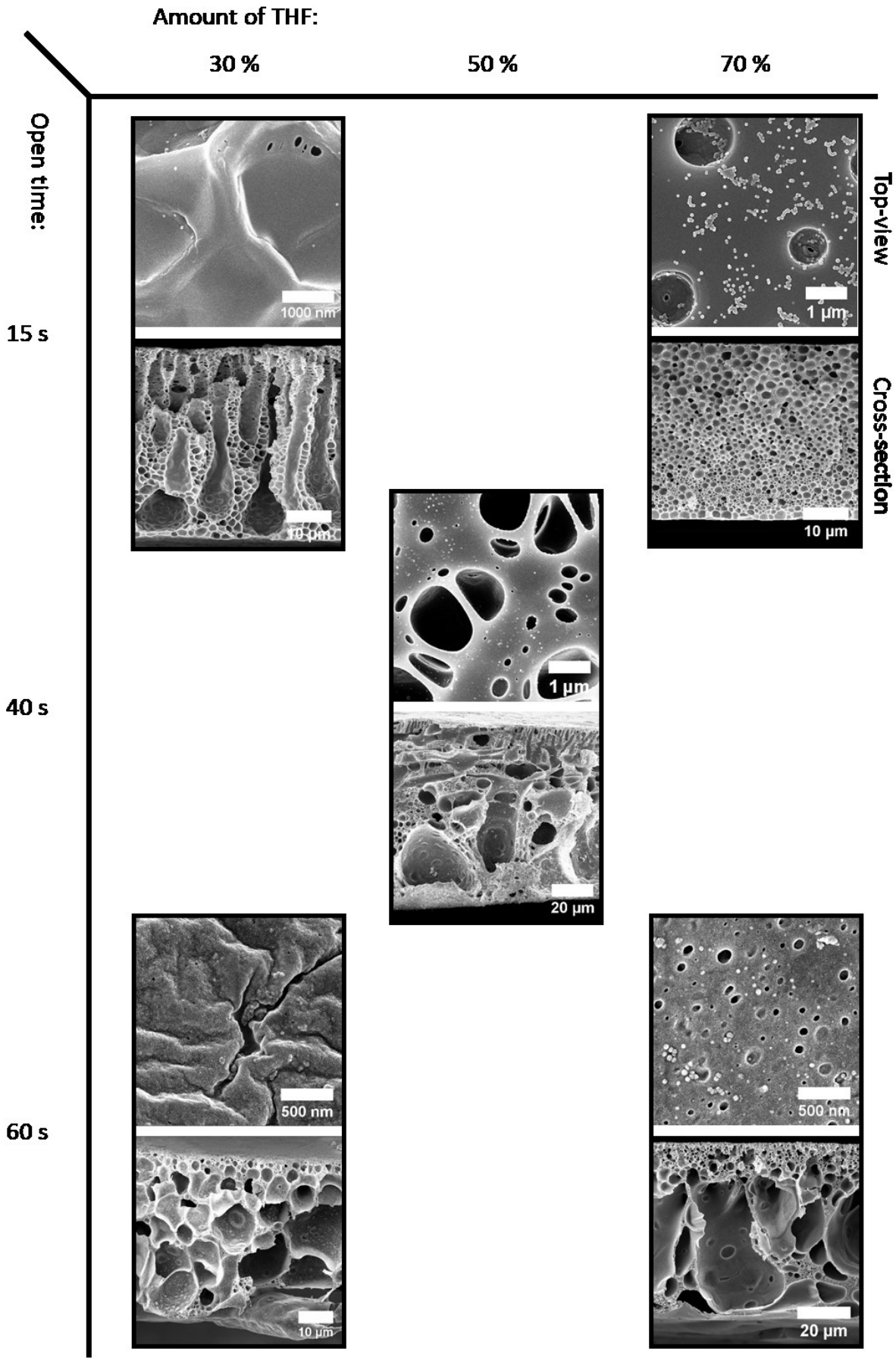

Figure 96: Membranes made from PS_{546}-b-PI_{24}-b-$PNIPAAm_{202}$ containing a hydrophilic content of 26 mol%. The open-time for is shown on the left side, and both a top-view and cross-section is shown for each film.

The micrographs show a top-view of each membrane to assess their porosity, and a cross-section to determine the membrane symmetry and thickness, which are summarised in Table 23. In all cases, porous structures are formed, but they differ significantly with the specific polymer used and the processing conditions. The pore-size differs considerably: PS_{546}-*b*-PI_{24}-*b*-$PNIPAAm_{202}$ cast from 50 % THF and immersed after 40 s exhibits pores of several µm; whereas PS_{546}-*b*-PI_{24}-*b*-$PNIPAAm_{168}$ cast from 30 % THF and immersed after 60 s shows pores of several nm. The thickness of the formed membranes exhibits a similar variation: PS_{546}-*b*-PI_{24}-*b*-$PNIPAAm_{168}$ cast from 70 % THF and immersed after 15 s has a thickness of 17 µm; whereas the same polymer forms films with a thickness of 84 µm when casting from a solution with 30 % THF and immersed after 60 s.

In general, it appears that short open-times with a low THF content lead to integral asymmetric membranes. All triblock terpolymers cast from a solvent mixture containing 30 % THF and immersed after 30 s show asymmetry along the cross-section. On the other hand, when the same open-time and higher THF concentrations are used, symmetric structures were found predominantly. Investigation of the cross-sections can only provide qualitative information regarding the degree of pore symmetry, and it remains challenging to quantify pore asymmetry in membranes. All structures are porous when considering their cross-section and top-view to varying degrees. The high influence of the processing parameters is also apparently looking at the membrane pore-size, which was estimated from the top-view micrographs. Theoretically, the pore-size should scale with the length of the hydrophilic segment, but this effect seems to be overlayed by the influence of the processing parameters. A more comprehensive investigation of the obtained effects is detailed in chapter 7.2.6 after the complete analysis of the obtained membranes.

7.2.5 Temperature Responsive Membranes

The membranes we prepared here should ideally exhibit temperature-responsive properties due to the PNIPAAm segment collapsing within the membrane pores. The water-flux measurements were carried out to confirm the nature of the pores formed. Therefore, a round piece was stamped out of the formed membrane and placed into a water-flux cell. After applying a transmembrane pressure of 0.3 mbar, water is pumped through the membrane to confirm if an interconnected and extended porous material is formed and if heating the membrane permits the PNIPAAm-segment to collapse, resulting in an increase in the water-flux (Figure 97). The membrane patch in the flow cell was held in position by a rubber ring, which causes tension on the membrane. Due to the brittleness of the prepared membranes, this tension results in the membranes breaking in many cases, requiring a new patch and/or membrane to be prepared.

Therefore, a round patch of the prepared film with a diameter of 24 mm was cut, placed in an Amicon flux-cell, and held in place with a rubber ring. A pressure of 0.3 mbar was then applied to measure the water-flux for a specific membrane. The water passing through the membrane was collected for a defined time, typically 10 min, and then the water was weighed to determine the water-flux. For the temperature-dependent measurements, the water reservoir and the flux-cell itself was heated to various temperatures, and the water-flux determined in a similar manner. The water-flux through the membrane should change upon heating the hydrophilic segment of the triblock terpolymer over the transition temperature. The segment should collapse to result in larger cavities or pores, permitting a higher water-flux through the membrane.

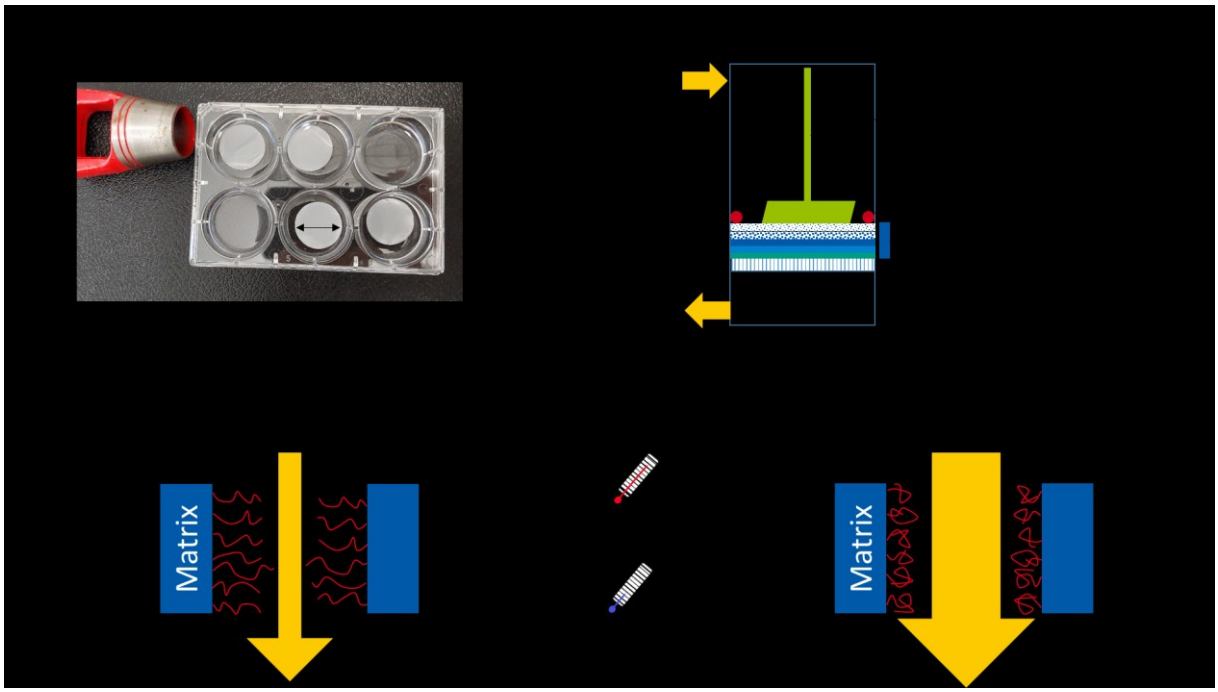

Figure 97: Water-flux measurements a) showing several prepared stamped patches for water-flux measurements and the location of the membrane in a schematic water-flux cell, and b) the expected change in water-flux upon the collapse and swelling of the hydrophilic segment within the membrane cavity.

Two main trends for the change in water-flux upon heating could be observed: the water-flux increases upon heating as expected; however, for all samples there is also a constant decrease in the water-flux during the measurement. Exemplary plots are shown in Figure 98.

Figure 98: Water-flux with increasing temperature for various membranes: a) PS_{546}-b-PI_{24}-b-$PNIPAAm_{168}$ cast from a solvent mixture containing 30 % THF after an open-time of 60 s; and b) PS_{546}-b-PI_{24}-b-$PNIPAAm_{202}$ cast from a solvent mixture containing 70 % THF after an open-time of 60 s.

In general, the water-flux decreases throughout the measurement, which is observed for all water-flux measurements and is attributed to membrane compression. Despite the membrane being very brittle, it can be compressed during the measurement, which leads to a lower water-flux. This effect was observed for all measured membranes. Nevertheless, for some membranes, *e.g.,* PS_{546}-*b*-PI_{24}-*b*-$PNIPAAm_{168}$, an increase in water-flux was observed upon heating the applied water. The SEM micrographs of the membrane shown in Figure 98a (formed from PS_{546}-*b*-PI_{24}-*b*-$PNIPAAm_{168}$ was cast from 30 % THF and immersed after 60 s) reveals a sponge-like structure. It is the membrane with the smallest pores according to the observed cross-sections. This observation does not necessarily indicate

that the other membranes do not show temperature-responsive behaviour. The PNIPAAm segments reach out into the interior of the pore and collapse upon heating to result in a bigger cavity, and consequently in a higher water-flux. If the cavity itself is already very large, the collapsing PNIPAAm segment will have a relatively small impact on the total cavity size, which means that the effect may not be measurable using the current setup.

7.2.6 Analysis of Variances on the Formation of Polymeric Membranes

As described above, the Analysis of Variances (ANOVA) can reveal effects that are not obvious at first sight, *e.g.*, two interacting factors. While the thickness and asymmetry of all structures could be assessed, not all membranes were suitable for water-flux measurements. Additionally, not all membranes displayed temperature-dependent water-flux. Analysis of variances was used to investigate the results, in attempts to find a consistent explanation of how the three input factors influence the three output factors. The collected results are summarised in Table 23.

In accordance with previous considerations, the experiment plan for the membrane formation consisted of three parameters with two levels each, including a centre point. The previously formed membranes were investigated by scanning electron microscopy (SEM) to determine their thickness and asymmetry. The water-flux of the formed membranes was assessed where possible, and the results are summarised in Table 23.

Table 23: Summary of the membranes formed and their properties.

PNIPAAm / mol%	THF / %	Open-time / s	Thickness[a] / µm	Asymmetry[b]	Water-flux[c] / L/(m²h)	Temperature response[d] / °C
15	30	15	57	1	2833	-
	30	60	72	1	0	-
	70	15	11	0	0	-
	70	60	40	1	0	-
	50	40	80	1	71	32
21	30	15	46	1	0	-
	30	60	84	0	1096	34
	70	15	17	1	0	-
	70	60	82	1	736	-
	50	40	69	0	70	29
26	30	15	41	1	320	-
	30	60	43	1	363	-
	70	15	37	0	1333	-
	70	60	62	1	700	33
	50	40	81	1	931	35

a) Measured *via* SEM; b) determined from the SEM cross-section, 0 = symmetric, 1 = asymmetric; c) determined at the start of the measurement; and d) temperature response given when effect observable.

While measuring a set of parameters and understanding that a certain trend should evolve automatically lets the experimenter adjust his results towards the assumed direction. Therefore, the results given here were measured and randomised to reduce the expectation error of the operator but reordered for higher clarity.

Only two output factors could be determined for all prepared membranes: the thickness, a qualitative factor, and the asymmetry, an attributive factor. The asymmetry is described using discrete values with two levels, symmetric and asymmetric, which decreases the information of such a factor drastically.

Nevertheless, the main effects of these values were determined by averaging all output factors for every input factor. In detail, the main effect of the ratio of PNIPAAm on the thickness is determined by averaging all membrane thicknesses of one triblock terpolymer and plotting the average value for all three triblock terpolymers. This procedure is done for all six combinations of input and output factors and plotted in Figure 99.

Figure 99: Main effects of the input parameters to the membrane fabrication. a) for the thickness in µm and b) for the asymmetry.

This procedure helps to quantify the main effects already observed and discussed previously. The thickness of the formed membranes has a clear maximum at the centre point of the experimental space. The maximum thickness of a membrane is reached at a PNIPAAm ratio of 21 %, 50 % THF, and an open-time of 40 s. Increasing amounts of each factor lead to thinner membranes. The amount of THF and the open-time appear to have a greater impact on the membrane thickness than the chain length of the hydrophilic block.

Short open-times also give the triblock terpolymers a short time to self-assemble and therefore more material can be washed out during the precipitation process; this leads to the formation of thinner membranes. Long open-times, on the other hand, give the triblock terpolymers more time to self-assemble and therefore the material can be packed more effectively to produce thicker and typically asymmetric membranes, which increases the membrane thickness compared to the short open-times. The thickest membranes are found at an intermediate open-time of 40 s.

Similar observations of two competing effects were also uncovered for the amount of THF in the casting mixture. For all membranes, equal wt% of polymers were dissolved in the same total volume of solvent; due to the different molecular weights, the number of polymer chains in solution differ, and therefore, the viscosity of the casting solution differs for the different polymers. The polymer solutions of the same polymer but with different amounts of THF in the casting solution show a different trend. Low amounts of THF in the casting mixture lead to a lower viscosity, the material spreads less, and the membranes are thicker. At higher amounts of THF, the solution is less viscous, and the cast film can spread more. These complex interactions also lead to a maximum film thickness obtained at intermediate values.

By comparing the membrane thickness formed with the resulting water-flux and thermo-response, it becomes apparent that only membranes with a thickness greater than 60 µm show a thermo-response

under water-flux. On the other hand, the thickness of a membrane cannot be directly linked to its water-flux. The triblock terpolymer with 26 % PNIPAAm cast from a 70 % THF solution and immersed after 15 s has a thickness of 37 µm and a water-flux of 1333 L/(m^2h). The triblock terpolymer with 21 % PNIPAAm cast from a 30 % THF solution and immersed after 60 s has a thickness of 84 µm and a water-flux of 1096 L/(m^2h).

Asymmetry, as mentioned previously, is challenging to investigate or quantify since it is a qualitative value. To obtain a statistically significant result from the asymmetry, more data is necessary. Another option is to weigh the asymmetry using a Lickert-scale, which is predominantly used for surveys to quantify the asymmetry on a scale from 1 to 10. A third method requires several experts to estimate whether the shown micrograph of a membrane is considered asymmetric and then averaging the values obtained.

According to the main effects presented in Figure 99b, the polymer composition likely effects the membrane symmetry. The SEM micrographs, on the other hand, do not show any obvious trends in terms of the membrane asymmetry with variable hydrophilic/hydrophobic ratios. The same applies to the processing parameters. The main effect diagram only shows the averaged values as one spot, which may lead to false conclusions regarding trends that are not significant. This method confirms what was already expected from the SEM micrographs: most membranes are asymmetric, but there are no obvious trends with the input parameters. Longer open-times and lower amounts of THF in the casting mixture tend to result in more asymmetric structures, but this observation is not statistically significant.

The results summarised in Table 23 can be used to fit the output factors based on the input factors. The toolbox utilised here is the Analysis of Variances (ANOVA), and the results are given in Table 24.

Table 24: ANOVA table for the mathematical fitting of the output factors(thickness and asymmetry) based on the input factors (hydrophilic segment length of the polymer, vol% THF and open-time).

Output Factor	Input Factor	Degrees of Freedom	Sum of Squares	p-test
Thickness	Polymer	1	3.8	0.915
	THF	1	736	0.161
	open-time	1	2732	0.015
	Polymer*THF	1	1079	0.097
	Error	10	3207	
	Total	14	7758	
Asymmetry	THF	1	0.083	0.514
	Open-time	1	0.079	0.524
	THF*open-time	1	0.750	0.068
	Error	11	2.021	
	Total	14	2.933	

The thickness and asymmetry of the membranes were analysed and fitted using several input factors, as well as various mathematical tools (see chapter 7.2.3). The fifteen experiments result in fourteen degrees of freedom, among which every input factor, as well as two interacting factors, take one degree of freedom. Three input factors and six two-way interacting factors are used for the initial model. Then the least significant factor is removed stepwise until the fit has the smallest residuals with

the least number of input factors. The results of both optimisations are shown in Table 24. The membrane thickness can be fitted using the hydrophilic/hydrophobic ratio of the triblock terpolymer, the amount of THF in the casting solution, and the open-time before immersing the polymer film into the water bath. The most significant input factor is the open-time, whilst the hydrophilic/hydrophobic ratio of the polymer is the least. However, a combination of the triblock terpolymer ratio and the amount of THF in the casting solution also presents a significant p-value.

The asymmetry of a membrane depends predominantly on a combination of the open-time and the amount of THF in the casting mixture. The single input factors—THF and open-time— alone have no significant influence on the asymmetry of the membrane. According to these experiments, the triblock terpolymer composition can be neglected in terms of the asymmetry of the formed membrane. The results of the ANOVA table (Table 24) can be transformed into fitting equations shown in Table 25:

Table 25: Fitting of the output factors(Thickness and asymmetry) using the input factors from the ANOVA analysis from Table 24 in order to predict a result with an uncertainty.

Output Factor	Formula	Error	R^2
Thickness / µm	0.616*A – 8.184*B + 15.07*C + 11.597*A*B + 54.446	5.12	0.587
Asymmetry	-0.083*B + 0.081*C – 0.081*B*C + 0.732	0.12	0.311
A = PNIPAAm ratio (%), B = amount of THF (%), C = open-time (s)			

Mathematical fitting of a reaction or process is also accompanied by an estimation of how trustworthy the fit is. The fit used to calculate the thickness has an R^2 value of 0.587, which means that the results of the calculation agree with ~60 % of the experimental observations. With a certainty of ~60 %, it is not possible to make sound predictions of the thickness of the resulting membrane. The asymmetry, on the other hand, is challenging to quantify. This results in an even less accurate mathematical fit with a certainty of ~30 %, and therefore more experiments are necessary to make more reliable predictions.

The mathematical fit of the membrane formation shows a relatively poor R^2 value. This may be due to the lack of data points or an unknown input factor that has a significant effect on the output factors and that was randomly varied during the experiments but not considered in the reaction plan. The membrane casting process was performed in a climate-controlled chamber to ensure a stable humidity of 50 % and a temperature of 25 °C. But this does not necessarily lead to the same humidity and temperature during every process because of minor errors in the device itself. Furthermore, the quality of the used solvents can also affect the membrane formation process. These inevitable errors that occur during the process can have a significant influence on the casting procedure. It was also not possible to find a link between the thickness or the asymmetry obtained from the SEM micrographs, water-flux, or its thermo-response. Therefore, a different method must be used.

7.3 Non-Invasive Membrane Characterisation Using 3D Single Particle Orbit Tracking

The characterisation of triblock terpolymer membranes was thus far performed *via* water-flux measurements and SEM. The SEM micrographs were recorded in the dry state, and therefore do not reflect the pore-size in the wet state under which the water-flux measurements were performed since the hydrophilic PNIPAAm segment collapses. The water-flux measurements indicate that to observe a stimuli-response under a water flow, the change in pore-size that is caused by the hydrophilic segment collapsing must be relatively high. Consequently, the void size within a membrane is an interesting, yet challenging factor to determine. A common technique used to determine the accessible voids for particles throughout the membrane is filtration of polydisperse particles. However, particles often exhibit complex interactions with the membrane surface, and again only offer limited insight into the pore-size along the membrane cross-section. Therefore, to gain better insight into the pore-size distribution in the swollen state along the membrane, it is necessary to monitor the diffusion of a single particle through the membrane. One suitable method is 3D single-particle orbit tracking (3D-SPOT), which is presented in the following section.

7.3.1 Environmental Requirements for Single-Particle Orbit Tracking

In collaboration with the University of Bayreuth, we performed single-particle orbit tracking to probe the structure of our prepared membranes.[226] In single-particle orbit tracking (SPOT), the focus of a laser beam is modulated so that the focus point rotates circularly around a fluorescent nanoparticle in the centre. The intensity of the emitted fluorescence increases upon movement of the particle closer to the focus. The rotation of the laser beam focus around the particle makes it possible to determine the direction of movement of the particle in two dimensions. Shifting the focus of the laser beam rotation in the third dimension enables a three-dimensional moving pattern of a fluorescent particle. The lateral position can be reconstructed from the amplitude and the phase of the modulation with a temporal resolution of approximately 5 ms, and a spatial resolution of approximately 10 nm.

During preliminary measurements, two major drawbacks became apparent: first, the high refractive index of the membrane compared to the solution limits the spatial resolution of the measurement; second, the diffusion speed of the particles exceeds the temporal resolution of the method. Therefore, the refractive index, as well as the viscosity of the surrounding solution, must be increased. Thiodiethanol (TDE) is characterised by a high refractive index of 1.52, has a higher viscosity, and is water-miscible. Furthermore, PNIPAAm remains temperature-responsive even in the presence of high amounts of TDE, and the investigation solution could be tuned in order to balance the thermo-responsive behaviour and high refractive index as compared in chapter 5.4.1.2.

As immersing a membrane in a water/TDE mixture could potentially affect its structural integrity, a small patch of a PS_{546}-*b*-PI_{24}-*b*-$PNIPAAm_{168}$ membrane; prepared using 50 % THF, and a 40 s open-time; was stored in pure TDE for 1 week before being characterised using SEM (Figure 100). The membrane proved stable after 1 week in TDE; however, certain changes are clearly visible by SEM. The membrane appears to be less porous and is denser due to the slightly better solubility of the hydrophobic segment in TDE compared to water. The number of pores observed in the top-view micrograph significantly decreases; but surprisingly, the pore-size is unchanged. Nevertheless, the membrane remains porous, and measurements in a water/TDE mixture are feasible.

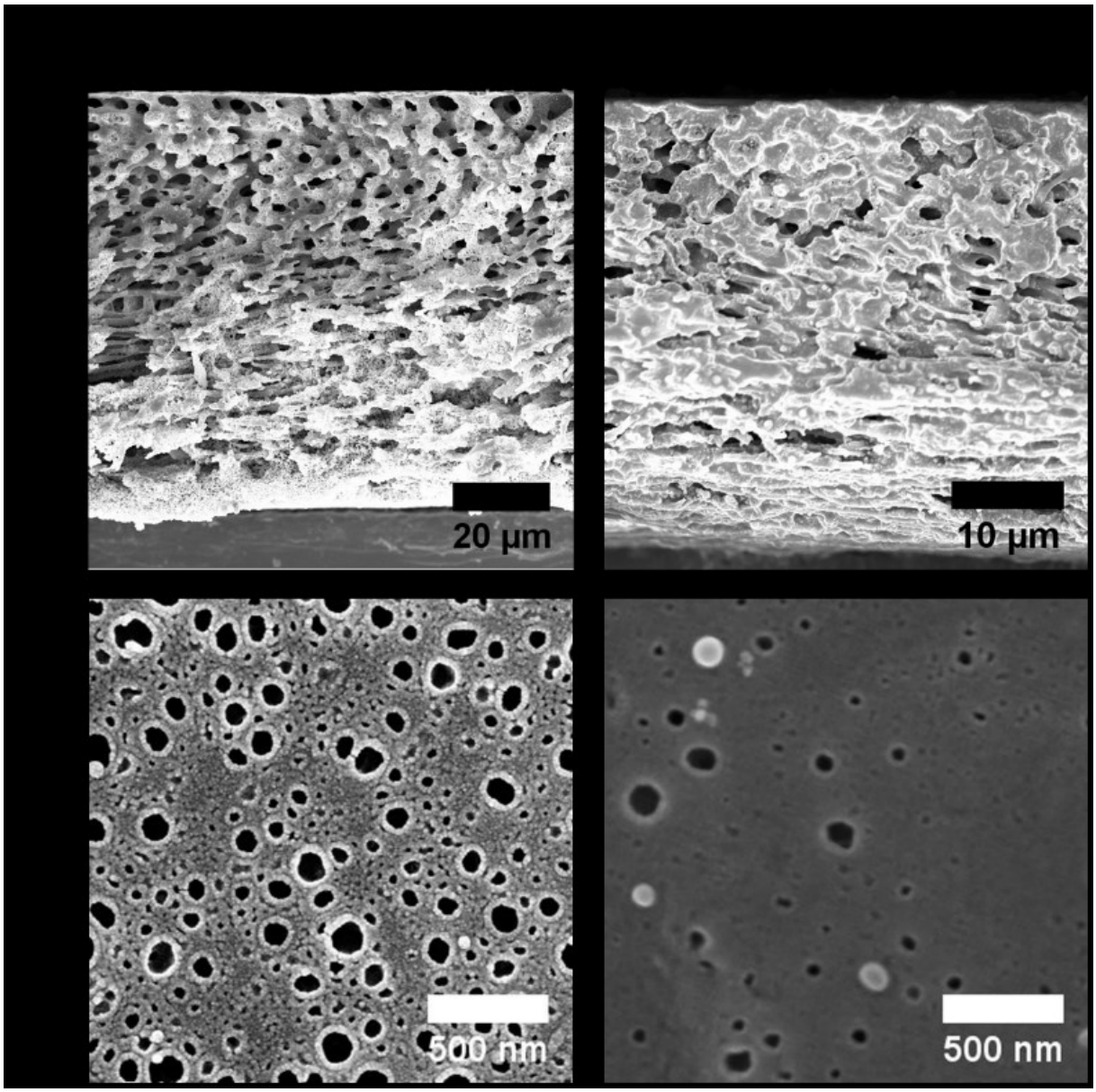

Figure 100: Membrane prepared from PS_{546}-b-PI_{24}-b-$PNIPAAm_{169}$ before and after soaking in thiodiethanol (TDE) for 1 week. The membrane was cast from a THF/DMF mixture (50/50 vol%) at a relative humidity of 50 % at 22 °C with an open-time of 40 s after immersion in water.

Environmental SEM (eSEM) measurements under high humidity were performed to assess the membrane structure in the wet state, where the PNIPAAm chains are swollen. Membrane patches, which were water-inflated and precooled, were placed into the sample chamber of the electron microscope. Micrographs were acquired while gently drying the outer layer of the membrane at a relative humidity of 62 %. This ensured the measurement conditions were, although not identical, somewhat comparable to those prevailing during the SPOT experiments. A comparison of both methods is shown in Figure 101. On comparing the micrographs in the dry and wet state, one can clearly see that the pores are significantly smaller in the swollen or wet state (Figure 101b); and that the porous structure is preserved along the membrane as observed in the cross-section (Figure 101a).

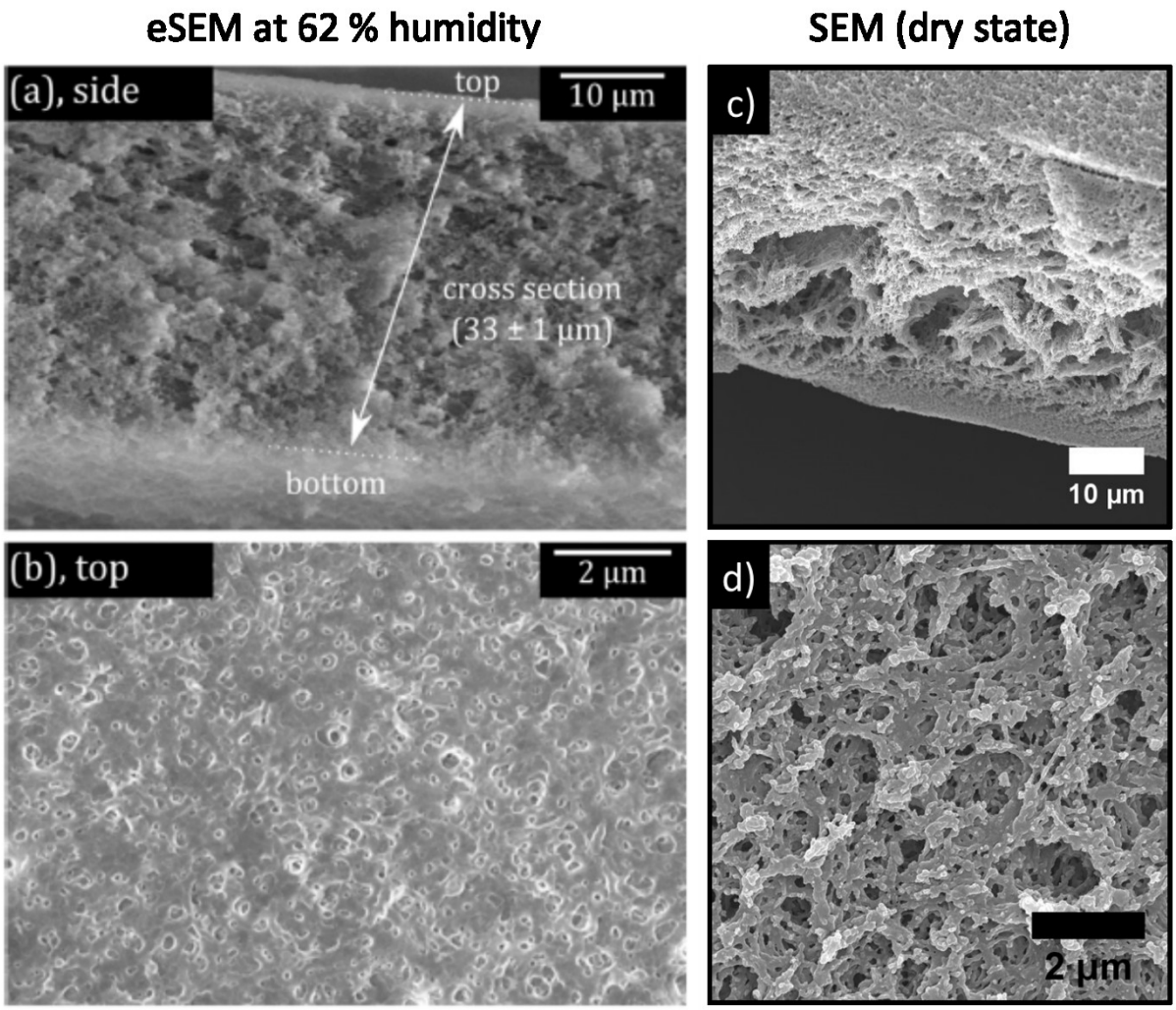

Figure 101: Micrographs of the PS_{43}-b-PI_{40}-b-$PNIPAAm_{17}$ triblock terpolymer membrane: eSEM measured at a relative humidity of 62 % showing the a) cross-section and b) top-view in comparison to the SEM micrographs recorded in the dry state showing the c) cross-section and d) top-view.

From the micrograph top-view, it is possible to determine the pore-size diameter and pore-size distribution of the prepared membrane in the wet and dry state *via* chord length analysis.[191, 233] The pore-size diameter was determined to be 360 ± 280 nm and 360 ± 10 nm in the dry and wet state, respectively. The mean pore-size is therefore in both cases the same. The broader distribution in the dry state arises from the higher roughness of the sample, which are misidentified as pores.

7.3.2 3D Single Particle Orbit Tracking Results

To determine the interior pore-size *via* the 3D-SPOT setup, the previously investigated membrane was immersed into a 1/1 vol% mixture of TDE and pH 8 buffer solution, a small amount (0.1 vol%) of Triton X-100, and three different tracer particles ranging from 25 to 100 nm in size were added. The trajectories of the various particles were determined, and their movement pattern was used to determine the pore-size distribution. A comparison between the pore-size obtained from the top-view and the diffusion lengths of the different particles is shown in Figure 102.

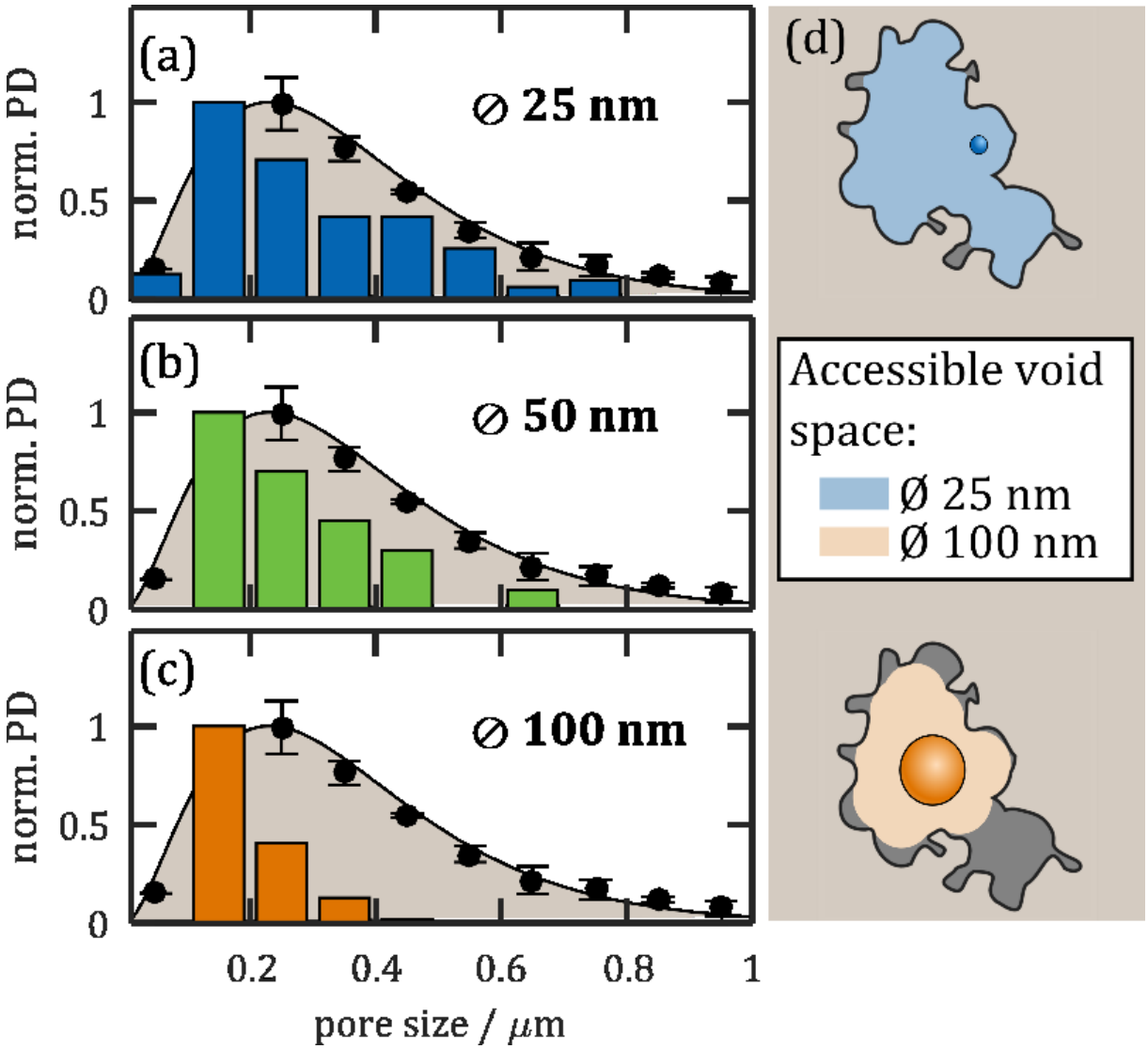

Figure 102: Normalised histograms of the confinement lengths obtained from the mean square displacement (MSD) for particles with a diameter of (a) 25 nm, (b) 50 nm, and (c) 100 nm. The black dots shown in the background refer to the normalised probability density of the pore-sizes obtained from the chord length analysis for the bottom-view eSEM micrograph. (d) Schematic depiction of particles with diameters of 25 and 100 nm within the same pore, showing the difference in accessible void space by the coloured area.

The overlayed pore-size distribution obtained from eSEM is in good agreement with the particle results from 3D single-particle orbit tracking. However, upon investigation of the pore-size using larger particles (100 nm) results in smaller pore-sizes compared to the investigations run with smaller particles (25 nm). The highly irregular pore morphology arises from the fabrication method used, resulting in a smaller accessible space for larger particles. Naturally, this effect is reversed for smaller particles as shown in Figure 102d. These results verify 3D-SPOT as a suitable non-invasive method for the determination of pore-sizes for membranes formed *via* the SNIPS process. A further advantage of this technique to be explored is the possibility to heat the device, which may be a suitable method to determine the change in void space between the collapsed and swollen PNIPAAm hydrophilic segment.

7.4 Thermo- and Photo-Responsive Block Copolymer Membranes

After investigating the thermo-response of the prepared triblock terpolymer asymmetric membranes intensively, we further extended our system and explored a photo- and thermo-responsive triblock terpolymer to form a dual-responsive membrane. We first synthesised a diblock macroinitiator and block extended it with a dual photo- and thermo-responsive hydrophilic segment. The response to both stimuli was then investigated *via* contact angle and water-flux measurements.

The synthesised macroinitiator, PS_{530}-*b*-PI_{229}, was block extended according to our previous protocols using a monomer to initiator ratio of 800 to 1 with 3 % SPA in the monomer mixture. This resulted in a hydrophilic block of P(NIPAAm$_{94}$-*co*-SPA$_{45}$), which accounts for 15 wt% of the triblock tetrapolymer. The triblock tetrapolymer was then dissolved in a 15 wt% mixture of THF/DMF (50/50 v/v). The solution was filtered, cast onto a glass substrate at 22 °C and 50 % relative humidity, and after an open-time of 60 s immersed into a water bath (Figure 103).

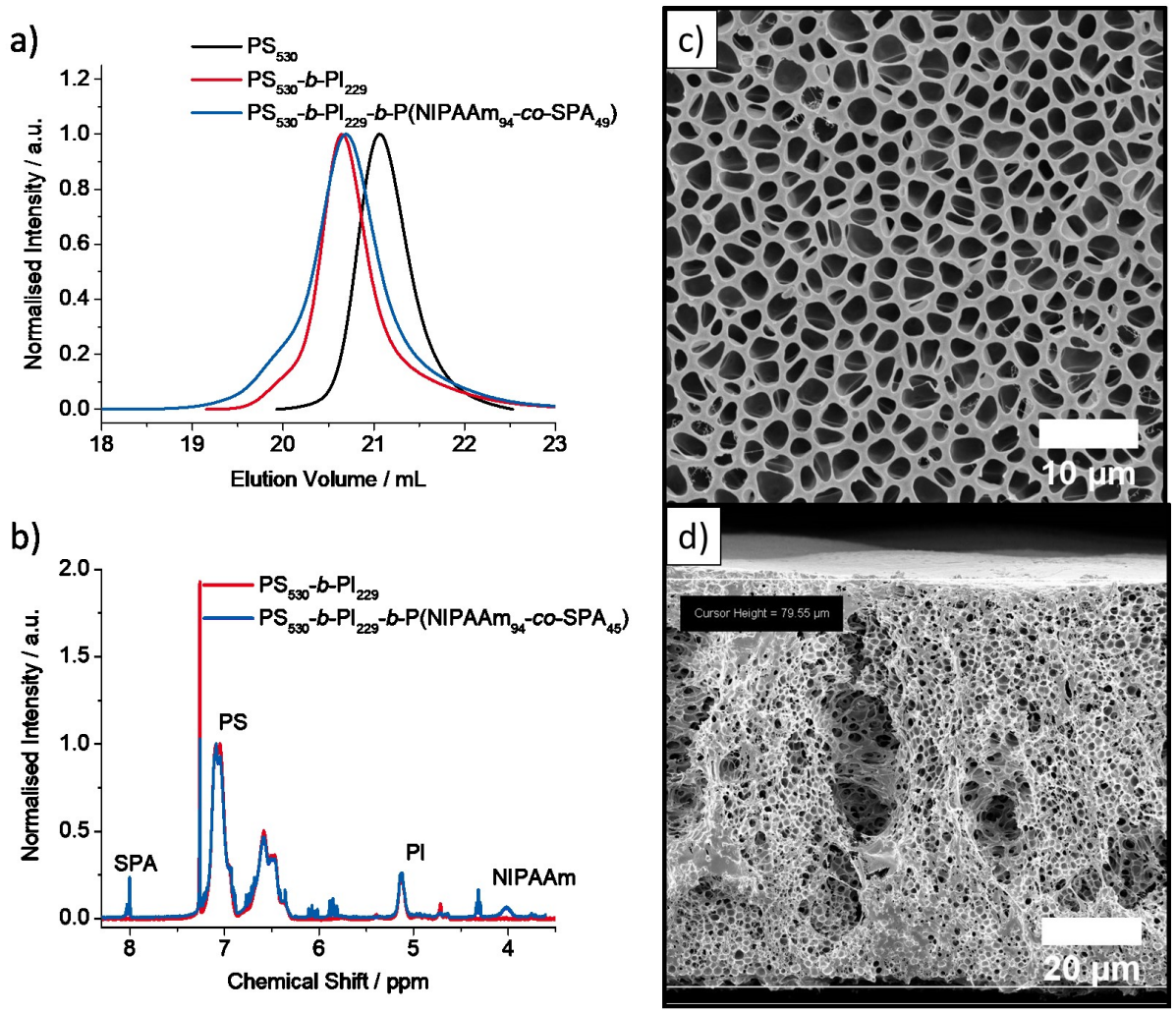

Figure 103: Analysis of the synthesised triblock tetrapolymer PS_{530}-b-PI_{229}-b-P(NIPAAm$_{94}$-co-SPA$_{45}$) via a) THF-SEC and b) ^{1}H-NMR in $CDCl_3$. SEM micrographs of the formed membrane showing the c) top-view and d) cross-section.

The synthesis of the triblock tetrapolymer containing SPA units was successful, with all relevant signals visible according to ^{1}H-NMR. The block extended polymer is monomodal by SEC. The membrane formed is comparable to the previous results of the triblock terpolymers without SPA, which makes this a promising starting system to investigate dual-responsive membranes. The thickness of the

membrane was determined to be 80 µm, which is comparable to the membranes formed using the PS-*b*-PI-*b*-PNIPAAm triblock terpolymers; however, the membrane formed is not asymmetric. According to previous investigations, symmetric membranes can still present a temperature response. In addition, the pore-size determined from the top-view micrograph is larger than most of the thermo-responsive membranes shown in chapter 7.2.4.

In chapter 5.4.2.2, it was shown that P(NIPAAm-*co*-SPA) exhibits a photo-response even in the solid-state. The membrane also changes in colour upon irradiation with UV light from white to violet, and back again upon irradiation with green light (Figure 104).

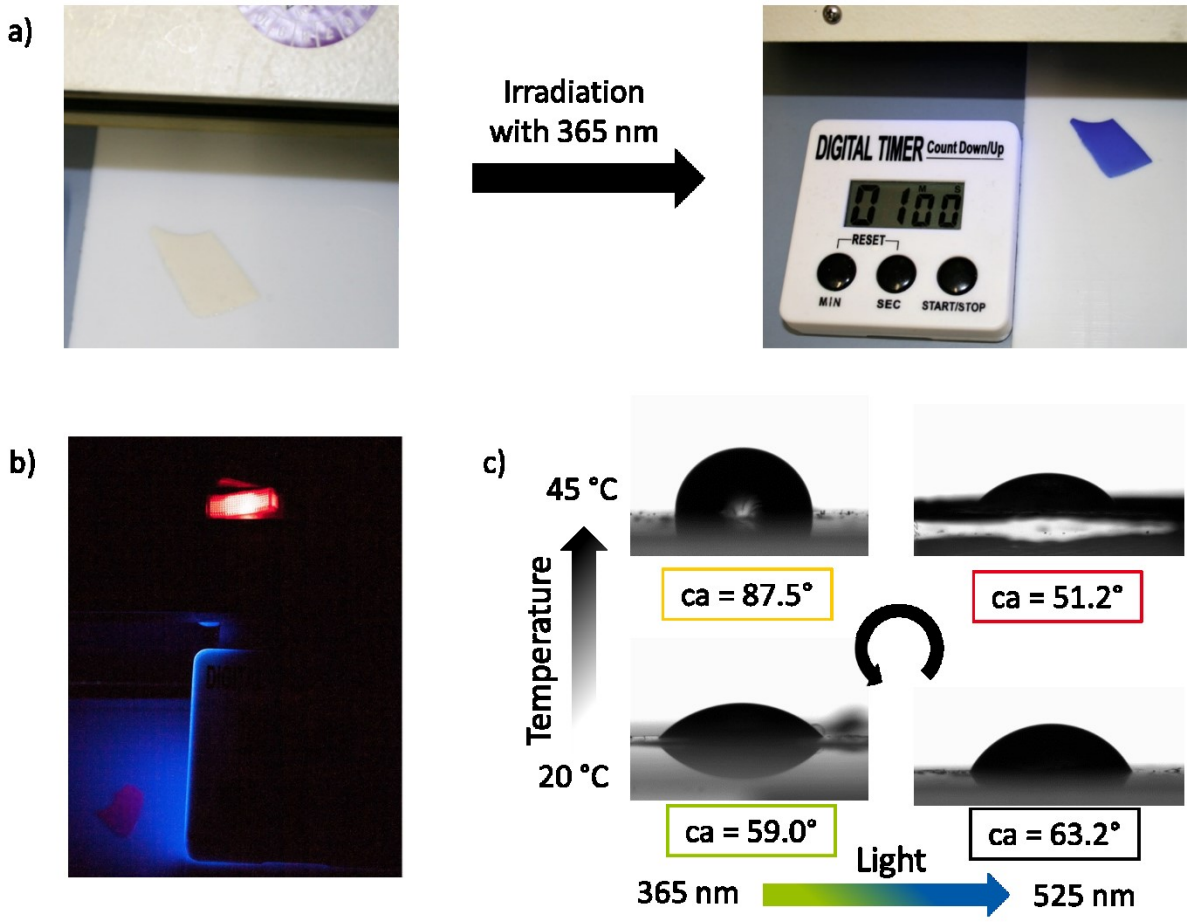

Figure 104: a) Photo-response of the PS_{530}-b-PI_{229}-b-P(NIPAAm$_{94}$-co-SPA$_{49}$) membrane upon irradiation at 365 nm. b) Red fluorescence of the membrane during irradiation at 365 nm. c) Contact angle measurements of a pH 8 buffer solution upon heating and irradiation of the membrane patches.

The photo-response of the membrane containing SPA is much faster than the photo-response of the dry copolymer films investigated previously. Within one minute of irradiation with a 365 nm UV light, the membrane patch switched to a saturated state, and no further colour change resulted from further irradiation. Fluorescence was also visible in the solid-state upon irradiation with a 365 nm UV light (Figure 104b). The contact angle of water droplets on the dry membrane was also determined in order to observe the four switching states of the dual-responsive hydrophilic segment. Below the LCST, the copolymer should be hydrophilic and the contact angle is expected to be rather low (>70°). Upon heating above the LCST, the contact angle of the membrane should increase. The photo-responsive SPA moiety can be switched from the hydrophobic spiropyran-form to the hydrophilic merocyanine-form, which should alter the contact angle of the membrane. The contact angle of the membrane was determined under several conditions: at room temperature; after irradiation with 525 nm light; after

heating to 45 °C; after irradiation with 365 nm for at least 2 min at 45 °C; and then after cooling back to room temperature. The contact angle was averaged over at least three measurements, and the results are shown in Figure 104c. Upon heating, the PNIPAAm chains in the swollen state collapsed, and this may be reflected in a higher contact angle above the transition temperature. The SP-form is less polar than the MC-form, which leads to an expected lower contact angle for the samples irradiated with 525 nm light. Both trends are observed, but the trends are not consistent for all transitions. Upon irradiation with 365 nm, the membrane exhibits a high contact angle at high temperatures (87.5°) and a significantly smaller contact angle at low temperatures (59.0°). At room temperature, the contact angle increases when the UV-irradiated sample is irradiated with green light from 59.0° to 63.2°. The only exception in this protocol is the green light-irradiated sample at high temperatures. Here no increase in contact angle is observed. However, during these experiments, once a colourless membrane is irradiated with UV light and becomes violet, it is not possible to switch back completely to their original colour. This can be attributed to the close proximity of the different SPA moieties within the membrane, which form inter-polyelectrolyte complexes that hinders the ability of the MC-form to switch back to the SP-form. An observation that was already noted before, where some block terpolymers could only be dissolved by long term irradiation with green light.

To evaluate the filtration performance of the PS_{530}-*b*-PI_{229}-*b*-P(NIPAAm$_{94}$-*co*-SPA$_{49}$) membrane, water-flux measurements were carried out (Figure 105). Since this dual-responsive membrane can exist in four switching states, the water-flux must be determined in all four states: at high and low temperature, and upon UV and green light irradiation (Figure 105b).

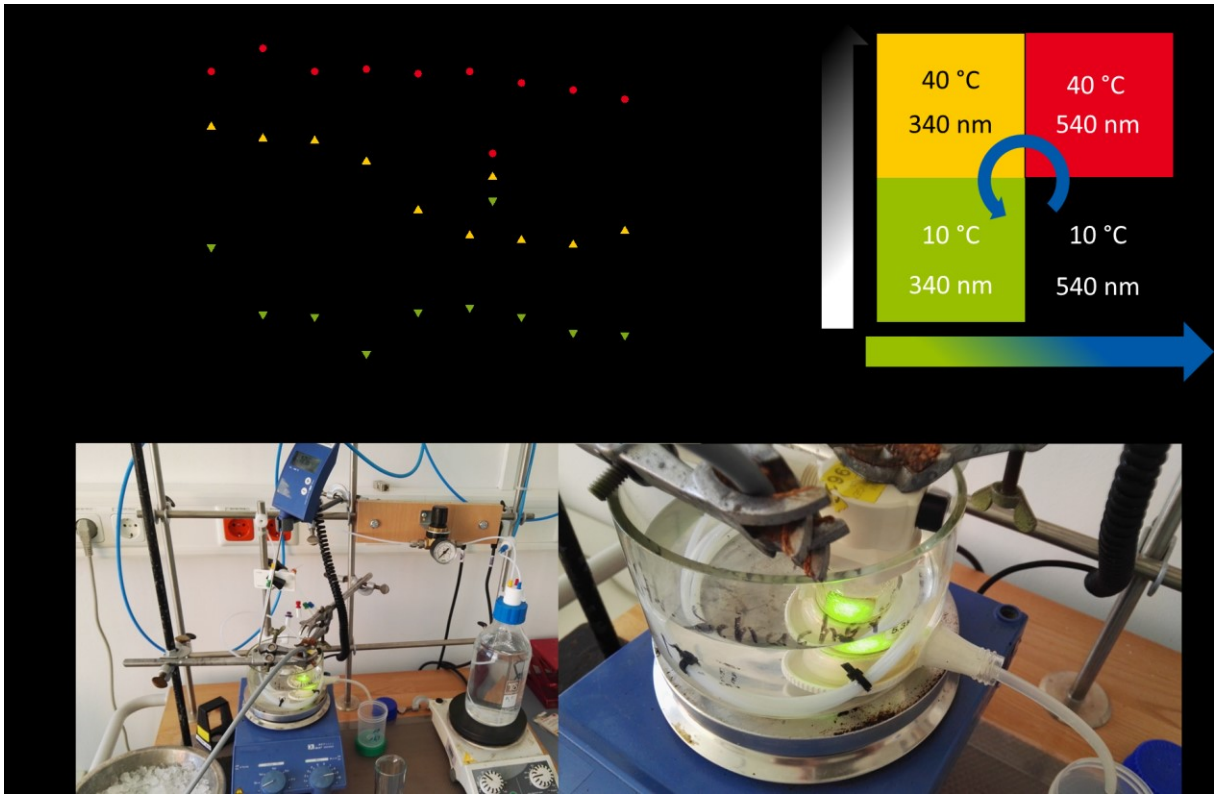

Figure 105: a) Water-flux with time of the PS_{530}-b-PI_{229}-b-P(NIPAAm$_{94}$-co-SPA$_{45}$) membrane, indicating its photo-switching behaviour; b) four switching cycles (arrow indicates the direction of the protocol), and c) the experimental setup used to irradiate and heat or cool the dual-responsive membrane.

The water-flux was determined at 10 °C whilst being irradiated with 540 nm light for 50 min. After which time, the temperature was increased to 40 °C and the water-flux determined for 80 min before

being irradiated at 340 nm at the same temperature (40 °C) for a further 80 min. Finally, the temperature was reduced again to 10 °C whilst irradiating with 340 nm light. During this measurement protocol, no significant change in the water-flux was observed. Although the membrane did change its colour from white to blue upon irradiation with 340 nm light. This behaviour agrees well with the colour changes observed previously for the P(NIPAAm-*co*-SPA) copolymers in chapter 5.4.2.2. However, it appears that the pore-size within the prepared membrane is too large to detect a measurable change in the water-flux as already observed for the PS-*b*-PI-*b*-PNIPAAm triblock terpolymer membranes. Therefore, the processing parameters should be further optimised to create smaller pores to increase the effect of the stimuli-induced collapse of the hydrophilic segment.

Although the membrane did not show the expected temperature-depended changes in water-flux upon irradiation, this experiment shows that it is possible to form porous structures using a block copolymer featuring photo- and temperature-responsive segment.

8 Summary and Conclusions

Within the scope of this thesis, various photo-responsive (spiropyran) and thermo-responsive (2-(2-(2-methoxyethoxy) ethoxy) ethyl acrylate or *N*-isopropylacrylamide) moieties were incorporated with copolymers or block terpolymers, and their dual-responsive behaviour in solution, micellar systems and polymeric membranes investigated. First, dual-responsive copolymers were synthesised using photo-responsive nitrobenzospiropyran acrylate (SPA) with a thermo-responsive moiety, either *N*-isopropylacrylamide (NIPAAm) or 2-(2-(2-methoxyethoxy) ethoxy) ethyl acrylate (TEGA). The copolymerisation of both combinations to form P(NIPAAm-*co*-SPA) and P(TEGA-*co*-SPA) is possible by free radical polymerisation thermally initiated with AIBN. A more sophisticated method, nitroxide-mediated polymerisation, was then applied since it permits the formation of well-defined hydrophobic copolymer macroinitiators that are suitable for block extension. This simplified the determination of the degree of polymerisation and enabled the formation of amphiphilic block terpolymers. Upon optimisation, a set of water-soluble copolymers from each thermo-responsive comonomer were prepared. The seven P(NIPAAm-*co*-SPA) copolymers contained 0 to 5.28 mol% of SPA according to ^{1}H-NMR and an absolute molar mass ranging from 32,000 to 124,000 g/mol. The five P(TEGA-*co*-SPA) copolymers contained 0 to 16 mol% of SPA and an absolute molar mass 37,000 to 58,000 g/mol. In both cases, the amount of SPA in the monomer mixture is reflected in the final copolymer composition. To investigate the dual responsive behaviour, the copolymers were dissolved in a pH 8 buffer solution, where the best photo-responsive behaviour is observed in the pH-range from 2 to 10. Upon irradiating the copolymers at 340 nm, a change in absorbance at 550 nm indicates the amount of SPA in the zwitterionic merocyanine form increases. This process could be reversed by irradiation at 540 nm and could be repeated at least three times. High amounts of SPA lead to a slower but more intensive photo-switching in both sets of copolymers. This behaviour was further confirmed in the solid-state for the P(NIPAAm-*co*-SPA) copolymers.

Heating the dissolved copolymer causes it to precipitate, which is best visualised by a change in transmission at 700 nm. For the same copolymer, the precipitation temperature is higher while the copolymer is irradiated with 340 nm light than while irradiated at 540 nm. The transition temperature in general decreases for increasing amounts of SPA in the copolymer. At the same time, the difference between the transition at 540 nm irradiation and the transition at 340 nm irradiation increases for increasing amounts of SPA. This could be confirmed for both sets of copolymers. The observed temperature difference is independent of the thermo-responsive moiety used. This indicates that the change in polarity originates from the switching of the SPA moiety, and should therefore be applicable for other thermo-responsive moieties not explored in this thesis.

Amphiphilic block copolymers were then prepared *via* NMP according to the optimal conditions found to prepare the water-soluble copolymers. A polystyrene macroinitiator was successfully block extended with dual-responsive copolymers, NIPAAm-*co*-SPA or TEGA-*co*-SPA. The NIPAAm-containing block terpolymers were purified by dialysis, while the TEGA-containing block copolymers required a more laborious purification. All polymeric material is precipitated and in a second work-up step, the additionally formed hydrophilic copolymer is dissolved in pH 8 buffer to collect the solid amphiphilic block terpolymer. The prepared amphiphilic block copolymers, PS_{456}-*b*-$PTEGA_{330}$ and PS_{456}-*b*-P($TEGA_{195}$-*co*-SPA_{16}), were then self-assembled. The size of the resulting micelles according to DLS and cryo-TEM were in good agreement, ranging from 37.2 nm for the block copolymer to 55.1 nm for the block terpolymer. The transition temperature of the NIPAAm-containing micelles is ~1 °C lower than the

water-soluble homopolymer. The transition temperature of the TEGA-containing micelles is 5 °C lower than that observed for PTEGA. The photo-responsive behaviour of the PS_{456}-*b*-P($TEGA_{195}$-*co*-SPA_{16}) block terpolymer micelles is accelerated compared to its analogous copolymer containing a comparable SPA content due to the close proximity of the SPA moieties. The transition temperature was determined to be 45 °C when irradiated at 540 nm, and 50 °C when irradiated at 340 nm. The hydrophilic segment contains 7.6 % of SPA and the temperature difference of 5 °C is in good agreement with the dual-responsive behaviour observed for the analogous copolymer. This indicates that the effect the SPA-moiety has on the transition temperature also applies to the dual-response of micellar systems.

Finally, appropriate block terpolymers were synthesised and used for the formation of membranes. A set of PS-*b*-PI-*b*-PNIPAAm triblock terpolymers with 15 to 26 mol% of NIPAAm was used to systematically investigate the formation of integral asymmetric polymeric membranes. Besides the length of the hydrophilic segment, the composition of the casting solution and open-time after film casting was varied. The film thickness was also investigated and the optimal film-forming conditions identified: a hydrophilic segment of 21 mol%, a casting mixture with 50 vol% THF, and an open-time of 40 s. The membrane formed from PS_{546}-b-PI_{24}-b-$PNIPAAm_{168}$ from a casting mixture with 30 vol% THF and an open-time of 60 s exhibited an increased water-flux with increasing temperature. It was also possible to form a dual stimuli-responsive membrane from PS_{530}-*b*-PI_{229}-*b*-P($NIPAAm_{94}$-*co*-SPA_{45}). The membrane was porous and changed colour upon irradiation, but no change in water-flux was observed. The contact angle, on the other hand, changed upon irradiation and/or heating. This indicates the membranes do indeed undergo changes upon the application of heat or light, but these changes do not manifest in a change in the water-flux.

Throughout this thesis, the expected dual-responsive behaviour of spiropyran-containing thermo-responsive polymers could be shown. The preliminary investigations of the photo-response also reveal the importance of dissolved ions. The effect of the solution ionic strength is quite complex. The synthesis of amphiphilic block copolymers used for the formation of micelles requires further optimisation in order to obtain well-defined block terpolymers to form micelles. Here, the dual-responsive behaviour needs to be further shown for the NIPAAm-containing block terpolymers as well. The formation of membranes via the SNIPS process from stimuli-responsive block terpolymer requires a more thorough investigation since the results of the investigated parameters are not predictable to a satisfying extend. Improvements in membrane formation could further lead to desirable highly responsive membranes, which exhibit variable water-flux upon irradiation and/or temperature changes. Throughout this thesis, the temperature difference between the transition temperatures of the 340 nm irradiated samples and 540 nm irradiated samples depends solely on the amount of SPA. We assigned this observation to the change in polarity from the non-polar spiropyran-form to the zwitterionic merocyanine-form. This affects the solvent hull around the copolymers and is therefore independent from the thermo-responsive moiety used. If this observation can be confirmed using other thermo-responsive moieties, we could gain a much deeper understanding of the effect of the light-responsive SPA moiety in polymeric materials for the preparation of better dual-responsive copolymers in the future.

9 Zusammenfassung und Ausblick

Gegenstand dieser Arbeit war die Synthese eines doppelt responsiven Materials aus einem Spiropyranmonomer (Licht-schaltbar) und N-Isopopylacrylamide (NIPAAm) oder Triethylenglycol acrylat (TEGA, beide Temperatur schaltbar) und die Untersuchung seines Schaltverhaltens in Lösung, an der Oberfläche von Mizellen sowie in den Poren von Membranen. Während des ersten Teils der Arbeit wurden doppelt schaltbare Copolymere bestehend aus lichtschaltbarem Benzonitrospiropyran acrylat (SPA) und einer temperaturschaltbaren Einheit, wobei es sich entweder um NIPAAm oder TEGA handelte, hergestellt. Es konnte nachgewiesen werden, dass beide Kombinationen in Copolymeren, P(NIPAAm-co-SPA) und P(TEGA-co-SPA) mittels freier radikalischer Polymerisation zugänglich sind. Im nächsten Schritt wurde eine kontrollierte radikalische Polymerisation, die Nitroxid-vermittelte Polymerisation (NMP) verwendet. Diese Polymerisationsmethode wurde gewählt, weil sie eine größere Kontrolle über die Polymerisation selbst sowie den Einsatz eines unimolekularen Initiators ermöglicht, wodurch der synthetische Fehler verringert werden kann. Eine kontrollierte radikalische Polymerisation wie die NMP ermöglicht die Verwendung von Makroinitiatoren. Die Verwendung von Makroinitiatoren hat zwei Vorteile: Zum einen können diese später zur Synthese von amphiphilen Blockterpolymeren verwendet werden, zum anderen vereinfacht eine Blockerweiterung die Bestimmung des Polymerisationsgrads und damit ebenso die Optimierung der Synthese. Während der Optimierung wurden Reaktionszeit, Temperatur, unimolekularer Initiator, Monomer/Initiator-Verhältnis und Verhältnis der beiden responsiven Monomere variiert. Auf Basis dieser Optimierung der Reaktionsbedingungen wurden je zwei Serien wasserlöslicher Copolymeren hergestellt, jeweils mit einer der zuvor genannten Temperatur-schaltbaren Einheiten (NIPAAm oder TEGA). Die Zusammensetzung der sieben P(NPAAm-*co*-SPA) Copolymer lag zwischen 0 bis 5.28 mol% SPA, bestimmt mittels ^{1}H-NMR Spektroskopie. Die absolute molare Masse wurde mittels statischer Lichtstreuung bestimmt und schwankte für die Proben zwischen 32,000 und 124,000 g/mol. Die fünf P(TEGA-*co*-SPA) Copolymere enthielten 0 bis 16 mol% SPA und hatten eine absolute molare Masse von 37,000 bis 58,000 g/mol. In beiden Fällen fand sich der Anteil SPA aus der initialen Monomermischung in der Zusammensetzung des Copolymers wieder. Durch den simultanen Verbrauch beider Monomere während der Polymerisation handelt es sich bei den hergestellten Serien um statistische Copolymere.

Im Absorptionsspektrometer wurden die hergestellten Copolymere anschließend sowohl auf ihre Licht- als auch Temperaturschaltbarkeit untersucht. In vorbereitenden Untersuchungen konnte der Einfluss des pH-Wertes auf die Lichtschaltbarkeit des verwendeten SPA Derivats untersucht. Das Copolymer P($NIPAAM_{538}$-*co*-SPA_6) wurde in Pufferlösungen von pH 2 bis pH 10 gelöst, mit 340 nm bzw. 540 nm bestrahlt und zeitabhängig ein Absorptionsspektrum der Lösung aufgenommen. Bei pH 8 zeigte sich die größte Änderung der Absorption sowie ein schnelles Schalten zwischen Spiropyran- und Merocyanine-Form. Der reversiblen Fotoschaltung wirken zwei Reaktionen entgegen: zum einen die Protonierung der offenen Merocyanine-Form bei zu geringen pH-Werten und zum anderen eine Hydrolyse der Esterbindung bei zu hohen pH-Werten. Während des Bestrahlens mit 340 nm änderte sich die Absorption des zuvor genannten Copolymers bei 550 nm, was einem Schalten der SPA-Einheit in die zwitterionische Merocyanine-Form zugeordnet wurde. Dieser Prozess konnte umgekehrt werden, indem die Probe mit 540 nm Licht bestrahlt wurde. Die Lichtschaltbarkeit bei pH 8 wurde für die zuvor synthetisierten Sets aus P(NIPAAm-*co*-SPA) und P(TEGA-*co*-SPA) für mindestens drei Zyklen wiederholt. Die Lichtschaltung der beiden Sets bei pH 8 folgte einer Kinetik erster Ordnung: Ein geringer Anteil SPA im Copolymer führte zu einer schnelleren aber auch weniger intensive Änderung der Absorption. Diese Ergebnisse ließen sich auch für dünne P(NIPAAm-*co*-SPA)-Filme mit einer

Schichtdicke von 10 – 20 µm bestätigen. Die Temperaturschaltbarkeit der Copolymere lässt sich ebenfalls im Absorptionsspektrometer nachweisen. Ein Erwärmen des Copolymers über die Übergangstemperatur führt zur Unlöslichkeit des Copolymers was sich in einer Trübung der Lösung manifestiert. Diese entstehende Trübung lässt sich gut durch eine Änderung der Transmission bei 700 nm detplektieren. Ein bei 340 nm bestrahltes Copolymer (SPA in der zwitterionischen Merocyanin-Form) wurde bei höheren Temperaturen wasserunlöslich als das gleiche Copolymer mit 540 nm bestrahlte Copolymer (SPA in der unpolaren Spiropyran-Form). Die Trübungstemperaturen für beide Phasenübergänge wurde bestimmt über die Halbwerthöhe zwischen der Transmission der gelösten Spezies und der Transmission der ungelösten Spezies. Die Übergangstemperaturen wurden für alle Copolymere und beide Strahlungszustände, 340 nm und 540 nm, bestimmt. Auch hier zeigten sich vergleichbare Trends zwischen beiden Serien an Copolymeren. Zum einen fielen die Trübungstemperaturen der Copolymere mit steigendem Anteil an hydrophoben SPA im Copolymer. Diese Beobachtung fand sich sowohl für die Copolymere, deren SPA-Einheit in der Merocyanine-Form, als auch für die Copolymere deren SPA-Einheit in der Spiropyran-Form vorliegt. Zum anderen stieg der Temperaturunterschied zwischen den Übergangstemperaturen in der Merocyanine-Form und der Spiropyran-Form mit dem Anteil an SPA im Copolymer an. Der entstehende Temperaturunterschied war unabhängig von der verwendeten temperatur responsiven Einheit.

Das doppelt responsive Schaltverhalten der wasserlöslichen Copolymere soll auf komplexere Polymerarchitekturen wie Mizellen angewendet werden. Dazu wurde ein Polystyrol Makroinitiator, der später den Kern der Mizellen bilden soll, mit einem wasserlöslichem P(NIPAAm-*co*-SPA) bzw. P(TEGA-*co*-SPA) Segment erfolgreich blockerweitert. Die Synthesebedingungen stimmten mit denen für die Synthese der Copolymere überein, jedoch führte eine Fällung zu einer bimodalen Verteilung in der SEC. Das gefällte Copolymer bestand aus erweitertem Blockterpolymer und zusätzlich entstandenem Copolymer. Blockterpolymere mit NIPAAm ließen sich aufarbeiten mittels Dialyse und die Blockterpolymere mit TEGA wurden gefällt und anschließend wurde das überschüssige Copolymer mit pH 8-Puffer herausgelöst. Die Blockterpolymere wurden in THF gelöst und anschließend pH 8 TRIS-Puffer tropfenweise zugegeben. Nach dem vollständigen Verdampfen des THFs wurde die stabile trübe Suspension charakterisiert. Die hergestellten Mizellen wurden mittels DLS auf ihr hydrodynamisches Volumen untersucht; die PS-*b*-P(NIPAAm-*co*-SPA) Mizellen hatten einen hydrodynamischen Radius von 50 – 80 nm und die PS-*b*-P(TEGA-*co*-SPA) Mizellen wiesen einen hydrodynamischen Radius von 25 – 75 nm auf. Die Mizellen aus den Blockcopolymeren PS_{456}-*b*-$PTEGA_{330}$ und PS_{456}-*b*-P($TEGA_{195}$-*co*-SPA_{16}) wurden ebenfalls mittels cryo-TEM untersucht und die Größenbestimmung von beiden Methoden stimmt überein: sie schwankt zwischen 37.2 nm für das Blockcopolymer und 55.1 nm für das Blockterpolymer.

Die Untersuchung des Schaltverhaltens der Mizellen folgte dem gleichen Messschema wie die zuvor hergestellten Copolymere. Die Licht responsiven Mizellen aus PS_{456}-*b*-P($NIPAAm_{165}$-*co*-SPA_{11}) und PS_{456}-*b*-P($TEGA_{196}$-*co*-SPA_{16}) wurden für drei Schaltzyklen mit 340 nm bzw. 540 nm bestrahlt. Das Blockterpolymer mit NIPAAm zeigte kein verändertes Absorptionsspektrum durch Bestrahlung, wohingegen das TEGA Blockterpolymer ein ähnliches Schaltverhalten wie die zuvor untersuchten Copolymere zeigt. Die Lichtschaltung von Mizellen aus PS_{456}-*b*-P($TEGA_{195}$-*co*-SPA_{16}) ist beschleunigt gegenüber einem Copolymer mit einem gleichwertigen Anteil SPA im hydrophilen Segment. Dies lässt sich vermutlich darauf zurückzuführen, dass sich die einzelnen SPA-Einheiten aufgrund der Nähe in der Mizellenkorona gegenseitig beeinflussen. Anschließend wurde das Verhalten der Mizellen auf Temperatur untersucht. Die Trübungstemperatur der Mizellen mit NIPAAm lag etwa 1 °C unter der des

Homopolymers PNIPAAm. Die Trübungstemperatur der Mizellen mit TEGA hingegen lag 5 °C unter der des Homopolymers PTEGA. Die Trübungstemperatur der Mizellen aus PS_{456}-*b*-P($TEGA_{195}$-*co*-SPA_{16}) lag bei 45 °C, während die Mizellen mit 540 nm Licht bestrahlt wurden und bei 50 °C, während die Mizellen mit 340 nm bestrahlt wurden. Das hydrophile Segment hatte einen Anteil von 7.6 % SPA und zeigte somit eine Temperaturdifferenz zwischen den beiden Bestrahlungszuständen von 5 °C, was mit den Ergebnissen, die zuvor für die Copolymere gefunden wurden übereinstimmt. Das zeigt, dass der Effekt der Lichtschaltung von SPA auf die Trübungstemperatur auf die Schaltbarkeit von Mizellen Anwendung findet.

Im letzten Teil der Arbeit wurden die bisherigen Erkenntnisse genutzt, um Blockterpolymer herzustellen, die sich für die Herstellung von Membranen eignen. Die hergestellten Blockterpolymere sollen im SNIPS-Prozess (Self-assembly non-solvent induced phase separation) verwendet werden, um integral asymmetrische Membranen herzustellen. Das hydrophile, doppelt responsiven Segment ordnet sich in diesem Prozess an der Poreninnenseite an und kann, ähnlich wie die zuvor untersuchten Mizellen, stimuli-abhängig Kollabieren wodurch der Durchfluss von Wasser durch die Membran verändert werden kann. Der SNIPS-Prozess ist sehr komplex, weshalb zunächst eine Serie aus PS-*b*-PI-*b*-PNIPAAm Triblockterpolymeren hergestellt wurde mit einem hydrophilen Anteil von 15 bis 26 mol%, um den Einfluss verschiedener Faktoren auf die Membranherstellung systematisch zu untersuchen. Neben der Länge des hydrophilen Blocks wurde auch die Verhältnisse von THF zu DMF in der Blockterpolymerlösung und die Wartezeit nach dem Rakeln variiert, um ihren Einfluss auf Membrandicke und Asymmetrie zu untersuchen. Die besten Ergebnisse entstanden bei 21 mol% hydrophilem Anteil, 50 % THF in der Filmziehlösung und einer Wartezeit von 40 Sekunden. Eine Membran aus PS_{546}-*b*-PI_{24}-*b*-$PNIPAAm_{168}$ (21 mol% NIPAAm) mit 30 % THF in der Filmziehlösung und einer Wartezeit von 60 s zeigte, dass der Durchflussfluss durch eine Membran bei steigender Temperatur sprungartig anstieg. Durch die erhöhte Temperatur kollabierten die PNIPAAm Segmente in den Poren der Membran, was zu einem erhöhten Durchfluss führt. Das Kollabieren der wasserlöslichen Ketten beeinflusste die tatsächliche Porengröße, jedoch ist die Änderung der Porengröße bei sehr großen Poren vernachlässigbar gering, weshalb keine Änderung im Durchfluss beobachtet werden kann. Die Porengröße einer Membran mit kollabierten Ketten lässt sich mittels SEM bestimmen. Gequollene PNIPAAm-Segmente hingegen müssen in wässrigem Zustand untersucht werden. Dazu wurde die Porengröße mittels eSEM bei 62 % Luftfeuchtigkeit ermittelt und mit dem Bewegungsspielraum eines Quantum-Dots in der Membran verglichen. Die Porengröße ist in beiden Fällen vergleichbar, auch wenn kleinere Partikel einen größeren Bewegungsspielraum haben als große Partikel. Es war möglich eine Membran aus dem Triblockterpolymer PS_{530}-*b*-PI_{229}-*b*-P($NIPAAm_{94}$-*co*-SPA_{45}) herzustellen und diese auf beide Stimuli (Licht und Temperatur) zu untersuchen. Die Membran war wasserdurchlässig, zeigte aber keine Änderung des Durchflusses und Untersuchungen mittels SEM zeigten eine sehr große Porosität. Die Membran änderte die Farbe bei Bestrahlung, was auf eine Lichtschaltbarkeit schließen lässt. Um die Temperaturschaltbarkeit nachweisen zu können, wurde der Kontaktwinkel bei unterschiedlichen Temperaturen mit gleichzeitiger Bestrahlung mit 365 nm bzw. 525 nm gemessen. Eine Membranprobe, die bei 20 °C mit 365 nm bestrahlt wird zeigt einen Kontaktwinkel von 59°. Wird diese Membran nun erwärmt auf 45 °C, wird das hydrophile Segment wasserunlöslich und der Kontaktwinkel steigt auf 63°. Wird eine kalte Membran mit 525 nm bestrahlt schaltet die SPA-Einheit in die unpolare Spiropyran-Form und der Kontaktwinkel steigt auf 87°. So kann eine doppelte Schaltbarkeit der Membran gezeigt werden.

Während dieser Arbeit konnte das erwartete doppelt responsive Verhalten von Copolymeren bestehend aus einem licht responsiven SPA und einer temperatur responsiven Einheit nachgewiesen werden. Jedoch haben sich während der Bearbeitung dieses Themengebiets einige Fragen ergeben die nach dem Anfertigen dieser Arbeit beantwortet werden müssen. Das Schaltverhalten in Lösung wurde sehr ausführlich untersucht, eine interessante Ergänzung zu der Arbeit wäre die Untersuchung, ob der Einfluss der Polaritätsänderung der Spiropyran-Einheit auch auf andere Temperatur-schaltbare Polymere einen vergleichbaren Einfluss hat. Die bisherigen Ergebnisse lassen vermuten, dass der gemessene Temperaturunterschied zwischen den Übergangstemperaturen beider Bestrahlungszuständen einen Grenzwert aufweist und die Synthese eines Copolymers mit einer anderen temperatur responsiven Einheit könnte bestimmen, wo dieser liegt. Die Ähnlichkeit im Schaltverhalten von Copolymeren und Mizellen wurde nur an wenigen Punkten gezeigt. Auch hier könnten zusätzliche Untersuchungen z. B. bezüglich der Schaltgeschwindigkeit auf Licht weitere Erkentnisse zum Schaltverhalten einer Spiropyraneinheit in Copolymeren liefern. Abschließend ist zu bemerken, dass die Herstellung von Membranen mittels des SNIPS-Prozessen sehr komplex ist und die einzelnen Einflussfaktoren für das von uns untersuchte System noch nicht vollständig bestimmt sind. Ein umfangreicheres Verständnis über die Herstellung der Membranen würde dazu führen, dass die Porengröße genauer eingestellt werden kann und es möglich ist, eine Membran herzustellen die das gleiche Schaltverhalten wie die gelösten Copolymere aufweist.

10 Experimental Part

10.1 Instruments

10.1.1 200 W Hg(Xe) Lamp

For irradiation in solution, a 200 W Hg(Xe) lamp from LOT-QuantumDesign (Darmstadt, Germany) was used. The light was filtered using a UV (U340 from Edmund Optics, Karlsruhe, Germany) and green filter (VG-9 from Edmund Optics) coupled into a glass fibre, which was placed over the sample. The estimated light intensity for the aqueous setup was 10.6 mW/cm^2 for both wavelength filters.

10.1.2 Absorption Spectroscopy in the UV and Visible Range (UV-Vis)

The UV-Vis measurements were performed on an Agilent (Santa Clara, USA) Cary 60 UV-Vis spectrophotometer with a Peltier single cell holder at a given temperature. For solid-state UV-Vis measurements, the solid samples were placed into a custom-made sample holder with the LEDs placed in front of them. The measurements in solution for both irradiation- and temperature-dependent studies were performed in a cuvette (Hellma Optics, Jena, Germany) with a path length of 1 cm. The irradiation source was in both cases placed in a custom-made holder to ensure the position remained the same for every measurement.

10.1.3 Dynamic Light Scattering (DLS)

DLS measurements were performed on an ALV DLS/SLS consisting of an ALV Laser CGS3 Goniometer with an ALV Avalanche correlator and a He-Ne laser (λ = 633 nm). The CONTIN algorithm was applied to analyse the obtained correlation functions. Apparent hydrodynamic radii were calculated according to the Stokes-Einstein equation.

10.1.4 dn/dc Measurements

The dn/dc values required for static light scattering were determined on an optilab rEX from Wyatt technologies with Astra 5.3.4.16 as analysis software.

10.1.5 Gas Chromatography (GC)

Gas chromatography was performed on a Shimadzu GC-2010 plus with an AOC-20s autosampler, an FID, and a flame ionisation detector flushed with hydrogen. The stationary phase was a PerkinElmer Elite 5MS with a length of 30 m, an inner diameter of 0.25 mm, and a 0.25 µm coating of 95 % dimethyl/5 % diphenyl polysiloxane. Helium was used as the mobile phase.

10.1.6 Gas Chromatography Coupled with Mass Spectrometry (GC-MS)

The gas chromatography with mass spectrometry was performed on a Shimadzu GC-2010 equipped with an AOC-20s autosampler using helium as the mobile phase. The stationary phase consists of a Phenomenex Zebron ZB-5MS with a length of 30 m and an inner diameter of 0.25 mm and coated with a 0.25 µm layer of 95 % dimethyl/5 % diphenyl polysiloxane. A GC-QP2010S MS-quadrupole detector was used.

10.1.7 Infrared Spectroscopy (IR)

Infrared spectra were recorded on a PerkinElmer Frontier FT-IR/NIR spectrometer equipped with a heatable Golden Gate ATR unit from Specac and measured in the range of 4000–450 cm^{-1}.

10.1.8 Light Emitting Diodes (LEDs)

For irradiation in the solid-state, two LEDs at 365 nm (0.8 mW) and two LEDs with a wavelength of 590 nm (22 cd) from Roithner (Vienna, Austria) were placed in front of the sample to result in an estimated light intensity of 3.4 mW/cm^2 for the 365 nm light source, and 4.5 mW/cm^2 for the 590 nm LED in the setup used.

10.1.9 Nuclear Magnetic Resonance Spectroscopy (NMR)

NMR measurements were carried out on either a 300 or 600 MHz Bruker NMR spectrometer (Karlsruhe, Germany). The solvent used is specified accordingly, and each spectrum is referenced to the residual solvent signal.

10.1.10 Profilometer

The profilometer images were taken on a NanoSight LM10 from Malvern (Germany, Kassel).

10.1.11 Scanning Electron Microscopy (SEM)

Samples for SEM were prepared as follows: for the top-view, membrane slices were cut and then placed on a glass surface before being dried under vacuum for 6 h; for the cross-sectional view, membrane slices were deep-frozen in liquid nitrogen, broken, and then placed on a glass surface before being dried under vacuum for 6 h. The samples were then coated with gold with an approximate thickness of 8 nm using a BAL-TEC SCD005 sputtering device (Balzers, Liechtenstein). SEM measurements were performed on a Zeiss (LEO) 1530 Gemini FESEM operating at 8 to 10 kV using an InLens or SE2 detector.

10.1.12 Size Exclusion Chromatography (SEC)

Various size exclusion chromatography systems were applied with different eluents, and these systems are described below.

Size exclusion chromatography in chloroform ($CHCl_3$-SEC) was performed on a Shimadzu system equipped with a CBM-20A system controller, an LC-10AD VP pump, an RID-10A refractive index detector, an SPD-10AD vp UV detector at 365 nm using a 94:2:4 (by volume) mixture of chloroform, *iso*propanol and trimethylamine at a flow rate of 1 mL min^{-1} at 40 °C on a PSS SDV guard/linear S (5 µm particle size). The system was calibrated with polystyrene, poly(methyl methacrylate) and polyethylene glycol standards from PSS (Mainz, Germany) with a molecular range of 400–100,000 g/mol.

Size exclusion chromatography in tetrahydrofuran with triple detection (THF-triple-SEC) was performed on a Shimadzu system equipped with a CBM-20A system controller, an LC-10AD VP pump, an RID-10A refractive index detector, a SPD-10AD VP UV detector at 365 nm, a PSS ETA-2010 viscosity detector, and a PSS SDL 7000 MALLS detector with an irradiation wavelength of 660 nm.

Tetrahydrofuran (THF) was used as eluent at a flow rate of 1 mL/min at 30 °C on a PSS SDV guard/linear M. The system was calibrated with polystyrene standards from PSS (Mainz, Germany) with a molecular weight range of 400–1,000,000 g/mol.

Size exclusion chromatography in *N*,*N*-dimethylacetamide (DMAc-SEC) was performed on a Shimadzu system equipped with a SCL-10A VP system controller, an LC-10AD VP pump, an RID-10A refractive index detector, a SPD-10AD VP UV detector at 365 nm in DMAc with 0.21 % LiCl at a flow rate of 1 mL/min on two PSS GRAM guard columns (1000 Å and 30 Å). The system was calibrated with polystyrene standards from PSS (Mainz, Germany) with a molecular weight range of 400–1,000,000 g/mol.

Size exclusion chromatography in tetrahydrofuran (THF-SEC) was performed on an Agilent 1260 system equipped with a G1330B pump, a PSS TC6001 oven at 30 °C, a G1362A refractive index detector, and a G1315D UV detector at 365 nm. THF was used as eluent at a flow rate of 1 mL/min on three PSS SDV guard columns (100/1,000/100,000 Å). The system was calibrated with polystyrene, poly(methyl methacrylate), polyethylene glycol, and polyisoprene standards from PSS (Mainz, Germany) with a molecular weight range of 200–2,000,000 g/mol[1].

10.1.13 Static Light Scattering (SLS)

Static light scattering measurements were performed using an ALV Laser CGS3 Goniometer equipped with an ALV Avalanche correlator and a He-Ne laser (λ = 633 nm). All SLS measurements were performed at 25 °C. To determine the molecular weight, three measurements of 30 s each with a difference of less than 5 % were performed at angles between 30 and 150 ° with a step-width of 10 °. The copolymers were dissolved in HPLC-grade THF at concentrations of 1, 2, 3, 5, and 10 g/L. The q^2+kc values were plotted in a Zimm-plot against K_c/R to determine the mass averaged molecular weight.

10.1.14 Transmission Electron Microscopy (TEM)

For TEM from aqueous solutions, copper grids were rendered hydrophilic through argon plasma cleaning for 30 s (Diener Electronics). A total of 15 µL of the respective sample solution was then applied to the grid, and excess sample removed by blotting with filter paper. TEM images were then acquired on a 200 kV FEI Tecnai G2 20 microscope equipped with a 4K Eagle HS CCD and a 1K Olympus MegaView camera for overview images.

10.1.15 Turbidimetry

Cloud points were measured in a Crystal 16 from Avantium Technologies connected to a chiller (Julabo FP 40) at a wavelength of 500 nm.

10.1.16 Water-Flux

Water-flux measurements were performed in an amicon ultrafiltration cell with an effective area of 4.1 cm^2, and at a typical pressure of 0.5 bar with deionised water.

10.2 Reagents

All solvents and chemicals were purchased from Sigma-Aldrich, ABCR, Alfa Aesar, Th. Geyer, VWR, Acros Organics, TCI, Carbolution, or Carl Roth, and were used as received if not explicitly stated otherwise. Commercially received liquid monomers were passed over a column containing basic aluminium oxide prior to use to remove the inhibitor. The solvent, 1,4-dioxane, was dried over sodium and benzophenone and distilled before use in polymerisations. The inhibitor in *N*-isopropyl acrylamide (NIPAAm) was removed by recrystallization from hexane. The initiator, 1-*tert*-butyl-3,3-dipropyl-5,5-diethyl-4-(1-phenylethoxy)-piperazin-2-one, was kindly provided by Christoph Hörenz. BlocBuilder-MA was kindly provided by Oliver Zuman and Robert Schroot.

10.3 Synthesis

10.3.1 Initiators

10.3.1.1 1-tert-butyl-3,3-dipropyl-5,5-diethyl-4-(1-phenylethoxy)-piperazin-2-one

10.3.1.1.1 3-Nitropentane

Sodium nitrite (1.21 eq., 27.5 g, 0.399 mol) was dissolved in DMSO (246 mL). After the addition of 3-bromopentane (1 eq., 50 g, 0.331 mol) the solution turned yellow and was then allowed to stir for an additional 4 h at ambient temperature. Ice (200 mL) was subsequently added, and the mixture extracted with pentane (3 × 50 mL). The combined organic phase was washed with water (3 × 50 mL), dried over magnesium sulfate, and then filtered before removing the solvent under reduced pressure. The crude product, 3-nitropentane (25. g, 65.8 % yield), was used without further purification.

^{1}H-NMR (300 MHz, $CDCl_3$): δ = 4.31 (m, 1H, -CH-), 2.03–1.88 (m, 2H, -CH_2-), 1.83–1.69 (m, 2H, -CH_2-), 0.94 (t, j = 7.41, 6H, 2 × -CH_3) ppm.

10.3.1.1.2 *N-tert*-Butyl-(2-ethyl-2-nitrobutyl)amine

A 37 % aqueous solution of formaldehyde (1.2 eq., 13 mL, 0.262 mol) was slowly added to a mixture of 3-nitropentane (1 eq., 25.5 g, 0.218 mol) and *tert*-butylamine (1 eq., 18.5 mL, 0.177 mol) in an ice bath with stirring for 10 min. The mixture was then heated to 50 °C and stirred for an additional 16 h before being extracted with pentane (100 mL). The organic phase was washed with water, dried over anhydrous magnesium sulfate, and then filtered before the solvent was evaporated under reduced pressure. The product was obtained by vacuum distillation ($1 \cdot 10^{-3}$ mbar, 50 °C) as a slightly yellow liquid (20.15 g, 45.7 % yield).

^{1}H-NMR (300 MHz, $CDCl_3$): δ = 2.92 (s, 2H, -CH_2-), 1.96 (q, j = 7.45, 4H, 2 × -CH_2-), 1.04 (s, 9H, 3 × -CH_3), 0.84 (t, j = 7.45, 6H, 2 × -CH_3) ppm.

10.3.1.1.3 *N-tert*-Butyl-(2-ethylbutane)-1,2-diamine

N-tert-Butyl-(2-ethyl-2-nitrobutyl) amine (1 eq., 20 g, 0.1 mol) was dissolved in a mixture of 1:1.5 mixture of water and acetic acid (370 mL). Zinc powder (13.8 eq., 89.6 g, 1.37 mol) was then added in small portions with vigorous stirring. The mixture was then heated to 80 °C, stirred for 2 h, and filtered directly. The solvent was removed under reduced pressure and the residue dissolved in water

(200 mL). An aqueous NaOH solution was added to obtain a pH of 12. The solution was then extracted with diethyl ether. The solvent was evaporated under reduced pressure, and the crude product purified by distillation ($6 \cdot 10^{-1}$ mbar, 40 °C). The product was obtained as a colourless liquid (9.1 g, 52 % yield).

^{1}H-NMR (300 MHz, $CDCl_3$): δ = 2.32 (s, 2H, -CH_2-), 1.41–1.22 (m, 4H, 2 × -CH_2-), 1.03 (s, 9H, 3 × -CH_3), 0.79 (t, j = 7.5, 6H, 2 × -CH_3) ppm.

10.3.1.1.4 1-*tert*-Butyl-3,3-dipropyl-5,5-diethyl-2-piperazinone

N-*tert*-Butyl-(2-ethylbutane)-1,2-diamine (1 eq., 8.82 g, 51.2 mmol) was mixed with chloroform (6.2 mL, 0.768 mol, 1.5 eq.) and 3-heptanone (12 eq., 78.2 mL, 0.630 mol). The mixture was cooled using an ice bath, and powdered KOH (5 eq., 16.9 g, 0.256 mol) was then slowly added to obtain a brown solution. The mixture was stirred for 19 h at room temperature. Subsequent filtration and evaporation of the solvent yielded the crude product, which was then purified by column chromatography using a 10:1 vol% mixture of hexane and diethyl ether as eluent. The product, 1-*tert*-butyl-3,3-dipropyl-5,5-diethyl-2-piperazinone, was obtained as a yellow liquid (2.89 g, 20 % yield).

^{1}H-NMR (300 MHz, $CDCl_3$): δ = 3.15 (s, 2H, -CH_2-), 1.62–1.55 (q, 4H, 2 × -CH_2-), 1.42 (s, 9H, 3 × -CH_3), 1.43–1.35 (q, 4H, 2 × -CH_2), 0.88–0.81 (m, 12H, 4 × -CH_3) ppm.

10.3.1.1.5 1-*tert*-Butyl-3,3-dipropyl-5,5-diethyl-2-piperazinon-4-oxyl

1-*tert*-Butyl-3,3-dipropyl-5,5-diethyl-2-piperazinone (1 eq., 600 mg, 2 mmol) was dissolved in dichloromethane (10 mL). *m*-Chloroperbenzoic acid (2 eq., 690 mg, 4 mmol) was then added in small portions over 40 min. The solution became orange, and a white precipitate formed. The mixture was allowed to stir for 6 h before the product was hydrolysed using an aqueous Na_2CO_3 solution. The aqueous layer was extracted with DCM (2 × 20 mL), and the combined organic phases dried over anhydrous sodium sulfate. After filtration, the solvent was removed under reduced pressure to obtain the crude product, which was purified by column chromatography using a hexane/EtOAc (5:1) mixture as eluent. The pure product was obtained as an orange solid (908 mg, 85 % yield).

^{1}H-NMR (300 MHz, $CDCl_3$, after reduction of the radical with phenylhydrazine): δ = 2.97 (s, 2H, -C-CH_2-N-), 1.93–1.62 (m, 4H, 2 × -CH_2-), 1.62–1.26 (m, 4H, 2 × -CH_2-), 1.31 (s, 9H, 3 × -CH_3), 0.92–0.72 (m, 12H, 4 × -CH_3) ppm.

10.3.1.1.6 1-*tert*-Butyl-3,3-dipropyl-5,5-diethyl-4-(1-phenylethoxy) piperazin-2-one

1-*tert*-Butyl-3,3-dipropyl-5,5-diethyl-2-piperazinon-4-oxyl (1.1 eq., 908 mg, 2.9 mmol), 1-bromoethyl benzene (1 eq., 0.36 mL, 2.65 mmol), Cu(0) (1.05 eq., 177 mg, 2.78 mmol), $Cu(OTf)_2$ (1 mol%, 9.6 mg, 0.0026 µmol), and *N*,*N*,*N*',*N*',*N*''-pentamethyldiethylenetriamine (PMDETA, 4 mol%, 22.1 µL, 106 µmol) were dissolved in benzene (7 mL) in a sealed tube and stirred for 48 h at 75 °C. After which time, the copper was removed by passing the mixture through a short AlO_x column, and then the solvent was removed under reduced pressure. The crude product was then purified by column chromatography using a mixture of hexane/MTBE (10:1 vol%). After concentrating the product under reduced pressure, the obtained solid was redissolved in 1,4-dioxane and freeze-dried. The pure product was obtained as a white solid (180 mg, 20 % yield).

^{1}H-NMR (300 MHz, $CDCl_3$): δ = 7.36–7.27 (m, 5H, Ar-H), 4.79–4.61 (m, 1H, Ar-CH-CH_3), 3.26–2.92 (m, 2 H, -C-CH_2-N-), 2.22–0.44 (m, 23H, 4 × -CH_2-, 5 × -CH_3), 1.38 (s, 9H, 3 × -CH_3) ppm.

10.3.1.2 BlocBuilder-MA

10.3.1.2.1 Diethyl 2,2-dimethyl-1-(1,1-dimethylamino) propylphosphonate

Pivalaldehyde (1 eq., 4.3 mL, 41 mmol) was measured into a round bottom flask equipped with a septum and subsequently deoxygenated by bubbling with argon for 20 min. After which time, *tert*-butylamine (1 eq., 4.29 mL, 41 mmol) was added dropwise at room temperature. The mixture was then heated to 35 °C for 2 h. The aqueous phase that formed was then removed, and the organic phase heated to 60 °C for an additional 2 h. Diethyl phosphite (1.45 eq., 7.72 mL, 60 mmol) was added dropwise at 40 °C directly followed by the dropwise addition of boron trifluoride diethyl ether (1 mL), and the reaction mixture allowed to react for 1 h at 60 °C. The formed α-aminophosphonate was acidified with 5 % HCl before being washed with DCM. The subsequent basification was performed with $NaHCO_3$ before being washed again with DCM to obtain the product as a colourless liquid (6.3 g, 55 % yield).

^{1}H-NMR (300 MHz, $CDCl_3$): δ = 4.25–4.00 (m, 4H, -CH_2-O-), 2.73 (d, j = 17.8 1H, -CH-), 1,42–1.21 (m, 6H, -O-CH_2-CH_3), 1.09 (s, 9H, -N-C(CH_3)$_3$), 1.03 (s, 9H, -CH-C(CH_3)$_3$) ppm.

10.3.1.2.2 Diethyl (1-(tert-butyl(hydroxy)amino)-2,2-dimethylpropyl)phosphonate radical (SG1 Nitroxide Radical)

m-Chloroperbenzoic acid (1.6 eq., 22.7 g, 131.7 mmol) was dissolved in DCM (200 mL) and dried over anhydrous $MgSO_4$. The mixture was filtered into a round bottom flask and cooled in an ice bath. The previously obtained α-aminophosphonate (1 eq., 23 g, 82.3 mmol) was slowly added at 0 °C over 2 h. The reaction mixture was then allowed to return to room temperature overnight and an orange liquid formed. Upon evaporation of the solvent, a colourless solid precipitated which was filtered off. The crude product was purified *via* column chromatography using a 1:1 vol% hexane/ethyl acetate solvent mixture as eluent to yield the SG1 radical as an orange liquid (5.82 g, 24 % yield).

FT-IR: υ = 1360 (-N-O·), 1247 (-P=O) cm^{-1}.

10.3.1.2.3 BlocBuilder-MA (2-[*N*-tert-butyl-*N*-(1-diethoxyphosphoryl-2,2-dimethylpropyl)aminoxy]-2-methyl propionic acid

In a Schlenk flask, 2-bromo 2-methyl propionic acid (1.5 eq., 780 mg, 5.1 mmol), SG1 (1eq., 1 g, 3.4 mmol), copper(0) powder (1.05 eq., 237.4 mg, 3.6 mmol), $Cu(OTf)_2$ (0.01 eq., 12.3 mg, 34 µmol), *N,N,N',N',N''*-pentamethyldiethylenetriamine (PMDETA) (0.04 eq., 23.6 mg, 136 µmol), and 2,2'-bipyridyl (2 eq., 1.06 g, 6.8 mmol) were dissolved in acetonitrile (10 mL), and the mixture deoxygenated by three freeze-pump-thaw cycles before being stirred overnight at room temperature. The brown mixture was diluted with aqueous NaOH (1 M, 50 mL) and extracted with DCM (3 × 30 mL). After acidification with concentrated HCl and extraction with DCM (3 × 30 mL), the organic phases were combined and dried over anhydrous $MgSO_4$. The solvent was removed under reduced pressure to yield the product as a colourless solid (2.28 g, 30 % yield).

^{1}H-NMR (300 MHz, $CDCl_3$): δ = 4.39–3.96 (m, 4H, CH_3-CH_2-O-), 3.40 (d, 1H, -CH-$PO(OEt)_2$), 1.77 (s, 3H, -$C(CH_3)_2$), 1.54 (s, 3H, -$C(CH_3)_2$), 1.38–1.28 (m, 6H, $PO(OEt)_2$), 1.23 (s, 9H, -$C(CH_3)_3$), 1.11 (s, 9H, -$C(CH_3)_3$) ppm.

10.3.2 Monomers

10.3.2.1 2-(2-(2-methoxyethoxy) ethoxy) ethyl acrylate (TEGA)

Triethylene glycol monomethyl ether (1 eq., 19.7 mL, 122.6 mmol) and triethylamine (1 eq., 16.1 mL, 122.6 mmol) were dissolved in DCM (100 mL), and the solution cooled to -20 °C. To that mixture, acryloyl chloride (1 eq., 10 mL, 122.6 mmol) dissolved in dichloromethane (50 mL) was added dropwise. The reaction mixture was then allowed to return to room temperature overnight. The turbid solution was then extracted with saturated sodium hydrogen carbonate (2 × 30 mL) followed by water (2 × 30 mL). The organic phase was dried over anhydrous $MgSO_4$, filtered, and the solvent removed under reduced pressure. The crude product was then purified by column chromatography using THF as eluent to obtain TEGA as a colourless liquid (17.37 g, 65 % yield).

^{1}H-NMR (300 MHz, $CDCl_3$): δ = 6.52 (d, j = 9.00, 1H, -C=C-H), 6.1 (dd, j = 10.3, 17.2, 1H, H_2C=C-H), 5.78 (d, j = 10.4, 1H, -C=C-H), 4.24 (t, 4.80 2H, COO.CH_2-), 3.75–3.4 (tt, j = 4.80, 27.7, 10H, -CH_2-), 3.30 (s, 3H, -CH_3) ppm.

10.3.2.2 Synthesis of 2-((3´,3´-dimethylspiro[chromene-2,2´-indolin]-6-yl)oxy) acrylate (BSP)

Trimethyl-6-hydroxyspiro-(2H-1-benzopyran-2,2'indoline) (1 eq., 500 mg, 1.7 mmol) and triethylamine (2.5 eq., 0.6 mL, 4.3 mmol) were dissolved in DCM (20 mL) before being deoxygenated by purging with argon for 30 min. The reaction mixture was then cooled to -30 °C before acryloyl chloride (1.45 eq., 0.2 mL, 2.47 mmol) dissolved in DCM (5 mL) was added over 30 min dropwise to the cold solution. The reaction mixture was then allowed to return to room temperature and stirred for a further 24 h. The clear red solution was then extracted with a saturated $NaHCO_3$ solution (2 × 30 mL), and then with deionised water (2 × 30 mL). The aqueous phases were then combined and extracted with DCM (2 × 50 mL). The combined organic phases were then dried over anhydrous $MgSO_4$, filtered, and the solvent removed under reduced pressure after the addition of a small amount of silica powder. The red powder was purified by column chromatography using a 4:1 mixture of *n*-hexane and ethyl acetate as eluent. The combined fractions were concentrated under reduced pressure to obtain the product as a white powder (467 mg, 78.9 % yield).

^{1}H-NMR (300 MHz, $CDCl_3$): δ = 7.19 (dt, j = 7.55, 0.78 Hz, 1H, CH), 7.08 (dd, j = 7.22, 0.67 Hz, 1H, CH), 6.84 (m, 4H, CH), 6.71 (d, j = 8.38 Hz, 1H, CH), 6.59 (dd, j = 16.38, 0.78 Hz, 1H, CH), 6.54 (d, j = 7.77 Hz, 1H, CH), 6.31 (dd, j = 17.3, 10.49 Hz, 1H, CH), 5.99 (dd, j = 10.33, 0.89 Hz, 1H, CH), 5.73 (d, j = 10.27 Hz, 1H, CH), 2.74 (s, 3H, CH_3), 1.32 (s, 3H, CH_3), 1.17 (s, 3H, CH_3) ppm.

10.3.2.3 Benzospiropyran ethyl acrylate (BSPA)

10.3.2.3.1 Synthesis of 2-bromoethylacrylate

2-Bromoethanol (1 eq., 5 mL, 70 mmol) and trimethylamine (1 eq., 9.71 mL, 70 mmol) were dissolved in DCM, and the mixture cooled to 0 °C. Over 1 h, a solution of acryloyl chloride (1 eq., 5.71 mL, 70 mmol) in DCM was added to the cooled mixture. The reaction was then allowed to return to room

temperature overnight before being filtered, and the filtrate extracted with saturated $NaHCO_3$ (3 × 10 mL) and water (3 × 10 mL). The combined organic phase was dried over anhydrous $MgSO_4$, filtered, and evaporated under reduced pressure. The product was collected as a colourless oil (4.21 g, 27.9 % yield) by vacuum distillation (0.1 mbar, 30 °C) and analysed *via* ^{1}H-NMR.

^{1}H-NMR(300 MHz, $CDCl_3$): δ = 3.53 (t, j = 6.15, 2H, CH_2), 4.45 (t, j = 6.15, 2H, CH_2), 5.87 (d, j = 10.42, 1H, CH_2), 6.13 (dd, j = 10.42, 17.30, 1H, CH), 6.44 (d, j = 17.30, 1H, CH_2) ppm.

10.3.2.3.2 Synthesis of 2-((3´,3´-dimethylspiro[chromene-2,2´-indolin]-6-yl)oxy) ethylacrylate (BSPA)

2-Bromoethylacrylate (1 eq., 1.22 g, 6.8 mmol), 3´,3´-dimethylspiro[chromene-2,2´-indolin]-6-ol (1 eq., 2 g, 6.8 mmol), and a grain of KI were suspended in butanone. The mixture was purged with argon before being heated to 90 °C for 15 h. The reaction mixture was then cooled to room temperature, filtered, and concentrated under reduced pressure. 2-((3´,3´-Dimethylspiro[chromene-2,2´-indolin]-6-yl)oxy) ethylacrylate (459 mg, 17.9 % yield) was purified by column chromatography using an 8 % ethyl acetate in hexane solution as eluent.

^{1}H-NMR (300 MHz, $CDCl_3$): δ = 1.21 (s, 3H, CH_3), 1.35 (s, 3H, CH_3), 4.12 (t, j = 4.70, 2H, CH_2), 4.52 (t, j = 4.70, 2H, CH_2), 5.75 (d, j = 10.18, 1H, CH-arom.), 5.88 (d, j = 10.39, 1H, CH_2), 6.20 (dd, j = 10.39, 17.29, 1H, CH), 6.53 (m, 2H), 6.69 (m, 2H), 6.85 (m, 2H), 7.11 (d, j = 10.44, 1H, CH-arom.), 7.21 (t, j = 7.61, 1H, CH-arom.) ppm.

10.3.2.4 2-(3´,3´-dimethyl-6-nitrospiro[chromene-2,2´-indolin]-1´-yl)ethyl acrylate (SPA)

10.3.2.4.1 Synthesis of 1-(2-hydroxyethyl)-2,3,3-trimethyl-3H-indolium bromide

A mixture of 2,3,3-trimethyl-3H-indol (1 eq., 2.72 mL, 16 mmol) and 2-bromoethanol (1.25 eq., 1.48 mL, 20 mmol) in acetonitrile (20 mL) was deoxygenated by purging with argon before being heated under reflux at 100 °C for 26 h. The solvent was removed under reduced pressure, and the solid resuspended in *n*-hexane (25 mL). The collected solid was then recrystallised from chloroform and used directly in the following step.

10.3.2.4.2 Synthesis of 9,9,9a-trimethyl-2,3,9,9a-tetrahydro-oxazolo[2,3-a]indole

1-(2-Hydroxyethyl)-2,3,3-trimethyl-3H-indolium bromide was dissolved in water and mixed with KOH (0.66 g, 12 mmol). The mixture turned from pink to yellow within 10 min at room temperature. The mixture was then extracted with diethyl ether (3 × 20 mL), dried over anhydrous $MgSO_4$, filtered, and the solvent removed under reduced pressure to obtain the product as a yellow oil (0.855 g, 33.5 %), which was analysed *via* ^{1}H-NMR.

^{1}H-NMR (300 MHz, $CDCl_3$): δ = 1.89 (s, 3H, CH_3), 1.31 (s, 3H, CH_3), 1.42 (s, 3H, CH_3), 3.44–3.86 (m, 4H, 2 × -CH_2), 6.76 (d, j = 7.80, 1H, CH-arom.), 6.93 (t, j = 7.38, 1H, CH-arom.), 7.13 (d, j = 7.32, 1H, CH-arom.), 7.19(t, j = 7.62, 1H, CH-arom.) ppm.

10.3.2.4.3 Synthesis of 2-(3´,3´-dimethyl-6-nitro-3´H-spiro[chromene-2,2´-indol]-1´-yl)-ethanol

9,9,9a-Trimethyl-2,3,9,9a-tetrahydro-oxazolo[2,3-a]indole (1 eq., 0.85 g, 4.2 mmol) and 2-hydroxy-5-nitrobenzaldehyde (1.5 eq., 1.05 g, 6.3 mmol) were dissolved in ethanol (10 mL), and the solution

heated under reflux for 3 h. After cooling to room temperature, the remaining solution was filtered and washed with ethanol. The product was obtained as red crystals (0.632 g, 33 % yield), which was analysed *via* ^{1}H-NMR.

^{1}H-NMR (300 MHz, DMSO-d_6): δ = 1.10 (s, 3H, -CH_3), 1.20 (s, 3H, -CH_3), 3.19 (dq, j = 7.02, 44.8, 2H, -CH_2), 3.44 (t, j = 6.92, 2H, -CH_2), 4.72 (s, 1H, -OH), 6.01 (d, j = 10.34, 1H, CH-arom.), 6.64 (d, j = 7.68, 1H, CH-arom.), 6.78 (t, j = 7.38, 1H, CH-arom.), 6.87 (d, j = 9.00, 1H, CH-arom.), 7.11 (m, 3H, 3 × CH-arom.), 8.00 (dd, j = 2.82, 9.00, 1H, CH-arom.), 8.21 (d, j = 2.82, 1H, CH-arom) ppm.

10.3.2.4.4 Synthesis of 2-(3´,3´-dimethyl-6-nitrospiro[chromene-2,2´-indolin]-1´-yl)ethyl acrylate (SPA)

2-(3´,3´-Dimethyl-6-nitro-3´H-spiro[chromene-2,2´-indol]-1´-yl)-ethanol (1 eq., 0.5 g, 1.42 mmol) and trimethylamine (1 eq., 0.197 mL, 1.42 mmol) were dissolved in DCM (10 mL), deoxygenated by purging with argon, and the mixture cooled to -35 °C. A solution of acryloyl chloride (1 eq., 0.116 mL, 1.42 mmol) in DCM (5 mL) was then slowly added, after which the reaction mixture was allowed to return to room temperature overnight. The solution was then extracted with saturated $NaHCO_3$ (2 × 20 mL) and water (2 × 20 mL). The organic phases were combined, dried over anhydrous $MgSO_4$, filtered, and concentrated under reduced pressure. The crude product was purified *via* column chromatography using chloroform as eluent to yield the product as a yellow solid (107.6 mg, 0.265 mmol, 18.6 % yield).

^{1}H-NMR (300 MHz, DMSO-d_6): δ = 1.06 (s, 3H, -CH_3), 1.19 (s, 3H, -CH_3), 3.36–3.51 (dt, j = 5.13, 45.8, 2H, -CH_2), 4.16–4.35 (dt, j = 5.50,54.8, 2H, -CH_2), 5.90 (d, j = 10.6, 1H, -CH), 5.96 (d, j = 10.6, 1H, CH-arom.), 6.09 (dd, j = 10.3, 17,2 1H, CH), 6.26 (d, j = 17.3, 1H, CH), 6.72 (d, j = 7.74, 1H, CH-arom.), 6.80 (t, j = 7.35, 1H, CH-arom.), 6.85 (d, j = 9.00, 1H, CH-arom.), 7.12 (m, 2H, 2 × CH-arom.), 7.20 (d, j = 10.4, 1H, CH-arom.), 7.99 (dd, j = 2.73, 8.97 1H, CH-arom.), 8.21 (d, j = 2.64, 1H, CH-arom.) ppm.

10.4 General Polymerisation Procedure

In a typical polymerisation, the NMP initiator was mixed with the monomer using a molar ratio of 1/400, where the monomer contained 5 mol% of the photo-responsive moiety. The polymerisation mixture was then deoxygenated by three consecutive freeze-pump-thaw cycles before being back-filled with argon. The sealed vial was then heated to 110 °C in a pre-heated and thermostatted oil bath or a metal block overnight. Residual monomer was removed by precipitation in a non-solvent. The obtained polymer was stored at room temperature in the dark.

10.4.1 PS Macroinitiator Synthesis

In a typical synthesis, a mixture of 1-*tert*-butyl-3,3-dipropyl-5,5-diethyl-4-(1-phenylethoxy) piperazin-2-one (NMP initiator, 50 mg, 120 µmol) and styrene (11.4 mL, 96 mmol, M/I = 800) was deoxygenated by three consecutive freeze-pump-thaw cycles in a sealed Schlenk tube before back-filling with argon. The reaction mixture was then heated at 105 °C for 24 h. After cooling to room temperature, the reaction mixture was precipitated twice in methanol and the product collected by filtration to yield the PS macroinitiator as a white powder (6.39 g, 61.4 % yield).

$CHCl_3$-SEC (PS standards): M_n = 28,700 g/mol; $Đ$ = 1.14.

10.4.2 PS-*co*-PI Macroinitiator Synthesis

In a typical synthesis, 1-*tert*-butyl-3,3-dipropyl-5,5-diethyl-4-(1-phenylethoxy) piperazin-2-one (NMP initiator, 11.7 mg, 24 µmol, M/I = 2000), styrene (5.15 mL, 44.9 mmol, 80 %) and isoprene (1.12 mL, 11.2 mmol, 20 %) were mixed in a sealed Schlenk flask before the mixture was deoxygenated by three consecutive freeze-pump-thaw cycles and back-filling with argon. The reaction mixture was then heated at 115 °C for 15 h. The macroinitiator was purified by precipitation twice in methanol to yield a white powder (1.29 g, 23.6 % yield) containing 19.4 % isoprene according to ^{1}H-NMR, and characterised by an M_n of 39,600 g/mol and $Đ$ of 1.22 from $CHCl_3$-SEC calibrated using PS standards.

10.4.3 PS-*b*-PI Block Extension

In a typical block extension, the PS macroinitiator (M_n = 30,000 g/mol, 1 g, 33 µmol) was dissolved in isoprene (6 mL, 60 mmol, M/I = 1800), and the mixture deoxygenated by three consecutive freeze-pump-thaw cycles in a sealed Schlenk tube before being back-filled with argon. The reaction mixture was then heated at 115 °C for 72 h, and the product purified by precipitation in methanol twice. The product was collected by filtration as a white powder (1.51 g, 30 % yield). According to ^{1}H-NMR in $CDCl_3$, the product contained 53.4 % isoprene, and a corresponding M_n and dispersity of 52,500 g/mol and 1.20, respectively.

10.4.4 PS-*b*-P(NIPAAm-*co*-SPA) Block Extension

In a typical procedure, the PS macroinitiator (M_n 52,300 g/mol, $Đ$ 1.18, 200 mg, M/I = 1476:1), NIPAAm (579 mg, 5.12 mmol, 95 %) and SPA (579 mg, 256 µmol, 5 %) were dissolved in 1,4-dioxane (6 mL). The reaction mixture was then deoxygenated by three freeze-pump-thaw cycles, back-filled with argon, and then heated to 100 °C in a pre-heated oil bath for 6 h. The colour changed from red to green, and then to blue during this time. The resulting polymer was purified by precipitation in cold Et_2O to obtain the block terpolymer (140 mg). Characterisation by ^{1}H-NMR and SEC indicates a composition of PS_{88}-*b*-P($TEGA_{10}$-*co*-SPA_2)^{71200} with a corresponding dispersity of 1.14.

10.4.5 PS-*b*-P(TEGA-*co*-SPA) Block Extension

In a typical procedure, the PS macroinitiator (M_n 52,300 g/mol, $Đ$ 1.18, 1.5 g, M/I = 1333:1), TEGA (7.4 g, 34 mmol, 95 %) and SPA (0.77 g, 1.9 mmol, 5 %) were dissolved in 1,4-dioxane (6 mL). The reaction mixture deoxygenated by three consecutive freeze-pump-thaw cycles, back-filled with argon, and then heated at 110 °C in a pre-heated and thermostatted oil bath for 6 h. The colour changed from red to green, and then to blue during the polymerisation. The resulting polymer was purified by precipitation in cold Et_2O to obtain the block terpolymer (1.2 g). Characterisation by ^{1}H-NMR and SEC indicates a composition of PS_{63}-*b*-P($TEGA_{33}$-*co*-SPA_4)^{85400} was obtained, with a corresponding dispersity of 1.59.

10.5 General Micelle Formation Procedure

In a typical procedure, the amphiphilic block terpolymer was dissolved in THF before water was slowly added to obtain a concentration of 0.5 mg/mL. The THF was then slowly evaporated to form micelles.

10.6 General Membrane Casting Procedure

Membranes were prepared *via* the SNIPS process. Diblock terpolymer films were cast from a 15 wt% solution of DMF and THF with a 200 µm doctor blade onto polished (with chloroform and 2-propanol) glass sheets using a Coatmaster 510 (Erichsen GmbH, Germany). The film-casting was carried out in a climate chamber from PlasLabs to control both the relative humidity and temperature during the process. Relative humidities of 30, 50, and 70 % were used. Typically after 30 s exposure to air (open-time), the cast films were immersed into a deionised water bath for the final membrane formation. During the next 60 min, the films typically started to lift off the glass surface. After 24 h, the membranes were taken out of the water bath and stored in deionised water until required.

11 References

1. Grimm, O.; Wendler, F.; Schacher, F., Micellization of Photo-Responsive Block Copolymers. *Polymers* **2017,** *9* (9), 396.

2. Wei, M.; Gao, Y.; Li, X.; Serpe, M. J., Stimuli-responsive polymers and their applications. *Polym. Chem.* **2017,** *8* (1), 127-143.

3. Shahinpoor, M.; Schneider, H.-J., *Intelligent Materials*. 2007.

4. Huang, W. M.; Ding, Z.; Wang, C. C.; Wei, J.; Zhao, Y.; Purnawali, H., Shape memory materials. *Mater. Today* **2010,** *13* (7-8), 54-61.

5. Lendlein, A.; Jiang, H.; Junger, O.; Langer, R., Light-induced shape-memory polymers. *Nat. Chem.* **2005,** *434* (7035), 879-82.

6. Muthyala, R., *Chem. Appl. Leuco Dyes*. 2002.

7. Bamfield, P., *Chromic Phenomena*. Royal Chemical Society: 2010; p P001-P562.

8. Armistead, W. H.; Stookey, S. D., Photochromic Silicate Glasses Sensitized by Silver Halides. *Science* **1964,** *144* (3615), 150-4.

9. Evans, R. A.; Hanley, T. L.; Skidmore, M. A.; Davis, T. P.; Such, G. K.; Yee, L. H.; Ball, G. E.; Lewis, D. A., The generic enhancement of photochromic dye switching speeds in a rigid polymer matrix. *Nat. Mater.* **2005,** *4* (3), 249-53.

10. Hirshberg, Y., Reversible Formation and Eradication of Colors by Irradiation at Low Temperatures. A Photochemical Memory Model. *J. Am. Chem. Soc.* **1956,** *78* (10), 2304-2312.

11. Gindre, D.; Boeglin, A.; Fort, A.; Mager, L.; Dorkenoo, K. D., Rewritable optical data storage in azobenzene copolymers. *Opt. Express* **2006,** *14* (21), 9896-901.

12. Walker, E.; Rentzepis, P. M., A new dimension. *Nat. Photonics* **2008,** *2* (7), 406-408.

13. Ameri, T.; Dennler, G.; Lungenschmied, C.; Brabec, C. J., Organic tandem solar cells: A review. *Energy Environ. Sci.* **2009,** *2* (4), 347-363.

14. Lechner, M. D.; Gehrke, K.; Nordmeier, E. H., *Makromolekulare Chemie: Ein Lehrbuch für Chemiker, Physiker, Materialwissenschaftler und Verfahrenstechniker*. Springer Berlin Heidelberg: 2014.

15. Tieke, B., *Makromolekulare Chemie: Eine Einführung*. Wiley: 2012.

16. Webster, O. W., Living polymerization methods. *Science* **1991,** *251* (4996), 887-93.

17. Waldron, C.; Zhang, Q.; Li, Z.; Nikolaou, V.; Nurumbetov, G.; Godfrey, J.; McHale, R.; Yilmaz, G.; Randev, R. K.; Girault, M.; McEwan, K.; Haddleton, D. M.; Droesbeke, M.; Haddleton, A. J.; Wilson, P.; Simula, A.; Collins, J.; Lloyd, D. J.; Burns, J. A.; Summers, C.; Houben, C.; Anastasaki, A.; Li, M.; Becer, C. R.; Kiviaho, J. K.; Risangud, N., Absolut “copper catalyzation perfected”; robust living polymerization of NIPAM: Guinness is good for SET-LRP. *Polym. Chem.* **2014,** *5* (1), 57.

18. Szwarc, M.; Levy, M.; Milkovich, R., Polymerization Initiated by Electron Transfer to Monomer. A New Method of Formation of Block Polymers1. *J. Am. Chem. Soc.* **1956,** *78* (11), 2656-2657.

19. Otsu, T.; Yoshida, M., *Makromol. Chem., Rapid Commun.* **1982,** *3* (2), 127-132.

20. Matyjaszewski, K.; Gaynor, S. G.; Greszta, D.; Mardare, D.; Shigemoto, T.; Wang, J.-S., Unimolecular and bimolecular exchange reactions in controlled radical polymerization. *Macromol. Symp.* **1995,** *95* (1), 217-231.

21. Matyjaszewski, K.; Spanswick, J., Controlled/living radical polymerization. *Mater. Today* **2005,** *8* (3), 26-33.

22. Jenkins, A. D.; Jones, R. G.; Moad, G., Terminology for reversible-deactivation radical polymerization previously called "controlled" radical or "living" radical polymerization (IUPAC Recommendations 2010). *Pure Appl. Chem.* **2009,** *82* (2), 483-491.

23. Braunecker, W. A.; Matyjaszewski, K., Controlled/living radical polymerization: Features, developments, and perspectives. *Prog. Polym. Sci.* **2007,** *32* (1), 93-146.

24. Moad, G.; Rizzardo, E.; Thang, S. H., Living Radical Polymerization by the RAFT Process – A Third Update. *Aust. J. Chem.* **2012,** *65* (8), 985-1076.

25. Hawker, C. J.; Bosman, A. W.; Harth, E., New Polymer Synthesis by Nitroxide Mediated Living Radical Polymerizations. *Chem. Rev.* **2001,** *101* (12), 3661-3688.

26. Reyhani, A.; Nothling, M. D.; Ranji-Burachaloo, H.; McKenzie, T. G.; Fu, Q.; Tan, S.; Bryant, G.; Qiao, G. G., Blood-Catalyzed RAFT Polymerization. *Angew. Chem., Int. Ed.* **2018,** *57* (32), 10288-10292.

27. Hawker, C. J.; Barclay, G. G.; Orellana, A.; Dao, J.; Devonport, W., Initiating Systems for Nitroxide-Mediated "Living" Free Radical Polymerizations: Synthesis and Evaluation. *Macromolecules* **1996,** *29* (16), 5245-5254.

28. Benoit, D.; Grimaldi, S.; Robin, S.; Finet, J.-P.; Tordo, P.; Gnanou, Y., Kinetics and Mechanism of Controlled Free-Radical Polymerization of Styrene andn-Butyl Acrylate in the Presence of an Acyclic β-Phosphonylated Nitroxide†. *J. Am. Chem. Soc.* **2000,** *122* (25), 5929-5939.

29. Benoit, D.; Chaplinski, V.; Braslau, R.; Hawker, C. J., Development of a Universal Alkoxyamine for "Living" Free Radical Polymerizations. *J. Am. Chem. Soc.* **1999,** *121* (16), 3904-3920.

30. Benoit, D.; Harth, E.; Fox, P.; Waymouth, R. M.; Hawker, C. J., Accurate Structural Control and Block Formation in the Living Polymerization of 1,3-Dienes by Nitroxide-Mediated Procedures. *Macromolecules* **2000,** *33* (2), 363-370.

31. Atkins, P. W.; De Paula, J., *Physikalische Chemie*. Wiley-VCH: 2013.

32. Kortekaas, L.; Browne, W. R., The evolution of spiropyran: fundamentals and progress of an extraordinarily versatile photochrome. *Chem. Soc. Rev.* **2019,** *48* (12), 3406-3424.

33. Iwamura, M.; Ishikawa, T.; Koyama, Y.; Sakuma, K.; Iwamura, H., 1-Pyrenylmethyl esters, photolabile protecting groups for carboxylic acids. *Tetrahedron Lett.* **1987,** *28* (6), 679-682.

34. Barltrop, J. A.; Plant, P. J.; Schofield, P., Photosensitive protective groups. *Chem. Commun.* **1966,** (22), 822-823.

35. Furuta, T.; Torigai, H.; Sugimoto, M.; Iwamura, M., Photochemical Properties of New Photolabile cAMP Derivatives in a Physiological Saline Solution. *J. Org. Chem.* **1995,** *60* (13), 3953-3956.

36. Sheehan, J. C.; Umezawa, K., Phenacyl photosensitive blocking groups. *J. Org. Chem.* **1973,** *38* (21), 3771-3774.

37. Wuts, P. G. M., Protection for the Phosphate Group. In *Greene's Protective Groups in Organic Synthesis*, Wuts, P. G. M., Ed. John Wiley & Sons, Inc.: Hoboken, New Jersey, 2014; Vol. 5, pp 1203-1262.

38. Jiang, J.; Tong, X.; Zhao, Y., A New Design for Light-Breakable Polymer Micelles. *J. Am. Chem. Soc.* **2005,** *127* (23), 8290-8291.

39. Jiang, J.; Tong, X.; Morris, D.; Zhao, Y., Toward Photocontrolled Release Using Light-Dissociable Block Copolymer Micelles. *Macromolecules* **2006,** *39* (13), 4633-4640.

40. Lee, J.-E.; Ahn, E.; Bak, J. M.; Jung, S.-H.; Park, J. M.; Kim, B.-S.; Lee, H.-i., Polymeric micelles based on photocleavable linkers tethered with a model drug. *Polymer* **2014,** *55* (6), 1436-1442.

41. Liu, X.; He, J.; Niu, Y.; Li, Y.; Hu, D.; Xia, X.; Lu, Y.; Xu, W., Photo-responsive amphiphilic poly(α-hydroxy acids) with pendent o-nitrobenzyl ester constructed via copper-catalyzed azide-alkyne cycloaddition reaction. *Polym. Adv. Technol.* **2015,** *26* (5), 449-456.

42. Song, Z.; Kim, H.; Ba, X.; Baumgartner, R.; Lee, J. S.; Tang, H.; Leal, C.; Cheng, J., Polypeptide vesicles with densely packed multilayer membranes. *Soft matter* **2015,** *11* (20), 4091-4098.

43. Zhu, C.; Bettinger, C. J., Photoreconfigurable Physically Cross-Linked Triblock Copolymer Hydrogels: Photodisintegration Kinetics and Structure–Property Relationships. *Macromolecules* **2015,** *48* (5), 1563-1572.

44. Wang, X.; Liu, G.; Hu, J.; Zhang, G.; Liu, S., Concurrent Block Copolymer Polymersome Stabilization and Bilayer Permeabilization by Stimuli-Regulated "Traceless" Crosslinking. *Angew. Chem. Int. Ed.* **2014,** *53* (12), 3138-3142.

45. Li, Y.; Qian, Y.; Liu, T.; Zhang, G.; Liu, S., Light-Triggered Concomitant Enhancement of Magnetic Resonance Imaging Contrast Performance and Drug Release Rate of Functionalized Amphiphilic Diblock Copolymer Micelles. *Biomacromolecules* **2012,** *13* (11), 3877-3886.

46. Xie, Z.; Hu, X.; Chen, X.; Mo, G.; Sun, J.; Jing, X., A Novel Biodegradable and Light-Breakable Diblock Copolymer Micelle for Drug Delivery. *Adv. Eng. Mater.* **2009,** *11* (3), B7-B11.

47. Greco, C. T.; Epps, T. H.; Sullivan, M. O., Mechanistic Design of Polymer Nanocarriers to Spatiotemporally Control Gene Silencing. *ACS Biomater. Sci. Eng.* **2016,** *2* (9), 1582-1594.

48. Gupta, M. K.; Balikov, D. A.; Lee, Y.; Ko, E.; Yu, C.; Chun, Y. W.; Sawyer, D. B.; Kim, W. S.; Sung, H.-J., Gradient release of cardiac morphogens by photo-responsive polymer micelles for gradient-mediated variation of embryoid body differentiation. *J. Mater. Chem. B* **2017,** *5*, 2019-2033.

49. Bertrand, O.; Gohy, J.-F.; Fustin, C.-A., Synthesis of diblock copolymers bearing p-methoxyphenacyl side groups. *Polym. Chem.* **2011,** *2* (10), 2284-2292.

50. Schumers, J.-M.; Bertrand, O.; Fustin, C.-A.; Gohy, J.-F., Synthesis and self-assembly of diblock copolymers bearing 2-nitrobenzyl photocleavable side groups. *J. Polym. Sci., Part A: Polym. Chem.* **2012,** *50* (3), 599-608.

51. Song, D.-P.; Wang, X.; Lin, Y.; Watkins, J. J., Synthesis and Controlled Self-Assembly of UV-Responsive Gold Nanoparticles in Block Copolymer Templates. *J. Phys. Chem. B* **2014,** *118* (44), 12788-12795.

52. Soliman, S. M. A.; Nouvel, C.; Babin, J.; Six, J.-L., o-nitrobenzyl acrylate is polymerizable by single electron transfer-living radical polymerization. *J. Polym. Sci., Part A: Polym. Chem.* **2014,** *52* (15), 2192-2201.

53. Jana, S.; Saha, A.; Paira, T. K.; Mandal, T. K., Synthesis and Self-Aggregation of Poly(2-ethyl-2-oxazoline)-Based Photocleavable Block Copolymer: Micelle, Compound Micelle, Reverse Micelle, and Dye Encapsulation/Release. *J. Phys. Chem. B* **2016,** *120* (4), 813-824.

54. Xu, Z.; Yan, B.; Riordon, J.; Zhao, Y.; Sinton, D.; Moffitt, M. G., Microfluidic Synthesis of Photoresponsive Spool-Like Block Copolymer Nanoparticles: Flow-Directed Formation and Light-Triggered Dissociation. *Chem. Mater.* **2015,** *27* (23), 8094-8104.

55. Liu, G.; Dong, C.-M., Photoresponsive Poly(S-(o-nitrobenzyl)-l-cysteine)-b-PEO from a l-Cysteine N-Carboxyanhydride Monomer: Synthesis, Self-Assembly, and Phototriggered Drug Release. *Biomacromolecules* **2012,** *13* (5), 1573-1583.

56. Jiang, X.; Lavender, C. A.; Woodcock, J. W.; Zhao, B., Multiple Micellization and Dissociation Transitions of Thermo- and Light-Sensitive Poly(ethylene oxide)-b-poly(ethoxytri(ethylene glycol) acrylate-co-o-nitrobenzyl acrylate) in Water. *Macromolecules* **2008,** *41* (7), 2632-2643.

57. Yuan, W.; Guo, W., Ultraviolet light-breakable and tunable thermoresponsive amphiphilic block copolymer: from self-assembly, disassembly to re-self-assembly. *Polym. Chem.* **2014,** *5* (14), 4259-4267.

58. Yang, F.; Cao, Z.; Wang, G., Micellar assembly of a photo- and temperature-responsive amphiphilic block copolymer for controlled release. *Polym. Chem.* **2015,** *6* (46), 7995-8002.

59. Jiang, X.; Jin, S.; Zhong, Q.; Dadmun, M. D.; Zhao, B., Stimuli-Induced Multiple Sol−Gel−Sol Transitions of Aqueous Solution of a Thermo- and Light-Sensitive Hydrophilic Block Copolymer. *Macromolecules* **2009,** *42* (21), 8468-8476.

60. Yao, C.; Wang, X.; Liu, G.; Hu, J.; Liu, S., Distinct Morphological Transitions of Photoreactive and Thermoresponsive Vesicles for Controlled Release and Nanoreactors. *Macromolecules* **2016**.

61. Shrivastava, S.; Matsuoka, H., Photocleavable amphiphilic diblock copolymer micelles bearing a nitrobenzene block. *Colloid Polym. Sci.* **2016,** *294* (5), 879-887.

62. Fang, J.-Y.; Lin, Y.-K.; Wang, S.-W.; Li, Y.-C.; Lee, R.-S., Synthesis and characterization of dual-stimuli-responsive micelles based on poly(N-isopropylacrylamide) and polycarbonate with photocleavable moieties. *React. Funct. Polym.* **2015,** *95*, 46-54.

63. Sun, T.; Li, P.; Oh, J. K., Dual Location Dual Reduction/Photoresponsive Block Copolymer Micelles: Disassembly and Synergistic Release. *Macromol. Rapid Commun.* **2015,** *36* (19), 1742-1748.

64. Wu, W.-C.; Kuo, Y.-S.; Cheng, C.-H., Dual-stimuli responsive polymeric micelles: preparation, characterization, and controlled drug release. *J. Polym. Res.* **2015,** *22* (5), 80.

65. Jin, Q.; Cai, T.; Wang, Y.; Wang, H.; Ji, J., Light-Responsive Polyion Complex Micelles with Switchable Surface Charge for Efficient Protein Delivery. *ACS Macro Lett.* **2014,** *3* (7), 679-683.

66. Kalva, N.; Parekh, N.; Ambade, A. V., Controlled micellar disassembly of photo- and pH-cleavable linear-dendritic block copolymers. *Polym. Chem.* **2015,** *6* (38), 6826-6835.

67. Wu, Y.; Hu, H.; Hu, J.; Liu, T.; Zhang, G.; Liu, S., Thermo- and Light-Regulated Formation and Disintegration of Double Hydrophilic Block Copolymer Assemblies with Tunable Fluorescence Emissions. *Langmuir : the ACS journal of surfaces and colloids* **2013,** *29* (11), 3711-3720.

68. Huo, H.; Ma, X.; Dong, Y.; Qu, F., Light/temperature dual-responsive ABC miktoarm star terpolymer micelles for controlled release. *Eur. Polym. J.* **2017,** *87*, 331-343.

69. He, L.; Hu, B.; Henn, D. M.; Zhao, B., Influence of cleavage of photosensitive group on thermally induced micellization and gelation of a doubly responsive diblock copolymer in aqueous solutions: A SANS study. *Polymer* **2016,** *105*, 25-34.

70. Tao, Z.; Peng, K.; Fan, Y.; Liu, Y.; Yang, H., Multi-stimuli responsive supramolecular hydrogels based on Fe3+ and diblock copolymer micelle complexation. *Polym. Chem.* **2016,** *7* (7), 1405-1412.

71. Kumar, S.; Dory, Y. L.; Lepage, M.; Zhao, Y., Surface-Grafted Stimuli-Responsive Block Copolymer Brushes for the Thermo-, Photo- and pH-Sensitive Release of Dye Molecules. *Macromolecules* **2011,** *44* (18), 7385-7393.

72. Wang, X.; Jiang, G.; Li, X.; Tang, B.; Wei, Z.; Mai, C., Synthesis of multi-responsive polymeric nanocarriers for controlled release of bioactive agents. *Polym. Chem.* **2013,** *4* (17), 4574-4577.

73. Cao, Z.; Wu, H.; Dong, J.; Wang, G., Quadruple-Stimuli-Sensitive Polymeric Nanocarriers for Controlled Release under Combined Stimulation. *Macromolecules* **2014,** *47* (24), 8777-8783.

74. Han, D.; Tong, X.; Zhao, Y., Fast Photodegradable Block Copolymer Micelles for Burst Release. *Macromolecules* **2011,** *44* (3), 437-439.

75. Han, D.; Tong, X.; Zhao, Y., Block Copolymer Micelles with a Dual-Stimuli-Responsive Core for Fast or Slow Degradation. *Langmuir* **2012,** *28* (5), 2327-2331.

76. Cabane, E.; Malinova, V.; Meier, W., Synthesis of Photocleavable Amphiphilic Block Copolymers: Toward the Design of Photosensitive Nanocarriers. *Macromol. Chem. Phys.* **2010,** *211* (17), 1847-1856.

77. Zhao, H.; Sterner, E. S.; Coughlin, E. B.; Theato, P., o-Nitrobenzyl Alcohol Derivatives: Opportunities in Polymer and Materials Science. *Macromolecules* **2012,** *45* (4), 1723-1736.

78. Zhao, H.; Gu, W.; Thielke, M. W.; Sterner, E.; Tsai, T.; Russell, T. P.; Coughlin, E. B.; Theato, P., Functionalized Nanoporous Thin Films and Fibers from Photocleavable Block Copolymers Featuring Activated Esters. *Macromolecules* **2013,** *46* (13), 5195-5201.

79. Xuan, J.; Han, D.; Xia, H.; Zhao, Y., Dual-Stimuli-Responsive Micelle of an ABC Triblock Copolymer Bearing a Redox-Cleavable Unit and a Photocleavable Unit at Two Block Junctions. *Langmuir : the ACS journal of surfaces and colloids* **2014,** *30* (1), 410-417.

80. Li, L.; Lv, A.; Deng, X.-X.; Du, F.-S.; Li, Z.-C., Facile synthesis of photo-cleavable polymers via Passerini reaction. *Chem. Commun.* **2013,** *49* (76), 8549-8551.

81. Schumers, J.-M.; Gohy, J.-F.; Fustin, C.-A., A versatile strategy for the synthesis of block copolymers bearing a photocleavable junction. *Polym. Chem.* **2010,** *1* (2), 161-163.

82. Gungor, E.; Armani, A. M., Photocleavage of Covalently Immobilized Amphiphilic Block Copolymer: From Bilayer to Monolayer. *Macromolecules* **2016,** *49* (16), 5773-5781.

83. Lee, R.-S.; Li, Y.-C.; Wang, S.-W., Synthesis and characterization of amphiphilic photocleavable polymers based on dextran and substituted-ε-caprolactone. *Carbohyd. Polym.* **2015,** *117*, 201-210.

84. Shota, Y.; Hidemi, T.; Shuya, Y.; Seiichi, N.; Kazuo, Y., Synthesis of Amphiphilic Diblock Copolymer Using Heterobifunctional Linkers, Connected by a Photodegradable N-(2-Nitrobenzyl)imide Structure and Available for Two Different Click Chemistries. *Bull. Chem. Soc. Jpn.* **2016,** *89* (4), 481-489.

85. Gao, Y.; Qiu, H.; Zhou, H.; Li, X.; Harniman, R.; Winnik, M. A.; Manners, I., Crystallization-Driven Solution Self-Assembly of Block Copolymers with a Photocleavable Junction. *J. Am. Chem. Soc.* **2015,** *137* (6), 2203-2206.

86. Coumes, F.; Malfait, A.; Bria, M.; Lyskawa, J.; Woisel, P.; Fournier, D., Catechol/boronic acid chemistry for the creation of block copolymers with a multi-stimuli responsive junction. *Polym. Chem.* **2016,** *7* (28), 4682-4692.

87. Katz, J. S.; Zhong, S.; Ricart, B. G.; Pochan, D. J.; Hammer, D. A.; Burdick, J. A., Modular Synthesis of Biodegradable Diblock Copolymers for Designing Functional Polymersomes. *J. Am. Chem. Soc.* **2010,** *132* (11), 3654-3655.

88. Gamys, C. G.; Schumers, J.-M.; Vlad, A.; Fustin, C.-A.; Gohy, J.-F., Amine-functionalized nanoporous thin films from a poly(ethylene oxide)-block-polystyrene diblock copolymer bearing a photocleavable o-nitrobenzyl carbamate junction. *Soft matter* **2012,** *8* (16), 4486-4493.

89. Zhao, H.; Gu, W.; Sterner, E.; Russell, T. P.; Coughlin, E. B.; Theato, P., Highly Ordered Nanoporous Thin Films from Photocleavable Block Copolymers. *Macromolecules* **2011,** *44* (16), 6433-6440.

90. Yang, L.; Lei, M.; Zhao, M.; Yang, H.; Zhang, H.; Li, Y.; Zhang, K.; Lei, Z., Synthesis of the light/pH responsive polymer for immobilization of α-amylase. *Mater. Sci. Eng. C.* **2017,** *71*, 75-83.

91. Natansohn, A.; Rochon, P., Photoinduced Motions in Azo-Containing Polymers. *Chem. Rev.* **2002,** *102* (11), 4139-4176.

92. Kumar, G. S.; Neckers, D. C., Photochemistry of azobenzene-containing polymers. *Chem. Rev.* **1989,** *89* (8), 1915-1925.

93. Berkovic, G.; Krongauz, V.; Weiss, V., Spiropyrans and Spirooxazines for Memories and Switches. *Chem. Rev.* **2000,** *100* (5), 1741-1754.

94. Assaid, I.; Bosc, D.; Hardy, I., Improvements of the Poly(vinyl cinnamate) Photoresponse in Order to Induce High Refractive Index Variations. *J. Phys. Chem. B* **2004,** *108* (9), 2801-2806.

95. Irie, M., Diarylethenes for Memories and Switches. *Chem. Rev.* **2000,** *100* (5), 1685-1716.

96. Stobbe, H.; Leuner, K., Farblose Alkylfulgide. (8. Abhandlung über Butadiënverbindungen.). *Ber. Dtsch. Chem. Ges.* **1905,** *38* (3), 3682-3685.

97. Irie, M.; Mohri, M., Thermally irreversible photochromic systems. Reversible photocyclization of diarylethene derivatives. *J. Org. Chem.* **1988,** *53* (4), 803-808.

98. Tanio, N.; Irie, M., Photooptical Switching of Polymer Film Waveguide Containing Photochromic Diarylethenes. *Jpn. J. Appl. Phys.* **1994,** *33* (Part 1, No. 3A), 1550-1553.

99. Fukaminato, T.; Sasaki, T.; Kawai, T.; Tamai, N.; Irie, M., Digital photoswitching of fluorescence based on the photochromism of diarylethene derivatives at a single-molecule level. *J. Am. Chem. Soc.* **2004,** *126* (45), 14843-9.

100. Stellacci, F.; Toscano, F.; Gallazzi, M. C.; Zerbi, G., From a photochromic diarylethene monomer to a dopable photochromic polymer: optical properties. *Synth. Met.* **1999,** *102* (1-3), 979-980.

101. Nishi, H.; Kobatake, S., Photochromism and Optical Property of Gold Nanoparticles Covered with Low-Polydispersity Diarylethene Polymers. *Macromolecules* **2008,** *41* (11), 3995-4002.

102. Seno, R.; Kobatake, S., Synthesis and characterization of amphiphilic silica nanoparticles covered by block copolymers branching photochromic diarylethene moieties on side chain. *Dyes Pigm.* **2015,** *114*, 166-174.

103. Griffiths, J., II. Photochemistry of azobenzene and its derivatives. *Chem. Soc. Rev.* **1972,** *1* (4), 481-493.

104. Hartley, G. S., The Cis-form of Azobenzene. *Nat. Chem.* **1937,** *140* (3537), 281-281.

105. Krollpfeiffer, F.; Mühlhausen, C.; Wolf, G., Zur Kenntnis der Lichtempfindlichkeit von Aryl-β-naphtylamin-azofarbstoffen. *Liebigs Ann. Chem.* **1934,** *508* (1), 39-51.

106. Bleger, D.; Schwarz, J.; Brouwer, A. M.; Hecht, S., o-Fluoroazobenzenes as readily synthesized photoswitches offering nearly quantitative two-way isomerization with visible light. *J. Am. Chem. Soc.* **2012,** *134* (51), 20597-600.

107. Ringsdorf, H.; Schmidt, H.-W., Electro-optical effects of azo dye containing liquid crystalline copolymers. *Makromol. Chem.* **1984,** *185* (7), 1327-1334.

108. Angeloni, A. S.; Caretti, D.; Carlini, C.; Chiellini, E.; Galli, G.; Altomare, A.; Solaro, R.; Laus, M., Photochromic liquid-crystalline polymers. Main chain and side chain polymers containing azobenzene mesogens. *Liq. Cryst.* **1989,** *4* (5), 513-527.

109. Moriya, K.; Seki, T.; Nakagawa, M.; Mao, G.; Ober, C. K., Photochromism of 4-cyanophenylazobenzene in liquid crystalline-coil AB diblock copolymers: the influence of microstructure. *Macromol. Rapid Commun.* **2000,** *21* (18), 1309-1312.

110. Frenz, C.; Fuchs, A.; Schmidt, H.-W.; Theissen, U.; Haarer, D., Diblock Copolymers with Azobenzene Side-Groups and Polystyrene Matrix: Synthesis, Characterization and Photoaddressing. *Macromol. Chem. Phys.* **2004,** *205* (9), 1246-1258.

111. Wang, G.; Tong, X.; Zhao, Y., Preparation of Azobenzene-Containing Amphiphilic Diblock Copolymers for Light-Responsive Micellar Aggregates. *Macromolecules* **2004,** *37* (24), 8911-8917.

112. Hu, J.; Yu, H.; Gan, L. H.; Hu, X., Photo-driven pulsating vesicles from self-assembled lipid-like azopolymers. *Soft matter* **2011,** *7* (24), 11345-11350.

113. Pearson, S.; Vitucci, D.; Khine, Y. Y.; Dag, A.; Lu, H.; Save, M.; Billon, L.; Stenzel, M. H., Light-responsive azobenzene-based glycopolymer micelles for targeted drug delivery to melanoma cells. *Eur. Polym. J.* **2015,** *69*, 616-627.

114. Se, K.; Kijima, M.; Fujimoto, T., Photochemical isomerization of azobenzene incorporated in poly(N,N-dimethyl-4-vinylphenethylamine-block-styrene) diblock copolymer by cross linkage. *Polymer* **1997,** *38* (23), 5755-5760.

115. Ueki, T.; Nakamura, Y.; Lodge, T. P.; Watanabe, M., Light-Controlled Reversible Micellization of a Diblock Copolymer in an Ionic Liquid. *Macromolecules* **2012,** *45* (18), 7566-7573.

116. Concellón, A.; Blasco, E.; Martínez-Felipe, A.; Martínez, J. C.; Šics, I.; Ezquerra, T. A.; Nogales, A.; Piñol, M.; Oriol, L., Light-Responsive Self-Assembled Materials by Supramolecular Post-Functionalization via Hydrogen Bonding of Amphiphilic Block Copolymers. *Macromolecules* **2016,** *49* (20), 7825-7836.

117. Concellón, A.; Clavería-Gimeno, R.; Velázquez-Campoy, A.; Abian, O.; Piñol, M.; Oriol, L., Polymeric micelles from block copolymers containing 2,6-diacylaminopyridine units for encapsulation of hydrophobic drugs. *RSC Adv.* **2016,** *6* (29), 24066-24075.

118. Dilthey, W.; Berres, C., Die Halochromie acylierter Aminochalkone und verwandter Verbindungen. (Heteropolare Kohlenstoffverbindungen. II. *J. prakt. Chem.* **1926,** *112* (1), 299-313.

119. Löwenbein, A.; Katz, W., Über substituiertespiro-Dibenzopyrane. *Ber. Dtsch. Chem. Ges.* **1926,** *59* (7), 1377-1383.

120. Hirshberg, Y.; Fischer, E., Photochromism and reversible multiple internal transitions in some spiroPyrans at low temperatures. Part II. *J. Chem. Soc.* **1954**, 3129-3137.

121. Bergmann, E. D.; Weizmann, A.; Fischer, E., Structure and Polarity of Some Polycyclic Spirans. *J. Am. Chem. Soc.* **1950,** *72* (11), 5009-5012.

122. Koelsch, C. F., Steric Factors in Thermochromism of Spiropyrans and in Reactivities of Certain Methylene Groups. *J. Org. Chem.* **1951,** *16* (9), 1362-1370.

123. Raymo, F. M.; Giordani, S., Signal Processing at the Molecular Level. *J. Am. Chem. Soc.* **2001,** *123* (19), 4651-4652.

124. Lee, S. K.; Neckers, D. C., Benzospiropyrans as photochromic and/or thermochromic photoinitiators. *Chem. Mater.* **1991,** *3* (5), 852-858.

125. Balmond, E. I.; Tautges, B. K.; Faulkner, A. L.; Or, V. W.; Hodur, B. M.; Shaw, J. T.; Louie, A. Y., Comparative Evaluation of Substituent Effect on the Photochromic Properties of Spiropyrans and Spirooxazines. *J. Org. Chem.* **2016,** *81* (19), 8744-8758.

126. Smets, G., Photochromic behaviour of polymeric systems and related phenomena. *Pure Appl. Chem.* **1972,** *30* (1-2), 1-24.

127. Krongauz, V. A.; Goldburt, E. S., Crystallization of poly(spiropyran methacrylate) with cooperative spiropyran-merocyanine conversion. *Macromolecules* **1981,** *14* (5), 1382-1386.

128. Gonzalez-De Los Santos, E. A.; Lozano-Gonzalez, M. J.; Johnson, A. F., Photoresponsive polyurethane-acrylate block copolymers. I. Photochromic effects in copolymers containing 6-nitro spiropyranes and 6?-nitro-bis-spiropyranes. *J. Appl. Polym. Sci.* **1999,** *71* (2), 259-266.

129. Lee, H. I.; Wu, W.; Oh, J. K.; Mueller, L.; Sherwood, G.; Peteanu, L.; Kowalewski, T.; Matyjaszewski, K., Light-induced reversible formation of polymeric micelles. *Angew. Chem. Int. Ed.* **2007,** *46* (14), 2453-7.

130. Kotharangannagari, V. K.; Sánchez-Ferrer, A.; Ruokolainen, J.; Mezzenga, R., Photoresponsive Reversible Aggregation and Dissolution of Rod–Coil Polypeptide Diblock Copolymers. *Macromolecules* **2011,** *44* (12), 4569-4573.

131. Berman, E.; Fox, R. E.; Thomson, F. D., Photochromic Spiropyrans. I. The Effect of Substituents on the Rate of Ring Closure. *J. Am. Chem. Soc.* **1959,** *81* (21), 5605-5608.

132. Zhang, Y.; Chen, S.; Pang, M.; Zhang, W., Synthesis and micellization of multi-stimuli responsive block copolymer based on spiropyran. *Polym. Chem.* **2016**.

133. Wang, X.; Hu, J.; Liu, G.; Tian, J.; Wang, H.; Gong, M.; Liu, S., Reversibly Switching Bilayer Permeability and Release Modules of Photochromic Polymersomes Stabilized by Cooperative Noncovalent Interactions. *J. Am. Chem. Soc.* **2015,** *137* (48), 15262-75.

134. Chen, J.; Zeng, F.; Wu, S.; Chen, Q.; Tong, Z., A core-shell nanoparticle approach to photoreversible fluorescence modulation of a hydrophobic dye in aqueous media. *Chem. Eur. J.* **2008,** *14* (16), 4851-60.

135. Guragain, S.; Bastakoti, B. P.; Ito, M.; Yusa, S.-i.; Nakashima, K., Aqueous polymeric micelles of poly[N-isopropylacrylamide-b-sodium 2-(acrylamido)-2-methylpropanesulfonate] with a spiropyran dimer pendant: quadruple stimuli-responsiveness. *Soft Matter* **2012,** *8* (37), 9628.

136. Menon, S.; Ongungal, R. M.; Das, S., Photocleavable glycopolymer aggregates. *Polym. Chem.* **2013,** *4* (3), 623-628.

137. Jin, Q.; Liu, G.; Ji, J., Micelles and reverse micelles with a photo and thermo double-responsive block copolymer. *J. Polym. Sci., Part A: Polym. Chem.* **2010,** *48* (13), 2855-2861.

138. Roy, D.; Brooks, W. L. A.; Sumerlin, B. S., New directions in thermoresponsive polymers. *Chem. Soc. Rev.* **2013,** *42* (17), 7214-7243.

139. Fujishige, S.; Kubota, K.; Ando, I., Phase transition of aqueous solutions of poly(N-isopropylacrylamide) and poly(N-isopropylmethacrylamide). *J. Phys. Chem.* **1989,** *93* (8), 3311-3313.

140. Weber, C.; Hoogenboom, R.; Schubert, U. S., Temperature responsive bio-compatible polymers based on poly(ethylene oxide) and poly(2-oxazoline)s. *Prog. Polym. Sci.* **2012,** *37* (5), 686-714.

141. Wolf, B. A.; Willms, M. M., Measured and calculated solubility of polymers in mixed solvents: Co-nonsolvency. *Makromol. Chem.* **1978,** *179* (9), 2265-2277.

142. Mukherji, D.; Marques, C. M.; Stuehn, T.; Kremer, K., Co-non-solvency: mean-field polymer theory does not describe polymer collapse transition in a mixture of two competing good solvents. *J Chem Phys* **2015,** *142* (11), 114903.

143. Bittrich, E.; Kuntzsch, M.; Eichhorn, K.-J.; Uhlmann, P., Complex pH- and temperature-sensitive swelling behavior of mixed polymer brushes. *J. Polym. Sci., Part B: Polym. Phys.* **2010,** *48* (14), 1606-1615.

144. Heskins, M.; Guillet, J. E., Solution Properties of Poly(N-isopropylacrylamide). *J. Macromol. Sci., A* **1968,** *2* (8), 1441-1455.

145. Schild, H. G., Poly(N-isopropylacrylamide): experiment, theory and application. *Prog. Polym. Sci.* **1992,** *17* (2), 163-249.

146. Schild, H. G.; Tirrell, D. A., Microcalorimetric detection of lower critical solution temperatures in aqueous polymer solutions. *J. Phys. Chem.* **1990,** *94* (10), 4352-4356.

147. Halperin, A.; Kröger, M.; Winnik, F. M., Poly(N-isopropylacrylamide) Phase Diagrams: Fifty Years of Research. *Angew. Chem. Int. Ed.* **2015,** *54* (51), 15342-15367.

148. Hofmann, C.; Schönhoff, M., Do additives shift the LCST of poly (N-isopropylacrylamide) by solvent quality changes or by direct interactions? *Colloid Polym. Sci.* **2009,** *287* (12), 1369-1376.

149. Yamauchi, H.; Maeda, Y., LCST and UCST behavior of poly(N-isopropylacrylamide) in DMSO/water mixed solvents studied by IR and micro-Raman spectroscopy. *J Phys Chem B* **2007,** *111* (45), 12964-8.

150. Mukherji, D.; Wagner, M.; Watson, M. D.; Winzen, S.; de Oliveira, T. E.; Marques, C. M.; Kremer, K., Relating side chain organization of PNIPAm with its conformation in aqueous methanol. *Soft matter* **2016,** *12* (38), 7995-8003.

151. Schild, H. G.; Tirrell, D. A., Microcalorimetric detection of lower critical solution temperatures in aqueous polymer solutions. *J. Phys. Chem. B* **1990,** *94* (10), 4352-4356.

152. Lutz, J.-F., Polymerization of oligo(ethylene glycol) (meth)acrylates: Toward new generations of smart biocompatible materials. *J. Polym. Sci., Part A-1: Polym. Chem.* **2008,** *46* (11), 3459-3470.

153. Hedir, G. G.; Arno, M. C.; Langlais, M.; Husband, J. T.; O'Reilly, R. K.; Dove, A. P., Poly(oligo(ethylene glycol) vinyl acetate)s: A Versatile Class of Thermoresponsive and Biocompatible Polymers. *Angew. Chem. Int. Ed.* **2017,** *56* (31), 9178-9182.

154. Hua, F.; Jiang, X.; Li, D.; Zhao, B., Well-defined thermosensitive, water-soluble polyacrylates and polystyrenics with short pendant oligo(ethylene glycol) groups synthesized by nitroxide-mediated radical polymerization. *J. Polym. Sci., Part A: Polym. Chem.* **2006,** *44* (8), 2454-2467.

155. Langer, M.; Brandt, J.; Lederer, A.; Goldmann, A. S.; Schacher, F. H.; Barner-Kowollik, C., Amphiphilic block copolymers featuring a reversible hetero Diels-Alder linkage. *Polym. Chem.* **2014,** *5* (18), 5330-5338.

156. Zhao, B.; Li, D.; Hua, F.; Green, D. R., Synthesis of Thermosensitive Water-Soluble Polystyrenics with Pendant Methoxyoligo(ethylene glycol) Groups by Nitroxide-Mediated Radical Polymerization. *Macromolecules* **2005,** *38* (23), 9509-9517.

157. Masson, P.; Beinert, G.; Franta, E.; Rempp, P., Synthesis of polyethylene oxide macromers. *Polymer Bulletin* **1982,** *7* (1), 17-22.

158. Neugebauer, D.; Rydz, J.; Goebel, I.; Dacko, P.; Kowalczuk, M., Synthesis of Graft Copolymers Containing Biodegradable Poly(3-hydroxybutyrate) Chains. *Macromolecules* **2007,** *40* (5), 1767-1773.

159. Lutz, J.-F.; Akdemir, Ö.; Hoth, A., Point by Point Comparison of Two Thermosensitive Polymers Exhibiting a Similar LCST: Is the Age of Poly(NIPAM) Over? *J. Am. Chem. Soc.* **2006,** *128* (40), 13046-13047.

160. Darling, S. B., Directing the self-assembly of block copolymers. *Prog. Polym. Sci.* **2007,** *32* (10), 1152-1204.

161. Riess, G., Micellization of block copolymers. *Progress in Polymer Science* **2003,** *28* (7), 1107-1170.

162. Blanazs, A.; Armes, S. P.; Ryan, A. J., Self-Assembled Block Copolymer Aggregates: From Micelles to Vesicles and their Biological Applications. *Macromol. Rapid Commun.* **2009,** *30* (4-5), 267-77.

163. Kim, J. K.; Yang, S. Y.; Lee, Y.; Kim, Y., Functional nanomaterials based on block copolymer self-assembly. *Prog. Polym. Sci.* **2010,** *35* (11), 1325-1349.

164. Kataoka, K.; Harada, A.; Nagasaki, Y., Block copolymer micelles for drug delivery: design, characterization and biological significance. *Advanced Drug Delivery Reviews* **2001,** *47* (1), 113-131.

165. Bates, F. S.; Fredrickson, G. H., Block Copolymers - Designer Soft Materials. *Phys. Today* **1999,** *52*, 32-38.

166. Brendel, J. C.; Schacher, F. H., Block Copolymer Self-Assembly in Solution-Quo Vadis? *Chem. - Asian J.* **2018,** *13* (3), 230-239.

167. Letchford, K.; Burt, H., A review of the formation and classification of amphiphilic block copolymer nanoparticulate structures: micelles, nanospheres, nanocapsules and polymersomes. *Eur. J. Pharm. Biopharm.* **2007,** *65* (3), 259-69.

168. Nicolai, T.; Colombani, O.; Chassenieux, C., Dynamic polymeric micelles versus frozen nanoparticles formed by block copolymers. *Soft matter* **2010,** *6* (14).

169. Kelley, E. G.; Murphy, R. P.; Seppala, J. E.; Smart, T. P.; Hann, S. D.; Sullivan, M. O.; Epps, T. H., Size evolution of highly amphiphilic macromolecular solution assemblies via a distinct bimodal pathway. *Nat. Commun.* **2014,** *5*, 3599.

170. Torchilin, V. P., Structure and design of polymeric surfactant-based drug delivery systems. *J. Controlled Release* **2001,** *73* (2-3), 137-172.

171. Rabnawaz, M.; Liu, G., Preparation and Application of a Dual Light-Responsive Triblock Terpolymer. *Macromolecules* **2012,** *45* (13), 5586-5595.

172. Yang, H.; Jia, L.; Wang, Z.; Di-Cicco, A.; Lévy, D.; Keller, P., Novel Photolabile Diblock Copolymers Bearing Truxillic Acid Derivative Junctions. *Macromolecules* **2011,** *44* (1), 159-165.

173. Zhang, W.; Zhou, X.; Li, H.; Fang, Y.; Zhang, G., Conformational Transition of Tethered Poly(N-isopropylacrylamide) Chains in Coronas of Micelles and Vesicles. *Macromolecules* **2005,** *38* (3), 909-914.

174. Nuopponen, M.; Ojala, J.; Tenhu, H., Aggregation behaviour of well defined amphiphilic diblock copolymers with poly(N-isopropylacrylamide) and hydrophobic blocks. *Polymer* **2004,** *45* (11), 3643-3650.

175. Ke, X. X.; Wang, L.; Xu, J. T.; Du, B. Y.; Tu, Y. F.; Fan, Z. Q., Effect of local chain deformability on the temperature-induced morphological transitions of polystyrene-b-poly(N-isopropylacrylamide) micelles in aqueous solution. *Soft matter* **2014,** *10* (28), 5201-11.

176. Kim, M. R.; Cheong, I. W., Stimuli-triggered Formation of Polymersomes from W/O/W Multiple Double Emulsion Droplets Containing Poly(styrene)-block-poly(N-isopropylacrylamide-co-spironaphthoxazine methacryloyl). *Langmuir* **2016,** *32* (36), 9223-8.

177. Yan, Q.; Yuan, J.; Yuan, W.; Zhou, M.; Yin, Y.; Pan, C., Copolymer logical switches adjusted through core-shell micelles: from temperature response to fluorescence response. *Chem. Commun. (Cambridge, U. K.)* **2008,** (46), 6188-90.

178. Mohanty, K.; Purkait, M. K., *Membrane Technologies and Applications*. 2011.

179. Lai, Z.; Bonilla, G.; Diaz, I.; Nery, J. G.; Sujaoti, K.; Amat, M. A.; Kokkoli, E.; Terasaki, O.; Thompson, R. W.; Tsapatsis, M.; Vlachos, D. G., Microstructural optimization of a zeolite membrane for organic vapor separation. *Science* **2003,** *300* (5618), 456-60.

180. Chang, C. H.; Gopalan, R.; Lin, Y. S., A comparative study on thermal and hydrothermal stability of alumina, titania and zirconia membranes. *J. Membr. Sci.* **1994,** *91* (1-2), 27-45.

181. Lee, W.; Ji, R.; Gösele, U.; Nielsch, K., Fast fabrication of long-range ordered porous alumina membranes by hard anodization. *Nature Materials* **2006,** *5*, 741.

182. Li, H.-J.; Cao, Y.-M.; Qin, J.-J.; Jie, X.-M.; Wang, T.-H.; Liu, J.-H.; Yuan, Q., Development and characterization of anti-fouling cellulose hollow fiber UF membranes for oil–water separation. *J. Membr. Sci.* **2006,** *279* (1-2), 328-335.

183. Lonsdale, H. K.; Merten, U.; Riley, R. L., Transport properties of cellulose acetate osmotic membranes. *J. Appl. Polym. Sci.* **1965,** *9* (4), 1341-1362.

184. Wu, D.; Xu, F.; Sun, B.; Fu, R.; He, H.; Matyjaszewski, K., Design and preparation of porous polymers. *Chem. Rev.* **2012,** *112* (7), 3959-4015.

185. Wan, Y.; Shi, Y.; Zhao, D., Supramolecular Aggregates as Templates: Ordered Mesoporous Polymers and Carbons†. *Chem. Mater.* **2008,** *20* (3), 932-945.

186. Jenekhe, S. A.; Chen, X. L., Self-assembly of ordered microporous materials from rod-coil block copolymers. *Science* **1999,** *283* (5400), 372-5.

187. Grande, D.; Penelle, J.; Davidson, P.; Beurroies, I.; Denoyel, R., Functionalized ordered nanoporous polymeric materials: From the synthesis of diblock copolymers to their nanostructuration and their selective degradation. *Microporous Mesoporous Mater.* **2011,** *140* (1-3), 34-39.

188. Gorzolnik, B.; Davidson, P.; Beurroies, I.; Denoyel, R.; Grande, D., Novel Functional Mesoporous Materials Obtained from Nanostructured Diblock Copolymers. *Macromol. Symp.* **2010,** *287* (1), 127-134.

189. van de Witte, P.; Dijkstra, P. J.; van den Berg, J. W. A.; Feijen, J., Phase separation processes in polymer solutions in relation to membrane formation. *J. Membr. Sci.* **1996,** *117* (1-2), 1-31.

190. Ulbricht, M., Advanced functional polymer membranes. *Polymer* **2006,** *47* (7), 2217-2262.

191. Abetz, V., Isoporous block copolymer membranes. *Macromol. Rapid Commun.* **2015,** *36* (1), 10-22.

192. Urbas, A.; Fink, Y.; Thomas, E. L., One-Dimensionally Periodic Dielectric Reflectors from Self-Assembled Block Copolymer−Homopolymer Blends. *Macromolecules* **1999,** *32* (14), 4748-4750.

193. Hillmyer, M. A., Polydisperse block copolymers: Don't throw them away. *J. Polym. Sci., Part B: Polym. Phys.* **2007,** *45* (24), 3249-3251.

194. Noro, A.; Cho, D.; Takano, A.; Matsushita, Y., Effect of Molecular Weight Distribution on Microphase-Separated Structures from Block Copolymers. *Macromolecules* **2005,** *38* (10), 4371-4376.

195. Lynd, N. A.; Meuler, A. J.; Hillmyer, M. A., Polydispersity and block copolymer self-assembly. *Prog. Polym. Sci.* **2008,** *33* (9), 875-893.

196. Hörenz, C. Amphiphilic (Block) Copolymers with Crosslinkable Moieties: from Functional Building Blocks to Nanostructured Materials. Jena, 2017.

197. Schacher, F. H. Funktionale Nanostrukturierte Systeme basierend auf wohldefinierten Blockcopolymeren: Schaltbare Membranen, Kompartmentierte Mizellen und Interpolyelektrolyt-Komplexe. 2009/05/15, Bayreuth, 2009.

198. Shishatskiy, S.; Nistor, C.; Popa, M.; Nunes, S. P.; Peinemann, K. V., Polyimide Asymmetric Membranes for Hydrogen Separation: Influence of Formation Conditions on Gas Transport Properties. *Adv. Eng. Mater.* **2006,** *8* (5), 390-397.

199. Phillip, W. A.; O'Neill, B.; Rodwogin, M.; Hillmyer, M. A.; Cussler, E. L., Self-assembled block copolymer thin films as water filtration membranes. *ACS Appl. Mater. Interfaces* **2010,** *2* (3), 847-53.

200. Nunes, S. P.; Peinemann, K.-V., *Membrane Technology*. 2006.

201. Cetintas, M.; de Grooth, J.; Hofman, A. H.; van der Kooij, H. M.; Loos, K.; de Vos, W. M.; Kamperman, M., Free-standing thermo-responsive nanoporous membranes from high molecular weight PS-PNIPAM block copolymers synthesized via RAFT polymerization. *Polym. Chem.* **2017,** *8* (14), 2235-2243.

202. Mocan, M.; Wahdat, H.; van der Kooij, H. M.; de Vos, W. M.; Kamperman, M., Systematic variation of membrane casting parameters to control the structure of thermo-responsive isoporous membranes. *Journal of Membrane Science* **2018,** *548*, 502-509.

203. Grimm, O.; Schacher, F., Dual Stimuli-Responsive P(NIPAAm-co-SPA) Copolymers: Synthesis and Response in Solution and in Films. *Polymers* **2018,** *10* (6), 645-661.

204. Grimm, O.; Maßmann, S. C.; Schacher, F. H., Synthesis and solution behaviour of dual light- and temperature-responsive poly(triethylene glycol-co-spiropyran) copolymers and block copolymers. *Polymer Chemistry* **2019,** *10* (21), 2674-2685.

205. Bleger, D.; Hecht, S., Visible-Light-Activated Molecular Switches. *Angew. Chem. Int. Ed.* **2015,** *54* (39), 11338-49.

206. Klajn, R., Spiropyran-based dynamic materials. *Chem. Soc. Rev.* **2014,** *43* (1), 148-84.

207. Hammarson, M.; Nilsson, J. R.; Li, S.; Beke-Somfai, T.; Andreasson, J., Characterization of the thermal and photoinduced reactions of photochromic spiropyrans in aqueous solution. *J. Phys. Chem. B* **2013,** *117* (43), 13561-71.

208. Wolff, C.; Kind, J.; Schenderlein, H.; Bartling, H.; Feldmeier, C.; Gschwind, R. M.; Biesalski, M.; Thiele, C. M., Studies of a photochromic model system using NMR with ex-situ and in-situ irradiation devices. *Magn. Reson. Chem.* **2016,** *54* (6), 485-91.

209. Hirshberg, Y.; Fischer, E., Photochromism and reversible multiple internal transitions in some spiropyrans at low temperatures. Part I. *J. Chem. Soc.* **1954**, 297-303.

210. Gibbons, O.; Carroll, W. M.; Aldabbagh, F.; Yamada, B., Nitroxide-mediated controlled statistical copolymerizations ofN-isopropylacrylamide withN-tert-butylacrylamide. *J. Polym. Sci., Part A: Polym. Chem.* **2006,** *44* (21), 6410-6418.

211. Schulte, T.; Siegenthaler, K. O.; Luftmann, H.; Letzel, M.; Studer, A., Nitroxide-Mediated Polymerization ofN-Isopropylacrylamide: Electrospray Ionization Mass Spectrometry, Matrix-Assisted Laser Desorption Ionization Mass Spectrometry, and Multiple-Angle Laser Light Scattering Studies on Nitroxide-Terminated Poly-N-isopropylacrylamides. *Macromolecules* **2005,** *38* (16), 6833-6840.

212. Hörenz, C.; Pietsch, C.; Goldmann, A. S.; Barner-Kowollik, C.; Schacher, F. H., Phase Inversion Membranes from Amphiphilic Diblock Terpolymers. *Adv. Mater. Interfaces* **2015,** *2* (8), 1500042.

213. Harrisson, S.; Couvreur, P.; Nicolas, J., Simple and efficient copper metal-mediated synthesis of alkoxyamine initiators. *Polym. Chem.* **2011,** *2* (8), 1859.

214. Miele, S.; Nesvadba, P.; Studer, A., 1-tert-Butyl-3,3,5,5-tetraalkyl-2-piperazinon-4-oxyls: Highly Efficient Nitroxides for Controlled Radical Polymerization. *Macromolecules* **2009,** *42* (7), 2419-2427.

215. Lessard, B.; Tervo, C.; Marić, M., High-Molecular-Weight Poly(tert-butyl acrylate) by Nitroxide-Mediated Polymerization: Effect of Chain Transfer to Solvent. *Macromol. React. Eng.* **2009,** *3* (5-6), 245-256.

216. Harrisson, S.; Couvreur, P.; Nicolas, J., Use of solvent effects to improve control over nitroxide-mediated polymerization of isoprene. *Macromol. Rapid Commun.* **2012,** *33* (9), 805-10.

217. Schroot, R.; Friebe, C.; Altuntas, E.; Crotty, S.; Jäger, M.; Schubert, U. S., Nitroxide-Mediated Polymerization of Styrenic Triarylamines and Chain-End Functionalization with a Ruthenium Complex: Toward Tailored Photoredox-Active Architectures. *Macromolecules* **2013,** *46* (6), 2039-2048.

218. Fleming, C. L.; Li, S.; Grotli, M.; Andreasson, J., Shining New Light on the Spiropyran Photoswitch: A Photocage Decides between cis- trans or Spiro-Merocyanine Isomerization. *Journal of the American Chemical Society* **2018**.

219. Rini, M.; Holm, A. K.; Nibbering, E. T.; Fidder, H., Ultrafast UV-mid-IR investigation of the ring opening reaction of a photochromic spiropyran. *J. Am. Chem. Soc.* **2003,** *125* (10), 3028-34.

220. Futami, Y.; Chin, M. L. S.; Kudoh, S.; Takayanagi, M.; Nakata, M., Conformations of nitro-substituted spiropyran and merocyanine studied by low-temperature matrix-isolation infrared spectroscopy and density-functional-theory calculation. *Chem. Phys. Let.* **2003,** *370* (3-4), 460-468.

221. Evans, L., UV-Vis Spectrophotometry. biochrom, Ed. 2018.

222. Hammarson, M.; Nilsson, J. R.; Li, S.; Beke-Somfai, T.; Andreasson, J., Characterization of the thermal and photoinduced reactions of photochromic spiropyrans in aqueous solution. *J Phys Chem B* **2013,** *117* (43), 13561-71.

223. Cao, K.; Xu, J.-t.; Wang, X.-s., Synthesis and characterization of Fe(II)-coordinated PS-b-P[NIPAM-co-(VBC-Fe-DMAP)] block copolymers. *Chinese Journal of Polymer Science* **2012,** *30* (5), 674-681.

224. Shinde, V. S.; Girme, M. R.; Pawar, V. U., Thermoresponsive polystyrene-b-poly(N-isopropylacrylamide) copolymers by atom transfer radical polymerization. *Indian J. Chem., Sect. A: Inorg., Bio-inorg., Phys., Theor. Anal. Chem.* **2011,** *50* (6), 781-787.

225. Mukherji, D.; Marques, C. M.; Kremer, K., Collapse in two good solvents, swelling in two poor solvents: defying the laws of polymer solubility? *J. Phys. Condens. Matter* **2018,** *30* (2), 024002.

226. Zalami, D.; Grimm, O.; Schacher, F. H.; Gerken, U.; Kohler, J., Non-invasive study of the three-dimensional structure of nanoporous triblock terpolymer membranes. *Soft matter* **2018,** *14* (48), 9750-9754.

227. Dunn, P. M., James Lind (1716-94) of Edinburgh and the treatment of scurvy. *Arch. Dis. Child.* **1997,** *76* (1), F64-F65.

228. Efron, B.; Cox, D. R.; Kass, R.; Barndorff-Nielsen, O. E.; Hinkley, D. V.; Fraser, D. A. S.; Dempster, A. P.; Efron, B., R. A. Fisher in the 21st century (Invited paper presented at the 1996 R. A. Fisher Lecture)Comment by D. R. CoxComment by Rob KassComment by Ole E. Barndorff-NielsenComment by D. V. HinkleyComment by D. A. S. FraserComment by A. P. DempsterRejoinder by Bradley Efron. *Statistical Science* **1998,** *13* (2), 95-122.

229. Armitage, P., A History of Mathematical Statistics from 1750 to 1930. . *Statistics in Medicine* **1999,** *18* (12), 1572-1573.

230. Box, J. F., R. A. Fisher and the Design of Experiments, 1922-1926. *The American Statistician* **1980,** *34* (1), 1-7.

231. Hahn, J.; Filiz, V.; Rangou, S.; Clodt, J.; Jung, A.; Buhr, K.; Abetz, C.; Abetz, V., Structure formation of integral-asymmetric membranes of polystyrene-block-Poly(ethylene oxide). *J. Polym. Sci., Part B: Polym. Phys.* **2013,** *51* (4), 281-290.

232. Fu, G. D.; Kang, E. T.; Neoh, K. G., Three-dimensionally ordered porous membranes prepared via self-assembly and reverse micelle formation from well-defined amphiphilic block copolymers. *Langmuir : the ACS journal of surfaces and colloids* **2005,** *21* (8), 3619-24.

233. Skaug, M. J.; Wang, L.; Ding, Y.; Schwartz, D. K., Hindered nanoparticle diffusion and void accessibility in a three-dimensional porous medium. *ACS Nano* **2015,** *9* (2), 2148-56.

12 Directories

12.1 Figures

12.2 Schemes

12.3 Tables

13 Declaration of Authorship / Selbstständigkeitserklärung

Ich erkläre, dass ich die vorliegende Arbeit selbstständig und unter Verwendung der angegebenen Hilfsmittel, persönlichen Mitteilungen und Quellen angefertigt habe.

_____ _____

Ort, Datum Oliver Grimm